



# Rich Dynamical Behavior in a Simple Chaotic Oscillator Based on Sallen Key High-Pass Filter

Saumen Chakraborty<sup>1</sup> · Saumendra Sankar De Sarkar<sup>2</sup> 

Received: 16 April 2022 / Revised: 8 February 2023 / Accepted: 9 February 2023

© The Author(s), under exclusive licence to Springer Science+Business Media, LLC, part of Springer Nature 2023

## Abstract

A chaotic oscillator has been designed based on a Sallen Key-type high-pass filter (HPF). The HPF has been converted to a chaotic oscillator using a parallel combination of a PN junction diode as a nonlinear element and an inductor as an energy storage element. The dynamics of the proposed system has been simulated numerically using fourth-order Runge–Kutta method. The circuit exhibits period-doubling route to chaos as well as period-adding route to chaos depending on the choice of system parameters. Striking features like antimonotonicity and coexistence of attractors are also observed. Bifurcation diagram, phase plane plots and spectrum of Lyapunov exponents have been employed to describe the chaotic behavior of the system. A hardware experiment has been carried out to verify the same in the laboratory using off-the-shelf components.

**Keywords** High-pass filter · Diode–inductor composite · Chaotic oscillator · Period-adding and period-doubling bifurcation · Antimonotonicity · Coexisting attractors

## List of Symbols

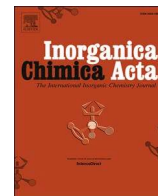
$C$	Capacitor
$R_1, R_2, R_a, R_b$	Resistor
$V_1, V_0$	Voltage
$k$	$R_1/2R_2$
$\omega_0$	Frequency of oscillation

---

✉ Saumendra Sankar De Sarkar  
ssdesarkar@gmail.com  
Saumen Chakraborty  
saumenbcc@gmail.com

<sup>1</sup> Department of Physics, Bidhan Chandra College, Asansol 713304, West Bengal, India

<sup>2</sup> Department of Physics, Raniganj Girls' College, Searsole Rajbari 713358, West Bengal, India



# Tris chelated meridional isomers of Co(III) complexes: Synthesis, crystal structure, protein binding, cytotoxicity studies and DFT/TDDFT calculation

Dama Saren<sup>a</sup>, Susobhan Das<sup>a</sup>, Aparup Paul<sup>a</sup>, Sharad S. Tat<sup>b</sup>, Manas Kumar Santra<sup>b</sup>,  
Tapan Kumar Si<sup>c</sup>, Horst Puschmann<sup>d</sup>, Subal Chandra Manna<sup>a,\*</sup>

<sup>a</sup> Department of Chemistry, Vidyasagar University, Midnapore 721102, West Bengal, India

<sup>b</sup> National Centre for Cell Science, NCCS Complex, Pune University Campus Ganeshkhind, Pune 411 007, Maharashtra, India

<sup>c</sup> Department of Chemistry, Bidhan Chandra College, Asansol 713304, West Bengal, India

<sup>d</sup> Department of Chemistry, University of Durham, South Road, Durham DH1 3LE, UK

## ARTICLE INFO

### Keywords:

Co(III) complexes  
Crystal structure  
Protein binding  
Cytotoxicity studies  
DFT/TD-DFT calculation

## ABSTRACT

Two mononuclear Co(III) complexes, [Co(L<sup>1</sup>)<sub>3</sub>] (**1**) and [Co(L<sup>2</sup>)<sub>3</sub>] (**2**) (HL<sup>1</sup>, 2-[(2-methoxy-ethylimino)-methyl]-phenol; HL<sup>2</sup>, 1-[(2-methoxy-ethylimino)-methyl]-naphthalen-2-ol) have been synthesized and characterized by X-ray crystal structure determination, IR and mass spectroscopic techniques. Both the complexes are mononuclear with distorted octahedral geometries and the Co(III) center are coordinated with three bidentate (O, N) Schiff base ligands. Complexes **1** and **2** form 1D and 3D supramolecular structures, respectively, with weak C—H... $\pi$  interactions. Experimental UV–vis absorption spectra have been compared with the results obtained from DFT / TD-DFT calculation using B3LYP functional and LanL2DZ basis set. The interaction of the complexes with bovine serum albumin (BSA) and human serum albumin (HSA) were studied using electronic absorption and fluorescence spectroscopic methods and the results show that complexes potentially quench the fluorescence of BSA/HSA through ground state association mechanism. Cytotoxicity studies of these complexes have been performed against breast cancer cell lines and found that they have moderate anticancer activity.

## 1. Introduction

First row transition metals play important role in the biological system and among them cobalt plays a vital role as for example, cobalt (III) is an important component of vitamin B<sub>12</sub> co-enzyme. Generally, the oxidation states of cobalt are +2 and +3 in coordination compounds and play an important role for their potential biological activities [1] and also they can potentially be used in catalysts [2], luminescence [3] and functional materials [4].

Multi-dentate Schiff base ligands are potentially used for the synthesis of 3d, 3d/lanthanoid metal-based coordination compounds [5].

The Schiff base coordinated compounds are biologically important because of their antifungal [6], antibacterial [7], anticancer [8], antimicrobial [9], antioxidant activities [10], etc.

A literature survey shows that Schiff-base coordinated cobalt compounds are also potentially used as cytotoxic agents [11].

In the circulatory system serum albumins (SAs) take parts in many physiological processes and show a vital role for transport of many exogenous and endogenous compounds [12]. High binding ability of

serum albumins (SAs) with metal complexes was reported in the literature Human serum albumin (HSA) and bovine serum albumin (BSA) are widely used for the study of binding affinity with metal complexes and to explore the mechanism of interaction.

Density functional theory (DFT) is a widely used as computational technique to explicate the molecular structure, electronic, and spectroscopic properties of 3d metal complexes [13]. Electronic absorbance spectral properties of the complexes can be explained by time-dependent density functional theory (TD-DFT) [14].

The present manuscript reports the synthesis, crystal structure, DFT/TD-DFT calculation, photophysical property, and protein binding activity of two mononuclear cobalt(III) complexes. The electronic spectral properties of complexes were explained by the results of DFT/TDDFT computation and the interaction of complexes with serum albumins was studied using electronic absorption and fluorescence spectroscopic techniques. The cytotoxicity studies of the two complexes have also been executed using breast cancer cell lines MCF7 and MDA-MB-231.

\* Corresponding author.

E-mail address: [scmanna@mail.vidyasagar.ac.in](mailto:scmanna@mail.vidyasagar.ac.in) (S.C. Manna).

<https://doi.org/10.1016/j.ica.2023.121423>

Received 31 October 2022; Received in revised form 24 January 2023; Accepted 31 January 2023

Available online 3 February 2023

0020-1693/© 2023 Elsevier B.V. All rights reserved.



## Moral Dogma and Ethical Relativity in Joseph Conrad's *Almayer's Folly*

Subhadeep Ray<sup>a</sup>  and Goutam Karmakar<sup>b</sup> 

<sup>a</sup>Kazi Nazrul University; <sup>b</sup>University of the Western Cape

### ABSTRACT

This paper studies the intricate treatment of the abstract and dogmatic order of imperial, racial, and religious morality, and the issue of ethical commitment in the concrete and fleeting relationships between individual subjects in Joseph Conrad's debut novel, *Almayer's Folly* (1895). The novel is set in the Malay Archipelago, where the fading years of the imperial absolutism of Europe give way to conflicting trade and political interests. A pessimistic philosophical outlook in Conrad's text shows how all the overindulgent narcissistic moral orders accommodate hate and self-interest motivated conspiracy, and simultaneously violate ethical demands of the Other in human contact.

### KEYWORDS

Morality; ethics; other; empire; race

June 2022

## Mothers and Daughters: Reclaiming the Besieged Body of Woman in Ashapura Debi's Trilogy

Subhadeep Ray

Goutam Karmakar

Follow this and additional works at: <https://vc.bridgew.edu/jiws>



Part of the [Women's Studies Commons](#)

### Recommended Citation

Ray, Subhadeep and Karmakar, Goutam (2022) "Mothers and Daughters: Reclaiming the Besieged Body of Woman in Ashapura Debi's Trilogy," *Journal of International Women's Studies*: Vol. 24: Iss. 5, Article 25. Available at: <https://vc.bridgew.edu/jiws/vol24/iss5/25>

This item is available as part of Virtual Commons, the open-access institutional repository of Bridgewater State University, Bridgewater, Massachusetts.

This journal and its contents may be used for research, teaching, and private study purposes. Any substantial or systematic reproduction, re-distribution, re-selling, loan or sub-licensing, systematic supply, or distribution in any form to anyone is expressly forbidden. Authors share joint copyright with the JIWS. ©2022 Journal of International Women's Studies.



## Mothers and Daughters: Reclaiming the Besieged Body of Woman in Ashapura Debi's Trilogy

By Subhadeep Ray<sup>1</sup> and Goutam Karmakar<sup>2</sup>

### Abstract

This paper offers a close reading of the intergenerational trilogy by Ashapura Debi, one of the first-canonized women-novelists of post-independence India: *Pratham Pratisruti* (*The First Promise*), 1965, *Subarnalata*, 1967, and *Bakul Katha* (*Bakul's Story*), 1974. Reconstituting a history of almost two centuries and countering the colonial/postcolonial grand narratives, these novels act as a saga of Bengali Hindu lower and middle-class women's plight under and resistance against a patriarchal social order operating at the most intimate levels of domestic relationships. Ashapura Debi's treatment of the intricacies of gender inequality and a woman's response to the violence inflicted on her body in one of the centres of South-Asian modernity and its vicinity intervenes crucially in the twentieth century feminist discourse. At the same time, her narrative closely follows a promise, accompanied by a sense of commitment and responsibility, handed over from mother to daughter to granddaughter to rise as self-conscious individual subjects by overcoming personal and social reservations and taboos. This paper, therefore, examines the micro-physics of power exercised in gender relations as evident in the concerned trilogy. It focuses on the performing bodies of women amidst all sorts of physical and psychological oppressions and how they provide a critique of the broader aspects of social change, like reform and nationalist movements. While considering the intersections between the poststructuralist gender studies in the West—developed as a sustained critique of the mechanism of modern power being proposed by Michel Foucault among others—and Ashapura Debi's observations, this paper theoretically emphasizes how the factors of

---

<sup>1</sup> Subhadeep Ray, Ph.D. (English), is presently an Associate Professor of English at Bidhan Chandra College, Kazi Nazrul University, Asansol, India. He is also Visiting Professor of English at Kazi Nazrul University, Asansol, India, and was the principal investigator of a UGC MRP on Popular Science Writing and Bengal Renaissance. He is a regular contributor to the Columbia University Press - UMCS Joseph Conrad Project, and Conrad: Eastern and Western Perspectives book series (UMCS & CUP). He works on the British and Bengali Modernist Fiction within the framework of Comparative Literature. His areas of interest are Modernism, Marxism, Postcolonialism, Disability studies, Poststructuralism, Translation studies, and Science Fiction. His publications include chapters in *Disability in Translation* (Routledge, 2020), and *Science Fiction in India* (Bloomsbury, 2022). He is the author of *Bengal Renaissance and Scientific Temper* (BlueRose, 2019), and editor of *Thirst* by Eugene O'Neill (Levant, 2005). He can be reached at [subhadeep.ray.eng@gmail.com](mailto:subhadeep.ray.eng@gmail.com). ORCID ID: <https://orcid.org/0000-0002-6663-8045>

<sup>2</sup> Goutam Karmakar, Ph.D. (English), is an NRF Postdoctoral Fellow at the University of the Western Cape, South Africa. He is also an Assistant Professor of English at Barabazar Bikram Tudu Memorial College, Sidho-Kanho-Birsha University, Purulia, West Bengal, India. His forthcoming and recently published edited volumes are *Nation and Narration: Hindi Cinema and the Making and Remaking of National Consciousness* (Routledge, forthcoming), *The Poetry of Jibanananda Das: Aesthetics, Poetics, and Narratives* (Routledge, forthcoming), *Narratives of Trauma in South Asian Literature* (Routledge), *The City Speaks: Urban Spaces in Indian Literature* (Routledge, 2022), and *Religion in South Asian Anglophone Literature: Traversing Resistance, Margins and Extremism* (Routledge, 2021). He has been published in journals including *Intersections*, *Quarterly Review of Film and Video*, *Journal of Environmental Planning and Management*, *MELUS*, *South Asian Review*, *Journal of Graphic Novels and Comics*, *Interdisciplinary Literary Review*, *Journal of Gender Studies*, *Journal of Postcolonial Writing*, *National Identities*, *Nationalism and Ethnic Politics*, *Journal of Narrative and Language Studies*, *Asian Journal of Women's Studies*, and *Asiatic* among others. His research interests are South Asian Literature, Postcolonial Literature, Film Studies, Women and Gender Studies, and Ecological Studies. He can be reached at 4177972@myuwc.ac.za. ORCID ID: <https://orcid.org/0000-0002-9119-9486>.

contingency in Bengali women's lives posit new insights into what, after Judith Butler, may be called "gender trouble" as they undo many of the morally ordered gender roles.

*Keywords:* Ashapura Debi, Violence, Body, Performativity, South Asian feminism

### **Introduction: The Familiar is Political**

*Journals of Dorothy Wordsworth* was published in two volumes in 1897<sup>1</sup>, and in his editorial preface, William Knight writes rather dismissively:

All the journals contain numerous trivial details, which bear ample witness to the "plain living and high thinking" of the Wordsworth household—an in this edition, samples of these details are given—but there is no need to record all the cases in which the sister wrote, "To-day I mended William's shirts", or "William gathered sticks", or "I went in search of eggs", etc. etc. (qtd. in Kimber, 2021)

An interesting story concerning the problematic relationship between the writer, the editor, and the reader follows. Next to Knight's above remark in the margin of Katherine Mansfield's personal copy, the following words are found to be scribbled: "There is! Fool!" (Kimber, 2021). Mansfield's sharp refusal of Knight's reservation regarding Dorothy's inclusion of all the details of daily life shifts the attention to those very performances that link ontological queries and epistemological self-reflections within the feminist discourse. Marginalization of women being a global phenomenon incites a counter-movement on a global scale that recognizes the politics of the intimate and familiar relationships. Simultaneously, as Peace A. Medie and Alice J. Kang argue,

dominant scholarships on women, gender and politics, produced mostly but not exclusively by Western feminists and other scholars in the Global North, needs to examine a broader range of variables that may be independent and interactive causes of gender inequality and discrimination against women. (2018, p. 38)

Thus, in the case of a woman, devoid of Dorothy's type of socio-cultural upbringing and positioned in the post/colonial hinterland of South-Asia, it is through a dense network of repetitive *trivial* performances that the body is gendered, and any attempt to subvert any norm of the 'socially acceptable' set of performances is treated with disciplinary coercion. The trivia is also being energised by a self-conscious female subject in order to interrogate what Michel Foucault refers to as the "microphysics of power" (2008, p. 33) and participate in resisting the institutionalised regulations of the female body. That the enacting of the personal and familiar domestic world by anonymous women turns it into the political is succinctly suggested by one of the first canonised woman-authors of Independent India, Ashapura Debi (1909-1995)<sup>2</sup> in the author's preface to the first novel of her intergenerational trilogy, which is a saga of the plight of Bengali woman, *Pratham Pratisruti (The First Promise)*, 1965<sup>3</sup>, *Subarnalata*, 1967, and *Bakul Katha (Bakul's Story)*, 1974:

The history of times past is made up of stories about the rise and fall of the public world. And that restless, clamorous history written against a backdrop of light and darkness holds out inspiration, ardour and excitement for the future. But is not the mute, domestic space similarly

broken and built? From which flows forth the changing colours of a community, an age, and people's mentalities? (2004, p. xxxix)<sup>4</sup>

The present paper offers an engaged reading of the above trilogy, which, as a seminal literary text of the post-WWII South-Asian women's writings, focuses on the intersecting experiences of mothers and daughters of patriarchal oppression and violence. Ashapura's work anticipates the recent examinations of how violence and the threat of violence in a patriarchal society constrain the actions of women, harming the victims and benefiting the correlative privileged social groups. The trilogy in question demonstrates how women as a group are not only oppressed materially through violence, but there is always a credible, psychologically operating threat of greater harm, effectively transmitted to their physical and mental beings by obvious hurts – such as social ostracism of female kin (Cudd, 2006). Simultaneously, the trilogy focuses on the changing means, causes, and effects of women's interrelated rebellions and self-explorations towards empowerment over generations from within the domain of intimate relationships, set against a huge canvas of the rise and fall of colonial and early post-colonial social institutions. In the course of its epic journey, Ashapura's narrative covers the crucial phases of the establishment of British imperial rule, followed by the introduction of English education, displacing the Persian and native codes of teachings, and the Western medical system in place of the indigenous treatments, social reforms, diverging nationalist struggles with their iconic nation-mother correlations, the turn of the century women's movements culminating in the formation of women's organisations like the All India Women's Conference in 1927, the independence and accompanying catastrophes, and the initial hopes and despairs of India as a nation-state.<sup>5</sup> The three concerned novels thus provide three interlocked but independent reflections on a long course of history. They reconstitute the cultural modernity of Bengal, in particular, and the sub-continent, in general, by prioritizing women's experience to explore the micro-politics of gender relations and gender oppressions. Ashapura Debi's inscription of "the nerve-racking stresses and strains of day-to-day living" (Rangra, 1989, p. 71) in her texts forms her specific contributions to South-Asian feminist thought.

Ashapura Debi's radical intervention in the Bengali literary culture is characterized by a self-reflective narrative stance, in which the successor mirrors the precursor and vice versa, and they are mutually committed to each other by an emotional, physical, and intellectual bonding. Thus, the first novel that is centered around the character of Satyabati significantly opens with a disclaimer on the part of the third-person narrator, that she came to know about Satyabati's story only from the notebook of Bakul, who is Satyabati's granddaughter. Bakul, a reputed author of new India in the third book, is in quest of a self-realization that may relate her back to her grandmother through her mother, Subarnalata. Given these factors of intertextuality, Ashapura Debi's own aesthetic involvements can be addressed in terms of asking "the 'absent' women's question" (Chowdhury, 1998, p. 47) through the postcolonial lens. This study wishes to understand this constitution/re-constitution of the 'I' through active interactions between mothers and daughters, who challenge the very disciplinary laws they are subjected to, across time and space. This paper applies the poststructuralist concept of performativity in relation to the gendered body, as proposed most prominently by Judith Butler. In the author's introduction to *Undoing Gender*, Butler writes:

[T]he "I" that I am finds itself at once constituted by norms and dependent on them but also endeavors to live in ways that maintain a critical and transformative relation to them. This is not easy, because the "I" becomes, to a certain extent unknowable, threatened with unviability, with becoming undone altogether, when it no longer

incorporates the norm in such a way that makes this “I” fully recognizable. (2004, pp. 3-4)

A central performative effort of Ashapura's heroines is to narrate the history of their present, which, in the cases of Satyabati and Subarnalata, is forcefully eliminated by the grand narrative. Bakul's emergence as a writer suggests her engagement with a long-cherished dream of her mother, aunts, and grandmothers. Bakul's preoccupations mirror those of the author, who confirms in an important interview: “I chose to reveal the truth of my life, I feel partially, in the form of my creative writing” (Rangra, 1989, p. 75). This ‘truth’ interrogates the viability of extensively wide-ranging and diverging positions like the post-Cartesian “rejection of the body as an obstacle to pure rational thought” (Shildrick & Price, 1999, p. 2), Indian religious ‘sanctity’, the interface between taboos against the reproductive body in indigenous cultures and the colonial anxiety over the ‘native’ hygiene, and the post-colonial radicalism to free both body and mind by throwing off the shackles of social orthodoxy. This paper is organized around readings of three novels in two interrelated sections, and it draws upon socio-cultural histories to contextualize the different aspects of Ashapura Debi's treatment of society, sexuality, violence, and the body. This is due to the fact that the globally sensitive positions of feminism and gender studies must be realized through critical evaluations of localized representations of misery and might in the survival strategies of women belonging to a community culture. In India, in particular, social discrimination has outweighed the survival strategies of women throughout the centuries. In this context, Ashapura Debi sets the agenda for Indian feminism in respect of the socio-cultural forces of her own history in the following terms:

I believe, there were various changes taking place from outside and there are drastic changes in society. But in order to give proper respect and honour to the women folk many more basic changes in the society are required. (Rangra, 1989, p. 73)

### ***Pratham Pratisruti: Rise of a Defiant Mother***

In *The Idea of Justice*, Amartya Sen emphasizes *real-life* experiences as the foundational component in social understanding:

“Institutions and rules are, of course, very important in influencing what happens, and they are part and parcel of the actual world as well, but the realized actuality goes well beyond the organizational picture, and includes the lives that people manage—or do not manage—to live” (2004, p. 18).

In terms of the above observation, Ashapura Debi's fiction unfurls the uncut versions of ordinary women's lives in Bengal, using all the resources history holds out to her, and raises disturbing questions regarding women's dignity, freedom, and justice that tend to subvert any of the metaphysical idealizations of *matrisama*—mother-like, *sarbangsahā*—all-enduring, and ‘pure’ woman. In his reading of Rabindranath Tagore's novelistic take on the nineteenth and early-twentieth-century Bengali ideological clusters, *Chaturanga (Quartets)*, 1915-16, Sibaji Bandyopadhyay points out that “the binary opposition between ‘modernity’ and ‘tradition’—the binary staple to nearly all colonial discourses—covers up” many overlapping zones “by positing a causal connection between *hegemony* and *repression*” (2012, p. 47). Decoding these connections across conventional binaries, Ashapura Debi's narrative presents the characters as performing bodies, which are not simply aspects of nature, but effects of the complex

workings of power. But, in contrast to the Foucauldian account in *Discipline and Punish* (1977) and *History of Sexuality* (1979) of the shift from “the body as the object of penal repression” to “more subtle and implicit techniques for its normalization” (Turner, 2012, p. 68), an epical novel like *Pratham Pratisruti (The First Promise)* offers a nuanced understanding of the interplay between violence and surveillance. It needs to be remembered that while the Western understanding of social censorship is interlinked with industrial modernization, printing technology, and reformation movements, in the colonial context, no such linear shift can be traced from the “traditional” to the “modern” forms of censorship. Furthermore, again moving beyond Foucault’s explanation of the “political technology of body” (1977, p. 24), that is, the means by which “discipline produces subjected and practiced bodies”, or “‘docile’ bodies” (1977, p. 138), the novel revises the very process whereby regulatory norms achieve materialization of their control over subject bodies. Such a narrative strategy thus exposes what Butler explicates about the “forcible reiteration” of regulatory norms: “That this reiteration is necessary is a sign that materialization is never quite complete, that bodies never quite comply with the norms by which their materialization is compelled” (1999, p. 236). This critical evaluation of the process of materialization of power enables Ashapura to use her writing as an act of revolt, as stated by her: “All those unpronounced protests of mine have appeared in my writing and in figures of rebellious women, like Satyabati of *Pratham Pratisruti*” (qtd in Dev Sen, 1997, p. xiv).

Because women’s bodies are inextricably linked to disciplinary attempts to “form” and “mean” them over time, it is the same “bodies that matter” – to use the title of Butler’s (1996) seminal text—once they explore the scopes of “unsanctioned” acts,<sup>6</sup> which are performed as an offshoot of constantly repressed desires. In this manner, the bodily actions of marginalized women<sup>7</sup> engage the contingent and micro-level intricacies of experience. Satyabati’s grandaunt Mokshada, a childless widow since childhood, personifies ritualistic sanctity, and, is shown to have been practicing all the taboos, codes, and conducts most strictly and severely harshly to any other woman failing to be so stringent in following the conventional Hindu norms. The same Mokshada, turning into a shadow of her former self at the end of her life, discovers the frailty of her domestic authority, built on a series of compromises. Mokshada even steals fried fish—a food-item Bengali Hindu widows are prohibited from eating—from the kitchen. As Jasodhara Bagchi notices, the narrative is centrally preoccupied with “Satyabati’s search for a viable alternative” (2004, p. XII) to the life she is offered, but this search interacts with a great range of actions around her. Satyabati’s activities are affected by others’ activities, as well as affected by others’ activities; and it is this capacity to affect and be affected by others that establishes Satyabati as an individual subject. There is no narrative blueprint for her vulnerability and resistance to social oppression. As she shifts from finding a “way of inhabiting social structures” to seeking “oppositional spaces and ‘pathways’ to empowerment” (McNay, 2016, p. 45), she has to repeat her searches all over till her death in a distant land. Therefore, the relation between body, violence, and resistance in Satyabati’s story is to be seen within the symbolic structure through which she and her fellow beings form their self-identities. Ashapura’s textuality treats the myriad ways power operates, even at the level of individual relations, which often challenges the universalizing tendencies of socio-cultural, political, and economic institutions. Her narrative critically engages itself with the ways ‘I’ is, in Jacques Derrida’s words, “comprised and determined in advance by the fact that it belongs to the most suspended ‘we’” (2005, p. 77) to find what is out of joint in intriguing relationships between individuals’ self-entities and social determination.

In *Pratham Pratisruti*, the first notable encounter between an individual’s body and tradition in a violent way involves the problematic construction of masculinity. Being ruthlessly beaten by his father for questioning the ritual of offering food and water to God when there is no proof of the divine acceptance of them, Ramkali Chatterji, Satyabati’s father, leaves

home at a very young age to find shelter in the household of an indigenous medical practitioner who grooms Ramkali to become a renowned Ayurvedic doctor. Sumit Sarkar points out that “the internal conflicts that ensue” in a number of male characters in Tagore’s novels, suggest a journey “through self-examination and auto-critique, towards a non-instrumentalized recognition of the autonomy of the Other” (2002, p. 121). In this respect, Ashapura Debi’s postcolonial re-writing of the colonial Bengali feudal and middle-class Hindu male’s shifting approaches to Others – in forms of race, caste, religion, class, and gender—provides an alternative ‘non-instrumentalized’ commentary on the dualities of colonized masculinity. Ramkali, in particular, is characterised by a constant swing between his role as a conventional patriarch—the head of a large family—and, to use Derrida, Ramkali’s “avowal of the opposite”, and his “confession of an error that is not foreign to the truth” (2005, p. 50). Thus, Ramkali, as an orthodox father, performs *gauridaana*<sup>8</sup> by marrying his only daughter off when she is still a kid, but, simultaneously, he not only convinces her in-laws to allow his daughter to stay at her parental home till puberty, but also permits Satyabati to live a ‘tom-boy’ type of life by overcoming inhibitions in private and public spheres. For enjoying her relative liberty, Satyabati is, however, frequently threatened with the dire consequences of future rejection by her in-laws. The relationship between the father and the daughter develops into a sort of friendship silently maintained by mutual protection and understanding. But it is occasionally unbridled by Satyabati’s growingly eloquent protest against injustice to her fellow village women.

Satyabati’s gradual coming to sense how regulative orders “determine socially acceptable behaviour for two binary genders, structuring the repertoire for gender performance, and coercing compliance” (Threadcraft, 2016, p. 218) is, however, possible through her participation in actual events. An example from the first part of the narrative would explain her growth as a conscious individual subject. Beating wives over silly matters is considered a natural right of husbands in the countryside, Satyabati inhabits, but when her cousin, Jata, kicks his wife, the latter is knocked to the ground and turns senseless. Receiving the news Satyabati hurries to inform her father, who is on his way back home from some neighbouring village:

“[...] when Jatada’s wife was sitting down to eat, just after she’d finished the cooking, Jatada asked for a paan. His wife said that there wasn’t any paan. [...] He gave her a good hard kick on her backside. And she fell on her face in the courtyard –’ Satyabati burst into laughter” (Debi, 2004, p. 17-18).

Satyabati’s impulsive mockery of another woman’s suffering makes her a part of the vulgar act of violence, and, it is to be noted that she is chided by her father, whose ethical and philanthropic sides are derived from his profession and have affinities with the early nineteenth-century social reformers. Satyabati’s timely intervention saves the victim’s life, as Ramkali brings the victim to sense. In a dramatic reversal of the narrative, Ramkali, too, learns from his daughter about a profound reality of rural women’s experiences in colonial Bengal. Common villagers, including Satyabati, are confirmed that Ramkali has the power to bring the dead back to life, and when Ramkali tries to correct such a misconception, his daughter reveals a startling fact:

Even god can’t do a thing if you die, do you understand? Jata’s wife hadn’t died.’

[...]

But then Baba, if you hadn’t felt her pulse and given her the “essence of gold”, Jatada’s wife would have remained like that – lifeless! And then

they'd have put her on a bamboo bier and cremated her! (Debi, 2004, p. 23)

Satyabati's observation of the dubious status of the body of Jata's wife as both belonging to an individual and a sort of public property looks forward to Butler's thesis in *Undoing Gender*:

"The body implies mortality, vulnerability, agency: the skin and the flesh expose us ... to violence. The body can be the agency and instrument of all these as well, or the site where, "doing" and "being done to" become equivocal" (2004, p. 21).

The reach of the nineteenth-century colonial modernity in India was greatly controlled within the production of the colonial ethnography itself, marked by, as Kamlesh Mohan notices,

a coherent, intelligible, though distorted picture of the colonial society, whose members had to be controlled, enslaved, and conditioned to perceive themselves as communal and religious entities, their languages, science, literature and cultural traditions as gifts from the manly, intellectually superior, materially advanced and culturally dynamic Europe" (2014, p. 59).

In this context, the social reform movements, concerning female sexuality, were filtered by the traditional authorities of the institutions of family and religion. In the words of Jasodhara Bagchi "[o]ne of the major sources of control over women's lives are the injunctions contained in the religious scriptures. In India these formed the bases of Personal Laws, with which the state arbitrated over women's legal rights" (1995, p. 8). In *Pratham Pratisruti*, the sexuality of nineteenth century rural and mostly illiterate Bengali Hindu women is the object of fundamental prohibition, whose transgression is judged as deadly offensive and treated with ritual atrocities. These women are shown to be threatened mainly by widowhood and co-wifery, and their bodies are brought under absolute social control through the cyclic experiences of motherhood. The narrative interest lies in exposing how the enacting of these social customs by these women constitutes their vulnerability. The mental violence imposed by the *kulin*<sup>9</sup> Brahmin practice of polygamy is shown in the novel from the perspectives of the concerned husbands' first wives. The vicious cycle of the patriarchal law is suggested when Ramkali tries to stop a marriage ceremony, as he detects the groom to be dying. But the situation turns further critical for, according to Hindu custom, once the *lagna*—or the sacred period of the rituals of wedding—is over, the bride is bound to remain unmarried for her life. The girl instantly becomes an easy victim of social torture, and even an aged Brahmin of the village offers to marry her on that very day. Ramkali holds himself accountable for the entire calamity in the bride's family, and decides to marry his nephew, Rashu, who is already married, off to the same hapless girl, Patli. It is only later that Satyabati makes her father aware of the kind of humiliation and physical distress his action has invited for Sarada, Rashu's first wife. At her in-laws' home, Satyabati befriends her mother-in-law's niece, Saudamini, who is reported to have been abandoned by her abusive husband. Under constant social pressure, the steadfast Saudamini turns compliant and tricks to find shelter at her husband's home in Calcutta in exchange for nursing her ailing co-wife. Saudamini's husband, on the other hand, accepts his first wife because he finds her healthier than his second wife, who turned ill after a series of child births. Going against the grain, Ashapurna's narrative undermines the colonial



discursive binary between the village and the metropolis and shows how the Bengali middle-class family manoeuvres even the urban space to exploit and enjoy women's bodies. Furthermore, "Satyabati's own steady decision of going to her marital home prematurely is another instance of abhorrence at the prospect of a co-wife" (Bagchi, 2004, p. XI).

In her marital household, a mature Satyabati is found to perform her role as an obedient daughter-in-law, as when she takes care of her father-in-law, Nilambar Banerji, after he becomes paralyzed. However, she does not let her domestic propriety dismantle her own sense of right and wrong, and the strength of her character incurs both wrath and fear among her family members. So, she declares that she will not touch her father-in-law's feet when she discovers his womanizing and tactical acceptance of this by her mother-in-law, Elokeshi: "Surely, duty isn't about displaying respect even when one is feeling deeply disrespectful inside!" (Debi, 2004, p. 225). Bold Satyabati does not succumb to her parents-in-law's threat to leave the home. Elokeshi's pleas for her husband and her abuses of Satyabati show that women follow an unspoken rule that moral lapses in men can be forgiven:

[...] She's nothing but a vile, venomous snake! [...] A respectable man like him was ready to kill himself after hearing her taunts. Sadu [or Saudamini] felt the urge to rush to Satya and plead, 'Quickly beg forgiveness if you know what's good for you!' [...] Satya would not bend even if god himself descended from heaven and implored. (Debi, 2004, p. 227)

As the third person narrator confirms, instead of supernatural being, Satyabati prayed "to the living gods she knew" (Debi, 2004, p. 287). "Gender is", as Butler's reasoning informs, "a regulatory norm, but it is also one that is produced in the services of other kinds of regulations" and "sexual harassment codes," consisting of the systematic mistreatment of women by men in places like family (2004, p. 53). But, in carving out a self that does not always conform to patriarchal regulations, one is not expected to reject completely the very world in which she finds herself as an active agent. In her fictional mapping of women's struggles against patriarchal violence, Ashapura Debi thus draws on the complex relationship between the domestic world of repression and torture and the public sphere of social reforms that, at least to a certain extent could enable men enthusiasts to address the practical sides of women's sufferings. If Satyabati is one of the "unnamed women" in history who "set out to search for answers" (Banerjee Chakravorty, 1998, p. 288) to the gross inhumanity they experience, the journey of Ashapura's protagonist particularly finds two signposts, who establish the relationship between the home and the world: Ramkali, representing the traditional knowledge system, and the village English teacher, Bhabatosh Biswas, with his metropolitan affiliations. While her father adds fuel to Satyabati's aspiration to read and write—something that prepares her for participating in the nineteenth-century emancipation movement in her later career—Bhabatosh becomes a steady inspiration behind some of her iconoclastic steps. Satyabati's radical intervention in the traditional attitude toward the body is first signalled by her arrangement of a sahib doctor to treat her sick husband, Nabakumar. And, notwithstanding affliction and resentment, Satyabati forces her husband to shift from their joint family in the native village to a nuclear family in Calcutta and find a government job, mainly under the influence of Bhabatosh. This seminal journey is further intertwined with different stages of Satyabati's motherhood.

According to Indira Chowdhury, "we are better to understand *Pratham Pratisruti* if we consider infanticide, abandonment and consequent motherless as a metaphoric complex that holds much of the plot together" (1998, p. 49). Chowdhury further points out how "Satyabati is literally rendered motherless when she gives birth to her son" as her own mother's death is

announced by Elokeshi in a matter-of-fact tone with the statutory caution that she must not eat fish for the short mourning period (1998, p. 49). At this crucial moment, Satyabati feels a sense of guilt for ignoring her mother, and her own attempt to perform *differently* her motherhood takes recourse to metropolitan modernity as offering liberation through education. In *Gender Trouble*, Butler confronts Julia Kristeva's 'reification' of maternity for "[b]y relegating the source of subversion to a site outside of cultural itself, Kristeva appears to foreclose the possibility of subversion as an effective or realizable cultural practice" (1990, p. 119). The culturally subversive potentials of Satyabati's maternal strategies are to be understood in terms of the extent of the tragedy she undergoes within a vindictive order. The patriarchal agency sets the most wicked design to diminish her aspirations, which are able to constitute what Butler calls "an open assemblage that permits multiple convergences and divergences" even within the available cultural system and does not always show "obedience to a normative telos of definitional closure" (1990, p. 22). Satyabati's vehement efforts enable her sons, Sadhan and Saral, to join the educated urban middle class of the second half of the nineteenth century, but the emancipation of their mind is curtailed by the collusion between tradition and modernity to turn them suspicious of their 'dominating' mother. Subarnalata, Satyabati's daughter, represents a new hope for the mother, whose ambition is to groom her promising child in the image of the 'new woman'. When Satyabati teaches little Subarnalata alphabet, Saudamini warns her that one is "forbidden to touch books before age five", but Satyabati's reply suggests how she repeats the available symbolic codes with strategic differences: "That's a rule for boys. There are no such rules for girls. After all, she wouldn't even be allowed to do the *hathe-khari*<sup>10</sup> ritual" (Debi, 2004, p. 458). Arriving in Calcutta, Satyabati also performs the role of a surrogate mother of another girl, named Suhash, who is the illegitimate daughter of a distant relative of Satyabati, Shankari. Shankari, who elopes with her lover to end up in a rich household at the heart of the city as a cooking maid and single mother, invents a story of the early widowhood of her extremely beautiful daughter in order to protect Suhash from her lustful employers. As the turn of events brings Suhash under Satyabati's care, the adamant and ill-mannered girl grows up into an intelligent learner. Suhash ultimately marries Bhabatosh, who later becomes a Brahmo, and turns into a successful teacher, that is, truly a 'new woman'. Subarnalata, on the contrary, is forcefully snatched from Satyabati by Elokeshi and Satyabati's husband, Nabakumar, who, a weakling, arranges another *gauridaana* during the eight-year-old Subarnalata's short visit to her village home and in the absence of her mother: "They had carried in the bride and placed her on the groom's lap. [...] The rebellious bride had tripped in her attempt to escape" (Debi, 2004, p. 519). As Subarnalata meets the common fate of numerous girl children in contemporary Bengal, her mother, with a last stroke of defiance, leaves her homeland. The narrative ends with a suggestion that a meaningful mother-daughter relationship is impossible in the historical context it charts, but the spectre of Satyabati, with her agony and longing, continues to haunt a series of daughters and granddaughters in the subsequent volumes of the trilogy, telling of a changing history of Bengali women.

### ***Subarnalata and Bakulkatha: Nation, State, Family, Daughter, and Granddaughters***

In contrast to a tendency to generalize women's condition within feminist discourses, postcolonial feminist scholars are particularly attentive to the situatedness and context-specific understanding of women's subjecthood, and the external and internal processes acting directly upon a community living to shape gender identities, in contrast to many hegemonic discourses on colonial relations. For instance, in her biography of Pandita Ramabai Sarasvati (1858–1922), a pioneer in the women's emancipation movement in India, Uma Chakravarti discloses how male-centric works by talking about "the feminization of the colonized male in relation to the colonizing male" *reduces* "gender to a representational phenomenon rather than a material and ideological arrangement" (2013, p. xv). On the other hand, any discursive appreciation of

the “evocation of nation as mother”, and particularly a poor mother, for it “encompassed an inculcation of the ethic of *mota chal* and *mota kapar* (coarse, simple rice and thick, homely cloth)”<sup>11</sup> and thereby invited “subordinated and marginalized groups to take part equal part in nationalist rituals” (Bose, 2017, p. 13), somehow underrating the circumstantial and other constraints Bengali non-elite women were subjected to as well as their resistance against socio-economic deprivation even within an embattled household through history. The sequels of *Pratham Pratisruti*, *Subarnalata* and *Bakulkatha*, give new meaning to the relationships between the country, state, family, and citizens in a new way. The materiality of her fictional project is suggested by the author in unambiguous terms:

*Subarnalata* is the story of a particular time, a time that has passed, but whose shadow still hovers over our social system. *Subarnalata* is a symbol of the helpless cry of an imprisoned soul ... sociologists write down the history of a changing society and I have merely tried to draw a curve to depict the change” (qtd in Dev Sen, 1997, p. vii).<sup>12</sup>

The novel presents a bleak narrative of a community living together that desperately resists any social change inside the home while adjusting itself to the upheavals in the outside world. This textual strategy is noted by Naina Dey, who notes that “[s]tanding at the crossroads of time, when the history of the world was fast changing”, Ashapura Debi concentrates “essentially on the family, especially on the women in the family” (2007, p. 222), and this kind of narrative exposes how the rays of social change are reflected and refracted by the domestic space.

In Rabindranath Tagore’s novella *Char Adhyay (Four Chapters)*, 1934, the central woman character, Ela, reflects on why Bengali mothers-in-law are found to be torturing their respective daughters-in-law, and argues that those who know themselves as internally weak treat their weaker subjects in the cruelest manner and desperately try to maintain the power structure in such a way that the frail authority they exercise is never exposed. *Subarnalata*’s interaction with this dynamic is direct and violent since the day of her wedding, as noted in the last section. Much later, her daughter, Bakul, remaining unmarried after a heartbreaking love affair, reviews in *Bakulkatha* how terrible conditions are attached to a sense of futility in the institution of marriage in respect of her mother and grandmother:

‘Why is marriage so irrefutable? Why can’t one break it?’ Bakul’s maternal Grandmother Satyabati had left her husband and children, her familiar world for the light of the greater world, driven by this quest. ... *Subarnalata* ... had been married off in the most clandestine way when she was only nine, a ritual performed by her own paternal Grandmother, Satyabati’s mother-in-law. ‘I don’t call it MARRIAGE! It’s all but a child’s play!’ Satyabati had revolted. (Debi, 2021, p. 304)

Bearing the stigma of being deserted by her own mother, *Subarnalata* becomes an object of enduring reproach, and the unbearable rule of her mother-in-law, Muktakeshi, in the family derives from a past struggle to bring up eight children single-handedly. As Shivani Banerjee Chakravorty explains, “[...] the mothering of male children with a modicum of power that is so fragile that it requires fierce protection and subterfuge, and the need to create discord between family members to prevent insurgency” (1998, p. 290). *Subarnalata*’s entrapment is completed by her husband, Prabodhchandra Chatterji, who is physically attracted to his wife but finds himself incompatible with her indomitable interest in a larger world. Prabodh tries to get rid of his anxieties by thrashing his wife and chastising her, and these acts are followed by prolonged emotional blackmail meant to force *Subarnalata* to satisfy her husband’s desires and

simultaneously maintain the family peace. Subarnalata's exposition of her spouse's character throws light on a critically overlooked side of colonized masculinity in the turn of the century Calcutta, that is, the center of the South-Asian Enlightenment: he is like a "python, which wraps its cold body around his victim, and soon its caress begins to feel like shackles of iron cutting into the flesh. This embrace crushes the insides of the victim while keeping the external appearance intact" (Debi, 1997, p. 124). The portrait of domestic violence against women in *Subarnalata* thus becomes comparable with the much more organised form of criminality practised by the colonial masters<sup>13</sup>. Another powerful strategy adopted to control Subarnalata's physical vitality—or her energy to disobey the family norms—seems to contain her within the *anturghor*, the room for childbirth. The narrative shows how the "maternal body" is a "consequence of a system of sexuality in which the female body is required to assume maternity as the essence of itself and the law of its desire" (Butler, 1990, p. 125). Subarnalata's domain of activities helps us to "understand the boundaries of the body as the limits of the socially hegemonic" (Butler, 1990, p. 179; emphasis in the original), and, therefore, her unsanctioned activities interconnect corporeal and social liberation.

Subarnalata's confrontation with her in-laws' family is mainly three-fold: her sustained interest in education, her problematic involvement in the contemporary Swadeshi movement, and her effort to re-appropriate her role as a mother. It is in *Bakulkatha* that her husband retorts when their daughter Bakul is seen carrying a couple of books by Rabindranath Tagore:

"These books...the root of all evil! Good Lord, three generations of women with the same disease! I heard your grandmother had it, and your mother, I know, was the most affected with it [...] and now her daughter, too [...] what a nuisance!" (Debi, 2021, p. 31).

As this 'disease'—often received also as a type of insanity—connects mothers and daughters over space and time, it becomes a powerful medium to contest the normative "process of materialisation that stabilizes over time to produce the effect of boundary, fixity and surface" (Butler, 1999, p. 239). In *Subarnalata*, especially, the relentless pursuit of knowledge involves a differently performing body. Subarnalata befriends a next-door woman, to whom she gives signals by tapping on the wall and smuggles books from her through a hole in the wall. Subarnalata's attempt to collect books from a generous person by employing a teenage boy as a medium between them, however, proves disastrous as she is accused of having an adulterous affair. Subarnalata does leave the house in protest, but only to return as her father expresses his inability to give her shelter on account of social stigma. Suchorita Chattopadhyay further points out that:

"[a] motive which is intricately woven into the entire fabric of the narrative is the dream of a balcony, a *baranda* (verandah), which would usher in a breath of fresh air to counter the stale claustrophobic atmosphere of the household" (2012, p. 87).

The victimisation of Subarnalata under domestic tyrannies against a background of late-nineteenth and early-twentieth century cultural modernity informs the unresolved equations between the customary laws of Hindu families and statutory laws. Ironically, restrictions imposed on Subarnalata's struggles to read and write seem to defy Satyabati's emancipating activities, about which Subarnalata comes to know through a letter from her mother only after the latter's death:

“I started a school for girls soon after my arrival here [in Varanasi] .... When I first started, I had to beg people to send their girls. Now a lot of people bring their daughters voluntarily. The need to educate women has begun to be felt by many” (Debi, 1997, p. 160).

The French feminist Hélène Cixous’s “The Laugh of the Medusa” (1973/1976), translated into English almost a decade after the publication of *Subarnalata*, theorizes the indispensable connection between writing, history, and the body:

Women must write herself: must write about woman and bring woman to writing, from which they have been driven away as violently as from their bodies—for the same reasons, by the same law, with the same fatal goal. Woman must put herself into the text—as into the world and into history—by her own movement. (1976, p. 875).

Subarnalata’s wish to turn her experiences and feelings into a book materializes when a distant brother-in-law of hers, Jagu, opens a private press, and secretly agrees to print her writing. The text thus produced, however, incites a stream of rebukes, leading the author to burn all the poorly published copies into ashes. The incident serves as a commentary on the close bond between the advent of modernity and printing in Bengal. It is Bakul who finally attempts to revive her mother’s manuscript but fails.

Uma Chakravarti draws the attention of South-Asian feminists to a set of questions: “[...] in what way did the new laws of the colonial state affect women and how was this similar or different for men? Did the colonial state regard women as its direct subjects or as mediated through the family?” (2013, p. 159). In this connection, *Subarnalata* narrates multiple layers of patriarchal adjustments. The male adults of Subarnalata’s marital family are depicted to be either employed in colonial administration or engaged in trade; and they consider the British as the natural masters of Indians, while never allowing the *nabya*,<sup>14</sup> introduced by colonial modernity, to disturb the domestic hierarchies. Arrangements are thus made to allot women, except a few, in Sumit Sarkar’s phrase, “non-existent, at best marginal” place “in these new public spaces and urban spectatorship” (2014; p. 308). Thus, when Subarnalata actively responds to the call of the Swadeshi movement by mobilising the family kids to gather foreign clothes and set fire to them, her performance unsettles the public-private intercourse:

“One of the children replied, ‘We are destroying the symbol of oppression. We’ll stop wearing these stupid English garments [...]’ Prabhas: ‘Fighting the British, are you? And who is your leader? Your mother? Very well, then why is she still indoors? ... Let me go and inform the Viceroy he is about to lose his job!’” The narrative confirms that the “sarcasm” in her brother-in-law’s comment cannot “upset Subarnalata at all” (Debi, 1997, p. 75).

Subarnalata’s direct interactions with the contemporary political revolt become possible when she meets a young revolutionary at the residence of a mostly neglected sister-in-law, whose exceptional character establishes a life-long friendship between these two women. This “thin, ugly, unlettered sister-in-law” is “despised by all” but faces “a life of dire poverty with a unique courage” and accomplishes an “unheard of” action “in society of those days by marrying her daughters in families” of lower caste (Bose, 1976, p. 86). Subarnalata is mentally drawn towards the vagabond Swadeshi rebel, Ambika, and suffers not only slander but also physical assault at the hands of her husband. But, she also realises that the valorisation of women’s

traditional roles by political activists is a dangerous fallacy. When she charges Ambika that the country will never be free by keeping a whole section of its citizens practically inactive by attributing an emotive purity to them, Subarnalata articulates the postcolonial feminist critique which shows how the populist discourse of nationalism relegates the question of women's liberation in the name of "maintaining a distinctive and superior cultural identity in the sanctity of the home" (Devenish, 2019, p. xix). Citizenship as full and equal participation, all the same, remains an unreach goal for the third and fourth generations of women portrayed in the final novel of the trilogy, which offers a turn in woman's performativity through Bakul's niece Shampa, who marries a fatally wounded trade union worker, Satyaban, against her parents' wish. Among Subarnalata's own daughters, Chanpa, the eldest one, satisfies herself by following a type of wifhood; whereas Parul, an introvert girl who scarifies her studies under the pressure of her father and brother, finds her intellectual capacity as an object of her educated and other-wisely caring husband's suspicion. Parul chooses a secluded life for herself as she is deserted by a growingly self-seeking society. Bakul, using the pen-name Anamika, becomes successful as an author, but the clash between an unrepentant orthodoxy and a "new era" which is "racing against time, obliterating every bit of insight, wisdom, promises on the way" (Debi, 2021, p. 278), she is anxious about the outcome of the long struggles of her mother and grandmother.

### **Conclusion: Ideology of Self-Sufficiency**

The three novels are contextualized by the control over women's bodies within the normative structure of the post/colonial Bengali Hindu family, as well as by the unresolved "woman question" and tensions regarding sexuality—the production of the masculine/feminine binary in the contemporary public sphere. Cutting across the public/private, personal/political, rural/urban, and modern/traditional binaries, Ashapura Debi's narrative shows how the microcosm of the family is governed by the same rules as the macrocosm of social order. As Dipannita Dutta movingly points out, "Ashapura calls for [...] a sufficiency of the self" that is marked by "a resistance to different forms of domination in terms of both needs and rights." Her "thrust is on the emancipation of the self from the narrow confines of self-interest", and she insists on moving "beyond the solidified lines of the self and the other, which are socially constructed" (2015, p. 5-6). In an internally rifted setting, Satyabati, Subarnalata, and Bakul act on behalf of their respective generations of repressed women. While being torn apart between the dos and don'ts of social customs, they tend to cross the grid of paradigmatic 'good' womanhood. Their performance is often marked as 'deviant', as they undo indigenous, theological, colonial, and nationalist borders around a socially conscious body. The narrative of their lives provides South-Asian feminist writing and also gender activism with a specific ideological direction.

### **Notes**

1. The volumes were published in London by Macmillan and Co. Ltd.
2. Ashapura Debi is also one of the most prolific writers in the history of Bengali literature. In a career spanning over sixty years, she wrote one hundred and eighty-one published novels, thirty-eight anthologies of short-fiction, fifty-two children's books, and collections of essays, autobiographical reminiscences, and interviews. Having no formal education, she started writing at the age of thirteen and continued to rock the Bengali cultural atmosphere with her unconventional stance against both traditional customs and unchecked modernization.
3. This novel won the prestigious Jnanpith Award in 1976.
4. In an interview with Shivani Banerjee-Chakravorty, dated March 6, 1991, Ashapura Debi again confirms: "I write about what is most familiar to me, day-to-day experience in middle-class homes" (2000, p.24).

5. Internal evidence suggests that the narrative of *Pratham Pratisruti* begins in the eighteenth century.
6. See Patricia Ticineto Clough's (2012) analysis of Butler's theoretical combination of Lacan, Foucault, and Derrida.
7. Joan W. Scott's essay, "The Evidence of Experience", published in 1991 in the *Critical Inquiry* 17(1), serves as a key essay in Western feminist thought to examine how experiences are produced and subverted. Ashapurna Devi's fiction, in a number of ways, resonates strongly with the feminist credo that the personal is political, and provides us with a South-Asian version of the entire dynamics.
8. The medieval practice of marrying a girl child at the tender age of eight or so was abandoned. She was denied formal education and social liberty, forced to follow various rituals and expected to be an expert in cooking, spinning, and other household chores.
9. Kulin Brahmins observed strict caste rules and practiced polygamy. The great social reformer of Bengal, Iswar Chandra Vidyasagar (1820-1891) fought against this Hindu practice in the mid-nineteenth century.
10. The ritual of writing for the first time in life, is generally held as a part of the worship of the goddess of learning, Saraswati.
11. There are numerous cultural texts that support such discourse; to cite an example, poet Rajanikanta Sen's (1865-1910) call to wear simple clothes and eat coarse rice provided by a poor and distressed mother with pride.
12. This second novel of the trilogy has led the feminist movement in South-Asia and has been adapted for film and theatre.
13. In *Char Adhyay*, Tagore in fact warns about not repeating the colonial inhumanity in native relationships.
14. The new, or modern.

## References

- Bagchi, J. (1995). Introduction. In J. Bagchi (Ed.), *Indian Women: Myth and Reality*. Hyderabad: Sangam Books.
- Bagchi, J. (2004). Foreword. In A. Devi and I. Chowdhury (By and Trans.), *The First Promise (Pratham Pratisruti)*. Hyderabad: Orient BlackSwan.
- Bandyopadhyay, S. (2012). *Sibaji Bandyopadhyay Reader: An anthology of essays*. Delhi: Worldview.
- Banerjee Chakravorty, S. (1998). Carving a Self: Feminist Consciousness, the Family, and the Socialization Process: A Study of Ashapurna Devi's Trilogy. In R. T. Ames, T. P. Kasulis, & W. Dissanayake (Eds.), *Self as Image in Asian Theory and Practice*, (pp. 280-304). New York: State University of New York Press.
- Bose, A. (1976). Ashapurna Devi: Perspective of Bengali Novelist. *Indian Literature*, 19(3), 80-95.
- Bose, S. (2017). *The Nation as Mother and Other Visions of Nationhood*. Gurgaon: Penguin Random House.
- Butler, J. (1990). *Gender Trouble: Feminism and the Subversion of Identity*. New York: Routledge.
- Butler, J. (2004). *Undoing Gender*. New York: Routledge.
- Butler, J. (1999). Bodies that Matter. In J. Price and M. Shildrick (Eds.), *Feminist Theory and the Body: A Reader*, (pp. 235-245). New York: Routledge.
- Chakravarti, U. (2013). *Rewriting History: The Life and Times of Pandita Ranabai*. New Delhi: Zubaan Books.



- Chattopadhyay, S. (2012). Ashapura Devi's "Women": Emerging Identities in Colonial and Postcolonial Bengal. *Argument: Biannual Philosophical Journal*, 2(1), 75-96.
- Chowdhury, I. (1998). Rethinking Motherhood, Reclaiming a Politics: A Reading of Ashapura Debi's *Pratham Pratisruti*. *Economic and Political Weekly*, 33(44), 47-52.
- Cixous, H. (1976). The Laugh of the Medusa. Trans. Keith Cohen & Paula Cohen. *Signs*, 1(4), 875-893. <https://doi.org/10.1086/493306>
- Cudd, A. E. (2006). *Analyzing Oppression*. New York: Oxford University Press.
- Debi, A. (1997). *Subarnalata*. Trans. Gopa Majumdar. New Delhi: Macmillan India.
- Debi, A. (2004). *The First Promise (Pratham Pratisruti)*. Trans. Indira Chowdhury. Hyderabad: Orient BlackSwan.
- Debi, A. (2004). Author's Preface. *The First Promise (Pratham Pratisruti)*. Trans. Indira Chowdhury. Hyderabad: Orient BlackSwan.
- Debi, A. (2021). *Bakulkatha*. Trans. Lopamudra Banerjee. Kolkata: Avenel Press.
- Dey, N. (2007). Food, family, widowhood in Ashapura Devi's short fiction. In S. Dasgupta & M. Lal (Eds.), *Indian family in Transition*, (pp. 221-230). New Delhi: Thousand Oaks, London & Singapore: Sage Publications.
- Devenish, A. (2019). *Debating Women's Citizenship in India, 1930-1960*. New Delhi: Bloomsbury India.
- Dev Sen, N. (1997). Foreword. In A. Debi & G. Majumdar (By and Trans.), *Subarnalata*. New Delhi: Macmillan India.
- Derrida, J. (2005). *The Politics of Friendship*. London & New York: Verso.
- Dutta, D. (2015). *Ashapura Devi and Feminist Consciousness in Bengal: A Bio-critical Reading*. New Delhi: Oxford University Press.
- Foucault, M. (1977). *Discipline and Punish: The Birth of the Prison*. New York: Pantheon Books.
- Foucault, M. (2008). *Psychiatric Power: Lectures at the College de France*. Trans. Graham Burchell. Eds. Arnold I. Davidson and Jacques Lagrange. New York: St. Martins Press.
- Kimber, G. (2021, May 28). Nastiness and joy: A virtuosic biography of D.H. Lawrence. *Times Literary Supplement*.
- McNay, L. (2016). Agency. In L. Disch & M. Hawkesworth (Eds.), *The Oxford Handbook of Feminist Theory*, (pp. 39-60). New York: Oxford University Press.
- Medie, P. A. and Kang, A. J. (2018). Power, knowledge and the politics of gender in the Global South. *European Journal of Politics and Gender*, 1(1-2), 37-54. <https://doi.org/10.1332/251510818X15272520831157>
- Mohan, K. (2014). *Science and Technology in Colonial India*. New Delhi: Aakar Books.
- Rangra, R. (1989). Truth cannot be revealed in its entirety: An Interview of Ashapura Devi. *Indian Literature*, 32(5), 71-78.
- Sarkar, S. (2002). *Beyond Nationalist Frames: Relocating Postmodernism, Hindutva, History*. New Delhi: Permanent Black.
- Sarkar, S. (2014). *Modern Times: India 1880s-1950s: Environment, Economy, Cultural*. New Delhi: Permanent Black.
- Sen, A. (2009). *The Idea of Justice*. London, New York, Toronto & New Delhi: Penguin Books.
- Shildrick, M., & Price, J. (1999). Openings on the Body: A Critical Introduction. In J. Price & M. Shildrick (Eds.), *Feminist Theory and the Body: A Reader*, (pp. 1-14). New York: Routledge.
- Thereadcraft, S. (2016). Embodiment. In L. Disch & M. Hawkesworth (Eds.), *The Oxford Handbook of Feminist Theory*, (pp. 207-226). New York: Oxford University Press.

Turner, B. S. (2012). Embodied Practice: Martin Heidegger, Pierre Bourdieu and Michel Foucault. In B. S. Turner (Ed.), *Routledge Handbook of Body Studies*, (pp. 62-74). New York: Routledge.

# Disparity in Educational Participation in the Lenses of Educational Returns and Family Background: Evidence from India

Journal of Asian and African Studies  
1–26  
© The Author(s) 2023  
Article reuse guidelines:  
sagepub.com/journals-permissions  
DOI: 10.1177/00219096231158342  
journals.sagepub.com/home/jas  


**Anjan Ray Chaudhury**

Department of Economics, Durgapur Government College, India

**Sreemanta Sarkar**

Department of Economics, Bidhan Chandra College, Asansol, West Bengal, India

**Madhabendra Sinha**

Department of Economics, Bidhan Chandra College, Asansol, West Bengal, India.

## Abstract

The paper attempts to investigate the origin of inequality in educational participation across Indian social groups in terms of inequality in the expected monetary educational returns and other demand-side factors responsible behind educational decision. We employ the binary logit model of regression for the accomplishment of the objective of this study. In addition, we decompose the discrepancy in educational participation into 'response effect' and 'attribute effect' to examine whether there is any discrimination in educational participation against the members of the disadvantaged social groups.

**JEL Classification:** I21, I24, I26

## Keywords

Disparity, social groups, logistic regression, returns to education, educational participation

## Introduction

The theories concerning human capital consider educational participation as an investment to increase lifetime income and wealth (Becker, 1975; Mincer, 1974; Schultz, 1975). A person requires bearing the cost to attain education which at the same time enables him to earn money in future.<sup>1</sup> A cost–benefit analysis is thus considered necessary before travelling into the world of education. The optimal choice depends on the equality of marginal benefit of one additional year of schooling to the marginal cost. All persons in a particular society may not be attracted to

---

### Corresponding author:

Madhabendra Sinha, Department of Economics and Politics, Visva-Bharati University, Santiniketan, West Bengal 731235, India.

Email: madhabendras@gmail.com



# Plant type II arabinogalactan: Structural features and modification to increase functionality

Kanika Ghosh<sup>a,\*\*</sup>, Daisuke Takahashi<sup>b</sup>, Toshihisa Kotake<sup>b,c,\*</sup>

<sup>a</sup> Department of Chemistry, Bidhan Chandra College, Asansol, 713304, West Bengal, India

<sup>b</sup> Division of Life Science, Graduate School of Science and Engineering, Saitama University, 255 Shimo-Okubo, Sakura-ku, Saitama City, Saitama, 338-8570, Japan

<sup>c</sup> Green Bioscience Research Center, Graduate School of Science and Engineering, Saitama University, 255 Shimo-Okubo, Sakura-ku, Saitama City, Saitama, 338-8570, Japan

## ARTICLE INFO

### Keywords:

Type II arabinogalactans  
Structural analysis approach  
Chemical modifications

## ABSTRACT

Type II arabinogalactans (AGs) are a highly diverse class of plant polysaccharides generally encountered as the carbohydrate moieties of certain extracellular proteoglycans, the so-called arabinogalactan-proteins (AGPs), which are found on plasma membranes and in cell walls. The basic structure of type II AG is a 1,3-β-D-galactan main chain with 1,6-β-D-galactan side chains. The side chains are further decorated with other sugars such as α-L-arabinose and β-D-glucuronic acid. In addition, AGs with 1,6-β-D-galactan as the main chain, which are designated as 'type II related AG' in this review, can also be found in several plants. Due to their diverse and heterogenous features, the determination of carbohydrate structures of type II and type II related AGs is not easy. On the other hand, these complex AGs are scientifically and commercially attractive materials whose structures can be modified by chemical and biochemical approaches for specific purposes. In the current review, what is known about the chemical structures of type II and type II related AGs from different plant sources is outlined. After that, structural analysis techniques are considered and compared. Finally, structural modifications that enhance or alter functionality are highlighted.

## 1. Introduction

Most polysaccharides are derived from plant cell walls and considerable economic activity is concerned with the transfer of plant cell wall polysaccharides into various products, such as fuels, chemicals, and foods. Major constituents of plant cell walls are cellulose, hemicellulose, pectin, and lignin, but arabinogalactan-proteins (AGPs), a class of glycoprotein, are also commonly observed [1,2]. Arabinogalactans (AGs) form two main groups based on their structure: the arabino-4-galactans (1,4-β-D-galactans decorated with α-L-arabinose, α-L-Ara) are classified as type I AG and the arabino-3,6-galactans (1,3-β-D-galactan:1,6-β-D-galactan decorated with α-L-Ara) are classified as type II AG. While type I AGs usually link to the rhamnogalacturonan (RG) I backbone of pectin, type II AGs are generally found as the carbohydrate moieties of AGP, in which type II AGs account for more than 90% of their weight [3]. Acacia gum AG obtained from the acacia tree (*Acacia senegal*), also called gum arabic, and larch AG from larch wood

(*Larix* species), are extensively utilized as gelling, emulsifying, and moisturizing agents in foods. In plants, type II AGs perform important functions in several physiological events such as differentiation, cell-cell recognition, embryogenesis, and programmed cell death [4,5], but the amount of type II AGs in cell wall is generally low. Due to difficulty in achieving large-scale production and low economic value, they are hardly utilized by humans.

Unlike other biological macromolecules like DNA and RNA helices (chains of nucleic acids) and proteins (chains of amino acids), polysaccharides (chains of monosaccharides) are not synthesized from a template or blueprint that determines the arrangement of their constituent sugar residues, which form branching, not single linear, chains. The monosaccharide units in oligosaccharides and polysaccharides can interconnect at several points to form a wide variety of branched or linear structures. Therefore, the structures of polysaccharides are heterogenous although some of them contain repetitive features. The chemical characterization of heterogenous polysaccharides is

\* Corresponding author. Division of Life Science, Graduate School of Science and Engineering, Saitama University, 255 Shimo-Okubo, Sakura-ku, Saitama City, Saitama, 338-8570, Japan.

\*\* Corresponding author.

E-mail addresses: [ghosh.kanika7@gmail.com](mailto:ghosh.kanika7@gmail.com) (K. Ghosh), [kotake@mail.saitama-u.ac.jp](mailto:kotake@mail.saitama-u.ac.jp) (T. Kotake).

<https://doi.org/10.1016/j.carres.2023.108828>

Received 29 March 2023; Received in revised form 22 April 2023; Accepted 24 April 2023

Available online 2 May 2023

0008-6215/© 2023 The Authors. Published by Elsevier Ltd. This is an open access article under the CC BY license (<http://creativecommons.org/licenses/by/4.0/>).



# A Study of Conformal $\eta$ -Einstein Solitons on Trans-Sasakian 3-Manifold

Yanlin Li<sup>1</sup> · Somnath Mondal<sup>2</sup> · Santu Dey<sup>3</sup> · Arindam Bhattacharyya<sup>2</sup> · Akram Ali<sup>4</sup>

Received: 12 April 2022 / Accepted: 4 October 2022  
© The Author(s) 2022

## Abstract

We study conformal  $\eta$ -Einstein solitons on the framework of trans-Sasakian manifold in dimension three. Existence of conformal  $\eta$ -Einstein solitons on trans-Sasakian manifold is discussed. Then we find some results on trans-Sasakian manifold which are conformal  $\eta$ -Einstein solitons where the Ricci tensor is cyclic parallel and Codazzi type. We also consider some curvature conditions with addition to conformal  $\eta$ -Einstein solitons on trans-Sasakian manifold. We also use torse-forming vector fields in addition to conformal  $\eta$ -Einstein solitons on trans-Sasakian manifold. Finally, an example of conformal  $\eta$ -Einstein solitons on trans-Sasakian manifold is constructed.

**Keywords** Trans-Sasakian manifold · Einstein soliton · Conformal  $\eta$ -Einstein soliton · Codazzi type Ricci tensor ·  $\mathcal{C}$ -Bochner curvature tensor ·  $\mathcal{W}_2$  curvature tensor ·  $\mathcal{M}$ -projective curvature tensor

## 1 Introduction

The Ricci flow on a smooth manifold  $M$  with Riemannian metric  $g(t)$  is given by

$$\frac{\partial}{\partial t}g(t) = -2Ric,$$

where  $Ric$  is the Ricci tensor of the metric  $g(t)$ . A Ricci soliton is a solution of Ricci flow (see details [24, 25, 57]), defined on a pseudo-Riemannian manifold  $(M, g)$  by

---

Yanlin Li, Somnath Mondal, Santu Dey, Arindam Bhattacharyya and Akram Ali have contributed equally to this work.

---

✉ Yanlin Li  
liy1@hznu.edu.cn

Extended author information available on the last page of the article



## Review

# Geometry of para-Sasakian metric as an almost conformal $\eta$ -Ricci soliton

Sumanjit Sarkar<sup>a,\*</sup>, Santu Dey<sup>b</sup>, Ali H. Alkhaldi<sup>c</sup>, Arindam Bhattacharyya<sup>a</sup>

<sup>a</sup> Department of Mathematics, Jadavpur University, Kolkata-700032, India

<sup>b</sup> Department of Mathematics, Bidhan Chandra College, Asansol, Burdwan, West Bengal-713304, India

<sup>c</sup> Department of Mathematics, College of Science, King Khalid University, 9004 Abha, Saudi Arabia



## ARTICLE INFO

## Article history:

Received 20 January 2022

Received in revised form 4 August 2022

Accepted 20 August 2022

Available online 28 August 2022

## MSC:

53C15

53C21

53C25

53E20

## Keywords:

Ricci flow

Conformal  $\eta$ -Ricci soliton

Almost conformal  $\eta$ -Ricci soliton

Gradient almost conformal  $\eta$ -Ricci soliton

Para-Sasakian manifold

## ABSTRACT

In this paper, we initiate the study of conformal  $\eta$ -Ricci soliton and almost conformal  $\eta$ -Ricci soliton within the framework of para-Sasakian manifold. We prove that if para-Sasakian metric admits conformal  $\eta$ -Ricci soliton, then the manifold is  $\eta$ -Einstein and either the soliton vector field  $V$  is Killing or it leaves  $\phi$  invariant. Here, we show the characteristics of the soliton vector field  $V$  and scalar curvature when the manifold admits conformal  $\eta$ -Ricci soliton and vector field is pointwise collinear with the characteristic vector field  $\xi$ . Next, we show that a para-Sasakian metric endowed an almost conformal  $\eta$ -Ricci soliton is  $\eta$ -Einstein metric if the soliton vector field  $V$  is an infinitesimal contact transformation. We also display that the manifold is Einstein if it represents a gradient almost conformal  $\eta$ -Ricci soliton. We develop an example to display the existence of conformal  $\eta$ -Ricci soliton on 3-dimensional para-Sasakian manifold.

© 2022 Elsevier B.V. All rights reserved.

## 1. Introduction

In modern mathematics, the methods of paracontact geometry play an important role. The notion of almost paracontact manifold was first introduced by Sato [21]. After that he and Matsumoto [22] defined and studied a para-Sasakian manifold as special case of an almost paracontact manifold. Adati et al. [1] deduced some fundamental properties of para-Sasakian manifold. Later Kaneyuki and Williams [12] associated pseudo-Riemannian metric with an almost paracontact manifold after Takahashi [24] introduced pseudo-Riemannian metric in contact manifold, in particular, in Sasakian manifold. Zamkovoy in [27] proved that any almost paracontact structure admits a pseudo-Riemannian metric with signature  $(n + 1, n)$ . Para-Sasakian manifold (in short p-Sasakian manifold) was studied by many authors, namely: Calvaruso [4], Cappelletti et al. [6], Tripathi et al. [25] and many others.

A pseudo-Riemannian manifold  $(M, g)$  admits a Ricci soliton which is a generalization of Einstein metric (i.e.,  $S = ag$  for some constant  $a$ ) if there exists a smooth non-zero vector field  $V$  and a constant  $\lambda$  such that

\* Corresponding author.

E-mail addresses: [imsumanjit@gmail.com](mailto:imsumanjit@gmail.com) (S. Sarkar), [santu.mathju@gmail.com](mailto:santu.mathju@gmail.com) (S. Dey), [ahalkhaldi@kku.edu.sa](mailto:ahalkhaldi@kku.edu.sa) (A.H. Alkhaldi), [bhattachar1968@yahoo.co.in](mailto:bhattachar1968@yahoo.co.in) (A. Bhattacharyya).

## A study of conformal almost Ricci solitons on Kenmotsu manifolds

Sumanjit Sarkar\*

*Department of Mathematics, Jadavpur University  
Kolkata, West Bengal 700032, India  
[imsumanjit@gmail.com](mailto:imsumanjit@gmail.com)*

Santu Dey

*Department of Mathematics, Bidhan Chandra College  
Asansol, Burdwan, West Bengal 713304, India  
[santu.mathju@gmail.com](mailto:santu.mathju@gmail.com)*

Arindam Bhattacharyya

*Department of Mathematics, Jadavpur University  
Kolkata, West Bengal 700032, India  
[bhattachar1968@yahoo.co.in](mailto:bhattachar1968@yahoo.co.in)*

Received 29 August 2022

Accepted 21 October 2022

Published 28 November 2022

The goal of this paper is to study conformal almost Ricci solitons within the framework of Kenmotsu manifolds. First, we demonstrate that if the potential vector field is Jacobi along the Reeb vector field, then the soliton reduces to a conformal Ricci soliton. If the manifold is  $\eta$ -Einstein Kenmotsu manifold, we show that either the manifold is of constant scalar curvature or the potential vector field is an infinitesimal contact transformation. In addition, if we consider the soliton vector field as a contact vector field, then either the gradient of  $\lambda$  is pointwise collinear with the Reeb vector field or the manifold becomes  $\eta$ -Einstein. Lastly, we develop an example of a conformal almost Ricci soliton on the Kenmotsu manifold.

*Keywords:* Ricci flow; conformal Ricci flow; conformal almost Ricci soliton; Kenmotsu manifold.

Mathematics Subject Classification 2020: 53C15, 53C21, 53C25, 53E20

### 1. Introduction

Contact geometry methods play an important role in modern mathematics, which has evolved from the mathematical formalism of classical mechanics. In 1969, Tanno [1] classified the connected almost contact metric manifolds. In [2], a new class of

\*Corresponding author.



## Characterization of Almost $\eta$ -Ricci–Yamabe Soliton and Gradient Almost $\eta$ -Ricci–Yamabe Soliton on Almost Kenmotsu Manifolds

**Somnath MONDAL**

*Department of Mathematics, Jadavpur University, Kolkata-700032, India*

*E-mail: somnathmondal.math@gmail.com*

**Santu DEY<sup>1)</sup>**

*Department of Mathematics, Bidhan Chandra College*

*Asansol-4, West Bengal-713304, India*

*E-mail: santu.mathju@gmail.com*

**Arindam BHATTACHARYYA**

*Department of Mathematics, Jadavpur University, Kolkata-700032, India*

*Email: bhattachar1968@yahoo.co.in*

**Abstract** The prime object in this article is to study an almost  $\eta$ -Ricci–Yamabe soliton and gradient almost  $\eta$ -Ricci–Yamabe soliton within the framework of almost Kenmotsu manifolds. It is shown that normal almost Kenmotsu manifold admitting an almost  $\eta$ -Ricci–Yamabe soliton or gradient  $\eta$ -Ricci–Yamabe soliton is locally isometric to hyperbolic space  $\mathbb{H}^{2n+1}(-1)$ . Next, we prove that if a  $(\kappa, \mu)$  almost Kenmotsu manifold admits an almost  $\eta$ -Ricci–Yamabe soliton, then the manifold is  $\eta$ -Einstein. Besides, we find the condition for non-normal almost Kenmotsu manifolds acknowledging gradient almost  $\eta$ -Ricci–Yamabe soliton. Moreover, an almost  $\eta$ -Ricci–Yamabe soliton on  $(\kappa, \mu)$ '-almost Kenmotsu manifold has been studied. Lastly, we construct an example of a gradient almost  $\eta$ -Ricci–Yamabe soliton on a 3-dimensional Kenmotsu manifold.

**Keywords** Ricci soliton,  $(\kappa, \mu)$ -almost Kenmotsu manifold,  $(\kappa, \mu)$ '-almost Kenmotsu manifold,  $\eta$ -Ricci–Yamabe soliton

**MR(2010) Subject Classification** 53D15, 53C15, 53C25

### 1 Introduction and Motivations

Contact geometry methods play an important role in modern mathematics. Contact geometry has evolved from the mathematical formalism of classical mechanics. In 1969, Tanno [46] classified the connected almost contact metric manifolds whose automorphism groups have maximal dimensions as follows:

(a) Homogeneous normal contact Riemannian manifolds with constant  $\phi$ -holomorphic sectional curvature if  $k(\xi, X) > 0$ ;

---

Received April 20, 2022, accepted May 30, 2022

The first author is supported by UGC Junior Research Fellowship of India (Grant No. 1157/(SC) (CSIR-UGC NET DEC. 2016))

1) Corresponding author

# General Relativistic Space-Time with $\eta_1$ -Einstein Metrics

Yanlin Li <sup>1</sup>, Fatemah Mofarreh <sup>2</sup>, Santu Dey <sup>3</sup>, Soumendu Roy <sup>4</sup> and Akram Ali <sup>5,\*</sup><sup>1</sup> School of Mathematics, Hangzhou Normal University, Hangzhou 311121, China; liyl@hznu.edu.cn<sup>2</sup> Mathematical Science Department, Faculty of Science, Princess Nourah bint Abdulrahman University, Riyadh 11546, Saudi Arabia; fyalmofarrah@pnu.edu.sa<sup>3</sup> Department of Mathematics, Bidhan Chandra College, Asansol 713304, India; santu@bccollegeasansol.ac.in<sup>4</sup> Department of Science & Humanities, MLR Institute of Technology, Hyderabad 500043, India; soumendu1103mtma@gmail.com<sup>5</sup> Department of Mathematics, College of Science, King Khalid University, Abha 61421, Saudi Arabia

\* Correspondence: akali@kku.edu.sa

**Abstract:** The present research paper consists of the study of an  $\eta_1$ -Einstein soliton in general relativistic space-time with a torse-forming potential vector field. Besides this, we try to evaluate the characterization of the metrics when the space-time with a semi-symmetric energy-momentum tensor admits an  $\eta_1$ -Einstein soliton, whose potential vector field is torse-forming. In addition, certain curvature conditions on the space-time that admit an  $\eta_1$ -Einstein soliton are explored and build up the importance of the Laplace equation on the space-time in terms of  $\eta_1$ -Einstein soliton. Lastly, we have given some physical accomplishment with the connection of dust fluid, dark fluid and radiation era in general relativistic space-time admitting an  $\eta_1$ -Einstein soliton.

**Keywords:** general relativistic space-time; torse-forming vector fields;  $\eta_1$ -Einstein soliton; Einstein's field equation; dust fluid; dark fluid; radiation era; Laplacian equation

**MSC:** 53C44; 53C50; 53B50

**Citation:** Li, Y.; Mofarreh, F.; Dey, S.; Roy, S.; Ali, A. General Relativistic Space-Time with  $\eta_1$ -Einstein Metrics. *Mathematics* **2022**, *10*, 2530. <https://doi.org/10.3390/math10142530>

Academic Editors: Constantin Udriste and Vladimir Rovenski

Received: 1 June 2022

Accepted: 14 July 2022

Published: 21 July 2022

**Publisher's Note:** MDPI stays neutral with regard to jurisdictional claims in published maps and institutional affiliations.



**Copyright:** © 2022 by the authors. Licensee MDPI, Basel, Switzerland. This article is an open access article distributed under the terms and conditions of the Creative Commons Attribution (CC BY) license (<https://creativecommons.org/licenses/by/4.0/>).

## 1. Background and Motivations

Throughout the article, we shall utilize the following acronyms: GRS—general relativistic space-time, TFVF—torse-forming vector field, and EMT—energy-momentum tensor. Ricci's soliton is well known among theoretical physicists because it is linked to string theory. It is well known that the theoretical physicists are interested in the Ricci soliton due to its association with string theory. In recent times, Ricci solitons are quite interesting in the field of differential geometry and geometric analysis as they characteristically present the Einstein metric. As a result, Ricci solitons in pseudo-Riemannian settings are extensively studied, and Hamilton introduced the concept of Ricci flow and extended it to address Thurston's geometric hypothesis. A Ricci soliton is a location in Hamilton's Ricci flow that is fixed (see details [1,2]) and an obvious extension of Einstein's metric is defined on a pseudo-Riemannian manifold  $(M, g)$  by

$$\frac{1}{2}\mathcal{L}_V g + Ric = \Lambda_1 g, \quad (1)$$

where  $\mathcal{L}_V$  stands for the Lie-derivative in the way of  $V \in \chi(M)$ ,  $\Lambda_1$  is a constant and the Ricci tensor of  $g$  is presented by  $Ric$ . The Ricci soliton is classified as follows:

- (i) If  $\Lambda_1 < 0$ , then the Ricci soliton is said to be shrinking.
- (ii) for  $\Lambda_1 > 0$ , then it is said to be expanding.
- (iii) If  $\Lambda_1 = 0$ , then it is implied to be steady.

## Characterization of general relativistic spacetime equipped with different types of solitons

Santu Dey

*Department of Mathematics, Bidhan Chandra College  
Asansol — 4, West Bengal 713304, India  
santu.mathju@gmail.com  
santu@bccollegeasansol.ac.in*

Meraj Ali Khan\*

*Department of Mathematics  
University of Tabuk, K.S.A.  
meraj79@gmail.com*

Soumendu Roy

*Department of Mathematics  
Jadavpur University, Kolkata 700032, India  
soumendu1103mtma@gmail.com*

Peibiao Zhao

*Department of Applied Mathematics  
Nanjing University of Science and Technology  
Nanjing 210094, P. R. China  
pbzhao@njjust.edu.cn*

Received 21 April 2022

Accepted 25 July 2022

Published 19 August 2022

The aim of this paper is to study certain types of metrics such as conformal  $\eta$ -Ricci soliton and Yamabe soliton in general relativistic spacetime. Here, we have shown the nature of the soliton when the spacetime with semisymmetric energy-momentum tensor admits conformal  $\eta$ -Ricci soliton, whose potential vector field is torse-forming. We have studied certain curvature conditions on the spacetime that admits conformal  $\eta$ -Ricci soliton. Also, we have enriched the importance of the Laplace equation on the spacetime admitting conformal  $\eta$ -Ricci soliton. Next, we have given some applications of physical

\*Corresponding author.

## Geometry of almost contact metrics as a $*$ -conformal Ricci–Yamabe solitons and related results

Santu Dey

*Department of Mathematics, Bidhan Chandra College  
Asansol - 4, West Bengal 713304, India  
santu.mathju@gmail.com*

Soumendu Roy

*Division of Mathematics, School of Advanced Sciences  
Vellore Institute of Technology, Chennai 600127, India  
soumendu1103mtma@gmail.com  
soumendu.roy@vit.ac.in*

Fatma Karaca\*

*İstanbul Beykent University, Department of Mathematics  
İstanbul 34550, Türkiye  
fatmakaraca@beykent.edu.tr*

Received 2 August 2022  
Accepted 22 February 2023  
Published 11 April 2023

The goal of this paper is to study certain types of metric such as  $*$ -conformal Ricci–Yamabe soliton (RYS), whose potential vector field is torse-forming on Kenmotsu manifold. Here, we establish the conditions for solitons to be expanding, shrinking or steady and find the scalar curvature when the manifold admits  $*$ -conformal RYS on Kenmotsu manifold. Next, we developed the nature of the vector field when the manifold satisfies  $*$ -conformal RYS. Also, we have adorned some applications of torse-forming vector field in terms of  $*$ -conformal RYS on Kenmotsu manifold. We have also studied infinitesimal CL-transformation and Schouten–van Kampen connection on Kenmotsu manifold, whose metric is  $*$ -conformal RYS. We present an example of  $*$ -conformal RYS on three-dimensional Kenmotsu manifold, and verify some of our findings.

*Keywords:* Ricci–Yamabe soliton;  $*$ -conformal Ricci–Yamabe soliton; torse-forming vector field; conformal Killing vector field; Kenmotsu manifold.

Mathematics Subject Classification 2020: 53C15, 53C25, 53C44

\*Corresponding author.

## Applications of some types of solitons within the framework of Kählerian spacetime manifolds

Santu Dey\*

*Department of Mathematics, Bidhan Chandra College  
Asansol-4, West Bengal 713304, India  
santu.mathju@gmail.com*

Siraj Uddin

*Department of Mathematics, Faculty of Science  
King Abdulaziz University, Jeddah 21589, Saudi Arabia  
siraj.ch@gmail.com*

Received 24 November 2022

Revised 24 February 2023

Accepted 1 March 2023

Published 12 April 2023

In this paper, we study applications of some certain types of solitons such as conformal Ricci soliton, conformal  $\eta$ -Ricci-Yamabe soliton and  $\eta$ -Ricci soliton on Kählerian spacetime manifolds. Further, we have developed the characteristics of conformal Ricci soliton and conformal  $\eta$ -Ricci-Yamabe soliton on almost pseudo-symmetric Kählerian spacetime manifolds. Here, we have signalized the nature of solitons in terms of shrinking, steady or expanding and we have also presented the relationship between  $\lambda$  and  $\mu$  in terms of conformal  $\eta$ -Ricci-Yamabe soliton. Finally, we have embellished the classification of the potential function with respect to gradient  $\eta$ -Ricci soliton on Kählerian spacetime manifolds.

*Keywords:* Ricci flow;  $\eta$ -Ricci soliton; conformal Ricci soliton; conformal  $\eta$ -Ricci-Yamabe soliton; almost pseudo-symmetric manifolds; Kählerian spacetime manifolds.

Mathematics Subject Classification 2020: 53C15, 53C21, 53C25, 53D15

### 1. Background and Motivations

Ricci solitons have received a lot of attention by many geometers, mainly due to the intense works of Hamilton (and also Perelman). In the recent years, Ricci solitons are of much interest in the field of differential geometry and geometric analysis as it naturally extends Einstein metric. In 1982, Hamilton [20] introduced the concept of Ricci flow, which is an evolution equation for metrics on a Riemannian manifold.

\*Corresponding author.

## Geometry of almost contact metrics as an almost $*\text{-}\eta$ -Ricci–Bourguignon solitons

Santu Dey

*Department of Mathematics, Bidhan Chandra College,  
 Asansol-4, West Bengal 713304, India  
 santu.mathju@gmail.com  
 santu@bccollegeasansol.ac.in*

Young Jin Suh

*Department of Mathematics and RIRCМ,  
 Kyungpook National University,  
 Daegu 41566, South Korea  
 yjsuh@knu.ac.kr*

Received 11 August 2022

Accepted 18 March 2023

Published 12 May 2023

In this paper, we give some characterizations by considering almost  $*\text{-}\eta$ -Ricci–Bourguignon soliton as a Kenmotsu metric. It is shown that if a Kenmotsu metric endows a  $*\text{-}\eta$ -Ricci–Bourguignon soliton, then the curvature tensor  $R$  with the soliton vector field  $V$  is given by the expression  $(\mathcal{L}_V R)(V_1, \xi)\xi = 2\vartheta\{V_1(r)\xi - V_1(Dr) + \xi(Dr) - \xi(r)\xi - Dr\}$ . Next, we show that if an almost Kenmotsu manifold such that  $\xi$  belongs to  $(\kappa, -2)'$ -nullity distribution where  $\kappa < -1$  acknowledges a  $*\text{-}\eta$ -Ricci–Bourguignon soliton satisfying  $\Omega + \psi \neq \vartheta[(r + 4n^2) + \{\xi(\xi(r)) - \xi(Dr)\}]$ , then the manifold is Ricci-flat and is locally isometric to  $\mathbb{H}^{n+1}(-4) \times \mathbb{R}^n$ . Moreover if the metric admits a gradient almost  $*\text{-}\eta$ -Ricci–Bourguignon soliton and  $\xi$  leaves the scalar curvature  $r$  invariant on a Kenmotsu manifold, then the manifold is an  $\eta$ -Einstein. Also, if a Kenmotsu metric represents an almost  $*\text{-}\eta$ -Ricci–Bourguignon soliton with potential vector field  $V$  is pointwise collinear with  $\xi$ , then the manifold is an  $\eta$ -Einstein.

*Keywords:*  $(\kappa, \psi)$ -almost Kenmotsu manifold;  $(\kappa, \psi)'$ -almost Kenmotsu manifold;  $*\text{-}\eta$ -Ricci–Bourguignon soliton.

Mathematics Subject Classification 2020: 53D15, 53C15, 53C25

### 1. Introduction and Motivations

The scientists and mathematicians across many disciplines have always been fascinated to study indefinite structures on manifolds. When a manifold is endowed with a geometric structure, we have more opportunities to explore its geometric properties. In 1981, a new geometric flow, named Ricci–Bourguignon flow, was introduced by Jean-Pierre Bourguignon [5], which was constructed and based on



# Combined effects of temperature-dependent properties and magnetic field on electro-osmotic mobility at arbitrary zeta potentials

Amit Mondal<sup>a</sup>, Prashanta Kumar Mandal<sup>b</sup>, Subrata Maiti<sup>c</sup> and Gopal Chandra Shit<sup>d</sup>

<sup>a</sup>Department of Mathematics, Bidhan Chandra College, Asansol, India; <sup>b</sup>Department of Mathematics, Visva-Bharati, Santiniketan, Bolpur, India; <sup>c</sup>Department of BSH, University of Engineering & Management, Kolkata, India; <sup>d</sup>Department of Mathematics, Jadavpur University, Kolkata, India

## ABSTRACT

We analyze the thermo-electroosmotic mobility of power-law electrolyte solution under the action of a magnetic field in a wavy pattern micro-channel. The flow is driven by the combined effect of the pressure gradient and the electric potential applied externally in the axial direction. The variable properties such as the viscosity, zeta potential, electrical and thermal conductivity of electro-thermal flow are assumed to vary with temperature. The entire flow phenomena have been solved by employing the finite difference method. We have presented the variation of electroosmotic mobility with the effect of Joule heating and applied magnetic field. We have examined the coupling effects of axial velocity, thermal energy, and electric potential function for various values of the temperature-dependent properties. These temperature-dependent property variations lead to developing volumetric flow rates associated with the behavior of the power-law index. The Nusselt number is drastically influenced by the temperature-dependent zeta potential variation in comparison with the Newtonian and shear-thickening fluids. The numerical and analytical solutions are validated with the existing literature and obtained a good agreement.

## ARTICLE HISTORY

Received 14 January 2022  
Accepted 8 August 2022

## KEYWORDS

Electro-osmotic flow;  
power-law fluid;  
temperature-dependent  
properties; electro-osmotic  
mobility; magnetic field

## Nomenclature

$a'$	the amplitude of the wavy walls
$B_0$	magnetic field
$Br$	Brinkman number
$C_p$	specific heat
$d'$	constant height of the channel
$E_0$	a uniform electric field
$E_{x^*}$	applied electric field along $x^*$ -direction
$E_{y^*}$	applied electric field along $y^*$ -direction
$e$	charge of proton
$Ha$	Hartmann number

**CONTACT** A. Mondal  amitmondal009@gmail.com



# Study of Bird Diversity during Monsoon Season Related to Air Quality Atasansol, West Bengal

Debdyuti Sengupta<sup>1</sup>, Soumendra Nath Talapatra<sup>2</sup>

<sup>1</sup> Ph.D Scholar, Department of Environmental Science, Secom Skills University, Kendradangal, Birbhum, West Bengal, India

<sup>2</sup>Department of Bio-Science, Secom Skills University, Kendradangal, Birbhum, West Bengal, India

Corresponding author Email: [debdyutisenguptaindia\[at\]gmail.com](mailto:debdyutisenguptaindia[at]gmail.com)

Phone: +91-7550856044

**Abstract:** Qualitative and quantitative assessment of bird diversity as during monsoon season and correlated with available air quality parameters of Asansol, West Bengal. For bird diversity assessment, a total 500-meter line transects was done randomly weekly twice a day (2hrs. duration in each day) and call count methods in industrial and urban area compared to suburban area for the period of three months (June 2021 – August 2021). Different biodiversity indices were compared between the sites. Overall air quality data were correlated with the value of bird diversity. In the present findings, qualitative and quantitative assessment indicated that the variety of bird species were observed less numbers (11 types and 118 organisms) in site A1 compared to site A2 (20 types and 202 organisms). Different indices such as Shannon diversity index, Index of Dominance, and Margalef's species richness index values were higher in site B (2.40, 0.87 and 3.60) when compared to site A (2.00, 0.81 and 2.10) while Berger-Parker Dominance Index value was observed lower in site A2 (0.30) when compared to site A1 (0.36). The values (Mean  $\pm$  SD) of different air quality parameters ( $\mu\text{g}/\text{m}^3$ ) viz.  $\text{PM}_{2.5}$ ,  $\text{PM}_{10}$ ,  $\text{SO}_2$  and  $\text{NO}_2$  were  $56.66 \pm 2.13$ ,  $114.32 \pm 5.64$ ,  $11.22 \pm 0.64$  and  $29.01 \pm 1.90$ , respectively. Different diversity indices were lower in the site A1 may be due to the combinations of air pollutants or  $\text{PM}_{10}$  itself when compared to site A2. In future, it is suggested to study avifaunal diversity in dry seasons viz. winter and summer related to the air quality status.

**Keywords:** Bird diversity; Air quality; Industrial area; Urban area; Suburban area; Air quality bioindicator

## 1. Introduction

The study of bird diversity is very important because this indicates air quality of particular area. Several air pollutants viz. particulates and gaseous pollutants have an impact on bird species due to inhalation exposure.<sup>[1-2]</sup> A recent international study emphasized that decreasing of bird population in USA due to air pollutants especially ozone increasing rate.<sup>[3]</sup> Beside these, urbanization is also the causative reason for the declining of bird species.<sup>[4-5]</sup> Abnormal air quality due to industrial and automobile emissions that lead to air pollution. But present regulation of air pollution is based on human health hazards and no standards of pollutants have been proposed for avifauna or other chordates.

High diversity of avifauna indicates a healthy ecosystem and bird species fulfil several ecological functions in their habitats.<sup>[5-6]</sup> Moreover, insect feeder and raptors regulate disease vectors viz. mosquitoes and rodents. Scavenger birds, especially Pied Crow (*Corvus albus*) an important contributor for recycling of biomass and reducing disposable wastes.<sup>[5]</sup> Fruit eating birds help in seed dispersal of fleshy fruit.<sup>[7]</sup> Birds also participate in plant pollination.<sup>[8]</sup>

Several earlier studies have been reported bird diversity in different parts of West Bengal<sup>[9-13]</sup> but not related to air quality of urban and/or industrial area compared to suburban area. Chowdhury et al.<sup>[4]</sup> studied bird diversity related to traffic load near roadside parks without air quality assessment. Some international studies have been reported that air pollution causes the declining of the bird diversity<sup>[1-2,14]</sup> and it was observed a close relation between bird diversity in two parks of Kolkata and air pollution<sup>[15]</sup> but the

correlation between air quality parameters and bird diversity in Asansol urbanized area near industry, West Bengal is lacking.

The present study was attempted the bird diversity as qualitative and quantitative assessment during monsoon season and correlated with available air quality parameters of Asansol, West Bengal.

## 2. Materials and Methods

### Selection of study area

The study sites were selected as per heavily populated neighbourhoods, nearby residential buildings, nearby roads and continuous vehicular movements and nearby industries designated as site A1 (latitude = 23° 40' N and longitude = 86° 55' E) and suburban area comparatively lower vehicular movements, far from industrial vicinity designated as site A2 (latitude = 23° 67' N and longitude = 87° 22' E), Asansol, West Bengal. The study was carried out in these two habitats as per downwind direction for qualitative and quantitative assessment.

### Study design

A total 500-meter line transects was done randomly weekly twice a day (2hrs. duration in each day) and call count methods in industrial and urban area compared to suburban area for the period of three months (June 2021 – August 2021). The photographs of birds were taken during survey by using camera and was identified with the help of research articles.<sup>[16-18]</sup> Some unassuming bird species were identified based on their calls.<sup>[19]</sup>

**Air quality data**

All the secondary data of ambient air pollutants such as SO<sub>2</sub>, NO<sub>2</sub>, PM<sub>2.5</sub> and PM<sub>10</sub> related to Asansol air quality monitoring station, West Bengal were retrieved from Air Quality Information System of West Bengal Pollution Control Board, Kolkata to know the present status of air quality during monsoon season (June 2021 – August 2021).

**Qualitative and quantitative assessment of avifauna**

Bird diversity indices such as total specimens (N), Shannon diversity index (H'), Index of Dominance (C), Berger-Parker

Dominance Index, and Margalef's species richness index (S) were calculated.<sup>[20-24]</sup> The formulae are as follows:

$$\text{Shannon-Wiener diversity index (H')} = - [\sum \text{Pi ln Pi}] \dots (1)$$

where, Pi is proportion of species i relative to the total number of species, and lnPi is natural logarithm of this proportion.

$$\text{Index of Dominance (C)} = \sum (\text{ni/N})^2 \dots (2)$$

where, ni = importance value for each species (number of individuals), N = total number of importance value

$$\text{Berger-Parker Dominance Index} = N_{\text{max}} / N \dots (3)$$

where, N<sub>max</sub> is the number of Individuals of a species, and N is total population of birds.

$$\text{Margalef's species richness} = S - 1 \div \ln N \dots (4)$$

where, S = number of species, ln N = natural logarithm of the total number of individuals

The values of different biodiversity indices were calculated by using online tool namely Biodiversity calculator developed by AL Young Studio ([https://www.alyoung.com/labs/biodiversity\\_calculator.html?rand](https://www.alyoung.com/labs/biodiversity_calculator.html?rand)).

**Statistical analysis**

The Pearson correlation coefficient was analyzed to determine significant association between different air quality parameters and number of bird species during monsoon. All the data were considered the significance level at P<0.05 by using statistical software, PAST (PAleontological STatistics) software (version 3.26) developed by Hammer et al.<sup>[25]</sup>

**3. Results**

In the present findings, qualitative and quantitative assessment indicated that the variety of bird species were observed few in numbers in site A compared to site B (Table 1). The comparison revealed bird varieties of about 11 types in site A than varieties of about 20 types in site B. Common species of birds were *Corvus splendens*, *Columba livia*, *Acridotheres tristis*, *Acridotheres ginginianus*, *Spilopelia chinensis*, *Turdoides striata*, *Anas platyrhynchos domesticus*, *Copsychus saularis*, and *Dicrurus adsimilis* observed in both study sites. Moreover, few species were observed only in site B not in site A.

**Table 1:** List of avifauna in the study sites

Site A1				Site A2			
S. No.	Common Name	Scientific Name	Total No.	Sl. No.	Common Name	Scientific Name	Total No.
1.	House crow	<i>Corvus splendens</i>	15	1.	Indian pigeon	<i>Columba livia</i>	60
2.	Indian pigeon	<i>Columba livia</i>	42	2.	Spotted dove	<i>Spilopelia chinensis</i>	18
3.	Common mayna	<i>Acridotheres tristis</i>	12	3.	Jungle babbler	<i>Turdoides striata</i>	12
4.	Bank mayna	<i>Acridotheres ginginianus</i>	4	4.	Common mayna	<i>Acridotheres tristis</i>	8
5.	Spotted dove	<i>Spilopelia chinensis</i>	2	5.	Asian koel	<i>Eudynamis scolopaceus</i>	1
6.	Jungle babbler	<i>Turdoides striata</i>	8	6.	Vulture	<i>Gyps indicus</i>	2
7.	Indian little black cormorant	<i>Phalacrocorax sp.</i>	1	7.	House crow	<i>Corvus splendens</i>	25
8.	Domestic duck	<i>Anas platyrhynchos domesticus</i>	12	8.	White breasted water hen	<i>Amaurornis phoenicurus</i>	7
9.	Oriental magpie robin	<i>Copsychus saularis</i>	2	9.	Indian rose ringed parakeet	<i>Psittaciformes sp.</i>	12
10.	Cock	<i>Gallus gallus domesticus</i>	15	10.	Red vented bulbul	<i>Pycnonotus cafer</i>	2
11.	Bronzed drongo	<i>Dicrurus adsimilis</i>	5	11.	Red whiskered bulbul	<i>Pycnonotus jocosus</i>	1
				12.	Cattle egret	<i>Bubulcus ibis</i>	12
				13.	Bank mayna	<i>Acridotheres ginginianus</i>	5
				14.	Domestic duck	<i>Anas platyrhynchos domesticus</i>	11
				15.	Cock	<i>Gallus gallus domesticus</i>	9
				16.	Purple sunbird	<i>Cinnyris asiaticus</i>	4
				17.	Bronzed drongo	<i>Dicrurus adsimilis</i>	8
				18.	Oriental magpie robin	<i>Copsychus saularis</i>	2
				19.	Greater coucal	<i>Centropus sinensis</i>	1
				20.	Woodpecker	<i>Dinopium benghalense</i>	2

Table 2 evaluates the comparative diversity indices between the site A1 and A2. Higher value of the number of total organisms of about 202 in site A2 when compared to site A1

(118). Different indices such as Shannon diversity index, Index of Dominance, and Margalef's species richness index values were higher in site A2 (2.40, 0.87 and 3.60) when

compared to site A1 (2.00, 0.81 and 2.10) while Berger-Parker Dominance Index value was observed lower in site A2 (0.30) when compared to site A1 (0.36).

**Table 2:** Diversity indices compared between the site A1 and A2

Indices	Site A1	Site A2
Total No. of species	11	20
Total No. of organisms	118	202
Shannon-Wiener diversity index	2.00	2.40
Index of Dominance	0.81	0.87
Berger-Parker Dominance Index	0.36	0.30
Margalef's species richness	2.10	3.60

Fig 1 describes the values (Mean  $\pm$  SD) of different air quality parameters in which all the parameters were observed within the national ambient air quality standards except PM<sub>10</sub>. The value of PM<sub>2.5</sub>, PM<sub>10</sub>, SO<sub>2</sub> and NO<sub>2</sub> were 56.66  $\pm$  2.13  $\mu$ g/m<sup>3</sup>, 114.32  $\pm$  5.64  $\mu$ g/m<sup>3</sup>, 11.22  $\pm$  0.64  $\mu$ g/m<sup>3</sup> and 29.01  $\pm$  1.90  $\mu$ g/m<sup>3</sup>, respectively.

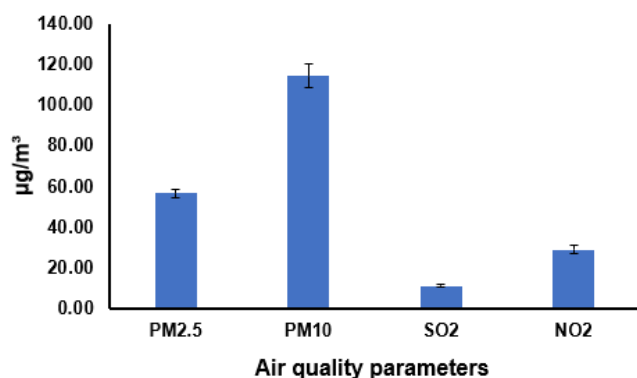


**Figure 1:** Average value of air quality parameters within the study area (Mean  $\pm$  SD; n = 27)

Table 3 estimates the Pearson correlation coefficient of air quality parameters and bird species availability in the site A1 and A2. In the site A, PM<sub>2.5</sub> and PM<sub>10</sub> were observed negative correlation ( $r = -0.024$  and  $r = -0.399$ ) while SO<sub>2</sub> and NO<sub>2</sub> shown positive correlation ( $r = 0.068$  and  $r = 0.715$ ) with the availability of bird species. In the site B, PM<sub>2.5</sub>, SO<sub>2</sub> and NO<sub>2</sub> were observed negative correlation ( $r = -0.132$ ,  $r = -0.234$  and  $r = -0.105$ ) while PM<sub>10</sub> shown positive correlation ( $r = 0.103$ ) with the availability of bird species.

**Table 3:** Correlation coefficient of air quality parameters and bird species availability in the site A1 and A2

Correlation coefficient of	Site A1	Site A2
PM <sub>2.5</sub> and bird species	$r = -0.024$	$r = -0.132$
PM <sub>10</sub> and bird species	$r = -0.399$	$r = 0.103$
SO <sub>2</sub> and bird species	$r = 0.068$	$r = -0.234$
NO <sub>2</sub> and bird species	$r = 0.715$	$r = -0.105$

#### 4. Discussion

The bird species are highly diverse and easily noticeable in the ecosystem. The diversity of avifauna declines due to environmental stresses especially abnormal air quality.<sup>[1-2,4,14-15]</sup>

In the present study sites common bird species such as *Corvus splendens*, *Columba livia*, *Acridotheres tristis*,

*Acridotheres ginginianus*, *Spilopelia chinensis*, *Turdoides striata*, *Anas platyrhynchos domesticus*, *Copsychus saularis*, and *Dicrurus adsimilis* observed in both study sites. Moreover, few more species such as *Eudynamis scolopaceus*, *Gyps indicus*, *Amaurornis phoenicurus*, *Psittaciformes sp.*, *Pycnonotus cafer*, *Pycnonotus jocosus*, *Bubulcus ibis*, *Cinnyris asiaticus*, *Centropus sinensis*, and *Dinopium benghalense* were recorded only in site B but in site A, one specimen of *Phalacrocorax sp.* was recorded. In the recent study, the variation of bird species due to air pollution has been found in the parks of Kolkata metropolitan area.<sup>[15]</sup>

Different diversity indices were higher in the site A2 due to less exposure of air pollutants compared to site A1 nearer to industrial vicinity and highly human interference as urbanized area. Moreover, all the air pollutants within the national ambient air quality standards except PM<sub>10</sub>. These pollutants may be safe for human but unsafe for bird's growth, metabolic activity, respiratory rate, etc. for declining diversity in site A1. On the other hand, the diversity was found a decreasing trend may be due to elevated average level of PM<sub>10</sub>, which has evidenced in the previous studies that particulates and other air pollutants decreased the diversity of avifauna.<sup>[2-3,14-15]</sup>

The negative value of the correlation coefficient, the  $r$  value indicates an increasing level of one parameter and decreasing in the other parameter. In the present study, there is a possibility of induction of air pollutants in site A1, which decreased the bird diversity as per decreased values of diversity indices, which is supported by earlier studies.<sup>[15,26]</sup> The relation between two variables could be established by correlation coefficient in which the parameters of air pollution and biodiversity of birds are interdependent and inversely related to each other.<sup>[15,27]</sup>

#### 5. Conclusion

The present study was conducted in the monsoon season to know the bird diversity related to air quality parameters in the industrial vicinity and urbanized area (site A) compared to suburban area far away from industries (site B) at Asansol, West Bengal. Different diversity indices were lower in the site A may be due to the combinations of air pollutants or PM<sub>10</sub> itself when compared to site A. In future, it is suggested to study avifaunal diversity in dry seasons viz. winter and summer related to the air quality status.

#### Conflict of interest

None

#### References

- [1] Brown RE, Brain JD, Wang N. The avian respiratory system: a unique model for studies of respiratory toxicosis and for monitoring air quality. *Environ Health Perspect.* 1997;105:188-200.
- [2] Sanderfoot OV, Holloway T. Air pollution impacts on avian species via inhalation exposure and associated outcomes. *Environ Res Lett.* 2017;12:083002.

- [3] Liang Y, Rudika I, Zou EY, Johnston A, Amanda D. Rodewald AD, et al. Conservation cobenefits from air pollution regulation: Evidence from birds. *Proceedings of the National Academy of Sciences USA*. 2020;117(49):30900-6.
- [4] Chowdhury R., Sarkar S, Nandy A, Talapatra SN. Assessment of bird diversity as bioindicators in two parks, Kolkata, India. *International Letters of Natural Sciences*. 2014;16:131-9.
- [5] Gatesire T, Nsabimana D, Nyiramana A, Seburanga JL, Mirville MO. Bird diversity and distribution in relation to urban landscape types in Northern Rwanda. *New Scientific World Journal*. 2014;2014:157824.
- [6] Stevenson T, Fanshawe J. *Field Guide to the Birds of East Africa: Kenya, Tanzania, Uganda, Rwanda, Burundi*. 1<sup>st</sup> edition, T&AD Poyser, London, UK, 2002.
- [7] Judd WS, Campbell CS, Kellogg EA, Stevens PF, Donoghue MJ. *Plant Systematics: A Phylogenetic Approach*, Sinauer Associates, Sunderland, Mass, USA, 3<sup>rd</sup> edition, 2008.
- [8] Singha Roy U, Purbasha Banerjee P, Mukhopadhyay SK. Study on avifaunal diversity from three different regions of North Bengal, India. *Asian Journal of Conservation Biology*. 2012; 1(2):120-9.
- [9] Das P, Aditya Bandyopadhyay S. A preliminary assessment of avifaunal diversity in and around Sarojini Naidu College campus, Kolkata, West Bengal, India. *International Journal of Fauna and Biological Studies*. 2016;3(2):56-61.
- [10] Mukhopadhyay S, Mazumdar S. Composition, diversity and foraging guilds of avifauna in a suburban area of southern West Bengal, India. *The Ring*. 2017;39:103-20.
- [11] Debnath S, Biswas S, Panigrahi AK. Present status and diversity of avian fauna in Purbasthali bird sanctuary, West Bengal, India. *Agric Sci Digest*. 2018;38(2):95-102.
- [12] Chowdhury S. Migratory wetland birds diversity in lower Chota Nagpur plateau with special reference to Purulia district, West Bengal, India. *Int J Adv Res*. 2020;8(10):357-67.
- [13] Li Z, Courchamp F, Blumstein DT. Pigeons home faster through polluted air. *Sci Rep*. 2016;6:1-6.
- [14] Roy Bhowmick S. Biodiversity assessment of bird species as bioindicators and the impact of air pollution on the ecological community. *International Journal of Pure and Applied Zoology*. 2021;9(2):18-25.
- [15] Ali S, Ripley SD. *Handbook of the Birds of India and Pakistan*. Oxford University Press. New Delhi, 1987.
- [16] Inskipp T, Lindsey N, Duckworth W. *An annotated checklist of the birds of the Oriental region*. Sandy, Bedfordshire, United Kingdom: Oriental Bird Club, 1996.
- [17] Grimmett R, Inskipp C, Inskipp T. *Pocket guide to the birds of the Indian subcontinent*. Oxford University Press, New Delhi, India, 1999.
- [18] Aynalem S, Bekele A. Species composition, relative abundance and distribution of bird fauna of riverine and wetland habitats of Infranz and Yiganda at Southern tip of Lake Tana, Ethiopia. *Trop Ecol*. 2008;49:199-209.
- [19] Shannon CE, Weiner W. *The Mathematical Theory of Communication*. Urbana, IL: University of Illinois Press, Urbana, 1949; 117 p.
- [20] Pielou EC. *The Measurement of Diversity in Different Types of Biological Collections*. *J Theore Biol*. 1966;3:131-44.
- [21] Margalef, R. *Perspectives in Ecological Theory*. Chicago II. University of Chicago Press, Chicago, 1968; 111 p.
- [22] Berger WH, & Parker FL. Diversity of planktonic foraminifera in deep-sea sediments. *Science*. 1970;168(3937):1345-7.
- [23] Stiling P. *Ecology: Theories and Applications* (3rd ed), Upper Saddle River, NJ: Prentice-Hall, Inc, 1999.
- [24] Hammer Ø, Harper DAT, Ryan PD. *PAST: Paleontological statistics software package for education and data analysis* *Palaeontologia Electronica*. 2001;4(1):9.
- [25] Marzluff, J M. Worldwide urbanization and its effects on birds. In: Marzluff JM, Bowman R, Donnelly R. (eds) *Avian Ecology and Conservation in an Urbanizing World*. Springer, Boston, MA, 2001; pp. 19-47.
- [26] Tanveer A, Shahzad M, Chaudhry AA. Avian fauna of Punjab University, Lahore. *Pak J Zool*. 2002;17:35-51.

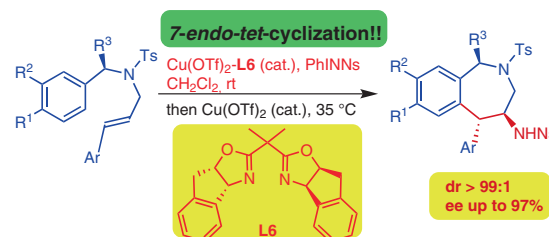


# Catalytic Enantioselective Synthesis of 4-Amino-5-aryltetrahydro-1*H*-benzo[*c*]azepines by an Aminoarylation Reaction

Sk Md Samim Akhtar<sup>1</sup>  
Saumen Hajra\*

Centre of Biomedical Research, Sanjay Gandhi Post-Graduate  
Institute of Medical Sciences Campus, Raebareilly Road, Lucknow  
226014, India  
Saumen.hajra@cblr.res.in  
saumen.hajra@gmail.com

Published as part of the Cluster  
Chemical Synthesis and Catalysis in India



Received: 26.05.2022

Accepted after revision: 28.07.2022

Published online: 28.07.2022 (Accepted Manuscript), 23.09.2022 (Version of Record)

DOI: 10.1055/a-1912-3285; Art ID: ST-2022-05-0230-C

**Abstract** A one-pot asymmetric aminoarylation reaction has been executed for the synthesis of *trans*-4-amino-5-aryltetrahydrobenzo[*c*]azepines with excellent diastereo- and enantioselectivity (*dr* > 99:1; *ee* ≤ 97%). The reaction progresses through aziridination of prochiral *N*-tosyl-*N*-cinnamylbenzylamines, followed by an intramolecular 7-*endo-tet* Friedel–Crafts cyclization of the tethered aziridines generated in situ, where the combination of Cu(OTf)<sub>2</sub> as a catalyst and PhINNs as a nitrene source was found to be effective. A chiral indenyl bis(oxazoline) was shown to be an efficient ligand for the catalytic enantioselective version of this one-pot transformation. This 7-*endo-tet* cyclization is contrary to the Baldwin cyclization rules.

**Key words** tetrahydrobenzazepines, asymmetric catalysis, aminoarylation, aziridines, Friedel–Crafts reaction, *endo-tet* cyclization

Nitrogen-containing heterocycles, such as azepines or their annulated variants, are ubiquitous structural motifs found in numerous natural and pharmaceutical products. However, tetrahydro-2-benzazepines remained an unprivileged class of heterocycles for a long period in medicinal and synthetic chemistry. Lately, this class of compounds has been found to elicit prominent biological activities, such as analgesic, antihypertensive, antitumor, and anti-Alzheimer's disease activities, among many others.<sup>2–7</sup> In particular, 4-amino-2-benzazepine<sup>3–6</sup> and 5-aryl-2-benzazepine motifs<sup>7</sup> are present in many compounds with profound bioactivities, such as compounds **A–F** (Figure 1). The dual ACE and NEP inhibitors AVE-7688 (Ilepatril) (**A**)<sup>3</sup> and MDL-100240 (**B**) are two advanced drug candidates for the potential treatment of hypertension and diabetic nephropathy.<sup>4</sup> The constrained dermorphin tetrapeptide analogue AN81 (**C**), a mixed  $\mu$ - $\delta$ -opioid agonist with subnanomolar binding affinity is a prospective analgesic. SBCHM01 (**D**) is a potent chimeric opioid agonist–neurokinin-1 antagonist for

the treatment of chronic pain.<sup>5</sup> Several reports state that the 5-aryltetrahydro-2-benzazepines **E** are HIV integrase inhibitors, antiarrhythmics, analgesics, or reuptake inhibitors of dopamine and serotonin, and powerful agents for the treatment of mental disorders and hypoxia.<sup>7</sup> Furthermore, the indolobenzazepin-7-one **F**, containing a 4-amino-5-aryl-2-benzazepine nucleus, was recently identified as having cytotoxic and antitumor properties as an inhibitor of tubulin polymerization.<sup>2,d,e</sup>

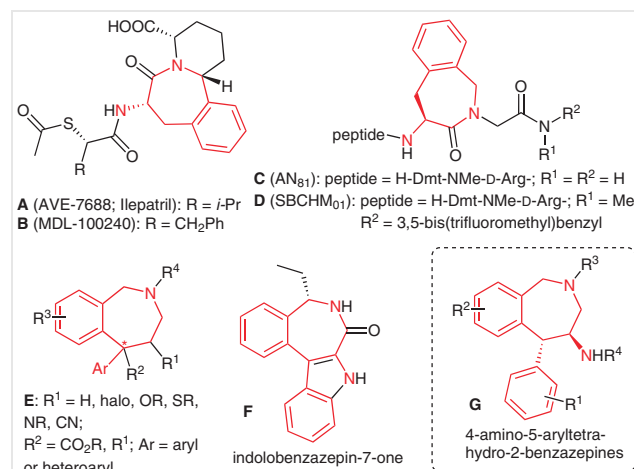
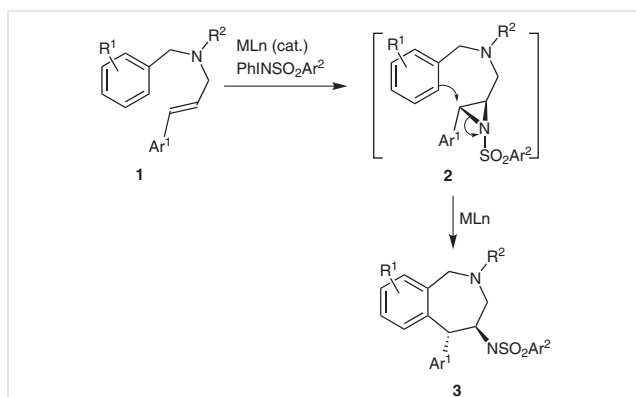


**Figure 1** Representative 4-amino- and 5-aryltetrahydro-2-benzazepine-motif-containing bioactive molecules

The promising pharmacological potential and the challenge of constructing the benzo-annulated seven-membered ring of tetrahydro-2-benzazepine heterocycles have recently attracted the attention of the synthetic community.<sup>8,9</sup> However, a catalytic asymmetric synthesis of tetrahydro-2-benzazepines, in particular, those having a vicinal 4-amino, 5-aryl unit, is still an unmet challenge.

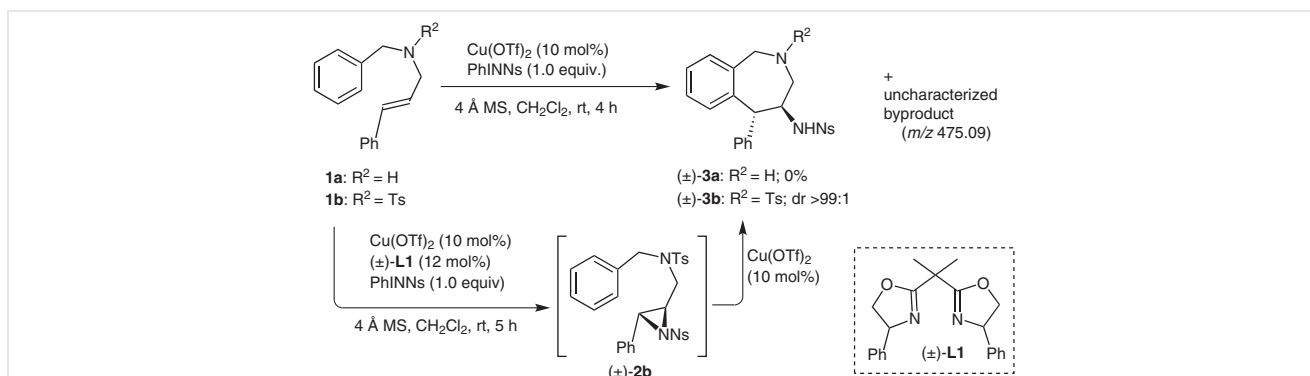
*N*-Benzyl-*N*-cinnamyl amines **1** were expected to generate the corresponding aziridines **2** by treatment with a suitable nitrene source. We envisioned a stereoselective intramolecular Friedel–Crafts cyclization of the in-situ-generated tethered aziridines **2** to give the tetrahydro-2-benzazepines **3** (Scheme 1), although such 7-*endo-tet* cyclizations have been rarely reported in the literature<sup>9f</sup>. Moreover, Baldwin's cyclization rules for the opening of three-membered rings to form cyclic structures seem to lie between those for tetrahedral and trigonal systems, with *exo*-modes being generally preferred.<sup>9a</sup> We hoped that a suitable chiral catalyst would also induce enantioselectivity in this overall process. Here, we report a highly efficient catalytic and enantioselective one-pot synthesis of *trans*-4-amino-5-aryltetrahydro-2-benzazepines **3** with high diastereo- (>99:1) and enantioselectivities (up to 97% ee) through an aminoarylation reaction.



**Scheme 1** Proposed 7-*endo-tet*-aminoarylation reaction

Iminoiodinanes and Lewis acids are routinely paired for aziridination of alkenes, and have been used for decades.<sup>10</sup> The couple's application in stereoselective aziridination reactions has been recently studied in our laboratory.<sup>11</sup> We found that the nitrenoid reagent PhINNs (Ns = nosyl), in combination with  $\text{Cu}(\text{OTf})_2$ , is an ideal precursor of a nitrene for delivery to an olefinic unit. Lewis acids such

as  $\text{Cu}(\text{OTf})_2$ , which can serve as dual-purpose catalysts, were expected to be effective in Friedel–Crafts reactions. At the outset, we employed the PhINNs– $\text{Cu}(\text{OTf})_2$  couple in the reaction of *N*-cinnamylbenzylamine (**1a**) under well-established conditions. Amine **1a** (5.0 equiv) was treated with PhINNs (1.0 equiv) in the presence of 0.1 equivalent of  $\text{Cu}(\text{OTf})_2$  catalyst and molecular sieves (MS 4Å) in  $\text{CH}_2\text{Cl}_2$  at room temperature (25 °C) (Scheme 2). However, this led to an intractable mixture, possibly as a result of the presence of the bare –NH group. It is reasonable to conclude that substrates with an exchangeable proton do not undergo the required reaction. Consequently, *N*-protection appeared to be inevitable to eliminate this issue. Accordingly, we planned to exploit the chemistry starting from *N*-tosyl-*N*-cinnamylbenzylamine (**1b**) under the aforementioned conditions at room temperature. Complete dissolution of the nitrenoid reagent required only four hours. Analysis of the reaction mixture after column chromatography revealed the formation of the expected 4-amino-5-phenyltetrahydro-2-benzazepine [(±)-**3b** ( $m/z$  600.12 [ $M + \text{Na}$ ]<sup>+</sup>)] with >99:1 diastereoselectivity in 69% yield, along with a considerable amount of an uncharacterized byproduct ( $m/z$  = 475.09), but with no trace of the aziridine (±)-**2b**. A detailed spectral analysis also confirmed that the cyclized product was *trans*-4-amino-5-phenyltetrahydro-2-benzazepine [(±)-**3b**]. Introduction of the phenyl BOX ligand (±)-**L1** into the reaction afforded aziridine (±)-**2b** exclusively, but a further attempt at a one-pot cyclization of the in-situ-generated aziridine (±)-**2b** with a supplementary amount of  $\text{Cu}(\text{OTf})_2$  gave a similar result to that of the reaction without ligand (±)-**L1**. These observations suggested that the reaction needed to be optimized at the Friedel–Crafts cyclization step. Hence, aziridine (±)-**2b** was prepared by an aziridination reaction in the presence of ligand (±)-**L1** and isolated by column chromatography. A spectral analysis confirmed its structure to be that of the *trans*-aziridine (±)-**2b**. A number of metal catalysts were screened under various conditions [for details, see the Supporting Information (SI); Table S1]. Ultimately  $\text{Cu}(\text{OTf})_2$  at the slightly elevated temperature of 35



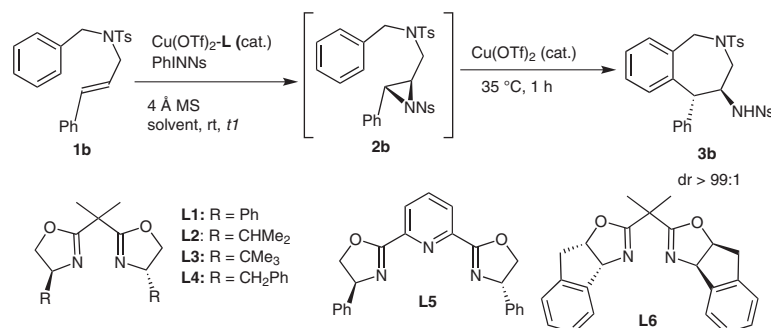
**Scheme 2** One-pot aminoarylation reaction of **1** using  $\text{Cu}(\text{OTf})_2$  catalyst with and without a ligand

°C was found to suppress the formation of the noncharacterized byproduct and afforded an excellent yield (91%) of the desired tetrahydrobenzazepine ( $\pm$ )-**3b**.

Meanwhile, it was evident that a nonracemic synthesis of *trans*-4-amino-5-aryltetrahydro-2-benzazepines **3b** could be achieved by the introduction of chiral copper(II) catalyst into the reaction with subsequent tuning. Consequently, we chose to investigate several chiral bisoxazoline (Box) ligand-chelated copper catalysts for enantioinduction in the reaction (Table 1). The bisoxazoline ligand **L1** was included in an aziridination reaction that provided aziridine **2b** as the sole product after five hours. One-pot treatment of **2b** with a supplementary amount of Cu(OTf)<sub>2</sub> at 35 °C took one hour to give the desired product **3b** with 69% ee in 71% yield (Table 1, entry 1). With the sterically demanding *tert*-butylbisoxazoline **L3**, there was no improvement in the yield (69%), but the ee dropped significantly to 32% (entry 3). A similar yield and selectivity were obtained in aminoarylation in the presence of the isopropyl bisoxazoline ligand **L2** (entry 2). Unlike the phenyl bisoxazoline ligand **L1**, the benzyl bisoxazoline ligand **L4** showed poor selectivity

(15%), even though it gave a better yield (entry 4). The Py-Box ligand **L5**, derived from *L*-phenylglycine, gave a maximum yield of 89% but provided no selectivity (entry 5). The bisoxazoline ligand **L6**, derived from (1*R*, 2*S*)-1-aminoin-dan-2-ol gave an improved yield and the highest enantioselectivity, and it was recognized as being the most suitable ligand (entry 6). Notably, unlike the phenyl rings on the oxazoline units in the phenyl Box ligand **L1**, those in the indenyl Box ligand **L6** are attached through an extra methylene bridge, which brings more rigidity to the structure. This structural strength of the indenyl Box ligand **L6** is responsible for providing the excellent enantioinduction. The absolute stereochemistry of the *trans*-cyclized product **3b** was assigned by analogy with reports in the literature.<sup>10,11</sup> After our search for an effective chiral catalyst, we screened several solvents. Halogenated solvents such as CHCl<sub>3</sub> and DCE gave decent selectivities in the series (entries 7 and 8), but CH<sub>2</sub>Cl<sub>2</sub> remained the ideal choice, as it provided the highest yield of 81% and the highest enantioselectivity of 96%. CH<sub>3</sub>CN also provided a moderate yield (77%), but a lower enantioselectivity (42%) (entry 9). The enantiomeric

**Table 1** Optimization of the Reaction Conditions for the One-Pot Catalytic Asymmetric Aminoarylation Reaction<sup>a</sup>



	Ligand	Solvent	Time <sup>b</sup> (h)	Yield <sup>c</sup> (%) of <b>3b</b>	ee <sup>d</sup> (%) of <b>3b</b>
1	<b>L1</b>	CH <sub>2</sub> Cl <sub>2</sub>	5	71	69 <sup>e</sup>
2	<b>L2</b>	CH <sub>2</sub> Cl <sub>2</sub>	5	58	29 <sup>e</sup>
3	<b>L3</b>	CH <sub>2</sub> Cl <sub>2</sub>	5	69	32 <sup>e</sup>
4	<b>L4</b>	CH <sub>2</sub> Cl <sub>2</sub>	5	80	15 <sup>e</sup>
5	<b>L5</b>	CH <sub>2</sub> Cl <sub>2</sub>	7	89	0
6	<b>L6</b>	CH <sub>2</sub> Cl <sub>2</sub>	5	81	96
7	<b>L6</b>	CHCl <sub>3</sub>	5	62	93
8	<b>L6</b>	DCE	5	59	88
9	<b>L6</b>	CH <sub>3</sub> CN	3	77	42
10	<b>L6</b>	C <sub>6</sub> H <sub>6</sub>	5	50	64

<sup>a</sup> Reaction conditions: Substrate **1b** (5 equiv), PhINNs (1.0 equiv), Box-Cu(II) complex [derived from Cu(OTf)<sub>2</sub> (10 mol%) and Box ligand **L** (12 mol%)], solvent, stirring at rt until complete dissolution of the nitrenoid reagent, then additional Cu(OTf)<sub>2</sub> (10 mol%), 35 °C, 1–2 h.

<sup>b</sup> Time for the aziridine formation.

<sup>c</sup> Isolated yield of **3b** after flash column chromatography.

<sup>d</sup> Determined by HPLC on a Chiralcel IA-3 column.

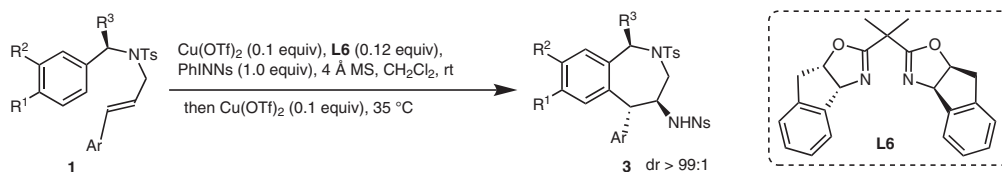
<sup>e</sup> The other enantiomer was formed predominantly.

leakage can be attributed to the high ligating affinity of the solvent molecules. The yield and selectivity did not improve in benzene (entry 10).

Earlier, it has been established that the enantioselectivity originates in the aziridination step and that the stereochemistry of the intermediate aziridine is relayed to the cyclized product.<sup>11b-h</sup> On this basis, we have previously accomplished asymmetric syntheses of dopamine D1 agonists (A-86929<sup>11c</sup> and dihydrexidine<sup>11d</sup>) and an antagonist (ecopipam<sup>11e</sup>), confirming the assigned absolute stereochemistry of both the newly generated stereocenters. Furthermore, Lewis acid-catalyzed intermolecular nucleophilic ring-opening reactions of chiral 2-arylaziridines mostly follow an S<sub>N</sub>2-type mechanism with inversion of configuration at the benzylic center affording a high stereoselectivity of the product.<sup>12</sup> Intramolecular nucleophilic ring-opening reactions of chiral 1,2-disubstituted aziridines also follow a similar S<sub>N</sub>2-type mechanism, providing excellent *trans*-diastereoselectivity (dr >99:1) irrespective of the ring size.<sup>11</sup> As in the earlier reports,<sup>11</sup> the other stereocenter of the aziridine in the present reaction remained undisturbed, affording an excellent diastereoselectivity of the cyclized product (dr > 99:1), so that the absolute configuration of the *trans*-cyclized product **3b** could be deduced by analogy.<sup>10,11</sup>

Having identified the optimal conditions for the catalytic enantioselective aziridination with the Cu(OTf)<sub>2</sub> catalyst and (1*R*, 2*S*)-1-aminoindan-2-ol-derived bis(oxazoline) ligand **L6** and the subsequent Friedel–Crafts cyclization of the in-situ-generated aziridine with additional Cu(OTf)<sub>2</sub>, we continued to investigate the scope of this one-pot protocol for the asymmetric synthesis of the *trans*-tetrahydro-2-benzazepine derivatives **3** (Table 2).<sup>13</sup> Substrates **1c** and **1i**, having electron-deficient aromatic rings at either end, experienced a slightly slower reaction but gave moderate yields of the cyclized products **3c** and **3i** (71 and 72%), respectively, and an excellent 95% enantioselectivity in both cases (Table 2; entries 2 and 8). Substrates **1d**, **1f**, and **1g**, containing electron-rich aromatic rings at either end, underwent faster reactions and provided improved yields of **3d**, **3f**, and **3g**, with enantioselectivities of 96, 97, and 96% respectively (Table 2, entries 3, 5, and 6). The electron-rich substrates **1e** and **1h**, in which both aromatic rings carried electron-rich methoxy substituents, underwent similar smooth reactions to afford the corresponding products in excellent yields and high ee values (entries 4 and 7). Substrates **1f** and **1g**, with a piperonyl ring (entries 5 and 6), gave the corresponding cyclized products directly at rt in the shortest reaction time without any halt at the corresponding aziridine intermediate; the reaction of substrate **1f** registered the highest yield and enantioselectivity (entry 5). Because of the electron-deficient nature of substrate **1c**,

**Table 2** Catalytic Asymmetric Aminoarylation for One-Pot Synthesis of *trans*-4-Amino-5-arylhexahydrobenzo[*c*]azepines **3**<sup>a,12</sup>



Entry	<b>1</b>	R <sup>1</sup> , R <sup>2</sup>	R <sup>3</sup>	Ar	Time <sup>b</sup> (h)	Product	Yield <sup>c</sup> (%)	ee <sup>d</sup> (%)
1	<b>1b</b>	H, H	H	Ph	6	<b>3b</b>	81	96
2 <sup>e</sup>	<b>1c</b>	F, H	H	4-FC <sub>6</sub> H <sub>4</sub>	10	<b>3c</b>	71	95
3	<b>1d</b>	H, OMe	H	4-MeC <sub>6</sub> H <sub>4</sub>	4	<b>3d</b>	84	96
4	<b>1e</b>	H, OMe	H	2-MeOC <sub>6</sub> H <sub>4</sub>	2	<b>3e</b>	83	87
5 <sup>f</sup>	<b>1f</b>	OCH <sub>2</sub> O	H	1-naphthyl	2	<b>3f</b>	87	97
6 <sup>f</sup>	<b>1g</b>	OCH <sub>2</sub> O	H	4-ClC <sub>6</sub> H <sub>4</sub>	2	<b>3g</b>	80	96
7	<b>1h</b>	OMe, H	H	3-MeOC <sub>6</sub> H <sub>4</sub>	4	<b>3h</b>	78	96
8	<b>1i</b>	OMe, H	H	4-FC <sub>6</sub> H <sub>4</sub>	7	<b>3i</b>	72	95
9	<b>1j</b>	H, H	Me	4-MeC <sub>6</sub> H <sub>4</sub>	6	<b>3j</b>	69	86

<sup>a</sup> Reaction conditions: **1** (5 equiv), PhINNs (1.0 equiv), Box-Cu(II) complex (derived from 10 mol% Cu(OTf)<sub>2</sub> and 12 mol% Box ligand **L6**), CH<sub>2</sub>Cl<sub>2</sub>, stirring at rt until complete dissolution of the nitrenoid reagent, then additional Cu(OTf)<sub>2</sub> (10 mol%), 35 °C, 1–2 h.

<sup>b</sup> Total time, including aziridine formation and subsequent cyclization.

<sup>c</sup> Isolated yield of **3** after flash column chromatography.

<sup>d</sup> Determined from HPLC on chiralpak IA 3 or IB 3 or IC 3 columns.

<sup>e</sup> Because of its electron-deficient nature, the corresponding aziridine did not cyclize in one pot. The reaction mixture was filtered through a short plug of silica gel and concentrated; the semicrude reaction mixture was then subjected to Friedel–Crafts cyclization with additional Cu(OTf)<sub>2</sub> in CH<sub>2</sub>Cl<sub>2</sub>.

<sup>f</sup> Compounds **1f** and **1g** gave the cyclized product **3f** and **3g** in one pot without the use of additional Cu(OTf)<sub>2</sub> at rt.



the corresponding aziridine **2c** did not cyclize in one pot. We therefore filtered the reaction solution through a short plug of silica gel and then processed the semicrude reaction mixture for Friedel–Crafts cyclization with additional  $\text{Cu}(\text{OTf})_2$ . Due to the presence of a preinstalled chiral center, substrate **1j** was expected to be a challenging one; however, the optimized chiral induction efficiently furnished a single diastereomer ( $\text{dr} > 99:1$ ) of the cyclized product **3j**. In terms of reactivity, substrate **1j** was comparable with **1b**, and therefore provided the desired product **3j** in good yield and selectivity (69% and 86%, respectively) (entry 9).

To support the seven-membered benzo[*c*]azepine structure **3** from the 7-*endo-tet* Friedel–Crafts cyclization, 2D NMR spectroscopic experiments (COSY and HMBC) of compound **3g** were carried out. The COSY spectrum defines all the  $^1\text{H}$ – $^1\text{H}$  couplings assigned to the product. The HMBC spectrum contained three two-bond-coupling peaks [H(e)–5–11, H(e)–5–16, and H(e)–5–4] of the dibenzylic proton [H(e)] (Figure 2), thereby confirming the seven-membered structural feature of *trans*-4-amino-5-aryltetrahydro-2-benzazepines **3** (for details, see SI).

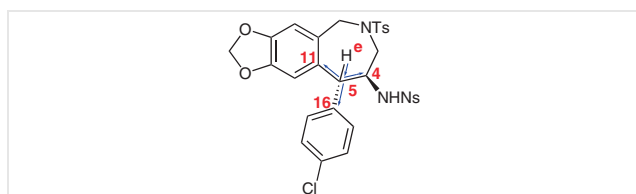


**Figure 2** HMBC two-bond couplings of compound **3g**

In summary, we have developed a highly efficient, one-pot, asymmetric synthesis of 4-amino-5-aryltetrahydrobenzo[*c*]azepines with excellent diastereo- and enantioselectivity ( $\text{dr} > 99:1$ ;  $\text{ee} \leq 97\%$ ). Catalytic enantioselective aziridination of the cinnamyl unit of *N*-sulfonyl-*N*-cinnamylbenzylamines and subsequent regio- and stereoselective 7-*endo-tet* Friedel–Crafts cyclization of tethered benzyl unit provides an excellent method. However, this 7-*endo-tet*-cyclization is contrary to Baldwin's cyclization rules. The developed protocol might open up a new avenue in tetrahydrobenzo[*c*]azepine-based medicinal and drug-discovery chemistry.

## Conflict of Interest

The authors declare no conflict of interest.

## Funding Information

This work was supported by SERB grants (Nos. SR/S1/OC-97/2012 and CRG/2020/000650).

## Supporting Information

Supporting information for this article is available online at <https://doi.org/10.1055/a-1912-3285>.

## References and Notes

- (1) Present address: Department of Chemistry, Bidhan Chandra College, Asansol-713304, India
- (2) (a) Xia, W.; Spector, S.; Hardy, L.; Zhao, S.; Saluk, A.; Alemane, L.; Spector, N. L. *Proc. Natl. Acad. Sci. U. S. A.* **2000**, *97*, 7494. (b) Spector, S.; Spector, N. L. US 6277844, **2001**. (c) Al-Qawasmeh, R. A.; Lee, Y.; Cao, M.-Y.; Gu, X.; Viau, S.; Lightfoot, J.; Wright, J. A.; Young, A. H. *Bioorg. Med. Chem. Lett.* **2009**, *19*, 104. (d) Keller, L.; Beaumont, S.; Liu, J.-M.; Thoret, S.; Bignon, J. S.; Wdzieczak-Bakala, J.; Dauban, P.; Dodd, R. H. *J. Med. Chem.* **2008**, *51*, 3414. (e) Pons, V.; Beaumont, S.; Tran Huu Dau, M. E.; Iorga, B. I.; Dodd, R. H. *ACS Med. Chem. Lett.* **2011**, *2*, 565. (f) Zhan, G.; Zhou, J.; Liu, R.; Liu, T.; Guo, G.; Wang, J.; Xiang, M.; Xue, Y.; Luo, Z.; Zhang, Y.; Yao, G. *J. Nat. Prod.* **2016**, *79*, 760. (g) Scott, L. J.; Goa, K. L. *Drugs* **2000**, *60*, 1095. (h) Grunewald, G. L.; Dahanukar, V. H.; Criscione, K. R. *Bioorg. Med. Chem.* **2001**, *9*, 1957. (i) Grunewald, G. L.; Caldwell, T. M.; Li, Q.; Criscione, K. R. *J. Med. Chem.* **2001**, *44*, 2849. (j) Bradshaw, B.; Evans, P.; Fletcher, J.; Lee, A. T. L.; Mwashimba, P. G.; Oehlich, D.; Thomas, E. J.; Davies, R. H.; Allen, B. C. P.; Broadley, K. J.; Hamrouni, A.; Escargueil, C. *Org. Biomol. Chem.* **2008**, *6*, 2138. (k) Miller, W. H.; Alberts, D. P.; Bhatnagar, P. K.; Bondinell, W. E.; Callahan, J. F.; Calvo, R. R.; Cousins, R. D.; Erhard, K. F.; Heerding, D. A.; Keenan, R. M.; Kwon, C.; Manley, P. J.; Newlander, K. A.; Ross, S. T.; Samanen, J. M.; Uzinskas, I. N.; Venslavsky, J. W.; Yuan, C.-K.; Haltiwanger, R. C.; Gowen, M.; Hwang, S.-M.; James, I. E.; Lark, M. W.; Rieman, D. J.; Stroup, G. B.; Azzarano, L. M.; Salyers, K. L.; Smith, B. R.; Ward, K. W.; Johanson, K. O.; Huffman, W. F. *J. Med. Chem.* **2000**, *43*, 22. (l) Clark, M. T.; Chang, J.; Navran, S. S.; Hoozor-Akbar, ; Mukhopadhyay, A.; Amin, H.; Feller, D. R.; Miller, D. D. *J. Med. Chem.* **1986**, *29*, 181. (m) Dalence-Guzman, M. F.; Berglund, M.; Skogvall, S.; Sterner, O. *Bioorg. Med. Chem.* **2008**, *16*, 2499. (n) Berglund, M.; Dalence-Guzman, M. F.; Skogvall, S.; Sterner, O. *Bioorg. Med. Chem.* **2008**, *16*, 2513.
- (3) (a) Tabrizchi, R. *Curr. Opin. Invest. Drugs (BioMed Cent.)* **2008**, *9*, 301. (b) Schäfer, S.; Steioff, K.; Linz, W.; Bleich, M.; Busch, A. E.; Löhn, M. *Eur. J. Pharmacol.* **2004**, *484*, 361. (c) Gross, O.; Koepke, M.-L.; Beirovski, B.; Schulze-Lohoff, M.; Segerer, S.; Weber, M. *Kidney Int.* **2005**, *68*, 456.
- (4) (a) Burnier, M. *Curr. Opin. Invest. Drugs (BioMed Cent.)* **2001**, *10*, 1957. (b) Rossi, G. P. *Cardiovasc. Drug Rev.* **2003**, *21*, 51.
- (5) (a) Vandormael, B.; Furla, D.-D.; Gramowski-Voß, A.; Kosson, P.; Weiss, D. G.; Schröder, O. H.-U.; Lipkowski, A.; Georgoussi, Z.; Tourwé, D. *J. Med. Chem.* **2011**, *54*, 7848. (b) Ballet, S.; Feytens, D.; Buysse, K.; Chung, N. N.; Tumati, S.; Keresztes, A.; Van Duppen, J.; Lai, J.; Varga, F.; Porreca, F.; Schiller, P. W.; Vanden Broeck, J.; Tourwé, J. *J. Med. Chem.* **2011**, *54*, 2467; and references cited therein.
- (6) (a) Flynn, G. A.; Giroux, E. L.; Dage, R. C. *J. Am. Chem. Soc.* **1987**, *109*, 7914. (b) Flynn, G. A.; Beight, D. W.; Huber, E. W.; Bey, P. *Tetrahedron Lett.* **1990**, *31*, 815. (c) Warshawsky, A. M.; Flynn, G. A.; Koehl, J. R.; Mehdi, S.; Vaz, R. J. *Bioorg. Med. Chem. Lett.* **1996**, *6*, 957. (d) Le Diguarher, T.; Ortuno, J.-C.; Shanks, D.; Guilbaud, N.; Pierré, A.; Raimbaud, E.; Fauchere, J.-L.; Hickman, J. A.; Tucker, G. C.; Casara, P. J. *Bioorg. Med. Chem. Lett.* **2004**, *14*, 767.

- (7) (a) Lafemina, R. L.; Young, S. D. GB 2271566 A, **1992**. (b) Johnson, R. E.; Busacca, C. A. US 5098901, **1991**. (c) Sherlock, M. H. US 3225031, **1963**. (d) Sherlock, M. H. US 3242164, **1966**. (e) Masatoshi, B.; Kenji, M.; Yutaka, B.; Noriyuki, I.; Mikio, H.; Hajime, F.; Eiichi, S. JP 5913761, **1984**. (f) Molino, B. F.; Liu, S.; Sambandam, A.; Guzzo, P. R.; Hu, M.; Zha, C.; Nacro, K.; Manning, D. D.; Isherwood, M. L.; Fleming, K. N.; Cui, W.; Olson, R. E. WO2007011820, **2007**. (g) Gámez-Montaña, R.; Chávez, M. I.; Roussi, G.; Cruz-Almanza, R. *Tetrahedron Lett.* **2001**, *42*, 9.
- (8) (a) Kamimura, A.; Taguchi, Y. *Tetrahedron Lett.* **2004**, *45*, 2335. (b) Van den Eynde, I.; Van Rompaey, K.; Lazzaro, F.; Tourwé, D. *J. Comb. Chem.* **2004**, *6*, 468. (c) Vieira, T. O.; Alper, H. *Org. Lett.* **2008**, *10*, 485. (d) Nandakumar, A.; Kiruthika, S. E.; Naveen, K.; Perumal, P. T. *Org. Biomol. Chem.* **2014**, *12*, 876. (e) Hu, Y.; Huang, H. *Org. Lett.* **2017**, *19*, 5070. (f) Pandey, A. K.; Han, S. H.; Mishra, N. K.; Kang, D.; Lee, S. H.; Chun, R.; Hong, S.; Park, J. S.; Kim, I. S. *ACS Catal.* **2018**, *8*, 742.
- (9) (a) Baldwin, J. E. *J. Chem. Soc., Chem. Commun.* **1976**, 732. (b) Dumoulin, D.; Lebrun, S.; Couture, A.; Deniau, E.; Grandclaudeon, P. *Tetrahedron: Asymmetry* **2010**, *21*, 195. (c) So, M.; Kotake, T.; Matsuura, K.; Inui, M.; Kamimura, A. *J. Org. Chem.* **2012**, *77*, 4017. (d) Allin, S. M.; Towler, J. M. R.; Elsegood, M. R. J.; Saha, B.; Bulman Page, P. C. *Synth. Commun.* **2012**, *42*, 872. (e) Quick, M. P.; Fröhlich, R.; Schepmann, D.; Wünsch, B. *Org. Biomol. Chem.* **2015**, *13*, 7265. (f) Palillero-Cisneros, A.; Gordillo-Guerra, P. G.; Aparicio-Solano, D. M.; Gnecco, D.; Mendoza, A.; Juárez, J. R.; Terán, J. L. *Tetrahedron: Asymmetry* **2015**, *26*, 95.
- (10) (a) Evans, D. A.; Faul, M. M.; Bilodeau, M. T. *J. Org. Chem.* **1991**, *56*, 6744. (b) Evans, D. A.; Faul, M. M.; Bilodeau, M. T.; Anderson, B. A.; Barnes, D. M. *J. Am. Chem. Soc.* **1993**, *115*, 5328. (c) Evans, D. A.; Faul, M. M.; Bilodeau, M. T. *J. Am. Chem. Soc.* **1994**, *116*, 2742.
- (11) (a) Hajra, S.; Maji, B.; Sinha, D.; Bar, S. *Tetrahedron Lett.* **2008**, *49*, 4057. (b) Hajra, S.; Maji, B.; Mal, D. *Adv. Synth. Catal.* **2009**, *351*, 859. (c) Hajra, S.; Bar, S. *Chem. Commun.* **2011**, *47*, 3981. (d) Hajra, S.; Bar, S. *Tetrahedron: Asymmetry* **2011**, *22*, 775. (e) Hajra, S.; Bar, S. *Tetrahedron: Asymmetry* **2012**, *23*, 151. (f) Hajra, S.; Sinha, D. *J. Org. Chem.* **2011**, *76*, 7334. (g) Hajra, S.; Akhtar, S. M. S.; Aziz, S. M. *Chem. Commun.* **2014**, *50*, 6913. (h) Akhta, S. M. S.; Bar, S.; Hajra, S. *Tetrahedron* **2022**, *103*, 132257.
- (12) For reviews, see: (a) Hu, X. E. *Tetrahedron* **2004**, *60*, 2701. (b) Singh, G. S.; Sudheesh, S.; Keroletswe, N. *ARKIVOC* **2018**, (i), 50. (c) Talukdar, R.; Saha, A.; Ghorai, M. K. *Isr. J. Chem.* **2016**, *56*, 445. For selected examples see: (d) Bhattacharyya, A.; Shahi, C. K.; Pradhan, S.; Ghorai, M. K. *Org. Lett.* **2018**, *20*, 2925. (e) Pradhan, S.; Chauhan, N.; Shahi, C. K.; Bhattacharyya, A.; Ghorai, M. K. *Org. Lett.* **2020**, *22*, 7903. (f) Tarannum, S.; Sk, S.; Das, S.; Wani, I. A.; Ghorai, M. K. *J. Org. Chem.* **2020**, *85*, 367.
- (13) **4-Amino-5-aryltetrahydro-2-benzazepines 3b-j; General Procedure**  
A two-necked, 25 mL, round-bottomed flask was charged with the Box ligand (1R,2S)-**L6** (0.011 g, 0.03 mmol, 0.12 equiv) and Cu(OTf)<sub>2</sub> (0.009 g, 0.025 mmol, 0.1 equiv). Anhyd CH<sub>2</sub>Cl<sub>2</sub> (1.2 mL) was added by syringe, and the resulting mixture was stirred for 30 min at rt. To this solution were added substrate **1** (0.467 g, 1.23 mmol, 5.0 equiv) in CH<sub>2</sub>Cl<sub>2</sub> (1.2 mL), PhINNs (0.1 g, 0.24 mmol, 1.0 equiv), and powered 4Å MS (0.2 g) and the mixture stirred at rt under argon. As soon as all the nitrenoid reagents were dissolved, additional Cu(OTf)<sub>2</sub> (0.007 g, 0.01 mmol, 0.1 equiv) was added to the reaction medium, which was then stirred at 35 °C under argon. The reaction, which was completed within 1 h, was quenched by dilution with EtOAc (10 mL). The mixture was then filtered through a short plug of silica gel that was washed with additional EtOAc (10 mL). The filtrate was concentrated by rotary evaporation under reduced pressure to give a crude mass that was purified by flash column chromatography (silica gel, EtOAc–hexane).  
**N-((4S,5R)-5-Phenyl-2-tosyl-2,3,4,5-tetrahydro-1H-2-benzazepin-4-yl)-4-nitrobenzenesulfonamide (3b)**  
White solid; yield: 91% (96% ee); mp 164–166 °C; [α]<sub>D</sub><sup>28</sup> –137 (c 0.30, CH<sub>2</sub>Cl<sub>2</sub>). HPLC [Daicel Chiralpak IA-3, hexane–EtOAc (60:40), 1.0 mL/min, λ = 254 nm]: t<sub>major</sub> = 6.1 min, t<sub>minor</sub> = 7.2 min. <sup>1</sup>H NMR (400 MHz, CDCl<sub>3</sub>): δ = 8.12 (d, J = 9.2 Hz, 2 H), 7.62 (d, J = 8.0 Hz, 2 H), 7.52 (d, J = 8.8 Hz, 2 H), 7.34 (d, J = 8.0 Hz, 2 H), 7.27–7.25 (m, 3 H), 7.19–7.17 (m, 3 H), 7.10 (d, J = 6.8 Hz, 4 H), 5.03 (d, J = 9.2 Hz, 1 H), 4.99–4.96 (m, 1 H), 4.34 (d, J = 9.2 Hz, 1 H), 3.86 (d, J = 10.8 Hz, 1 H), 3.24 (dd, J = 10.0, 2.0 Hz, 1 H), 3.18–3.14 (m, 1 H), 2.49 (s, 3 H). <sup>13</sup>C NMR (100 MHz, CDCl<sub>3</sub>): δ = 150.0, 144.6, 143.8, 140.5, 139.5, 132.9, 129.9, 128.9, 128.6, 128.5, 128.4, 128.3, 128.2, 127.7, 127.4, 127.1, 124.2, 62.9, 62.2, 53.8, 49.4, 21.6. DEPT-135 NMR (100 MHz, CDCl<sub>3</sub>): δ = 130.4, 129.4, 129.2, 129.1, 129.0, 128.7, 128.6, 128.1, 127.9, 127.5, 124.6, 63.3, 62.7, 54.2, 49.9, 22.0. ESI-MS: m/z [M + Na]<sup>+</sup> calcd for C<sub>29</sub>H<sub>27</sub>N<sub>3</sub>NaO<sub>6</sub>S<sub>2</sub>: 600.1239; found: 600.1238.

To Whom It May Concern

To

Dr. Amit BANERJEE, Ph.D.,

Principal Investigator, Microsystem Design-Integration Lab;

Assistant Professor, Bidhan Chandra College, West Bengal, INDIA;

Reference: Consulting Project with Organic Electronics Research Center (OERC), Ming Chi University of Technology, New Taipei City, Taiwan from 1st January, 2021- 31<sup>st</sup> December, 2023

Subject: Certificate of Completion

Dear Dr. Banerjee,

With reference to details mentioned above, we are pleased to provide you the certificate of satisfactory completion of our consulting project from 2021-2023 with Ming Chi University of Technology, New Taipei City, Taiwan.

As token of our gratitude, a consultation fee of 24000 NTD will be transferred to your institutional account, further disbursement of the same may be carried out according to your institutional and/or local tax norms.

We very much appreciate your support and opportunity to interact, guiding and advising in your domain of expertise in microelectronic technologies and devices.

With best regards,

Dr. Sajal Biring

Associate Professor, Department of Electronic Engineering

Head of research division

Organic Electronic Research Center

Ming Chi University of Technology

## Certificate of Appointment

*Certificate No. 001-2022*

*Date of Issue: 01/01/2022*

To

Dr. Amit Banerjee

Assistant Professor

Physics Department, Bidhan Chandra College

Kazi Nazrul University

Asansol, West Bengal, 713303, India

This certificate of appointment is hereby granted to you for the position as an adjunct research fellow in the Organic Electronics Research Center, Ming Chi University of Technology, New Taipei City, Taiwan due to your outstanding academic achievements. The appointment term is for one year starting from 1<sup>st</sup> January, 2022 till 31<sup>st</sup> December, 2023.

Director *Shan-Wei Liu*

Organic Electronics Research Center  
Ming Chi University of Technology



**Date:** 24/06/2022

**Venue:** Conference Room 2, CQuERE, TCG CREST

**Members:**

1. Prof. B.P. Das (Director, CQuERE, TCG CREST)
2. Prof. B.N. Dev (Professor, CQuERE, TCG CREST)
3. Prof. H. Inokawa (Professor, Research Institute of Electronics, Shizuoka University, Japan)
4. Prof. Amit Banerjee (Principal Investigator, Microsystem Design-Integration Lab/Assist. Prof. BC College)
5. Prof. S. Prasanna (Asst. Professor, CQuERE, TCG CREST)
6. Dr. T. Basu (Research Scientist, CQuERE, TCG CREST)
7. Ms. P. Chakraborty (Administrator, CQuERE, TCG CREST)

**Meeting minutes:**

1. Prof. Das has presented a few slides on the activities in CQuERE
2. Dr. Basu introduced Prof. Inokawa and the rest of the participants
3. Dr. Basu presented some ideas on the integrated photonic circuits platform and how it can be used for sensing and computation.
4. The possibility of international collaboration with the Research Institute for Electronics, Shizuoka University has been discussed.
5. Being an expert in the CMOS fabrication process and single-photon detectors, Prof. Inokawa has assured to extend his support for developing an integrated photonic circuit platform. The Research Institute of Electronics may provide know-how and fab support for the Integrated Photonics initiative on a long-term collaboration basis further supported by Microsystem Design-Integration design facility by Dr. Banerjee.
6. Possibility of organizing an international conference on integrated photonics has been discussed. Prof. Inokawa has agreed to visit India during the conference.
7. Dr. Banerjee has proposed a state-of-the-art corporate lab based on his preliminary discussions with High-Tech semiconductor corporations in Japan and Singapore.

# Review on the Evolution of 6G and Terahertz Communication for Highspeed Information Processing

Pia Sarkar<sup>a</sup>, Arijit Saha<sup>a</sup>, Aditya Banerjee<sup>b</sup>, Amit Banerjee<sup>c, \*</sup> (ORCID: 0000-0001-9612-4523), A. Y. Seteikin<sup>d, e</sup>, and I. G. Samusev<sup>e</sup> (ORCID: 0000-0001-5026-7510)

<sup>a</sup> B.P. Poddar Institute of Management and Technology, Kolkata, 700052 India

<sup>b</sup> Amity Institute of Applied Science, Amity University, Noida, 201301 India

<sup>c</sup> Physics Department, Bidhan Chandra College, Asansol, 713303 India

<sup>d</sup> Amur State University, Blagoveshchensk, 675027 Russia

<sup>e</sup> Immanuel Kant Baltic Federal University, Kaliningrad, 236000 Russia

\* e-mail: amitbanerjee.nus@gmail.com

Received September 20, 2022; revised October 14, 2022; accepted October 20, 2022

**Abstract**—The imminent development and deployment of 6G technology demands high-speed data transfer with least latency. Terahertz (THz) spectrum is anticipated to provide the essential higher bandwidth with potential to increase network capacity greatly and further realization of 6G communication. But there are several challenges in terahertz technology like dearth of efficient sources, detectors, communication systems and reliable infrastructure for network implementation that are yet to be addressed and may need several years in development. Currently a similar communication design would face path loss, fading, poor signal quality due to inevitable molecular absorption, attenuations due to rain, cloud, gaseous molecules. While enhanced signal transmission power may offset some effects at a higher energy consumption and cost of system design. Power optimization and management would be another challenge in THz frequencies. Spectral efficiency and capacity may be improved due by Non-Orthogonal Multiple Access (NOMA) technique combined with Multiple Input Multiple Output (MIMO) antenna system. However, stable successive interference cancellation technique used in NOMA is still another challenge. Further to our development of chip-integrable uncooled terahertz microbolometer arrays as chip-integrable sensing device, and reconfigurable graphene nanopatch antenna compatible with the same, this article explores the opportunity in communication and network application for high-speed information processing. This work reviews the opportunities and challenges in the development of sources, detectors, communication systems prospective for 6G Communication in general and specific to that with THz spectrum.

**Keywords:** millimeter wave communication, terahertz communication, absorption loss, diffraction loss, path loss

**DOI:** 10.3103/S1062873822700617

## INTRODUCTION

Wireless communication has been revolving through one generation to another generation. In 4G network sub 6 GHz frequencies have been used. But microwave frequencies have limitations in data usages as they are burdened by many wireless users due to ever increasing demand. To accommodate higher number of users, higher data transfer speed, higher frequency millimeter wave band (mmWave) are being used in 5G. New technologies and design methodologies are being used for wireless connection used in Internet of Technology (IoT), enabling AI (Artificial Intelligence) supported by clouds. But mmWave propagation characteristics are unfavorable and may fail to meet the extreme technological demands in various applications e.g. virtual reality (VR), 3D video or automotive vehicles etc where data transfer rate should extremely

high. These leads increasing interest to investigate and explore further into the Terahertz (THz) band. The Terahertz (THz: from 300 GHz–3 THz) band provides higher bandwidth, low latency with data rate of Tbps range, accommodating extreme number of wireless users with ultra-high speed transfer rate. THz antenna can offer high directivity and less eavesdropping. Indoor communication can be improved by easily beam tracking and using the path of reflection in Terahertz. Terahertz can also follow Non-Line of Sight (NLOS) propagation. As transmission distance in mmWave and THz frequencies are less and antenna sizes are small, they can consume less power. The effects of free space diffraction and noise generated from optical source are less in this frequency. Most importantly other than its qualities useful for communication, the Terahertz radiation is non-ionizing and



hence not harmful for health of user and living-beings in general.

Millimeter spectra are blocked by obstacles and cannot penetrate the wall, however same is not true for Terahertz frequencies up to certain limits. However, either of these frequencies are affected by loss due to penetration and scattering. Outdoor communication can be affected by atmospheric attenuation that limits transmission distance in mmWave, particularly in THz frequency. Designing smaller and compact hardware in mmWave communication system, leads to lower sensitivity and not cost effective. The recent developments in THz devices makes realizable THz signal generation and detections and enables THz system with sufficient output power and sensitivity. The advancement in THz devices can facilitate reliable THz communication. However, the THz communication for highspeed information processing is still in its infancy and may need several years in development. The technical challenges for high-speed data communication for 6G in general and specific to THz spectrum have been discussed here drawing out the research and development course.

#### LITERATURE SURVEY

Oluseun.D. Oyeleke et al. [1] summarized the scope and advanced applications in THz band. They predicted different types of loss that THz wave sustain during transmission. A. Moldovan et al. [2] compared between Line of Sight (LOS) and Non-Line of Sight (NLOS) propagation. In case of LOS, absorption loss and spreading loss are dominant whereas in NLOS, reflection loss predominates. Capacity has been estimated for both propagation mechanisms. Long Bao Le et al. [3] discussed about the comparison of 4G and 5G. They overviewed different technologies to improve 5G network. K. Tekbiyik et al. [4] overviewed the opportunities to use THz spectrum and discussed about different path loss models for some distances and frequency to estimate path loss. They summarized open research area in THz communication. Ian F. Akyildiz et al. [5] presented the prospects of THz spectrum and the roadmap for research work in this topic. C. Han et al. [6] discussed new architecture such as hybrid beamforming and open research issues of THz communication. G. Rongbin et al. [7] addressed state-of-the-art technologies like hybrid beamforming, precoding, high gain antenna array to tackle path loss. A.A.A. Olyman et al. [8] summarized the application of THz frequency as a pillar in 6G communication.

#### THE CHALLENGES

(i) Terahertz source and Transceiver design [9, 10]. As THz spectrum has high frequency, the transceiver bandwidth should be large. Generation of THz wave is challenging as conventional oscillator cannot produce

this high frequency. On the contrary, with respect to optical photon emitters this frequency is much low to generate. Enough power should be transmitted to tackle high path loss. Further investigation underway to obtain necessary gain and sensitivity of transceiver. Lack of proper transceiver design is an open research issue for THz communication.

(ii) Antenna and amplifier design [9]. Designing antennas and amplifiers in this frequency range is highly challenging task. The aperture of antenna should be small, and antenna should possess high gain and bandwidth. For smaller beamwidth, antenna gain increases. So, antenna should be designed such that beamforming should be narrow.

(iii) Realization of ADC and DAC [11]. High data rate can be achieved using several hundred GHz bandwidths. But design of Analog to Digital converter (ADC) and Digital to Analog converter (DAC) are challenging as sampling rate should be high enough to get data rate in Tbps. Realization of such high speed and resolution are difficult and may incur significant design and system costs. New state-of-the-art waveforms and modulation techniques should be introduced such that ADC and DAC can consume less power. But more power is consumed when number of bits increases for high resolution.

(iv) Proper channel modelling [9, 10]. There are many standard materials obstacles if observed between transmitter and receiver, THz wave cannot pass through that beyond certain extend and suffers data loss. As penetration loss is high reliable link cannot be established. So, THz wave can cover only short distance making it suitable for indoor communications. LOS transmission can be affected by spreading loss. In this case THz wave can consider NLOS (Non-Line of Sight) communication. However, in NLOS communication the size and shape of obstacles, incident angle and frequency can affect the reflection path, diffraction, and scattering phenomena. Frequency selective nature of the channel makes the channel-modelling extremely challenging. Further different types of propagation phenomena like reflection, scattering and diffraction can affect THz signal. These phenomena depend on type of objects and signal wavelength. In presence of an object (in between transmitter and receiver) of size comparable with wavelength causes diffraction. The signal bends around the obstacle. Knife-edge diffraction model can estimate the diffraction for a sharp knife shaped object.

(v) Suitable modulation technique [9]. Conventional modulation techniques are not applicable for THz frequency. There is lack of reliable coding in THz band. Handover is another challenging issue in THz cellular technology due to small cell size.

(vi) Path loss [10, 13]. Significant power can be lost during transmission. THz transmission distance is up to 10 m due to propagation and absorption loss. Change in humidity can change the attenuation, and

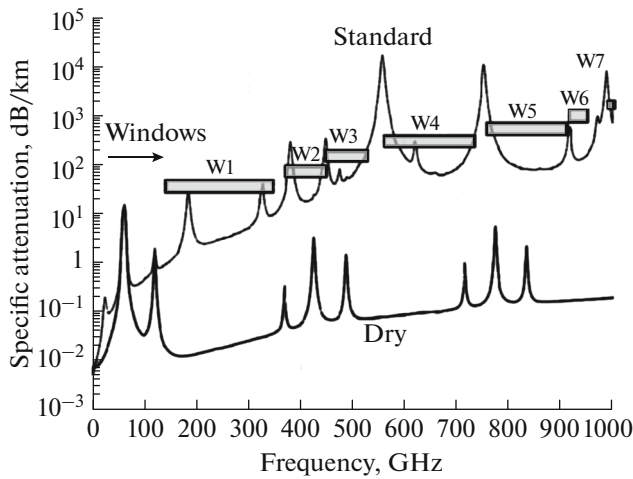


**Fig. 1.** Atmospheric attenuation vs. carrier frequency. The upper curve presents the attenuation in sea level and the lower curve represents for attenuation in dry air [14, 15]. (Image reproduced under a Creative Commons Attribution 4.0 License from [14]).

lead to path loss, loss in energy of radio wave while transmission occurs. When radio waves are radiated from source, power density will be lower due to spreading loss. Path loss varies with transmission distance, frequency, and channel. As per Friis law, received power varies inversely with path loss, and hence received power decreases with large value of path loss. So transmitted power should be significant to overcome the path loss.

(vii) Atmospheric absorption loss [10, 13]. Molecular absorption depends on frequency. Communication in THz band shows frequency selective nature. If medium changes THz wave absorption will be changed as per different molecules. Due to smaller wavelength THz wave cannot pass through oxygen and water vapor molecules. These molecules can absorb THz waves. In case of smaller transmission distance absorption loss can be ignored and transmission window is large. With increasing transmission distance molecular absorption increases and transmission window becomes narrower. Suitable transmission window should be determined where absorption loss will be less. If any material possesses low absorption coefficient value, the material cannot absorb the wave so much. Above 200 GHz water vapor causes high attenuation in THz frequency as visible from Fig. 1 [14, 15]. This attenuation can be predicted by taking the inputs of humidity, pressure, and temperature. Rain attenuation increases up to 100 GHz, whereas attenuation becomes nearly constant beyond 100 GHz [16–19].

As per Beer–Lambert Law, transmittance is related to absorbance and optical depth.

$$T = \frac{\Phi_e^r}{\Phi_e^t} = e^{-r}, \quad (1)$$

where  $\Phi_e^t$  and  $\Phi_e^r$  are transmitted and received radiant flux of material respectively.

Transmittance  $T(f, d)$  of any material is function of optical depth.

$$T(f, d) = \frac{P_{rx}(f)}{P_{tx}(f)} = e^{-k_{ac}(f)d}, \quad (2)$$

where  $P_{rx}(f)$  and  $P_{tx}(f)$  are received and transmitted power respectively,  $k_{ac}(f)$  is absorption coefficient. All of these values are dependent on frequency.

### SOME SOLUTIONS OF THE CHALLENGES

(i) High gain antenna [9]. Phased antenna array can be deployed to handle high path loss in THz frequency. Multiple patch antennas can transmit baseband and RF signal. Signal phase can be changed. These signals are received and combined by receiver antennas. Power amplifiers should be incorporated for each antenna which makes the system size more. As metal antennas can consume more power, graphene-based antennas can be used for low power consumption. To overcome the path loss in THz band, antenna gain should be high. Horn and parabolic antenna can satisfy this criterion, but large size of these antennas makes it difficult to use. Planar antennas can be fabricated easily, but directivity is poor and high gain cannot be achieved using these antennas. Massive Multiple Input Multiple Output (MIMO) antennas can meet the requirement of high gain. It can improve beam forming and spectral efficiency. Spatial multiplexing techniques are followed by multiple antennas to increase data rate. Further study is required for other applications.

(ii) Beam steering and modulation techniques [11]. Hybrid beamforming can reduce the number of ADC and DAC. Power efficiency can be improved by reducing the number of bits. But it can introduce distortion that has to be handled with care in communication. In case of 5G and beyond communication new multicarrier waveforms can be implemented such as Orthogonal Frequency Division Multiplexing (OFDM). OFDM technique can mitigate multi path fading and inter-symbol interference. But clock rate should be fast to operate processor for THz frequency. This makes the system complex. Multicarrier modulation can produce high peak-to-peak average power ratio. This modulation technique can be used in indoor communication.

More antenna elements with high gain should be implemented to tackle the path loss. Multi element antenna with high gain limit the spreading of beam. So, spreading loss can be reduced. As a result, single path dominates and THz channel shows frequency-flat nature. Single carrier waveform can be used in THz frequency. Thus peak-to-average power ratio can



be diminished. Single carrier waveform and phase modulation like Binary Phase Shift Keying (BPSK) and Quadrature Phase Shift Keying (QPSK) can be applied in THz communication. This enhances spectral efficiency.

(iii) On-chip integrable microelectronic sensors and sources in THz [20–30]. The current review work is an extension of our several reports on design and experimental realization of suitable on-chip integrable terahertz microbolometer arrays which can efficiently operate in room temperature as THz sensor. Further compatible design for reconfigurable graphene nanopatch antenna with the same has also been reported. The application extension of these THz sensor devices in communication and network systems are exciting. This along with suitable on-chip GaN based IMPATT based THz sources, design and simulation results of which has been also proposed by our group, are currently being explored for communication and high-speed information processing along with application in biomedical and advanced imaging. These THz source and sensor are designed and made so that they are compatible with state-of-the-art medium-scale semiconductor device processes for possible commercial production. Comprehensive literature studies on the design, development and fabrication of these devices and the current state-of-art have been extensively discussed in our previous reports [20–30].

## CONCLUSIONS

5G technology wireless communication using mm Wave can establish massive number of connections with very low latency, supporting data rate in Gbps. While this somewhat meets the current data transfer demands, due to escalating demand and rapid innovation in connected and centralized devices, the spectrum for wireless data transfer may fall short eventually. Terahertz spectrum with higher frequency is not used by any dedicated service this moment and has the potential to provide Tbps data rate for various application. Hence, Terahertz may be considered as one of the foundation pillars of 6G technology. The non-ionizing Terahertz radiation is not harmful for living-beings in general and hence a step forward towards a circular and sustainable technology supported economy. The paper summarizes the prospects, but challenges along with possible solutions in terahertz devices, Terahertz communications as a candidate for 6G technology. High Path loss, proper channel modelling, suitable antenna design, non-availability of power efficient transceiver and terahertz generator may draw the consideration of researchers for the viability of terahertz in 6G technology. However, some prospective design integration in recent times with chip-integrable room temperature detectors (e.g. terahertz microbolometer arrays) along with other advanced terahertz sources (e.g. IMPATT based), could possibility build compatible and compact com-

munication systems with potential application in 6G Communication specific to THz spectrum.

## FUNDING

This paper was partially supported by the Device Development Programme (DST/TDT/DDP-38/2021), by the Department of Science Technology, Ministry of Science and Technology, Government of India.

## CONFLICT OF INTEREST

The authors declare that they have no conflicts of interest.

## REFERENCES

- Oyeleke, O.D., Thomas, S., Idowu-Bismark, O., Nzerem, P., and Muhammad, I., *Int. J. Eng. Manuf.*, 2020, vol. 10, p. 54.
- Moldovan, A., Ruder, M.A., Akyildiz, I.F., and Gerstacker, W.H., *Proc. 2014 IEEE Globecom Workshops*, 2014, p. 388.
- Le, L.B., Lau, V., Jorswieck, E., Dao, N.D., Haghghat, A., Kim, D.I., and Le-Ngoc, T., *EURASIP J. Wireless Commun. Networking*, 2015, no. 1, p. 1.
- Tekbıyık, K., Ulusoy, E., Ekti, A.R., Yarkan, S., Baykaş, T., Görçin, A., and Kurt, G.K., *Proc. 2019 IEEE 30th Annual International Symposium on Personal, Indoor and Mobile Radio Communications*, 2019, p. 1.
- Akyildiz, I.F., Han, C., Hu, Z., Nie, S., and Jornet, J.M., *IEEE Trans. Commun.*, 2022, vol. 70, p. 4250.
- Han, C., Yan, L., and Yuan, J., *IEEE Wireless Commun.*, 2021, vol. 28, p. 198.
- Guo, R., Tang, Y., Zhang, C., Liu, S., and Zhao, Z., *Chin. J. Electron.*, 2022, vol. 31, no. 3, p. 488.
- Solyman, A.A., and Elhaty, I.A., *Int. J. Electr. Comput. Eng.*, 2021, vol. 11, no. 4, p. 3403.
- Mehta, L.R., *Int. J. Eng. Res. Appl.*, 2020, vol. 10, no. 7, p. 13.
- Alsharif, M.H., M.Albreem, A., and AA Solyman, *Comput., Mater. Continua*, 2021, vol. 66, no. 3, p. 2831.
- Song, H.J., and Lee, N., *IEEE Trans. Terahertz Sci. Technol.*, 2021, vol. 12, no. 2, p.105.
- Han, C., Wu, Y., Chen, Z., and Wang, X., arXiv: 1912.06040, 2019.
- Oyeleke, O.D., Thomas, S., Idowu-Bismark, O., Nzerem, P., and Muhammad, I., *Int. J. Eng. Manuf.*, 2020, vol. 10, p. 54.
- Tataria, H., Shafi, M., Molisch, A.F., Dohler, M., Sjoland, H., and Tufvesson, F., *Proc. IEEE*, 2021, vol. 109, no. 7, p. 1166.
- Attenuation by Atmospheric Gasses and Related Effects, Document ITU-R P.676-12, 2019.
- Rappaport, T.S., Xing, Y., Kanhere, O., Ju, S., Madanayake, A., Mandal, S., Alkhateeb, A., and Trichopoulos, G.C., *IEEE Access*, 2019, vol. 7, p. 78729.
- Rappaport, T.S., Sun, S., Mayzus, R., Zhao, H., Azar, Y., Wang, K., Wong, G.N., Schulz, J.K., Samimi, M., and Gutierrez, F., *IEEE Access*, 2013, vol. 1, p. 335.

18. Rappaport, T.S., Murdock, J.N., and Gutierrez, F., *Proc. IEEE*, 2011, vol. 99, no. 8, p. 1390.
19. Qingling, Z., and Li, J., *Proc. 2006 7th International Symposium on Antennas, Propagation & EM Theory*, 2006, p. 1.
20. Banerjee, A., Satoh, H., Tiwari, A., et al., *Jpn. J. Appl. Phys.*, 2017, vol. 56, 04CC07.
21. Banerjee, A., Satoh, H., Sharma, Y., Hiromoto, N., Inokawa, H., *Sens. Actuators, A*, 2018, vol. 273, p. 49.
22. Banerjee, A., Satoh, H., Elamaran, D., Sharma, Y., Hiromoto, N., Inokawa, H., *Jpn. J. Appl. Phys.*, 2018, vol. 57, 04FC09.
23. Banerjee, A., Satoh, H., Elamaran, D., Sharma, Y., Hiromoto, N., Inokawa, H., *J. Appl. Phys.*, 2019, vol. 125, 214502.
24. Elamaran, D., Suzuki, Y., Satoh, H., Banerjee, A., Hiromoto, N., Inokawa, H., *Micromachines*, 2020, vol. 11, no. 8, p. 718.
25. Banerjee, A., Vajandar, S., and Basu, T., in *Terahertz Biomedical and Healthcare Technologies*, Banerjee, A., Chakraborty, B., Inokawa, H., Roy, J.N., Eds., Amsterdam: Elsevier, 2020, p. 145.
26. Banerjee, A., Chakraborty, C., and Rathi, M., in *Terahertz Biomedical and Healthcare Technologies*, Banerjee, A., Chakraborty, B., Inokawa, H., Roy, J.N., Eds., Amsterdam: Elsevier, 2020, p. 225.
27. Banerjee, A., Chakraborty, C., Kumar, A., and Biswas, D., in *Handbook of Data Science Approaches for Biomedical Engineering*, Balas, V.E., Solanki, V.K. Kumar, R., and Khari, M., Eds., New York: Academic, 2020, p. 121.
28. Basu, T., Banerjee, A., and Vajandar, S., in *Terahertz Biomedical and Healthcare Technologies*, Banerjee, A., Chakraborty, B., Inokawa, H., Roy, J.N., Eds., Amsterdam: Elsevier, 2020, p. 75.
29. Biswas, A., Sinha, S., Acharyya, A., Banerjee, A., Pal, S., Satoh, H., Inokawa, H., *J. Infrared, Millimeter, Terahertz Waves*, 2018, vol. 39, p. 954.
30. Samanta, D., Karthikeyan, M.P., Banerjee, A., and Inokawa, H., *Nanomedicine*, 2012, vol. 16, p. 12. <https://doi.org/10.2217/nnm-2020-0386>



## Sulfide and Selenide Based Materials for Emerging Applications

Sustainable Energy Harvesting and Storage Technology

2022, Pages 179-194

# Chapter 9 - Sulfide and selenide-based flexible and semitransparent solar cells for building integrated photovoltaics

[Amit Banerjee<sup>a</sup>](#), [Aatreyee Sarkar<sup>b,c</sup>](#), [Shobha Shukla<sup>b</sup>](#), [Sumit Saxena<sup>b</sup>](#), [Aditya Banerjee<sup>d</sup>](#), [Asim Guchhait<sup>e</sup>](#),  
[Raghavendra Lawaniya<sup>c</sup>](#), [Avishek Kumar<sup>c</sup>](#), [Goutam Kumar Dalapati<sup>c</sup>](#)

[Show more](#)

Outline | Share Cite

<https://doi.org/10.1016/B978-0-323-99860-4.00025-3>

[Get rights and content](#)

## Abstract

Semiconductor materials based on Copper chalcogenides, also called kesterites, such as copper-zinc-tin-sulfide ( $\text{Cu}_2\text{ZnSnS}_4$ , CZTS), copper-zinc-tin-selenide ( $\text{Cu}_2\text{ZnSnSe}_4$ , CZTSe), and copper-zinc-tin-sulfide-selenide ( $\text{Cu}_2\text{ZnSn}(\text{S},\text{Se})_4$ , CZTSSe) are promising light absorbing materials for the next generation flexible and semitransparent thin film solar cells with protentional application in building integrated photovoltaics, among various other. These materials are environmentally friendly, earth abundant and can be synthesized easily using solution-based techniques (sol-gel spin coating, chemical bath deposition, spray coating) and physical vapor deposition (sputter, thermal evaporation). Thin film solar cells with kesterite absorbers can be efficiently integrated on patterned glass substrates for semitransparent solar cells for building integrated photovoltaic (BIPV) applications and holds enormous potential for large scale commercial application. This review chapter explores recent development with comprehensive discussion on materials, design, device integration and future perspectives with wide literature-survey and analysis on sulfide and selenide-based semitransparent and flexible solar cells for smart window applications.

[Recommended articles](#)

## References (0)

## Cited by (0)

[View full text](#)

Copyright © 2022 Elsevier Inc. All rights reserved.

## Research Article

# IoT-Based Response Time Analysis of Messages for Smart Autonomous Collision Avoidance System Using Controller Area Network

Anil Kumar Biswal,<sup>1</sup> Debabrata Singh,<sup>2</sup> Binod Kumar Pattanayak <sup>1</sup>,  
Debabrata Samanta <sup>3</sup>, Amit Banerjee <sup>4</sup>, A. Y. Seteikin,<sup>5,6</sup> and I. G. Samusev <sup>5</sup>

<sup>1</sup>Department of CSE, ITER, SOA Deemed to Be University, India

<sup>2</sup>Department of CA, ITER, SOA Deemed to Be University, India

<sup>3</sup>Department of Computer Science, CHRIST University, India

<sup>4</sup>Physics Department, Bidhan Chandra College, Asansol 713 303, India

<sup>5</sup>Immanuel Kant Baltic Federal, University, Kaliningrad, 236000, Russian Federation and Amur State University, Blagoveshchensk 675027, Russia

<sup>6</sup>Amur State University, Blagoveshchensk 675027, Russia

Correspondence should be addressed to Amit Banerjee; [amitbanerjee.nus@gmail.com](mailto:amitbanerjee.nus@gmail.com) and I. G. Samusev; [is.cranz@gmail.com](mailto:is.cranz@gmail.com)

Received 12 August 2021; Accepted 3 March 2022; Published 8 April 2022

Academic Editor: Rajesh Kaluri

Copyright © 2022 Anil Kumar Biswal et al. This is an open access article distributed under the Creative Commons Attribution License, which permits unrestricted use, distribution, and reproduction in any medium, provided the original work is properly cited.

Many accidents and serious problems occur on the road due to the rapid increase in traffic congestion in all sections of the country. Autonomous vehicles provide a solution to successfully and cost-effectively avoid this problem while minimizing user disruption. Currently, more engaging electromechanical elements with an analog interface are used to develop affordable automobiles for efficient and cost-effective operation for a smart driving platform with a semiautonomous automobile, strengthening the vehicle involvement of the driver while increasing safety. As a result, it takes longer for various car elements to respond, which causes more problems during message transmission. This project aims to create a Controller Area Network (CAN) for analyzing message response times by incorporating a few application nodes on the IoT platform, such as an antilock braking system, flexible cruise control, and seat belt section, for some real-time control system applications. These application nodes are car analytical parts that are linked to IoT modules to prevent collisions. An autonomous device for collision avoidance and obstacle detection in a vehicle can impact road accidents if the CAN protocol is implemented.

## 1. Introduction

In recent years, traffic congestion, driver drowsiness and reckless driving represent a big problem in the different areas around the world that are seriously affected by road accidents in the transport system [1]. Unconditional circumstances are controlled by intelligent autonomous vehicles because of the above. Therefore, through the implementation of collision avoidance mechanisms in the vehicle, the

automation domain offers a forum for monitoring reckless driving as well as driver fatigue [2]. The “Automotive Serial Controller Area Network” protocol is used for designing an intelligent control car with a huge range of serial bus communication control system [3].

Large types of embedded systems require high-speed communication platforms for providing automotive industrial control. But various industries are not supported with automation that needs to be operated with Controller Area

Network (CAN) protocol [4]. A serial communication bus like CAN was considered in the International Standardization Organization (ISO), which has replaced the complex wiring control with a two-wire bus, thereby adding a multi-master communication serial bus that can transmit messages to various parts of the network system [5].

Currently, the Automobiles are being constructed with microcontrollers and more electrical parts as we know that is the central part of the controlling unit and various types of devices or circuitries connected to it. This process is very complex to interpret and improve performance by using several connections and electrical lines linked to a microcontroller [6]. The communication area for the project is an implanted CAN networking system which provides effective data transfer, allowing multiple microcontrollers and devices to be connected with a popular CAN bus using the CAN protocol, then the connection of all items with the consideration of optimum priority and speed [7].

This protocol also offers a high-speed serial data frame communication interface, low-cost physical medium, short message frame length, and, at the same time, it adds a high-level detection or correction mechanism for errors in different communication network nodes [8]. The evolution of embedded systems and software has been used in modern times to build smart autonomous vehicles over 40-50 percent globally and this percentage of progress is only expected to increase with improving road safety and security features [9] [10]. Due to the process of digitization for constructing smart vehicles with the use of IoT modules that can create a huge number of datasets [11]. So that, the dimensionality reduction and security of datasets are required to be managed and also yield good results through the blockchain-big data technique [12]. In general, the protocols between the network (sensor) nodes for physical communication with the IoT data link layers, the sensor nodes, are described by the CAN protocol [13]. Here, the ultrasonic sensor node application process is used to measure the distance between the vehicle and the road barrier [14] [15].

This system determines the distance of the obstacle by an ultrasonic sensor to control the motor speed that has been designed using Arduino UNO, IoT modules, and CAN base serial communications protocol. When the sensor node is connected to the CAN bus, which provides a rapid response to measure the distance of an obstacle, the message is automatically forwarded to the Arduino Uno module to track the vehicle's engine movement and steering. This proposed system provides an environment to enhance the driver-vehicle platform to make a semi-autonomous vehicle system with the help of developing and implementing a digital driving system [16] [17]. The optimal response time calculation is impossible in the existing system, which takes maximum time to communicate with each part of the vehicle due to massive datasets. These datasets shorten the response time of an existing system that causes vehicle accidents while driving.

*1.1. Motivation of This Work.* Designing a process of response time analysis of a smart autonomous collision avoidance system messages based on IoT modules and CAN serial communications protocol to prevent any road

accidents by taking an optimized range of message length and message ID for providing timing response in conversion. In recent years, the autonomous operation has been extensively applied to vehicles for road safety issues.

### 1.2. Contribution to This Work

- (i) The smart vehicle is developed by the Controller Area Network (CAN) that is accessed in various real-time suits to link internal-level communication facilities to shared units of car control systems, e.g., industrial and home automation and medical equipment, which is a "broadcast" type of bus. In other words, there is no address part of sending or receiving nodes. The network can accept to receive or transmit the messages sent by all nodes, where the acceptance test is performed after receiving the message from each node
- (ii) The messages are checked by each node whether it is irrelevant to that particular node or not. When a message is pertinent, then it is received by that node. Otherwise, it is not accepted. The priority node can send the first message for transmission, which depends on an 11-bit identifier. Here, an identifier is uniquely identified all over the network and is used to tag the content of the message. A numeric value is added to each message, which controls its priority on the bus, thereby recognizing the contents of the message
- (iii) When the bus is not loaded by any task, then some nodes can be ready to communicate with each other. But during this period, where the CAN bus attempts to forward messages from more than two nodes concurrently, then the identifier field is uniquely defining the priority of the message through the network. The messages are securely transmitted in the sequence of priority without missing anyone, which is possible with this technique. If a numerical value of the identifier is lower, then it is treated as a higher priority. This means that the message with more prevalent ID bits (i.e., Bit 0) will overwrite all nodes so that only the predominant message will finally be acknowledged by each node after arbitration of the ID
- (iv) Using the Arduino controller and serial communication protocol on different device nodes, collision avoidance, and obstacle detection techniques are implemented on the smart vehicle via IoT modules. To detect any obstacle through a different ultrasonic sensor on the road, we can produce a message frame to relay the node to a vehicle's engine

The rest of the paper is structured as follows: the literature survey pertaining to this field is included in Section 2. Section 3 describes the network protocol model and the proposed system, and Section 4 represents the proposed framework and operating theory, along with its implementation processes and components. In Section 5, we describe the simulation setup and result from analysis, and in Section 6, we conclude our paper with some references.

## 2. Literature Survey

Control Area Network (CAN) is detailed in [18] that provides a communication network between control units in automotive industries. CAN provides vast advantages and then it is widely used in distinct industries including military, aviation, electronics, factories and many more. Here, the microcontrollers and devices communicate among themselves using CAN in the absence of a host computer and there is no need to follow heavy access of the main controller. In [19], The author describes CAN-BUS to be an essential network technology for communication which is implemented in the automobile network communication sector with some characteristics like real-time implementation, reliability, and flexibility.

In [20], the current wireless home automation requires a greater amount of RF recipients and thus the frequency range varies. Electromagnetic waves may lose messages, and the cost and complexity of multi-home automation will be significant. This process is crucial for detecting problem areas. Due to that, it allows controlling only limited devices. The author talks about a Controller Area Network (CAN) bus used to send and receive messages between automotive devices [21]. There are possibilities of errors when transmitting messages via the nodes. To detect those errors, a Controller Area Network Adaptive Fault Diagnostic Algorithm detects all of the CAN's defective nodes.

In [22], the authors discuss the current parameters of vital signs for patients in critical care units; patient's bedside are equipped with devices that keep intensivists and other medical staff informed. This information allows paramedical personnel to take the necessary measures for disease prevention and cure. Extracting CAN messages from automotive ECUs can be made successfully as detailed in [23]. It gives the details of the construction of software and hardware, which interfaces directly into the car with the CAN network.

It includes CAN bus transceiver behavioural models. Thermal behaviour can be allowed for different types of simulations for verification in reasonable CPU time from core verifications for detailed analysis of the integrity of signals [24]. This review examines the research done on the Controller Area Network (CAN) reliability analysis. In recent decades, schedulability analysis has been extended to an advanced technique that can determine whether or not the time limits of several jobs performed by a single CPU or a distributed system for nontrivial systems. [25]. This is a description and illustration of a reliability analysis method that focuses on auto systems based on CAN, that also considers the impact of the error on schedulability analysis [26].

In [27] proposed an automotive CAN cluster for processing messages by using a gateway mechanism. So, this is used for worst-case response analysis (WCRT) for finding lower and upper bound on the response time of the CAN cluster of automobiles. It is efficient to monitor a large-scale CAN cluster, and then its performance will be improved by reducing unnecessary conservation in process of designing. The WCRT analysis of CAN with sporadic message execution in a multicore automotive gateway protocol has been designed by Xie et al. [28]. This process is con-

structed on global and portioned scheduling to evaluate real message sets and guides the design optimization. This gateway technique can remove the bottleneck of the message execution with the use of a small message execution delay, but its real-time process can be improved through multiple execution units. Alaei et al. [29] proposed a method for improving message response time by using a statistical based algorithm. In this paper, the stuff bits were reduced through the Statistical Mask Calculation (SMC) which provided better performance than the existing process. But the validation will require to improve in the reliability of the CAN network by minimizing bit stuffing.

The CAN is generally applied in various sectors like industrial, home automation, transportation, medical sector, and thermal plant, etc. that shows worst-case response time (WCRT) at the time of execution. This occurs due to delay in the periodic frame of the message, desynchronization of the message frames, improper scheduling of frames, etc., which is the main reason for WCRT. But in this current or proposed system is improvising the process response time of message transmission in various units of the system that makes the whole process full of automation. This paper provides a technique for analyzing the response time of CAN through an enhanced method of bit stuffing, message format, and error handling mechanism to optimal way for the handling of huge datasets. The existing process of the CAN bus is designed to measure lower and upper bound on the response time by using a cluster gateway algorithm which is performed their activity on a large-scale cluster of the message. But it sometimes does not give perfect responses due to unnecessary conversion in the process. That is why this proposed approach algorithm provides a perfect observation to finding the response time of optimized or prioritized message conversion in CAN bus that helps to avoid the cause of the collision.

## 3. Proposed System

An automation domain that is a versatile way to monitor the motor movement from a collision due to any obstacle is the objective of the proposed method. The primary goal of this phase is to ensure protection from unconditional road accidents due to traffic congestion and reckless driving.

*3.1. Serial Communication Protocols.* The growing demand for transmission of message has been controlled through the different protocols for communication, which is based on applications to build in a networked and internet-connected environment [30] [31] [32]. But these protocols vary from one another at the time of communication. So the upper and lower end protocols form the transmission procedures covering the various communication nodes of automobiles [33]. The device's CAN control bus and address bus are referred to as the higher end. Together with the increased focus on the distributed systems and networking, the cost benefit and advanced capabilities of silicon technology have led to the need for new highly organized communication methods in the area of field bus application. The automobile expects scalable control systems with a high



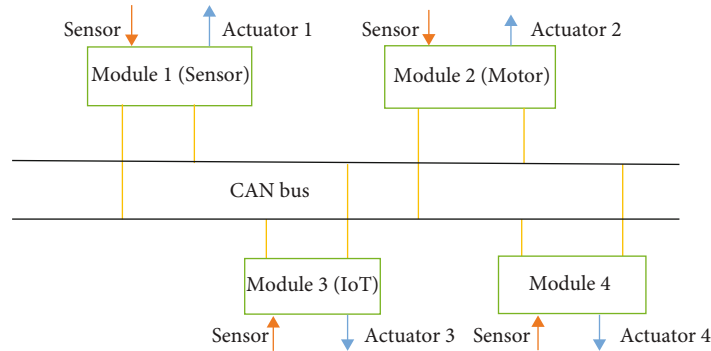


FIGURE 1: Illustration of a distributed CAN bus network.

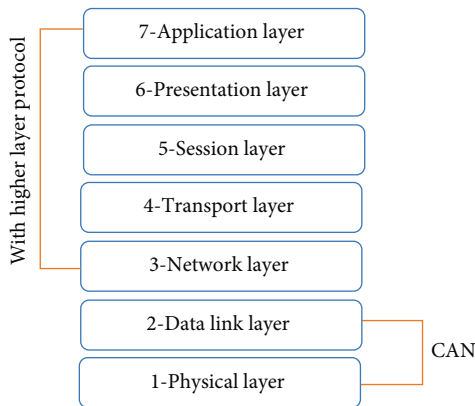


FIGURE 2: Controller Area Network (CAN) protocol defines in OSI model

standardization degree. The high level of standardization in the hardware and software modules leads to reusable systems that are ready to adapt in any single application setting to the various requirements and solutions [34]. The automotive vehicle has been developed by adding many electronic components with IoT modules for providing safety and to improve collision avoidance systems. Consequently, they need more and more hardwired, dedicated signal lines because of the complexity of the sharing data transmission control architecture of the system. This prompted the replacement by network architecture of the current wiring mode where the network system communicates via a common bus to all of the nodes. So this communication is ideally performed through CAN protocol which was developed by R. Bosch [35]. The CAN is used to communicate together in real time at speeding up to 1 Mbps, sensor and actuator via a two-wire serial data bus [36]. Focused on the concept of the “Shared Variables,” the Virtual Levelled Systems Architecture (VLSA) model forms the generic interface architecture that is central to the CAN protocol [37]. Individual tasks are handled by distributed controllers in the VLSA architecture, with each one responsible for a portion of the total control programme. Through their sensors and actuators, nodes in a distributed system interact with the real process. The nodes use a dynamic, priority-based arbitration system to send messages on the bus. Figure 1 shows illustration of a distributed CAN bus network.

The nodes use a dynamic arbitration method based on priority to pass messages on the bus [38]. The nodes filter out the corresponding messages by filtering the message algorithm. Any message sent on the bus is delivered to every node in your network. Based on the message received, the application will send control signals to the device via the actuators. Jitter occurs when data packets are sent over your network connection with a temporal delay. Congestion on the network, as well as route changes, are common causes.

*3.1.1. CAN Protocol.* The CAN is described as two protocol standards such as ISO 11898 and ISO 11519 [39]. The ISO 11898 standard monitors high speed communication up to 1Mbps in physical layer of OSI model. The upper limit for ISO 11519 is 125 kbps that is consisting of a sub-layer of Logical Link Control (LLC) and a sub-layer of Media Access Control (MAC) in data link layer [40] [41]. Controller Area Network (CAN) Protocol defines in OSI model represents in Figure 2.

To keep data and monitor information, the Data Link Layer constructs data frames. Generally, some additional services such as detecting frames with bit stuffing and also used to re-transmit faulty data frames at the time of communication.

The CAN Physical Layer in one given network transmits data between different nodes; it decides the mode of transmission of signals and thus addresses issues such as the encryption, timing and synchronization of the communicated data signal [42]. With the implementation of the CAN protocol, the receivers of the sensor nodes data set will be transmitted to the control unit of the device, which normalizes the physical and data link layers of the OSI communication model for the automation domain, while the higher-layer protocols such as CAL/CAN Open and the CAN Kingdom, System Net, define the application layer [41]. The upper layer of ISO/OSI model’s highest level, the application layer, communicates with an application program. The OSI layer closest to the end-user is the application layer.

*3.2. CAN Message Transfer.* The maximum load for utility is 94 bits and restricted format communications of varying but limited lengths are used by CAN. There is no particular address in the messages. Instead, it can be thought that the messages are addressed by four separate frame types for

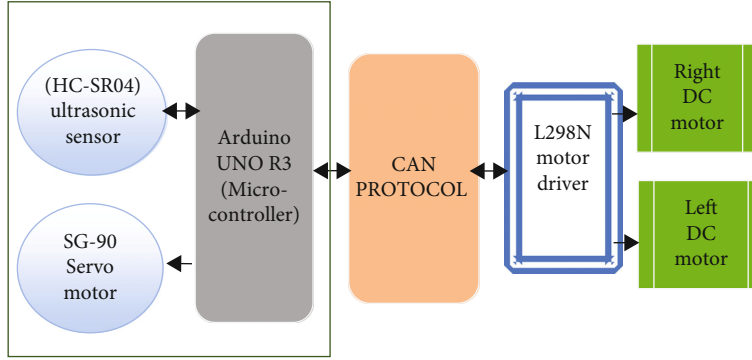


FIGURE 3: Proposed block diagram of smart autonomous collision avoidance system using the CAN protocol.

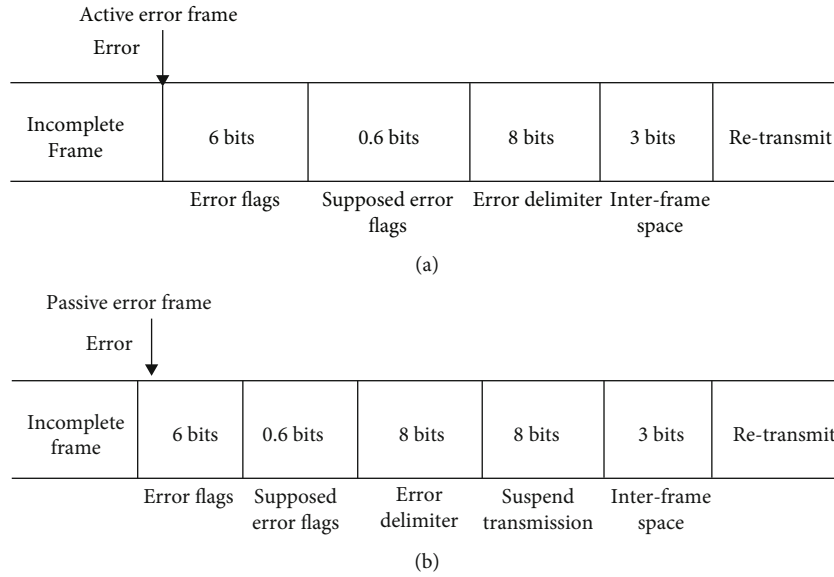


FIGURE 4: CAN error frame: (a) active error frame and (b) passive error frame.

```

1 : for i = j downto 1
2 :  $\pi_{i,2...n_i} = \pi_{i,1}$ 
3 :  $RT_i = WCRT(\pi_{i,2...n_i})$ 
4 : while ( $RT_i > DL_i$ ) do
5 : decrement  $\pi_{i,2...n_i}$  (maximum priority)
6 : if ( $\pi_{i,2...n_i} < \pi_{i,1}$ ) then
7 : return Fail
8 : endif
9 :  $RT_i = WCRT(\pi_{i,2...n_i})$ 
10 : endwhile
11 : endfor
12 : Return success

```

ALGORITHM 1: Message priority task algorithm.

communications such as a data frame, a remote frame, and an error frame for sending and reporting a detected data.

**3.2.1. Data Frame.** The CAN systems are used to transfer eight bytes of data frames with fixed data lengths through the network. Eight separate bit fields are composed of a message frame: frame start bit, data arbitration, control, data,

CRC frame, acknowledgement, frame end field and Inter-Data space. So this protocol is defined by two frameworks base and extended format [43] [44].

The CAN 2.0A specifies base format CAN systems with standard 11-bit frame identifiers. But the CAN 2.0B identifies extended a format CAN system that has 29-bit frame identification. Where the CAN 2.0B supports both 11 bit and 29 bit identifiers, but the CAN 2.0A only supports 11-bit frame. The extended format is used on complex heavy traffic networks where the number of messages generated by network transmitters is greater than the number of possible CAN ID codes that may be given to them. The Standard CAN 11-bit ID provides the Extended CAN 29bit for 2, or 2047 separate message ID, whereas the CAN 29bit ID is stretched to provide 2 or 538 million identifiers [45].

So the vehicular conflicts may arise due to cross-wind, unbalanced friction coefficients, also a flat tire, the driver's behaviour is taken into account. The CAN bus is used by the Arduino UNO R3 module system as it relies on many IoT control units residing in the vehicle's Engine Control Unit (ECU- L298N Motor Driver) which depends significantly on the selection of the braking mechanisms (such as



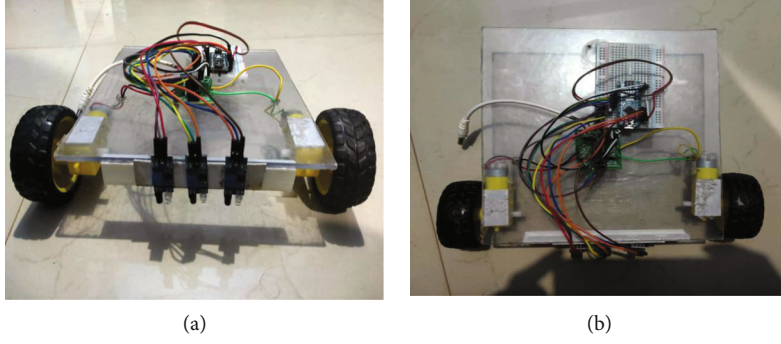


FIGURE 5: (a) Front and (b) top view of Smart Autonomous Collision Avoidance Vehicle.

TABLE 1: Details of Network Parameters.

Network parameters	Value in numbers (nos) (variable message ID)	Value in numbers (nos) (variable message length)
Message length	5-8	1-5000
Message ID	1-5000	1-500

hydraulic, pneumatic systems, electro-hydraulics, or even the electro-mechanics) and the usability of the Electronic Control Unit (ECU) as depicted in Figure 3 [46].

#### 4. Working Principle and Methodology

**4.1. Measuring Response Time of CAN.** Measurement of the CAN message worst-case latencies for real-time analysis can be conducted on a fixed priority response time analysis scheduling standard [47]. The response time can be calculated using a worst-case message queuing configuration. The typical way to express the worst case action is to assume a collection of streams of traffic and also producing a fixed priority of queue messages on a periodic basis [48].

In the proposed model with message streams (MS) is processed in CPU scheduling with three elements of the messages  $\langle J_i, Q_i, C_i \rangle$ , where  $J_i$  is the queuing jitter,  $Q_i$  is the queuing delay and  $C_i$  is the communication delay of message  $i$ . When lower priority messages are forwarded it take a long time to be delayed in the queue ( $Q_i$ ). Then the real-time need to send the message by bus, due to communication delay ( $C_i$ ). The response time of worst-case error messages of the CAN bus is generally calculated, which shows the overhead error  $EO_i$  in terms of  $E(t)$  denotes the maximum time required to signal and retrieve errors during the interval  $t$ . The response time analysis of worst-case (WR) can be determined by:

$$WR_i = J_i + Q_i + C_i,$$

$$Q_i = B_i + \sum_{j \in hp(i)} \left\lceil \frac{(Q_j + J_j + \tau_{bit})}{T_j} \right\rceil C_j + E(Q_i + C_i),$$

$$WR_i = J_i + B_i + \sum_{j \in hp(i)} \left\lceil \frac{(Q_j + J_j + \tau_{bit})}{T_j} \right\rceil C_j + P_k,$$

$$P_k = C_i + E(Q_i + C_i), B_i = \max_{\forall k \in lm(i)} (C_k),$$

$$C_i = \left( mh + 8P_i + 15 + \left\lceil \frac{(mh + 8P_i - 1)}{4} \right\rceil \right) T_{bit},$$

$$EO_i = 15_t au_{bit} + \max_{K \in hp(i) \cup \{i\}} (C_k + 31_t au_{bit}), \quad (1)$$

- (i) Captures the effect of external interference as an error in many frames, rather than allowing the interference pattern to be defined and that explanation gives the consequence of message transmissions.
- (ii) The period of interference does not reflect the potential delay, e.g. assuming that interference with duration  $15_t au_{bit}$  will in the worst case give an error overhead.
- (iii) Only allows relatively simple interference patterns with an initial burst and a residual error rate.
- (iv) Does not conveniently capture interference from multiple sources.

**4.1.1. Features of CAN Error Handling.** Error Active is the default mode for a node. When any of the two Error Counters rises above 127, the node goes into Error Passive mode, and when the Transmit Error Counter rises beyond 255, the node goes into Bus Off mode. When an Error Active node identifies errors, it transmits Active Error Flags. The signal was scattered throughout propagation due to several nodes exchanging sample thresholds. The CAN bus can cause errors which are also used for error finding and auto-checking tools to attain resources of source-based controlling, bit stuffing, CRC bit checks, as well as testing format of the message frame [49]. So, it is depicted in Figures 4(a) and 4(b).

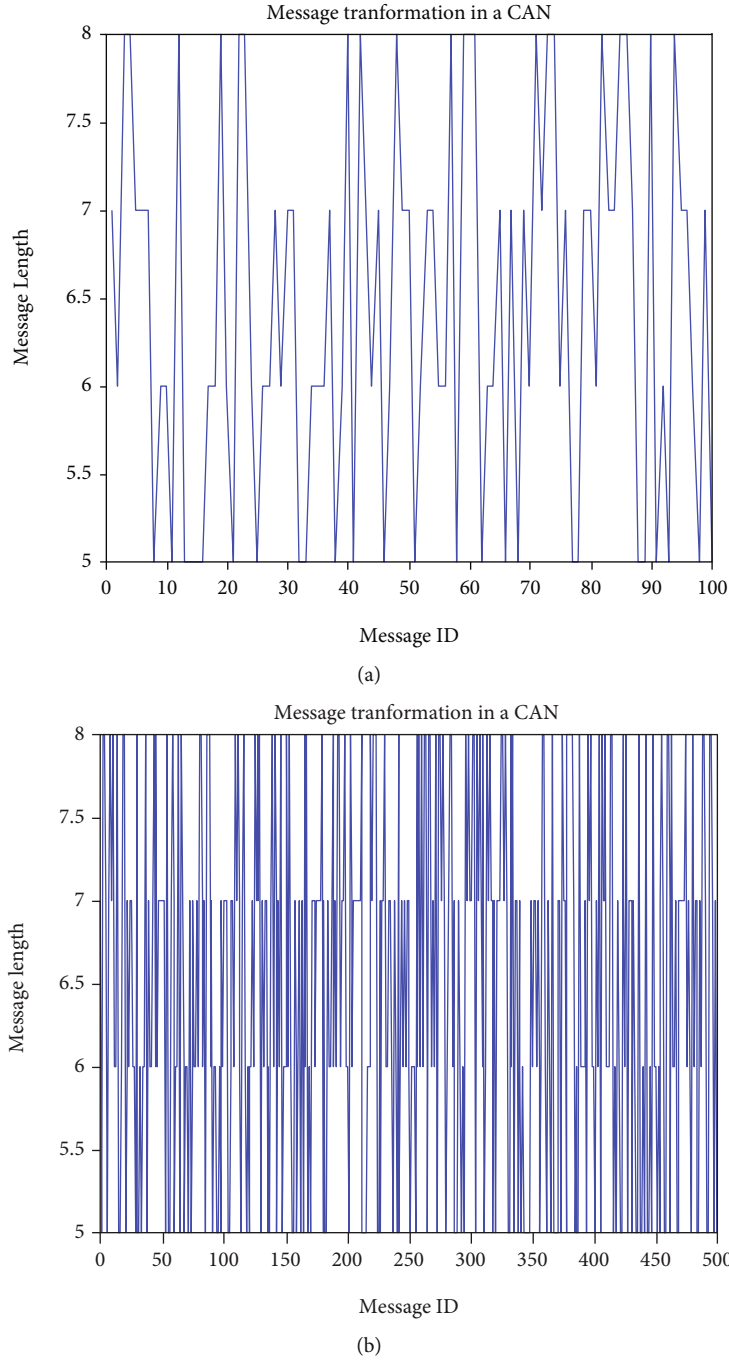


FIGURE 6: (a) Message length = 5 – 8 and ID = 100 nos and (b) message length = 5 – 8 and ID = 500 nos.

4.2. *Bit-Stuffing Effect and Retransmission of CAN Message Frame.* When a CAN node detects an error in a transmission, it sends an error flag consisting of six bits with the same polarity. The bit stuffing method prevents six consecutive bits from having the same polarity by adding a bit of opposite polarity after the fifth bit. If the number of bit-stuffing increases then the re-transmission of CAN messages can be increased. But the bit-stuffing decreases then the re-transmission of CAN messages can be decreased at the time of communication.

The message bit pattern is a set of stuffed bits that requires probability distribution of each bit frame format [50]. So, the distribution of communication time can be collected from the number of stuff bits that is defined as

$$CD_m(t) = CD_m(t) + \phi(b)\tau_{bit} \quad (2)$$

At the time when the message communication is not successfully transmitted to the destination, it is due to the delays

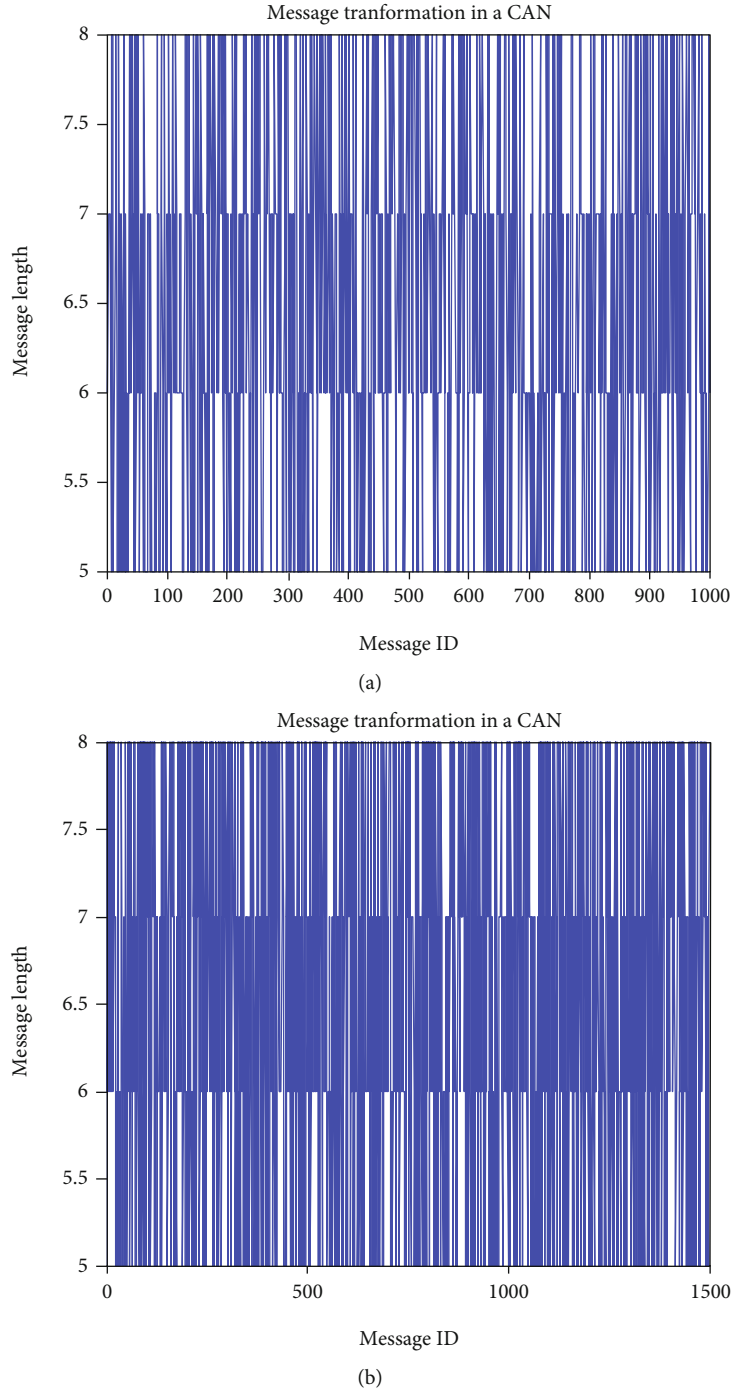


FIGURE 7: (a) Message length = 5 – 8 and ID = 1000 nos and (b) message length = 5 – 8 and ID = 1500 nos.

or occurrence of any noise. Due to that reason, the message may need to be re-transmitted which is denoted by  $RT_i$  for message  $i$ . So, It can be expressed as:

$$RT_i = \lceil S_i * PR_i \rceil \quad (3)$$

Where the total frames set defines as  $S_i$  of a message  $i$ , and the percentage of need for message re-transmission size can be defined by  $PR_i$ . In the case of non-complex data,  $PR_i=0$  and for other types of data, it is expressed as  $PR_i>0$ . Then the

worst-case communication time ( $WC_i$ ) can be calculated for message  $i$  without any error situation and can be expressed as

$$WC_i = S_i * p_k * \tau_{bit} \quad (4)$$

Here, when the bits are stuffed, then the worst case data packet size is denoted as  $p_k$ .

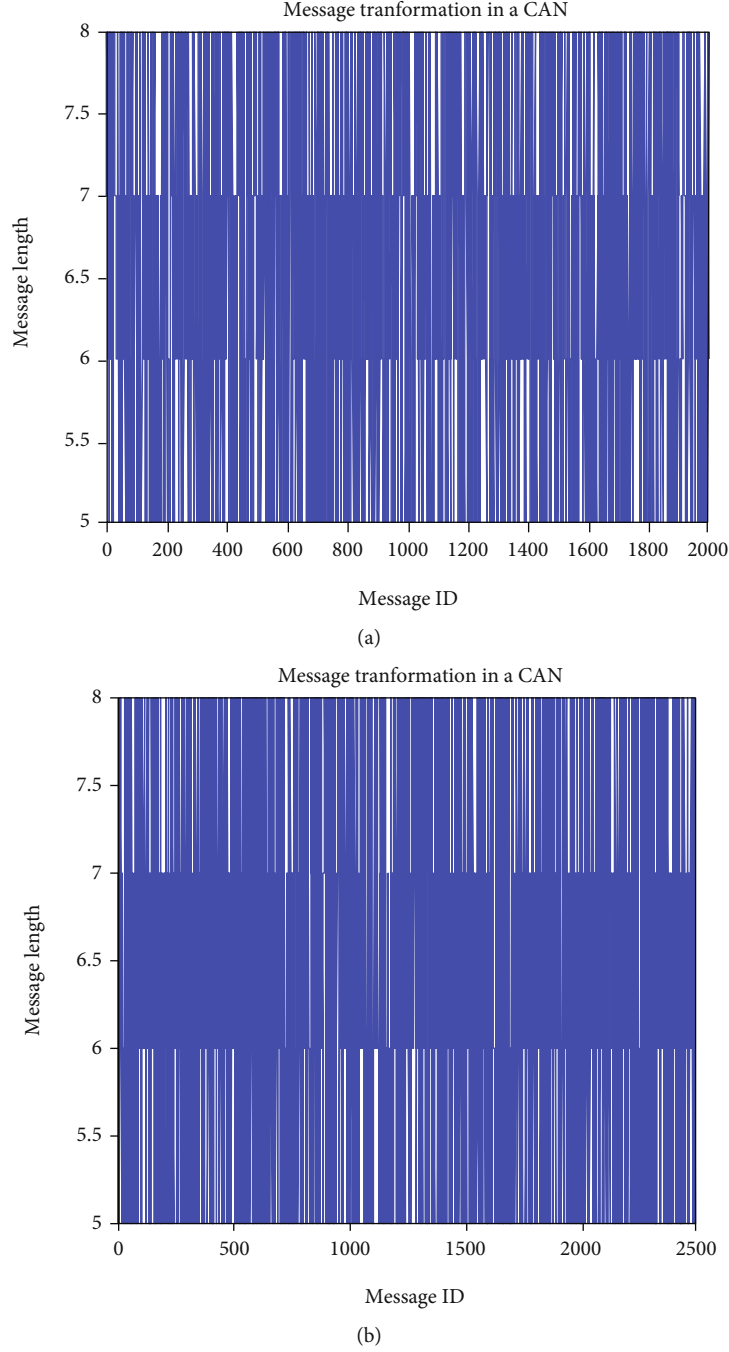


FIGURE 8: (a) Message length = 5 – 8 and ID = 2000 nos and (b) message length = 5 – 8 and ID = 2500 nos.

4.3. *Phase Communication Time and Optimal Action of Message Frame.* The instant jitter function can be expressed as  $j_{i,m} = P_{i,m} - (m * TS_i + \phi_i)$ , and according to that, system the jitter sum can be given as

$$J_S = \sum_{n=1}^t \sum_{m=1}^t j_{i,m} \quad (5)$$

where  $j_{i,m}$  denotes the instant jitter of the  $k^{\text{th}}$  data frame of the sensor node  $m$ , the beginning time of the communication is denoted as  $P_{i,m}$ ,  $\phi_i$  is the start-up phasing of the sys-

tem and the communication time interval of sensor node  $i$  is expressed as  $TS_i$ . So the alteration between the predicted starting and actual time of communication is expressed by the expression  $P_{i,m} - (m * TS_i + \phi_i)$ . The fitness can be calculated for optimal action of the system as

$$F(t) = J_S. \quad (6)$$

When a number of messages is used for transmission, then the crossover condition occurs and due to that,

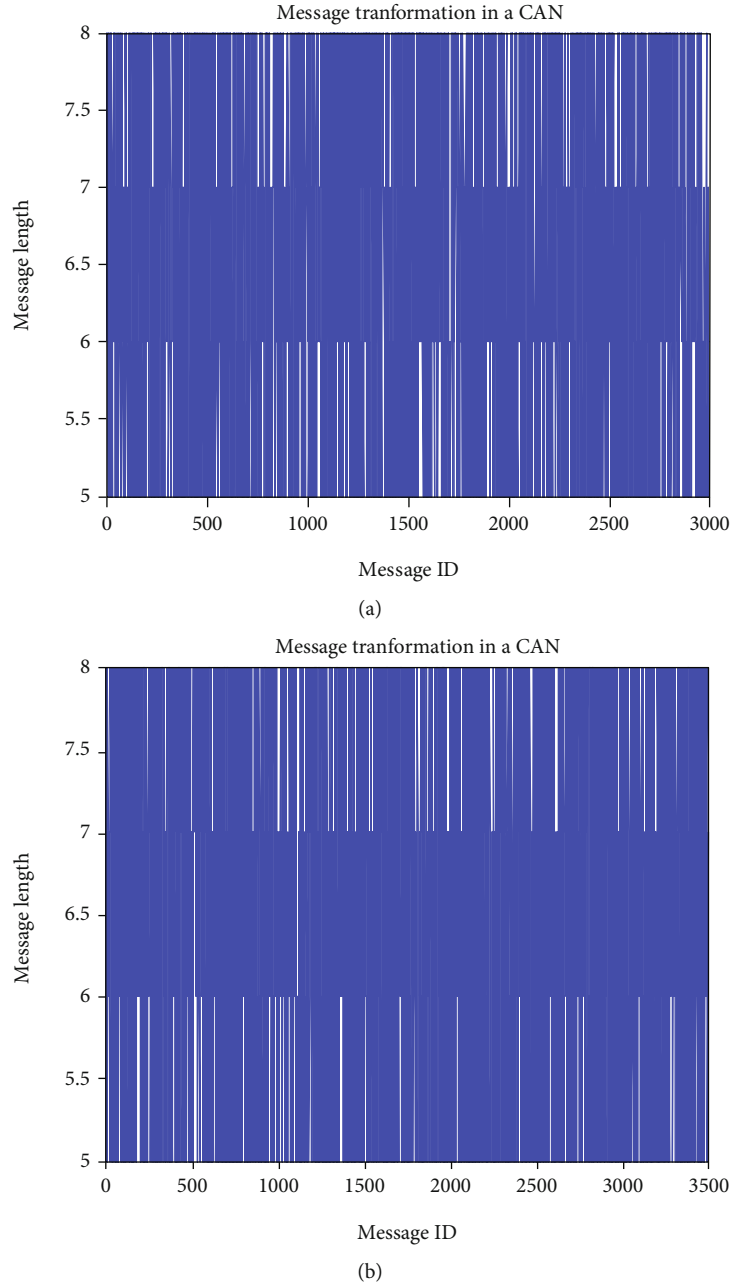


FIGURE 9: (a) Message length = 5 – 8 and ID = 3000 nos and (b) message length = 5 – 8 and ID = 3500 nos.

messages are queued according to their priorities. The successors are formed during processing by crossover action. It requires optimal scheduling; thus, we can choose a crossover probability of 1.0. Again, this process has improved the optimization by using efficient transformation probability as follows:

$$P_{trans} = \begin{cases} \frac{0.1(f_m - f)}{f_m - f_a}, & f \geq f_a, \\ 0.2, & f \leq f_a. \end{cases} \quad (7)$$

**4.4. Message Analysis in CAN Protocol.** The various level of ECUs is accessed in automotive applications to transfer signals as a form of message for steering of wheel speeds, gear selection and position of all controlled nodes of vehicles, measured through the CAN [47]. There can be more than 2500 separate signals in a high-end car, each essentially substituting an isolated connection in a conventional point-to-point connection unit [51].

These signals are used to read the location of a foot-brake; when it is pressed, the back-light section can be finding changes in signal to on brake light to avoid collision by ECU of IoT section of the CAN bus. When the messages

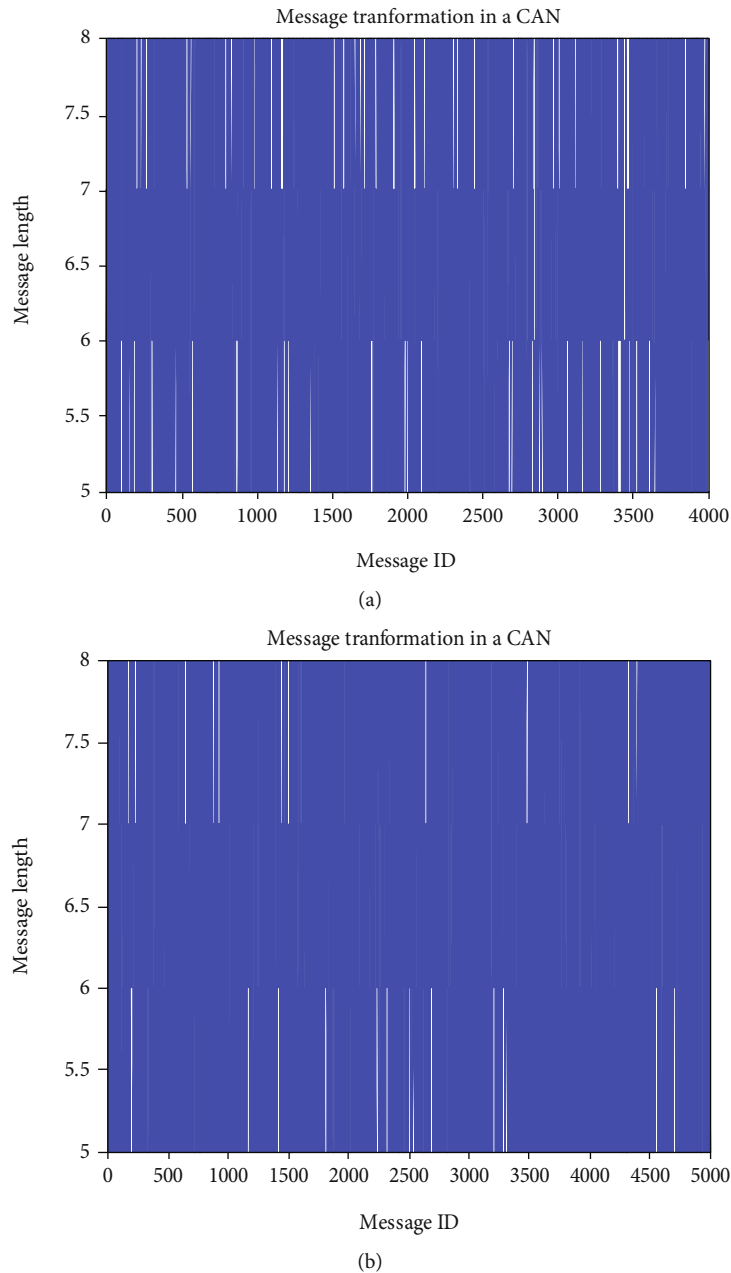


FIGURE 10: (a) Message length =5-8 and ID=4000 nos and (b) message length =5-8 and ID =5000 nos.

of CAN are linked with the deadline, then it responds within their time constraints as often as once every five milliseconds due to the stability and engine control system of an automobile.

**4.4.1. Message Formats.** The restricted data context is discussed in four message formats such as message frame, isolated node, error bit, and excess load bit [52]. A data frame starts with the begin-of-frame bit (BOF), 11-bit ID, and the distant transfer request (DTR) bit [53] [54]. The area of arbitration forms the ID and the DTR bit.

The control field contains six bits that also specify the length of bytes in the data field, which can range from 0 to

8 bytes. Whereas a CRC bit is used to verify whether the bit sequence has been modified or not in the data field. The transmitter uses the 2-bit acknowledgment field (ACK) to obtain correct frame recognition from of receiver. The end of a message frame signal is denoted in the 7-bit end of frame (EOF) which is expanded to a twenty-nine-bit ID recipient. A 21-bit extended database framework is also available.

- (i) Response time calculations under normal case
- (ii) Graph of maximum achievable utilization versus  $T_f$
- (iii) Graphs of response time of any message versus  $T_f$

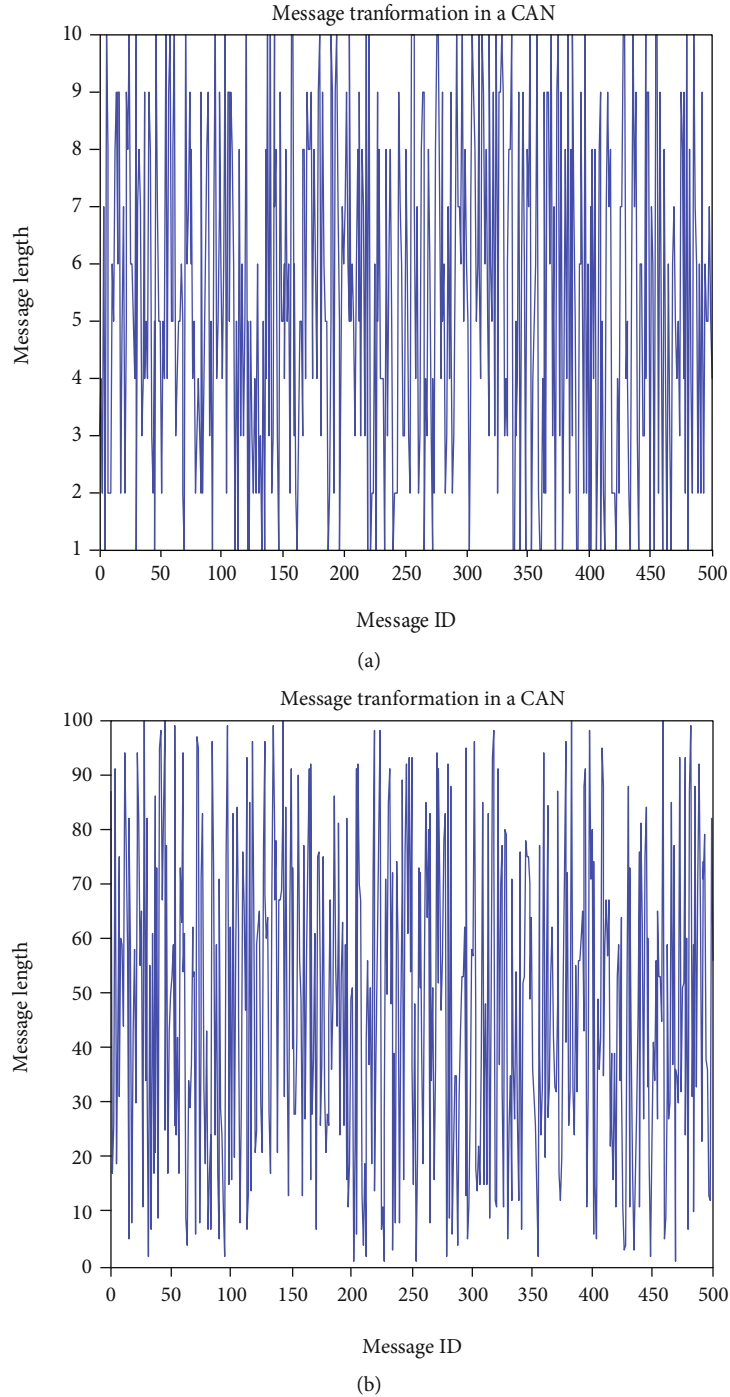


FIGURE 11: (a) Message length = 1-10 and ID =500 nos and (b) message length = 1-100 and ID =500 nos.

(iv) Worst case tolerable value for  $T_f$

Suppose for every first frame, message priorities are already assigned; that is  $\Pi_i, 1$  is assigned for each  $1 \leq i \leq m$  to first frame. In the absence of general losses, it can be assumed that messages are organized accordingly: that is  $i < j$  implies that  $\pi_i, 1 < \pi_j, 1$ . If all subsequent frames are assigned priority  $\pi_i, 2$   $n_i$ , assume that WCRT( $i, \pi_i, 2n_i$ ) will use the methods shown above to find the worst-case response time  $RT_i$  designed for message  $i$ . In order to deter-

mine whether a feasible priority assignment exists, one can then use the algorithm given below in Algorithm 1.

This algorithm is optimal in that it always identifies one of the priorities for the two levels allocated. This algorithm starts with the lowest priority message frame, and then the worst time complexity is  $O(n^2)$ . The algorithm is proposed for analyzing the response time of the priority of messages from message ID and length in the CAN network. However, this algorithm evaluates response time based on message ID and length.

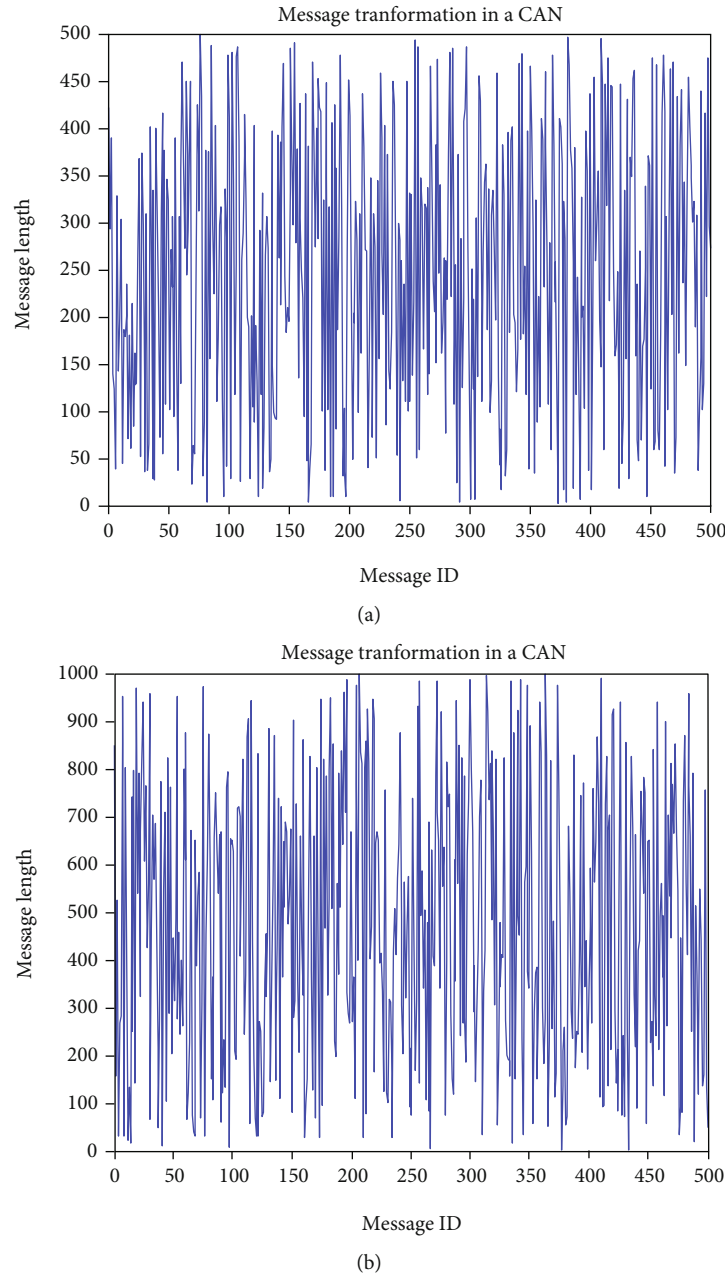


FIGURE 12: (a) Message length = 1-500 and ID =500 nos and (b) message length = 1-1000 and ID =500 nos.

4.5. *Components Description.* Different types of hardware components are required to design this proposed system:

4.5.1. *Arduino UNO R3 Controller.* It is an open-source and IDE microcontroller that controls every movement of sensor nodes and other system network nodes [55] [56]. The C or C++ language are simply used for programming.

4.5.2. *HC-SR04 Ultrasonic Ranging Module.* The sensor module is typically used in the 2 cm-400 cm range to measure the distance of the obstacle [57]. Thus, the angle of 15 degrees with a voltage of 5 V dc is made.

4.5.3. *L298N Dual Bridge Motor Driver Module.* L298N is a driver circuit with two inputs that makes the system to be independently enabled or disabled and the motor movement can also be controlled [58] [59]. In this case, the pulse of PWM is used to set the service period for signalling.

4.5.4. *DC Motors.* DC motor is accompanied by the two 150 rpm DC motors, which needs 12 V of voltage and 1-2 Amp current to start moving from right to left.

4.5.5. *SG 90 Microservo Motor.* It is a very lightweight server motor with high strength, which can rotate easily about 180



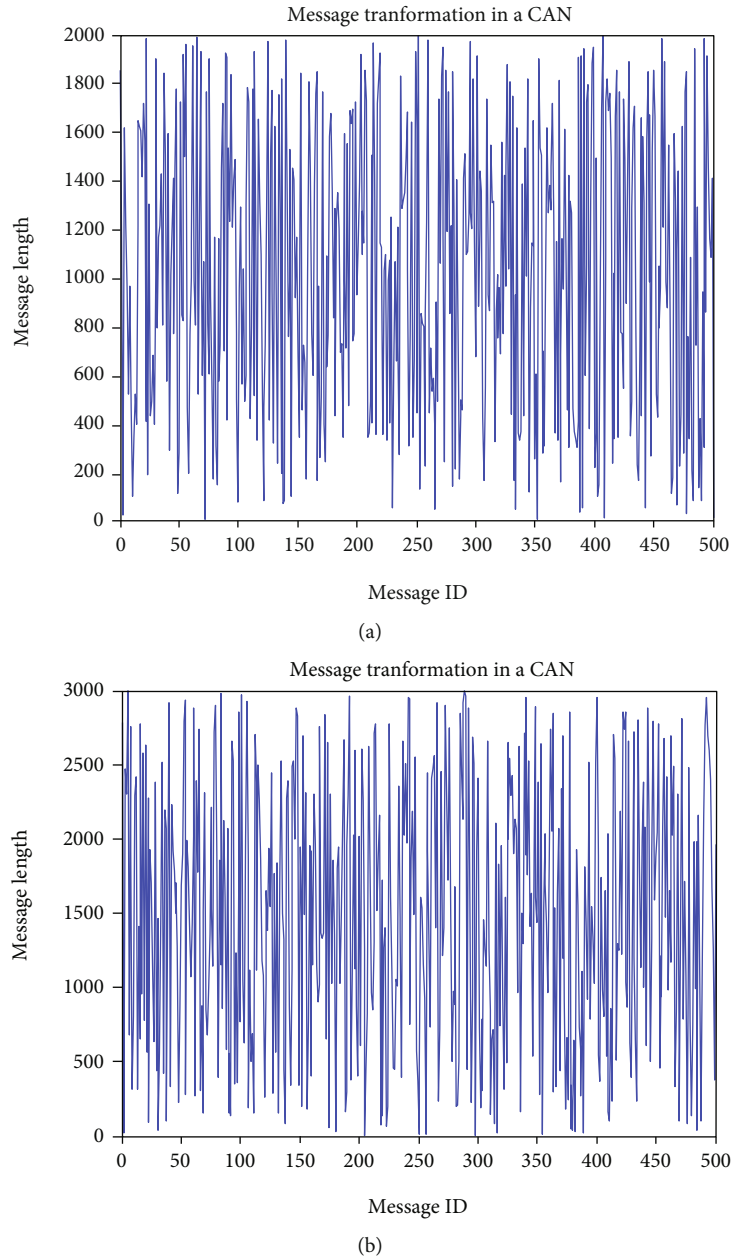


FIGURE 13: (a) Message length = 1-2000 and ID =500 nos and (b) message length = 1-3000 and ID =500 nos.

degrees (90 per path) [60] [61]. However, the movement is regulated through servo code, hardware and library.

## 5. Simulation Setup and Results Discussion

The intelligent self-employed vehicle is moving forward, which calculates the distance of an obstacle automatically. When an obstacle is detected within 20 cm via an ultrasonic sensor, the message frames obtained are transmitted to the controller. The CAN protocol code is received by the controller, which instructs the command to regulate motor movement from left to right and back. The collision avoidance algorithm was successfully implemented in order to reduce the problem. The front and top view of the Smart

Autonomous Collision Avoidance Vehicle is shown in Figures 5(a) and 5(b).

**5.1. Response Time Analysis.** One of the types of field bus control devices used in networking is CAN. It is a protocol system based on a packet. Communication can be accomplished using the CAN protocol between different devices. The CAN bus is used to control the unit of transmission and receiving unit, which is mainly implemented due to low costs. The CAN multi-master node cannot simultaneously be transmitting and accepting messages that consist of a message ID as well as the message frame is communicated consecutively to the bus.

The CAN carriers detect multiple access protocols with collision detection and message priority arbitration, and

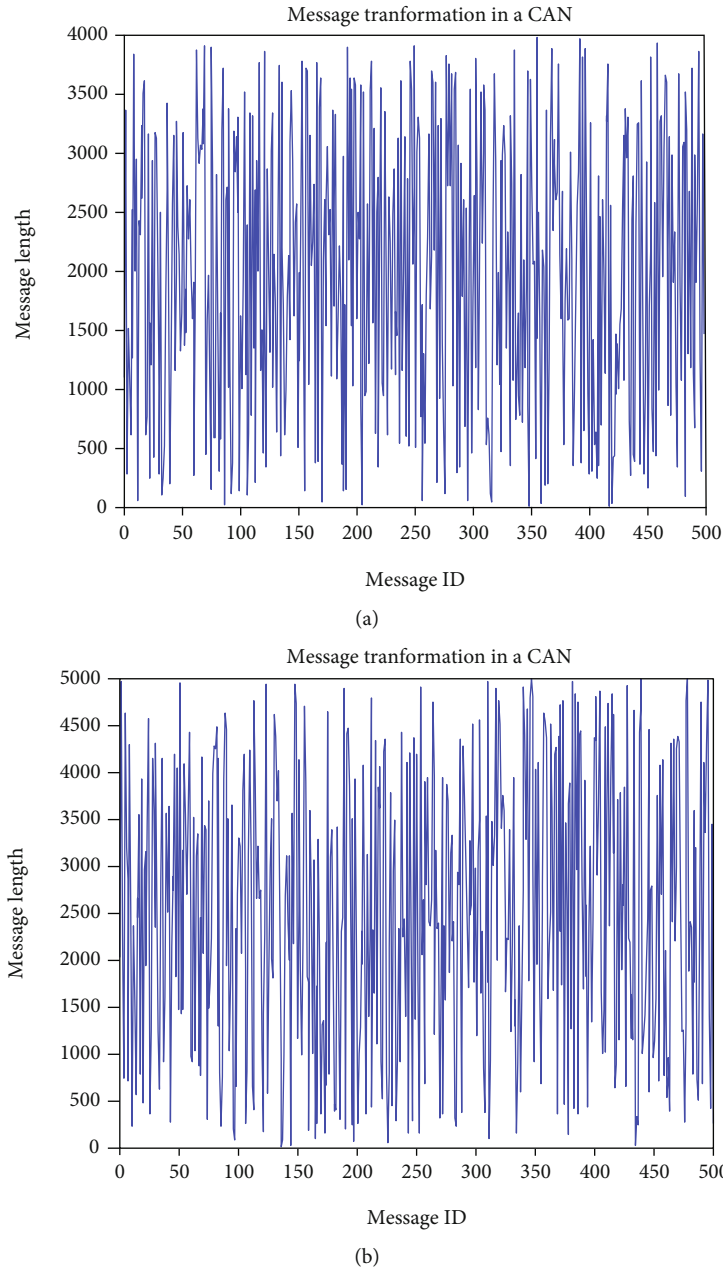


FIGURE 14: (a) Message length = 1-4000 and ID =500 nos and (b) message length = 1-5000 and ID =500 nos.

there are two types of protocols used in it. For flow control, the technique is used to confirm sensor data integrity, the cyclic redundancy checks (CRC) for an error control mechanism, which also manages the remote frames and the overload frames. CAN-based Database file (.dbc) is taken from the website CAN RT.dbc. It includes numerous attributes such as Name, Statement, ID, Duration, Signals, and Extended. We just take value for message length and message ID in this document which is shown in Table 1. So, these parameters observe the response of messages in the field of communication within the CAN network. After checking various data numbers, we get the following results, which are shown below. Figure 6 shows (a) message length

= 5 – 8 and ID = 100 nos and (b) message length = 5 – 8 and ID = 500 nos.

5.1.1. Result for Constant Message Length and Variable Message ID. Figure 7 shows (a) message length = 5 – 8 and ID = 1000 nos and (b) message length = 5 – 8 and ID = 1500 nos. Figure 8 shows (a) message length = 5 – 8 and ID = 2000 nos and (b) message length = 5 – 8 and ID = 2500 nos. Figure 9 shows (a) message length = 5 – 8 and ID = 3000 nos and (b) message length = 5 – 8 and ID = 3500 nos. Figure 10 shows (a) message length = 5 – 8 and ID = 4000 nos and (b) message length = 5 – 8 and ID = 5000 nos. In the simulation result, we got some figures which represent

different outcome from the use of CAN RT.dbc. Figures 6–10 represent that the message transformation is performed in the CAN network of two classes of inputs generated by taking fixed values for message length 5-8 and random values for message ID like 100 nos, 500 nos, 1000 nos, 1500 nos, 2000 nos, 2500 nos, 3000 nos, 3500 nos, 4000 nos, 5000 nos, respectively. When the simulation of the above network is performed by changing of message ID parameter, which shows response time (located through the white line) that varies through the process. The above analysis shows that the response time is more delayed by increasing message ID numbers. Similarly, the message is highly responded to at fewer messages ID which is shown in the above figures.

*5.1.2. Result for Constant Message ID and Variable Message Length.* We have some figures in the simulation outcome that show different outcomes from the use of CAN RT.dbc. In the CAN network, figures reflect the message conversion of two groups of inputs created by taking fixed values for message ID 500 numbers and random values for message length such as 1-10, 1-100, 1-500, 1-1000, 1-2000, 1-3000, 1-4000, 1-5000. When this network simulation is performed by changing the message length parameter with fixed message length and it shows no more changes in the response time of the process in the above figures. Figure 11 shows (a) message length = 1 – 10 and ID = 500 nos and (b) message length = 1 – 100 and ID = 500 nos. Figure 12 shows (a) message length = 1 – 500 and ID = 500 nos and (b) message length = 1 – 1000 and ID = 500 nos. Figure 13 shows (a) message length = 1 – 2000 and ID = 500 nos and (b) message length = 1 – 3000 and ID = 500 nos. Figure 14 shows (a) message length = 1 – 4000 and ID = 500 nos and (b) message length = 1 – 5000 and ID = 500 nos.

*5.2. Discussion.* In a practical scenario, several attributes such as Name, Statement, ID, Extended, Length, Signals have to be considered from the collected database. If all these attributes are combined, we can get an unschedulable framework in certain situations. Therefore, some of the attributes already in the database, such as Name, Statement, Expanded, and Signals, need to be removed. For communication, some powerful attributes such as ID and length have to be considered for a particular message.

We might easily get a very negative analysis to find errors if there are many such data and we compose them. We have shown from the simulation outcome that there was no difference in the simulation outcome for different message length values by holding the message ID unchanged. In other words, we can assume that message length variance has less influence than message ID. We take the message ID from 1 to 5000 in this paper and check the network conjunction result. We also shift the message's duration from 1 to 5000 and examine the transformation impact of this change in values.

The existing approaches tested in a limited range of message length and message ID values which is not provided a clear idea about the performance of the CAN network. But this paper is taking 1-5000 numbers values for message length and message ID. According to the proposed experi-

ment is evaluating performance in two ways like (i) constant message length with variance number of values (1-5000) for message ID and (ii) constant message ID with variance number of values (1-5000) for message length. Thus the performance is varied on the case of constant message length with variance number of values (1-5000) for message ID, but the consistent performance is evaluated on the case of constant message ID with variance number of values (1-5000) for message length.

## 6. Conclusion and Future Scope

While several solution algorithms and concepts have been developed over several years to solve conflict issues using CAN communication on the vehicle network, there have been few attempts to develop a solution to the handling of errors. This is a comparison-based analysis of the variable message ID and constant message length figures that we concluded that if we send no more messages at a time, then there would be more conflict on the network. The recipient will not get the real message due to conflict, and there will also be a risk of receiving more than one message at a single node. The CAN protocol is used to provide a secure and robust serial communication bus from sensor nodes to the control unit of an automated system. When the sensor node of the IoT module is received, a message frame can be transmitted to the destination node that can be responded to in time. The phase of communication time and the optimal action of the message frame are utilised to build a flexible format for transmission of a frame from sender end to receiver end, which implies that a system node can receive a message frame and respond to it via an acknowledged frame bit. The proposed scheme achieves high precision, determining the location of an obstacle and then monitoring the impact of collision time.

More number of experiments could be carried out and future directions are:

- (a) To assess the efficiency of the algorithms, a large number of experiments with more tasks have to be tested
- (b) Secondly, it is important to evaluate large-size problem cases using periodic preemptive tasks

A new automatically moving algorithm between the EDF algorithm and the ACO scheduling algorithm should be developed in the future to work with overloaded conditions.

## Data Availability

The IoT data that support the findings of this study are available on request from the corresponding author.

## Conflicts of Interest

The authors of this manuscript declared that they do not have any conflict of interest.

## Acknowledgments

This paper was partially supported by the Ministry of Science and Higher Education of the Russian Federation (Assignment No. 075-02-2021-1748) and Device Development Programme (DST/TDT/DDP-38/2021), by the Department of Science Technology, Ministry of Science and Technology, Government of India.

## References





- [1] G. Li, W. Lai, X. Sui et al., "Influence of traffic congestion on driver behavior in post-congestion driving," *Accident Analysis & Prevention*, vol. 141, p. 105508, 2020.
- [2] P. A. Hancock, T. Kajaks, J. K. Caird et al., "Challenges to human drivers in increasingly automated vehicles," *Human Factors*, vol. 62, no. 2, pp. 310–328, 2020.
- [3] U. Kiencke, S. Dais, and M. Litschel, "Automotive serial controller area network," *SAE Transactions*, vol. 95, pp. 823–828, 1986.
- [4] Y.-J. Kim, H.-Y. Lee, and J.-G. Chung, "4-bit data arrangement algorithm for can compression," in *2018 International SoC Design Conference (ISOCC)*, pp. 216–217, Daegu, Korea (South), 2018.
- [5] S. Dekanic, R. Grbic, T. Maruna, and I. Kolak, "Integration of can bus drivers and uds on aurix platform," in *2018 Zooming Innovation in Consumer Technologies Conference (ZINC)*, pp. 39–42, Novi Sad, Serbia, 2018.
- [6] I. Gonzalez and A. J. Calderon, "Integration of open source hardware arduino platform in automation systems applied to smart grids/micro-grids," *Sustainable Energy Technologies and Assessments*, vol. 36, article 100557, 2019.
- [7] G. Kornaros, O. Tomoutzoglou, D. Mbakoyiannis et al., "Towards holistic secure networking in connected vehicles through securing CAN- bus communication and firmware-over-the-air updating," *Journal of Systems Architecture*, vol. 109, p. 101761, 2020.
- [8] D.-S. Kim and H. Tran-Dang, "Industrial sensors and controls in communication networks," in *Computer Communications and Networks*, Springer International Publishing, Cham, 2019.
- [9] H. Lu, Q. Liu, D. Tian, Y. Li, H. Kim, and S. Serikawa, "The cognitive internet of vehicles for autonomous driving," *IEEE Network*, vol. 33, no. 3, pp. 65–73, 2019.
- [10] L. Chelouah, F. Semchedine, and L. Bouallouche-Medjkoune, "Localization protocols for mobile wireless sensor networks: a survey," *Computers & Electrical Engineering*, vol. 71, pp. 733–751, 2018.
- [11] G. T. Reddy, M. P. K. Reddy, K. Lakshmana et al., "Analysis of dimensionality reduction techniques on big data," *IEEE Access*, vol. 8, pp. 54776–54788, 2020.
- [12] N. Deepa, Q.-V. Pham, D. C. Nguyen et al., "A survey on blockchain for big data: Approaches, opportunities, and future directions," 2020, <https://arxiv.org/abs/2009.00858>.
- [13] A. L. Kun, S. Boll, and A. Schmidt, "Shifting gears: user interfaces in the age of autonomous driving," *IEEE Pervasive Computing*, vol. 15, no. 1, pp. 32–38, 2016.
- [14] J. Sanchez-Garcia, J. Garcia-Campos, M. Arzamendia, D. G. Reina, S. Toral, and D. Gregor, "A survey on unmanned aerial and aquatic vehicle multi-hop networks: Wireless communications, evaluation tools and applications," *Computer Communications*, vol. 119, pp. 43–65, 2018.
- [15] A. K. Biswal, D. Singh, B. K. Pattanayak, D. Samanta, and M.-H. Yang, "Iot-based smart alert system for drowsy driver detection," *Wireless Communications and Mobile Computing*, vol. 2021, 13 pages, 2021.
- [16] IndustryJournalPro, "Forward collision avoidance radar market research report 2019-2025," 2019, 2021, <https://industryjournalpro.com/forward-collision-avoidance-radar-market-research-report-2019-2025/>.
- [17] Hyundai, "12 Hyundai safety features that make driving today safer than ever," 2020, 2021, <https://www.hyundai.com/au/en/why-hyundai/myhyundai-news/issues/2020/issue-02/12-hyundai-safetyfeatures-that-make-driving-today-safer-than-ever>.
- [18] T. Nolte, M. Nolin, and H. A. Hansson, "Real-time server-based communication with can," *IEEE Transactions on Industrial Informatics*, vol. 1, no. 3, pp. 192–201, 2005.
- [19] W. L. Ng, C. K. Ng, B. M. Ali, N. K. Noordin, and F. Z. Rokhani, "Review of researches in controller area networks evolution and applications," *Proceedings of the Asia-Pacific Advanced Network*, vol. 30, pp. 14–21, 2013.
- [20] A. S. Shinde and V. B. Dharmadhikari, *Controller Area Network for Vehicle Automation*, CiteSeer, 2012.
- [21] G. Yu, C. Zhou, and S. Huang, "A protocol for automatic node-id binding in canopen networks," *JCM*, vol. 7, no. 10, pp. 765–773, 2012.
- [22] T. Vijayan, *Controller Area Network in Modern Home Automation*, CiteSeer, 2012.
- [23] C.-L. Wey, C.-H. Hsu, K.-C. Chang, P.-C. Jui, and M.-T. Shiue, "Emi prevention of can-bus-based communication in battery management systems," *International Journal of Engineering & Computer Science IJECS-IJENS*, vol. 13, no. 5, pp. 6–12, 2013.
- [24] K. C. Emani, K. Kam, M. Zawodniok, Y. R. Zheng, and J. Sarangapani, "Improvement of can bus performance by using error-correction codes," in *2007 IEEE Region 5 Technical Conference*, pp. 205–210, Fayetteville, AR, USA, 2007.
- [25] H. A. Hansson, T. Nolte, C. Norstrom, and S. Punnekkat, "Integrating reliability and timing analysis of can-based systems," *IEEE Transactions on Industrial Electronics*, vol. 49, no. 6, pp. 1240–1250, 2002.
- [26] R. I. Davis, A. Burns, R. J. Bril, and J. J. Lukkien, "Controller area network (can) schedulability analysis: refuted, revisited and revised," *Real-Time Systems*, vol. 35, no. 3, pp. 239–272, 2007.
- [27] G. Xie, G. Zeng, R. Kurachi, H. Takada, R. Li, and K. Li, "Exploiting Sparsity to Accelerate Fully Connected Layers of CNN-Based Applications on Mobile SoCs," *ACM Transactions on Embedded Computing Systems (TECS)*, vol. 17, no. 2, pp. 1–25, 2018.
- [28] G. Xie, G. Zeng, R. Kurachi et al., "Wcrt analysis and evaluation for sporadic message-processing tasks in multicore automotive gateways," *IEEE Transactions on Computer-Aided Design of Integrated Circuits and Systems*, vol. 38, no. 2, pp. 281–294, 2019.
- [29] R. Alaei, P. Moallem, and A. Bohlooli, "Statistical based algorithm for reducing bit stuffing in the controller area networks," *Microelectronics Journal*, vol. 101, p. 104794, 2020.
- [30] K. Liu, E. Fridman, and L. Hetel, "Networked control systems in the presence of scheduling protocols and communication delays," *SIAM Journal on Control and Optimization*, vol. 53, no. 4, pp. 1768–1788, 2015.



- [31] B. H. C. Orak, F. Y. Okay, M. Guzel, S. Murt, and S. Ozdemir, "Comparative analysis of iot communication protocols," in *2018 International symposium on networks, computers and communications (ISNCC)*, pp. 1–6, Rome, Italy, 2018.
- [32] K. T. Nguyen, M. Laurent, and N. Oualha, "Survey on secure communication protocols for the internet of things," *Ad Hoc Networks*, vol. 32, pp. 17–31, 2015.
- [33] S. Krishnamoorthy, *Design of an ASIC chip for a Controller Area Network (CAN) protocol controller*, [Ph.D. thesis], Texas Tech University, 2006.
- [34] J. Long, "Automobile electronic control network design based on can bus," in *2018 International Conference on Intelligent Transportation, Big Data & Smart City (ICITBS)*, pp. 9–12, Xiamen, China, 2018.
- [35] K. Pazul, *Controller area network (can) basics*, Microchip Technology Inc, 1999.
- [36] K. H. Johansson, M. Torngren, and L. Nielsen, "Vehicle applications of controller area network," in *Handbook of networked and embedded control systems*, Springer, 2005.
- [37] W. E. Lawrenz, *System design tools for networked systems in cars*, SAE Technical Paper, 1990.
- [38] Q. Zhu, Z. Dongmei, and S. Xunwen, "Distributed remote temperature monitoring and acquisition system based on can bus," in *2010 Prognostics and System Health Management Conference*, pp. 1–4, Macao, China, 2010.
- [39] SC HPL, "Introduction to the controller area network (can)," in *Application Report SLOA101*, Texas Instruments, 2002.
- [40] P. Santi, "Topology control in wireless ad hoc and sensor networks," *ACM Computing Surveys (CSUR)*, vol. 37, no. 2, pp. 164–194, 2005.
- [41] M. A. C. Aung and K. P. Thant, "Detection and mitigation of wireless link layer attacks," in *2017 IEEE 15th International Conference on Software Engineering Research, Management and Applications (SERA)*, pp. 173–178, London, UK, 2017.
- [42] Y. Liu, Q. Zhang, and L. Ni, "Opportunity-based topology control in wireless sensor networks," *IEEE Transactions on Parallel and Distributed Systems*, vol. 21, no. 3, pp. 405–416, 2010.
- [43] S. Hasnaoui, O. Kallel, R. Kbaier, and S. B. Ahmed, "An implementation of a proposed modification of can protocol on can fieldbus controller component for supporting a dynamic priority policy," in *38th IAS Annual Meeting on Conference Record of the Industry Applications Conference, 2003*, pp. 23–31, Salt Lake City, UT, USA, 2003.
- [44] S. Hong and W.-H. Kim, "Bandwidth allocation scheme in can protocol," *IEE Proceedings-Control Theory and Applications*, vol. 147, no. 1, pp. 37–44, 2000.
- [45] X. Wang and W. Guo, "The design of rs232 and can protocol converter based on pic mcu," *Computer and Information Science*, vol. 2, no. 3, pp. 176–181, 2009.
- [46] Q. Lin, Y. Zhang, A. Van Mieghem et al., "Design and experiment of a sun-powered smart building envelope with automatic control," *Energy and Buildings*, vol. 223, article 110173, 2020.
- [47] G. I. Mary, Z. C. Alex, and L. Jenkins, "Response time analysis of messages in controller area network: a review," *Journal of Computer Networks and Communications*, vol. 2013, Article ID 148015, 11 pages, 2013.
- [48] Y. Wang and M. Saksena, "Scheduling fixed-priority tasks with preemption threshold," in *Proceedings Sixth International Conference on Real-Time Computing Systems and Applications. RTCSA'99 (Cat. No. PR00306)*, pp. 328–335, Hongkong, 1999.
- [49] J. Van Waes, J. Lannoo, A. Degraeve, D. Vanoost, D. Pissoort, and J. Boydens, "Effectiveness of cyclic redundancy checks under harsh electromagnetic disturbances," in *2017 International Symposium on Electromagnetic Compatibility-EMC EUROPE*, pp. 1–6, Angers, France, 2017.
- [50] G. Leen and D. Heffernan, "Tcan: a new time-triggered controller area network," *Microprocessors and Microsystems*, vol. 26, no. 2, pp. 77–94, 2002.
- [51] K. Tindell, A. Burns, and A. J. Wellings, "Calculating controller area network (can) message response times," *Control Engineering Practice*, vol. 3, no. 8, pp. 1163–1169, 1995.
- [52] R. Sato and S. Fukumoto, "Response-time analysis for controller area networks with randomly occurring messages," *IEEE Transactions on Vehicular Technology*, vol. 69, no. 4, pp. 3893–3902, 2020.
- [53] S. Mubeen, J. Maki-Turja, and M. Sjodin, "Extending Worst Case Response-Time Analysis for Mixed Messages in Controller Area Network With Priority and FIFO Queues," *IEEE Access*, vol. 2, pp. 365–380, 2014.
- [54] G. Cena, I. C. Bertolotti, T. Hu, and A. Valenzano, "Can with extensible in-frame reply: protocol definition and prototype implementation," *IEEE Transactions on Industrial Informatics*, vol. 13, no. 5, pp. 2436–2446, 2017.
- [55] N. S. Kumar, B. Vuayalakshmi, R. J. Prarthana, and A. Shankar, "Iot based smart garbage alert system using arduino uno," in *2016 IEEE Region 10 Conference (TENCON)*, pp. 1028–1034, Singapore, 2016.
- [56] A. K. Biswal, D. Singh, and B. K. Pattanayak, "Iot-based voice-controlled energy-efficient intelligent traffic and street light monitoring system," in *Green Technology for Smart City and Society*, Springer, 2021.
- [57] V. Zhmud, N. Kondratiev, K. Kuznetsov, V. Trubin, and L. Dimitrov, "Application of ultrasonic sensor for measuring distances in robotics," *Journal of Physics: Conference Series*, vol. 1015, article 032189, 2018.
- [58] M. H. Y. Yumei, "High-precision servo controller of dc micro-motor based on dspic30f4011," *Electronic Measurement Technology*, vol. 10, 2010.
- [59] M. M. Maung, M. M. Latt, and C. M. Nwe, "Dc motor angular position control using pid controller with friction compensation," *International Journal of Scientific and Research Publications*, vol. 8, no. 11, p. 149, 2018.
- [60] S. K. Mostaque and B. Karmakar, "Low cost arduino based voice controlled pick and drop service with movable robotic arm," *European Journal of Engineering and Technology Research*, vol. 1, no. 5, pp. 29–33, 2018.
- [61] K. Neeraja, P. R. C. Rao, D. S. Maloji, and D. M. A. Hussain, "Implementation of security system for bank using open cv and rfid," *International Journal of Engineering & Technology*, vol. 7, no. 2-7, p. 187, 2018.

## Research Article

# Diagnose Diabetic Mellitus Illness Based on IoT Smart Architecture

Abhilash Pati,<sup>1</sup> Manoranjan Parhi,<sup>1</sup> Binod Kumar Pattanayak <sup>1</sup>, Debabrata Singh,<sup>1</sup>  
Debabrata Samanta <sup>2</sup>, Amit Banerjee <sup>3,4</sup>, Sajal Biring <sup>4,5</sup>,  
and Goutam Kumar Dalapati<sup>4,6</sup>

<sup>1</sup>Siksha 'O' Anusandhan University, Bhubaneswar, Odisha, India

<sup>2</sup>Department of Computer Science, CHRIST University, Bangalore, India

<sup>3</sup>Physics Department, Bidhan Chandra College, Asansol 713 303, India

<sup>4</sup>Organic Electronics Research Center, Ming Chi University of Technology, New Taipei City, Taiwan 24301

<sup>5</sup>Department of Electronic Engineering, Ming Chi University of Technology, New Taipei City, Taiwan 24301

<sup>6</sup>Sunkonnect, 1 Cleantech Loop, Singapore 637141

Correspondence should be addressed to Debabrata Samanta; [debabrata.samanta369@gmail.com](mailto:debabrata.samanta369@gmail.com),  
Amit Banerjee; [amitbanerjee.nus@gmail.com](mailto:amitbanerjee.nus@gmail.com), and Sajal Biring; [biring@mail.mcut.edu.tw](mailto:biring@mail.mcut.edu.tw)

Received 11 May 2022; Revised 14 July 2022; Accepted 28 July 2022; Published 25 August 2022

Academic Editor: Kuruva Lakshmana

Copyright © 2022 Abhilash Pati et al. This is an open access article distributed under the Creative Commons Attribution License, which permits unrestricted use, distribution, and reproduction in any medium, provided the original work is properly cited.

Obtaining a quick remote diagnosis of heart disease has proven problematic in recent days. To overcome such issues in e-Healthcare systems, Internet of Things (IoT) applications have been deployed using cloud computing (CC) approaches. There are still a number of disadvantages to using CC, including latency, bandwidth, energy usage, and security and privacy concerns. Fog computing (FC), a CC development, may be able to overcome these obstacles. DiaFog enabling remote users for real-time diagnosis of diabetic mellitus disease (DMD) has been proposed in this study, which is based on the combined ideas of IoT, cloud, and fog computing, as well as an ensemble deep learning (EDL) technique. The proposed system is trained with EDL approaches on the integrated dataset of two diabetes mellitus disease datasets (DMDDs), namely, Pima Indians Diabetes Dataset (PIDD) and Hospital Frankfurt Germany Diabetes Dataset (HFGDD), obtained from the UCI-ML and Kaggle repository, respectively, and the integrated dataset of these two. The suggested system has been used to demonstrate accuracy, precision, recall, *F*-measure, latency, arbitration time, jitter, processing time, throughput, energy consumption, bandwidth utilization, network utilization, scalability, and more. In the remote instantaneous diagnosis of diabetic patients, the integration of IoT-fog-cloud is useful. The results of the trials show the value of employing FC principles and their applicability for speedy diabetic patient remote diagnosis. PACS-key is describing text of that key PACS-key describing text of that key.

## 1. Introduction

The first digital revolution, i.e., the connection of numerous networks known as the Internet, is regarded as an all-time brilliant invention. The evolving phase continues, and we are now in the second digital revolution, the Internet of Things (IoT), which is essential to long-distance communications. The Internet of Medical Things (IoMT) is a cutting-edge network that offers a global healthcare system that can cure any condition of any location [1, 2]. The globe is becoming more industrialized, and the deceased rate is ris-

ing. However, the number of lifestyle illnesses has been increased in the same period. Type 2 diabetes, heart attack, hypertension attack, and obesity are among these disorders. The kind of nutrition, degree of stress, lack of physical activity, and environmental variables are all critical contributing factors to various disorders. In some instances, the side effects of these disorders may result in life-threatening symptoms such as paralysis, shortness of breath, irregular heartbeat, cardiac arrest, and chest discomfort, all of which need immediate medical treatment. Wearables sensors and IoT applications are becoming more popular for inexpensive

e-Healthcare systems [3, 4]. These IoT applications in e-Healthcare systems have enabled health professionals to monitor patients remotely while allowing patients to access e-Healthcare services easily.

*1.1. Diabetes Mellitus Disease (DMD).* Diabetes, also known as diabetes mellitus disease (DMD), is a common chronic metabolic illness characterized by high blood glucose levels that may lead to various health problems affecting the kidneys, heart, and eyesight. There are three basic forms of DMD, according to the World Health Organization (WHO) [5]:

- (i) Type 1 DMD (T1DMD) is an autoimmune disease that causes insulin levels to drop dramatically
- (ii) Type-2 DMD (T2DDMD) is caused by insulin-producing cells in the pancreas malfunctioning and insulin resistance in the peripheral organs
- (iii) Gestational DMD (GDMD) is a kind of diabetes that affects pregnant women who have blood glucose levels that are higher than usual

Because of the health risks associated with DMD, it is critical to keep an eye on vulnerable populations, such as children, the elderly, and pregnant women [6, 7].

*1.2. IoT-Fog-Cloud Integration Approach.* Primarily, IoT applications are based only on CC. The CC creates a complete bundle for the individuals. e-Healthcare systems are aimed at making patients' lives simpler and more convenient. Current e-Healthcare systems rely heavily on IoT-enabled smart devices. Real-world applications of CC and its enlarged variations, such as edge computing (EC) and FC, have lately emerged [8, 9]. Traditional cloud networking infrastructures include restrictions like lesser data transmission speed, mobile traffic management, and privacy and security issues. So to circumvent the limits and operate as a bridge between various terminals and cloud servers, FC was created [10]. The IoT is built on the combined concepts of FC and CC ideas [11]. FC is a feature of CC that allows for reduced latency in cloud servers [12]. Fog-based designs efficiently cope with e-Healthcare system issues such as scalability, readability, flexibility, and energy awareness [13]. The FC tries to improve node-to-node communication while saving bandwidth [14]. The FC may be utilized to enhance disease diagnosis and prediction accuracy [15, 16]. The IoT-fog-cloud integration architecture generally comprises three layers, as depicted in Figure 1.

*1.3. Ensemble Learning (EL) in Disease Diagnosis.* Ensemble learning (EL) classification-based algorithms have recently been suggested to tackle classification error concerns in machine learning (ML) applications. The researchers, hence, proposed some ensemble classifiers for software fault prediction in [17]. For multiclass imbalanced data classification, ensemble classifiers are also used [18, 19]. The support vector machine (SVM),  $k$ -nearest neighbors (KNN), naive Bayes (NB), decision tree (DT), artificial neural network (ANN), fuzzy decision tree, and logistic regression- (LR-) based learning approaches have been used for diabetes

prediction [20]. However, these methods suffer from low classification accuracy and computational complexity despite their popularity. Thus, a unique ensemble strategy is required to increase diabetes classification accuracy and deep learning (DL) in many datasets to justify that the proposed model is efficient.

*1.4. Research Gap and Motivation.* In recent years, the rising deceased rate from chronic diseases such as diabetes has posed a danger to people worldwide. Furthermore, bringing medical advantages closer to these patients in real-time is a societal challenge. Previously, diabetes patients used self-monitoring of blood glucose (SMBG) approaches such as pricking their fingers numerous times per day to test their blood glucose levels [8, 21]. There are several disadvantages to using such tactics. Then, emerged the idea of IoT health sensors, which replaced conventional sensors that lacked Bluetooth capabilities to automatically input users' detected data into smartphones through a specialized mobile application. A wide range of studies has been conducted employing the integration principles of IoT, CC, and FC, with most studies focusing on smart cities and smart homes. In e-Healthcare systems, the integration notion is also essential. It is worth noting that these studies are hardware-based yet have a real-time influence on society; nonetheless, they might be a one-time expenditure for a particular ailment. In recent days, fast remote diagnosis of any sickness has become a sought-after task.

*1.5. Research Questions.* The following research questions (RQs) have been considered in this study:

RQ1. What are the key outcomes of using a preprocessed integrated dataset for the diagnosis of DMDs?

RQ2. What are the major benefits of involving EL approaches with DL techniques in predicting a specific disease?

RQ3. What are the motives for using the integrated architecture in e-Healthcare systems, as well as the primary projected benefits?

RQ4. What is the primary objective of the IoT-fog-cloud integrated framework in processing e-Healthcare systems?

RQ5. Is it conceivable under the proposed work for the user to restrict third-party exposure to their clinical records?

*1.6. Objective and Key Contributions of the Research.* The rapid diagnosis of diabetes patients remotely is a need which is the main objective of this research. In this paper, DiaFog enabling remote users for real-time diagnosis of diabetes mellitus disease based on integrated concepts of IoT, cloud, and fog computing and ensemble deep learning (EDL) has been proposed. The proposed system is trained with EDL approaches on the integrated dataset of two diabetes mellitus disease datasets (DMDDs), namely, Pima Indians Diabetes Dataset (PIDD) and Hospital Frankfurt Germany Diabetes Dataset (HFGDD), obtained from the UCI-ML and Kaggle repository, respectively, and the integrated dataset of these two.

This paper's main goal and contributions may be described this way:



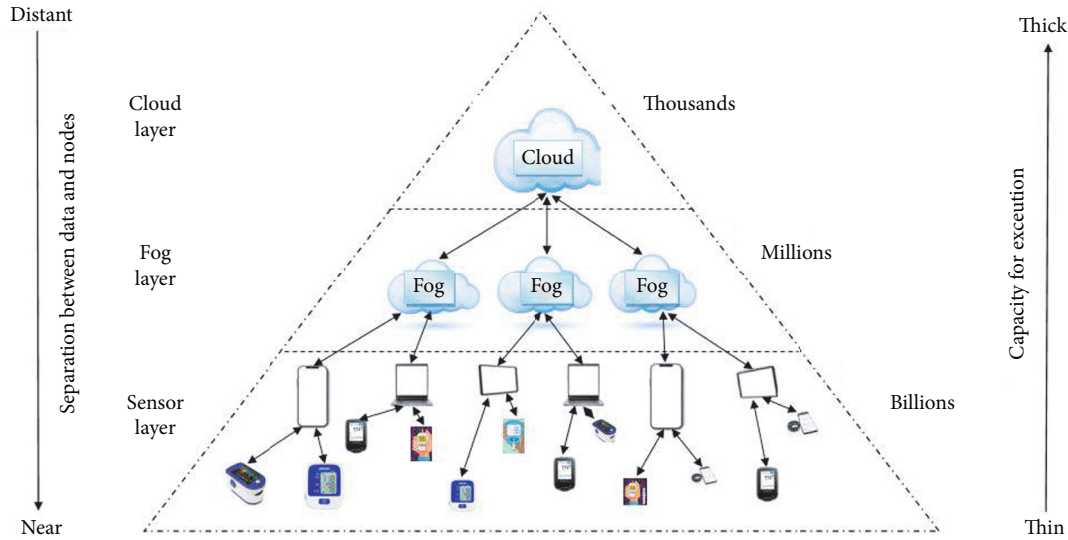


FIGURE 1: The architecture of IoT-fog-cloud integration.

- (i) Building a portable automated diabetes patient diagnostic system based on EDL techniques
- (ii) Using various frameworks and simulators previously recommended for IoT-fog-cloud integration for ultimate predictive analytics
- (iii) Examining the work in terms of numerous evaluation metrics as well as network metrics on the diabetes disease integrated dataset
- (iv) Addressing the findings and making comparisons of the findings with those of previous research investigations
- (v) Highlighting the major areas where further IoT-fog-cloud computing integrated studies can foster the application of the methods
- (vi) Identifying and analyzing prior work in diabetes disease diagnostics done by various authors in real time from afar

*1.7. The Organization of the Paper.* The following is the order in which the paper is organized: Section 2 discusses the spectrum of research work conducted in this field with a table containing the summary of these researches. Section 3 covers this work's architectural features, including the proposed work's design and the proposed model's working principle. Section 4 describes the efficient examination of the proposed work, comparing it with some related results considered in this research. Section 5 concludes with the study's pros and cons and the possible extensions to the proposed work.

## 2. Related Work

Kaur et al. have introduced a cloud IoT-based framework named CI-PDF for diabetes prediction considering accuracy, sensitivity, and specificity as evaluative parameters on the

PIDD dataset and claimed to have achieved 94.5% of prediction accuracy by combining neural network (NN) and DT approaches [22]. Priyadarshini et al. have presented Deep-Fog, a fog computing-based deep neural architecture for predicting stress type, diabetes, and hypertension attacks using standard datasets and open-source software tools, and claimed to have achieved a superior and competitive method in comparison to others [15]. Fernández-Caramés and Fraga-Lamas have introduced an IoT continuous glucose monitor- (CGM-) based system that claims to offer a translucent and truthful blood sugar data source from a population in a quick, flexible, scalable, and low-cost manner by accessing the collected blood sugar samples and warning them in the case of a dangerous situation being detected [21]. Barik et al. have introduced FogLearn, a fog computing-based framework for the application of  $K$ -means clustering in Ganga River Basin Management and real-world feature data for detecting diabetes patients suffering from diabetes mellitus and found that fog computing holds a lot of promise for medical and geospatial big data analysis [23]. Fernández-Caramés et al. have created and implemented a system that improves commercial CGMs in terms of IoT capabilities, allowing them to monitor patients remotely and alert them about the severity of their conditions. And they claimed to have developed a better technique for diagnosing patients' illnesses remotely in real time [6]. Gia et al. have developed a fog-based structure for remote health monitoring and fall detection. The system provides numerous progressive amenities such as ECG feature extraction, security, and locally distributed storage. In addition, the system operates accurately, and the wearable sensor node is energy efficient [24]. Devarajan et al. proposed an energy-efficient fog-assisted healthcare system that manages glucose levels based on evaluative measures such as energy efficiency, prediction accuracy, computational complexity, and latency on two datasets from the UCI repository diabetes dataset and the Physical Activity Monitoring Dataset (PAMAP2). The experimental results show that fog over cloud computing

has increased bandwidth efficiency, reduced latency, and enhanced accuracy [25]. Abdel-Basset et al. have suggested a novel framework based on computer-processed diagnosis and IoT to detect and observe type 2 diabetes patients and indicated the validity and robustness of the proposed algorithms considering accuracy and execution time as the performance evaluators [26]. Haq et al. have developed a filter method based on the DT-ID3 (Iterative Dichotomiser 3) model for essential feature selection in comparison to two ensemble learning algorithms, Ada Boost and RF, using prediction accuracy and computation time as evaluative measures, and found that the DT algorithm based on selected features improves the classifier's performance [27]. Kumari et al. have proposed an ensemble voting classifier that uses the ensemble of three ML algorithms, viz., LR, NB, and RF for the classification considering the evaluative measures like accuracy, precision, recall, and  $F1$ -score on PIDD and claimed to have achieved comparatively enhanced results on binary classifications [28]. Geetha and Prasad have built a hybrid model named T2DDP that doctors can effectively use to treat diabetic patients by employing supervised classification algorithms such as NB and ensemble algorithms like bagging with RF and AdaBoost for DT and found that the forecast will be submitted to the patient's cell phone at an early stage to make the immediate decisions about the health risk [29]. Shynu et al. have introduced efficient blockchain-based secure healthcare services for disease prediction in fog computing, considering purity, normalized mutual information (NMI), and accuracy as performance evaluators on PIDD and Cleveland heart disease dataset (CHDD) and thereby claimed that the proposed work efficiently clusters and predicts the disease compared to other methods [30]. Singh et al. have introduced an ensemble-based framework named eDiaPredict employing XGBoost, SVM, RF, NN, and DT to predict diabetes status among patients considering performance parameters like accuracy, sensitivity, specificity, Gini Index (GI), precision, the area under the curve (AUC), the area under the convex hull (AUCH), minimum error rate (MER), and minimum weighted coefficient (MWC) on PIDD and claimed that the proposed model could provide patients with a practical and precise prediction of diabetes based on glucose concentrations [31]. Rajput et al. have proposed a reference model for assisting rural people in India who have diabetes in characterizing two diabetes victims at an early stage using KNN, LR, SVM, RF, DT, and NB classifiers, considering accuracy, misclassification rate (MCR), recall, precision, prevalence, and  $F1$ -score as evaluative parameters on PIDD, and claimed to have achieved improved communication and interaction between patients [32]. Table 1 depicts an overview of the works conducted relating to this field.

### 3. Proposed Work: DiaFog

This section contains information on the various datasets, materials, and techniques employed in this study and the proposed work's architecture, design, and operation, designated as DiaFog.

**3.1. Materials and Methods.** This section is for the background study related to this research work. The simulation tool iFogSim, the simulating framework FogBus, one of the popular cloud service providers, Amazon Web Services (AWS), and the cloud computing platform Aneka are discussed briefly here, along with the datasets considered in training the model. In addition, a detailed discussion on the techniques considered in this research.

**3.1.1. Dataset Description.** DiaFog, the suggested model, is tested on three diabetic disease datasets: the Hospital Frankfurt Germany Diabetes Dataset (HFGDD), the Pima Indians Diabetes Dataset (PIDD), taken from the Kaggle and UCI-ML repository, respectively, and the Integrated Diabetes Dataset (IDD) of these two [33–35]. The HFGDD has 2000 persons, whereas the PIDD has 768 patients; both have nine columns. The binary result column contains two classes, each of which accepts the values “0” or “1,” with “0” indicating the absence of diabetes and “1” indicating the existence of diabetes illness. Additionally, there are 1316 normal individuals and 684 diabetic individuals in HFGDD, while there are 500 normal individuals and 268 diabetic individuals in PIDD. An experiment's IDD was created by combining characteristics from both datasets. The suggested filtering and normalizing approaches handle all datasets with some missing values. Table 2 provides a summary of these datasets. There are 2768 cases in the IDD, each with a unique attribute. A deep machine learning technique cannot be used for the short dataset with nominal values. As a result, all nominal data is transformed into numeric values for the EDL model to work. Table 3 shows a summary of the dataset's characteristics.

**3.1.2. Deep Learning (DL) and Activation Function (AF).** Deep learning (DL), hierarchical learning (HL), or deep structured learning (DSL), a subset of ML, is gaining interest in the categorization of data points [36]. The primary types of DL include the recurrent neural network (RNN), deep neural network (DNN), convolution neural network (CNN), and artificial neural network (ANN). An ANN is a system that uses weighted inputs to learn. These inputs are then processed to generate an output. As the ANN learns, new routes emerge. Paths with greater weightings in the model are considered more significant (or create more desired outcomes). The bulk of DL structures and algorithms employ the ANN framework. An ANN has neurons (interconnected nodes). A multilayer perceptron (MLP) is a feedforward ANN that employs backpropagation to train the network. It is utilized for supervised learning, parallel distributed computing, and algorithmic neurobiology. The dataset was trained using MLP, a DL approach. The MLP function approach is presented as follows [37, 38]:

$$V_q = \theta_q + \sum_{p=1}^n W_{qp} X_p, \quad (1)$$

$$Y_q = f_q(V_q). \quad (2)$$

TABLE 1: A summary of some related works done.

Author	Materials and methods	Dataset(s) used	Evaluative measures	Findings
Kaur et al. [22]	CI-PDF, a cloud IoT-based diabetes prediction platform, was introduced	PIDD	Accuracy, sensitivity, and specificity	Achieved 94.5% of prediction accuracy by combining DT and NN approaches
Priyadarshini et al. [15]	Introduced DeepFog, a deep neural architecture based on fog computing for forecasting stress, diabetes, and hypertension attacks	Stress, T2D, hypertension datasets	Accuracy, precision, recall, and <i>F1</i> -score	Achieved a superior and competitive method in comparison to others
Fernández-Caramés and Fraga-Lamas [21]	Introduced an IoT CGM-based system to remotely monitor patients by accessing blood sugar samples obtained and to notify them if a problematic scenario is discovered	Not mentioned	Prediction accuracy	This study claimed to be able to give a population with transparent and trustworthy blood sugar data quickly, easily, and affordably
Barik et al. [23]	Introduced the FogLearn framework for <i>K</i> -means clustering in Ganga River Basin Management using real-world feature data for diagnosing diabetes patients	PIDD	Accuracy	As a consequence, fog computing has great potential for extensive data analysis in medicine and geography
Fernández-Caramés et al. [6]	Designed and built a solution that allows continuous commercial CGMs to monitor patients remotely and warn them about their problems	Not mentioned	Prediction accuracy	The authors claimed to have developed a better technique for diagnosing patients' illnesses remotely in real time
Gia et al. [24]	A fog-based system for remote health monitoring and fall detection was introduced	Not mentioned	Energy efficiency	The suggested procedure is precise, and the worn sensor node saves energy
Devarajan et al. [25]	To manage blood glucose levels, propose an energy-efficient fog-assisted healthcare system	PAMAP2 and PIDD	Energy efficiency, accuracy, computational complexity, and latency	As a consequence, the fog over cloud computing has improved bandwidth efficiency, latency, and classification accuracy
Abdel-Basset et al. [26]	To diagnose and monitor type 2 diabetes patients, a new framework based on computer-assisted diagnostics and the IoTs was proposed	Personally collected data	Accuracy and execution time	The suggested algorithms were shown to be valid and resilient
Haq et al. [27]	Developed a filter method based on the ID3-DT model	Clinical data	Accuracy and computation time	Found that the decision tree algorithm based on selected features improves the classifier performance
Kumari et al. [28]	Proposed an ensemble voting classifier that employs the ensemble of three ML algorithms, viz., RF, LR, and NB	PIDD	Accuracy, precision, recall, and <i>F1</i> -score	Achieved comparatively enhanced results on binary classifications
Geetha and Prasad [29]	Proposed T2DDP is a hybrid model that uses supervised classification algorithms like NB and ensemble algorithms like bagging with RF and AdaBoost for DT to help physicians properly treat diabetic patients	PIDD	Accuracy, precision, recall, and <i>F1</i> -score	It was discovered that the predicted outcome would be sent to the patient's mobile phone at an early stage, allowing them to make quick judgments concerning the health risk
Shynu et al. [30]	Introduced efficient blockchain-based safe healthcare services for illness prediction in fog computing	PIDD and CHDD	Accuracy, purity, and NMI	In comparison to existing approaches, the suggested work efficiently clusters and predicts illness
Singh et al. [31]	eDiaPredict, an ensemble-based system that uses XGBoost, RF, SVM, NN, and DT to forecast diabetes status in patients, was introduced	PIDD	Accuracy, GI sensitivity, AUC, specificity, precision, AUCH, MER, and MWC	The proposed model can provide patients with a practical and precise prediction of diabetes based on glucose concentrations
Rajput et al. [32]	Proposed a reference model for aiding rural people in India who are suffering from diabetes	PIDD	Accuracy, MCR, recall, precision, prevalence, and <i>F1</i> -score	The authors stated that they were able to increase patient communication and engagement

TABLE 2: A brief description of considered datasets.

Dataset used	Number of characteristics	Number of instances
HFGDD	9 (8 considered as inputs)	768 (500 healthy and 268 diabetic)
PIDD	9 (8 considered as inputs)	200 (1316 healthy and 684 diabetic)
IDD	9 (8 considered as inputs)	2768 (1816 healthy and 952 diabetic)

TABLE 3: A brief description of considered features of the datasets.

Sl. no.	Features	Meaning	Values
1	Pregnancies	Number of times the women is pregnant	A numeric value (between 0 and 17)
2	Glucose	After 2 hours, plasma glucose concentration was determined in an oral glucose tolerance test (OGTT)	A numeric value (between 0 and 199)
3	Blood pressure	Diastolic blood pressure (in mmHg)	A numeric value (between 0 and 122)
4	Skin thickness	Thickness of triceps skin fold (in mm)	A numeric value (between 0 and 99)
5	Insulin	2-hour serum insulin (in $\mu\text{U/ml}$ )	A numeric value (between 0 and 846)
6	Body mass index (BMI)	Index mass of the body (weight in kg/height in $\text{m}^2$ )	A numeric value (between 14 and 80.6)
7	Diabetes pedigree function (DPF)	Diabetes mellitus family history	A numeric value (between 0.078 and 2.42)
8	Age	Age in years	A numeric value (between 1 and 120)
9	Outcome	Diabetes disease diagnosis	0: healthy and 1: diabetic

Here,  $V_q$  is the  $q$  number of linear combinations of  $p$  number of inputs,  $X_p$  is the  $p$  number of inputs,  $\theta_q$  is the  $q$  number of bias,  $W_{qp}$  is the weighted connection between the neuron  $j$  and the input  $X_p$ ,  $f_q(\cdot)$  is the  $q$  number of activation functions, and  $Y_q$  is the  $q$  number of outputs.

A DNN uses a layered NN with several layers of neurons. DNNs are made up of numerous linked perceptrons, each of which is a single neuron. In a DNN, dense layers are those where all inputs are densely connected to all outputs. DNNs may also have hidden layers. A hidden layer is a point between the NN's input and output where the activation function (AF) transforms the incoming data. It is called a hidden layer since it is not visible from the system's inputs or outputs. The deeper the NN, the more data recognition. The AF multiplies the input delivered to a node by weight and capacity. The function determines the signal's range. In DNN, each layer may be switched on or off, with the output of one layer feeding the input of the next layer ahead. A DNN has more hidden layers than other NNs. The dataset was trained using DNN, a DL algorithm. The DNN model is given as [38–40]

$$P_b^m(y) = W_t^m y x + B_t^m, \quad (3)$$

$$P_b^m(\hat{y}) = P_a^m(\hat{y}), \quad m = 1. \quad (4)$$

Here, each preactivation function  $P_b^m(y)$  is normally a linear operation involving the matrix  $W_t^m(y)$  and the bias  $B_t^m$ , which can be integrated into a parameter  $P_a^m$ .

$$P_b^m(\hat{H}^{m-1}) = P_a^m(\hat{H}^{m-1}), \quad m > 1. \quad (5)$$

The  $\hat{y}$  denotes the addition of 1 to the vector  $y$ . The form of hidden-layer activation functions  $H^m(y)$  is often the same at each level, but this is not always the case.

The activation function (AF) creates a weighted total and then adds bias to it to determine whether a neuron should be activated or not. The goal of these functions is to introduce nonlinearity into a neuron's output. ReLU (Rectified Linear Unit) became a prominent AF in DL and continues to give outstanding results today. It was built to solve the research's vanishing gradient issues. The sigmoid function has long been the most common AF in NNs. The sigmoid function's values are in the range  $[0, 1]$ , and because of its nature, tiny and big numbers sent through it will become values near zero and one, respectively. ReLU is the most often used AF, while the sigmoid function is the most commonly used AF for binary classification, which may be expressed as [37, 40, 41]

$$R(d) = \max(0, d), \quad (6)$$

$$S(d) = \frac{1}{1 + e^{-d}}. \quad (7)$$

Here,  $R(d)$  and  $S(d)$  are for ReLU and sigmoid AF, respectively, whereas the  $\max(\cdot)$  function finds the maximum value.

**3.1.3. Ensemble Learning (EL).** Ensemble learning (EL) may improve performance and accuracy in predictive analysis [42–44]. Ensemble approaches promise to reduce the bias and variance of the traditional learning algorithm's three flaws: the computational, symbolic, and statistical problems. Ensemble approaches include bagging, boosting, and stacking. Bagging is a strong, effective, and easy ensemble approach. This approach employs several copies of a training set utilizing



the bootstrap with any classification or regression model. Bagging works well with unstable nonlinear models (little changes in the training set create large changes in the model). Boosting is a model averaging meta-algorithm. A popular ensemble approach is a potent learning principle [45, 46]. Multiple classifiers are built by various learning algorithms on the same dataset of feature vectors, and their classifications are stacked. Voting and averaging are also simple ensemble procedures. They are simple to comprehend and use. Both techniques begin by building several classification models on a training dataset. Create each base model using multiple splits of the same training dataset and algorithm or utilizing the same dataset with alternative methods. This method uses majority voting to choose the final output prediction that obtains more than half of the votes. The ensemble technique could not create a reliable prediction if no guess receives more than 50% of the votes. In weighted averaging, each model's forecast is multiplied by a weight, and then, the average is determined. A smoother model is frequently the result of this procedure. Assume we have  $M$ -bootstrap samples of size  $N$  (approximations of  $M$ -independent subsets) indicated as  $\{s_1^1, s_2^1, s_N^1\}, \{s_1^2, s_2^2, s_N^2\}, \dots, \{s_1^M, s_2^M, s_N^M\}$ .

We might fit  $M$  nearly independent weak learners (one from each subgroup)  $w_1(s), w_2(s) \dots, w_M(s)$  using data coefficients  $d_1(s), d_2(s), \dots, d_M(s)$  and then aggregate them using either majority voting or weighted averaging to achieve an EDL model with reduced variance as

$$MV_M(s) = \operatorname{argmax}_p [\operatorname{card} (m | w_m(s) = P)], \quad (8)$$

$$WA_M(s) = \frac{1}{M} \sum_{m=1}^M d_m(s) \times w_m(s). \quad (9)$$

**3.1.4. iFogSim and FogBus.** The iFogSim simulator proved helpful in evaluating alternate scheduling strategies for fog and clouds [47]. A range of situations may be considered with iFogSim, including latency, energy usage, network congestion, and operating expenses. Performance indicators are measured by emulating fog/edge devices and cloud data centers. This study used iFogSim for several simulations. This study also uses the FogBus paradigm [9], integrating IoT, CC, and FC concepts. It uses blockchain to guarantee communication security, privacy, and data integrity. It links Aneka's platform-based fog setup with the cloud via HTTP RESTful APIs. It enables platform-independent IoT application execution and interaction interfaces while computing instances. It lets developers construct apps and customers operate several apps simultaneously, and service providers manage their resources.

**3.1.5. AWS and Aneka.** Amazon Web Service (AWS), a CC service provider, is the most reliable cloud computing company, providing excellent web services and security [48]. This platform is a perfect example of actual cloud computing since it allows for data security, integrity, and availability. It provides on-demand services. The IT resources are cheap, and there is no upfront commitment. The CC platform Aneka enables developers to establish APIs [49]. Its primary

design element is a service-oriented architectural (SOA) module. One of its primary features is its support for numerous programming models that describe the execution logic of programs using various abstractions. The framework's extensible SOA simplifies cloud administration and deployment while supporting various distributed application design patterns. Aneka uses cloud resources, whereas iFogSim and FogBus are used for different simulations and using fog resources.

**3.1.6. Platform and Languages Used.** The components of this work were written in a variety of programming languages. The Python programming language was used to create the preprocessing and EDL components. Jupyter python tool and SciKit Learn, Keras, and Tensorflow libraries were utilized in the EDL application. The approach, data filtering, and data processing in the intelligent gateway implementation are all made in Python to maintain compatibility with other services. We use the Pandas embedding library, a data structure library, to import the file into our Python environment. Numpy, Matplotlib, and additional libraries as needed are also loaded into the environment [50, 51]. In addition, the Android application is built using the App Inventor tool from MIT, and the web communications are carried out using the PHP programming language in this work.

**3.2. The Architecture.** DiaFog's architecture, as shown in Figure 2, incorporates a variety of techniques, hardware components, and software components required in this framework, as detailed below. The suggested study is based on previously specified frameworks and simulators for IoT-fog-cloud integration for ultimate predictive analytics.

**3.2.1. Hardware Components Used.** DiaFog consists of IoT health sensors, gateways, master PC node (MPN), fog worker node (FWN), and cloud data center node (CDCN), which are briefly covered here. The IoT health sensors collect data from diabetic patients and transfer it to gateway devices. For example, the "blood pressure sensor" measures systolic and diastolic pressures in mmHg. Gateways take patient data and share it with either MPN or FWNs. These gateways behave like fog. MPN assigns jobs to worker nodes using a resource manager or handles requests using a learned EDL model. When MPN and FWNs are overloaded, it forwards to CDCNs via cloud integrators, acting as a gateway device. FWN processes data using the learned EDL model and produces results as requested by gateway devices or MPNs. FWNs are Raspberry Pi devices in this work. CDCN is used to access cloud resources. MPN and FWNs are overloaded, and MPN forwards to CDCNs, acting as a gateway device.

**3.2.2. Software Components Used.** The proposed work comprises various software components, which are briefly discussed here. In the data preprocessing module, data from IoT health sensors such as blood pressure sensors is preprocessed and filtered before being sent to the cloud. Preprocessing of data improves model prediction accuracy. Preprocessed data from gateway devices are saved in a .csv file and utilized next. The data manager (DM) accepts preprocessed data from IoT health devices. Depending on the

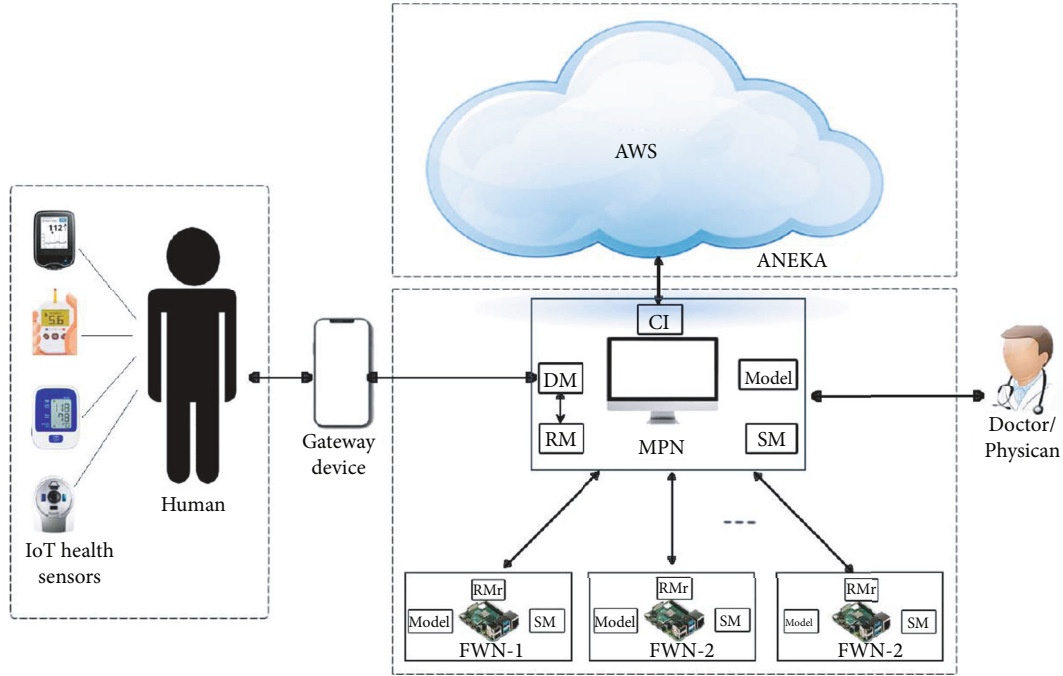


FIGURE 2: The architecture of DiaFog.

situation, it may combine data from many sources and change transmission frequency. The DM is in charge of deciding which FWNs to distribute the received data. The resource manager (RM) selects resources for programs to execute. The calculating server's RM determines each MPN and FWN's resource status. After collecting data, the RMs establish resources on FWNs and the cloud for applications. After receiving credentials from a gateway device, the MPN security manager (SM) validates them against the Credential Archive of Warehouse Service. In contrast, the FWN-SM oversees protected interactions of an FWN with others while conducting computations. The cloud integrator (CI) delivers storage and resource-providing instructions to the cloud. It gives context data for cloud-based instances like containers and virtual machines (VMs) to resource management. The resource monitor (RMr) allots resources to programs and tracks how successfully they are used in real time. A service provider-defined threshold is exceeded, an unexpected problem occurs, and the RM is notified. In this component, the dataset is used to train a DL approach to classify vector points (5vectors) generated by IoT health device preprocessing. On the other hand, it predicts and delivers results for the RM's tasks, a bagging classifier, and an EL approach for classification and averaging.

**3.3. The Design.** DiaFog's design begins with good dataset selection. The approach incorporates preprocessing of the raw patient dataset. The EDL model to be used at each design node is a step. An Android app is a vital tool for remote users. Experiment setup and implementation are the critical elements in the proposed study's design.

**3.3.1. Dataset Preprocessing.** The raw dataset is preprocessed and filtered here. The data were cleaned and normalized

before training and testing to improve the model's prediction accuracy. In this study, the mobile application collects eight things every time, and the 9th data in the dataset is utilized as the anticipated outcome. Table 4 shows a sample of the considered integrated dataset.

**3.3.2. Experimental Set-Up and Android App.** The set-up is implemented with some hardware configurations as evaluative hardware for the experiments in this work, including the primary gateway device (Xiaomi A2 with Android version 10), MPN (Dell with Core i3, Windows 10 64-bit OS, and 6 GB RAM), FWNs (five numbers of Raspberry Pi 4 with 4 GB SDRAM), and public cloud (AWS with Windows server and Aneka platform). In addition, 100 cell phones belonging to different people were utilized to test the scalability of the suggested concept.

The DiaFog.apk, an android interface built using MIT's App Inventor for this effort, will be utilized in a variety of Android-enabled gateway devices to gather data from remote users [52]. It serves as a connection point for IoT health devices and MPNs or FWNs [12]. As shown in Figures 3 and 4, the data input from the individuals is delivered to MPNs, and results are recorded.

**3.3.3. Implementation.** DiaFog's implementation section examines how the previously mentioned components are implemented. One of the most popular programming languages, Python, has been used to preprocess data and train the EDL model in recent years. For the predictive binary classification, the model uses ANN with a bagging classifier and majority voting classifier as EL techniques and DNN with a bagging classifier and weighted averaging as EL methods, as shown in Figure 5. Both EDL models were applied to the three datasets mentioned earlier: HFGDD,

TABLE 4: Samples from the preprocessed IDD dataset.

Sl. no.	Pregnancies	Glucose	Blood pressure	Skin thickness	Insulin	BMI	DPF	Age	Outcome
1	6	148	72	35	0	33.6	0.627	50	1
2	1	85	66	29	0	26.6	0.351	31	0
3	8	183	64	0	0	23.3	0.672	32	1
4	1	89	66	23	94	28.1	0.167	21	0
5	0	137	40	35	168	43.1	2.288	33	1
6	5	116	74	0	0	25.6	0.201	30	0
7	3	78	50	32	88	31	0.248	26	1
8	10	115	0	0	0	35.3	0.134	29	0
9	2	197	70	45	543	30.5	0.158	53	1
10	8	125	96	0	0	0	0.232	54	1

Fog Based Framework for Diabetes Disease Diagnosis

## Diabetes Disease Test

Enter Details:

user1@gmail.com

Master IP Address: 192.168.43.159

Contact Number: 9012345678

Age (in Years): 25

Blood Pressure: 66

Pregnancies: 1

Glucose: 89

Skin Thickness: 23

Pedigree Function: 0.167

Insulin: 94

BMI: 28.1

Submit

Job Submitted to 192.168.43.159

Please find the Result

You do not have Diabetes disease; No need to worry

FIGURE 3: Screenshot of the DiaFog app with diabetes response as no.

PIDD, and IDD. The results of the trials are then compared to determine which EDL model is the best. In the case of ANN, the ReLU function is used in all of the input, hidden, and output layers, but in the case of DNN, the ReLU function is used in both the input and hidden layers, and the sigmoid function is utilized at the output layer. The sizes of various layers in this study, including an input layer, a hidden layer, and an output layer, are 8, 3, and 2 in ANN and 8, 4, and 2 in DNN, respectively. The ninth feature is used to determine whether or not the patient has DMD. This proposed work's learning rate is 0.001 and 0.12 in ANN and DNN, respectively. In this study, the commonly used optimizer, Adam, is employed for modeling in both scenarios. Table 5 shows a summary of the DL approach setup. The Android app utilized in this project was created using MIT's App Inventor, and the online communications were done with PHP language. The data characteristics are stored in an excel file and then delivered to the MPN through HTTP post. The DM stationed within MPN is responsible for the subsequent conveyance of the data obtained. After any of the nodes have successfully processed the data supplied from the persons, the result is transmitted to the user's gateway device through the MPN.

**3.4. The Working Principle.** The working concept of this suggested work, DiaFog, is explained with several algorithm phases and a communication flow diagram. These networks are based on the master-slave idea, with MPN as the master and FWNs as slaves. The MPN, FWNs, and gateway devices are all on the same network. There are three ways to communicate: MPN alone, MPN with FWNs, or cloud only. In the first situation, MPN fulfills the task request and provides the result, whereas in the second case, FWN does so. When MPN detects insufficient resources, i.e., MPN and FWNs are overloaded, it forwards to CDCNs, acting as a gateway device. Algorithm 1 describes the primary function of the gateway device, whereas Algorithm 2 describes the primary role of the MPN. Besides, Algorithm 3 is for training the EDL model, and Algorithm 4 is for the test cases applied to the generated EDL model. This work's hardware components interact according to the prescribed framework. The communication chain shown in Figure 6 depicts a flow of work ordered by users remotely.



FIGURE 4: Screenshot of the DiaFog app with diabetes response as yes.

### 3.5. Algorithms Representing Detailed Working of DiaFog

## 4. Empirical Analysis

A short discussion on different network characteristics and evaluative metrics is addressed, followed by a discussion on the outcomes acquired by this suggested effort dubbed DiaFog. This section also includes an overview of comparisons with similar works done. The performance of every planned task must be evaluated for research purposes. This study is built on previously suggested frameworks and simulators for IoT-fog-cloud integration for ultimate predictive analytics. These include performance parameters (accuracy, precision, recall,  $F$ -measure, etc.) and network parameters (latency, arbitration time, processing time, throughput,

bandwidth consumption, jitter, network utilization, energy consumption, scalability, etc.).

**4.1. Performance Parameters.** The primary purpose of performance parameters is to find the confusion matrix, a real-to-anticipated-class matrix on which numerous evaluation metrics have been applied.  $T_1$ ,  $T_0$ ,  $F_1$ , and  $F_0$  are abbreviations for the confusion matrix's true positive, true negative, false positive, and false negative. Some of the performance measures for classification purposes explored in this study include accuracy (Acc), precision (Pre), recall (Rec), and  $F$ -measure (F-M). The "Acc" is defined as the number of correct predictions divided by the total number of input samples. The "Pre" is defined as the ratio of properly predicted positive observations to the total number of correctly predicted positive observations. The "Rec" is defined as the proportion of successfully expected positive observations to the total number of properly predicted positive observations. The "F-M" is the weighted average of "Pre" and "Rec." The detailed evaluation formulas are as follows:

$$\text{Acc} = \frac{(T_1 + T_0)}{(T_1 + T_0 + F_1 + F_0)}, \quad (10)$$

$$\text{Pre} = \frac{T_1}{(T_1 + F_1)}, \quad (11)$$

$$\text{Rec} = \frac{T_1}{(T_1 + F_0)}, \quad (12)$$

$$\text{F-M} = \frac{(2 \times \text{Pre} \times \text{Rec})}{(\text{Pre} + \text{Rec})}. \quad (13)$$

In this work, in order to validate the proposed EDL model, we evaluated it through six models. Here, model 1, model 2, and model 3 are the ANN along with the bagging Classifier and majority voting EL models applied on PIDD, HFGDD, and IDD datasets, respectively, whereas, model 4, model 5, and model 6 are the DNN along with the bagging classifier and weighted averaging EL models applied on PIDD, HFGDD, and IDD datasets, respectively. The observed results are then compared, as depicted in Table 6 and Figures 7–10. From experiments, it is revealed that model 6 outperforms other models in terms of the performance parameters like "Acc," "Pre," "Rec," and "F-M."

**4.2. Network Parameters.** Network characteristics are heavily influenced by the computing approach or level at which the fog-enabled IoT application is coordinated. Various network characteristics such as latency, arbitration time, total processing time, throughput, energy consumption, bandwidth, jitter, network utilization, and scalability are used to verify this suggested work. Layout 1 for MPN alone, layout 2 for MPN with 1 FWN, layout 3 for MPN with 2 FWNs, layout 4 for MPN with 3 FWNs, layout 5 for MPN with 4 FWNs, and layout 6 for CDCN only are the various configurations employed in this study for the assessment of various network metrics.

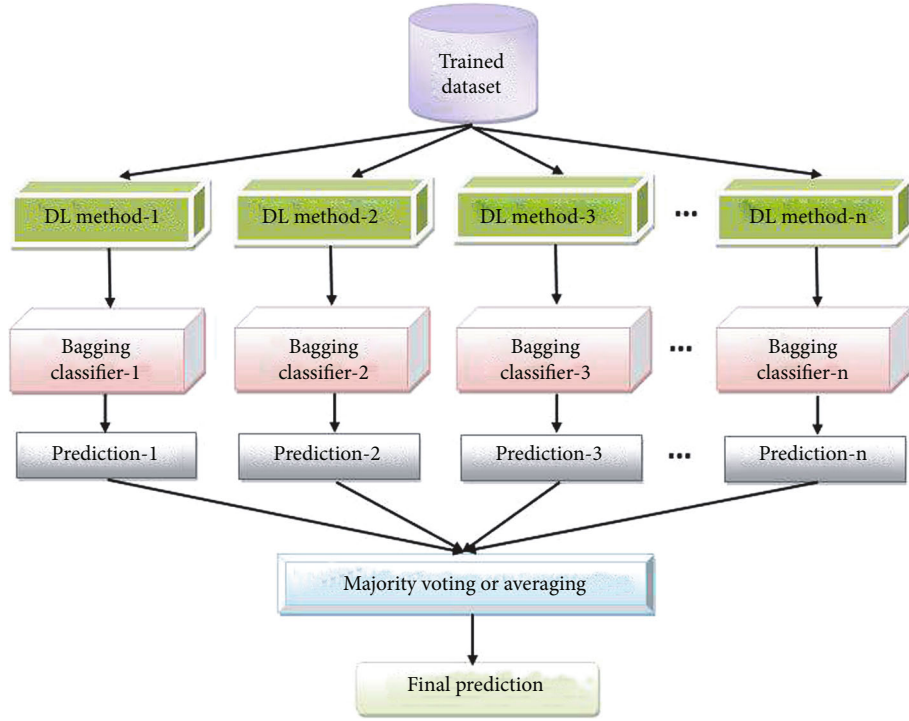


FIGURE 5: Basic diagram of the EDL model.

TABLE 5: Configuration of DL methods considered in DiaFog.

DL methods	No. of input layers	No. of hidden layers	No. of output layers	Optimizer used	Learning rate	AF at input layers	AF at hidden layers	AF at output layers
ANN	8	3	2	Adam	0.001	ReLU	ReLU	ReLU
DNN	8	4	2	Adam	0.120	ReLU	ReLU	Sigmoid

```

1 Inputs :  $USR_i$ 
  Output :  $RES_i$ 
  True: Gateway in active mode
  2 True Obtain  $ATB_i$  using  $IHD_i$  Submit  $USR_i$  to  $GTW_i$ ,  $GTW_i$  connected to  $MPN$  Send  $USR_i$  to  $MPN$  using  $GTW_i$  Obtain  $RES_i$  Reset to obtain  $ATB_i$  and submit  $USR_i$  again.
  
```

ALGORITHM 1: Gateway primary function.

```

1 Inputs :  $USR_i$ 
  Output :  $RES_i$ 
  True :  $MPN$  in active mode
  2 True Obtain  $USR_i$ ,  $MPN$  (Available) outcome = 0 return  $RES_H$  return  $RES_D$ ,  $FWN_i$  (Available) outcome = 0 return  $RES_H$ 
  return  $RES_D$ ,  $CDCN_i$  (Available) outcome = 0 return  $RES_H$  return  $RES_D$  Return  $RES_i$  to  $GTW_i$  using  $MPN$ 
  
```

ALGORITHM 2: MPN primary function.

Latency is the time it takes for data to flow across a network. It also refers to the time it takes for a data packet to be recorded, transferred, processed by several devices, and finally received and decoded. The variation in latencies is estimated by adding transmission time and queuing delay, as shown in Figure 11. Because all contact is done through

single-hop data transfers, the latency is nearly the same whether the work is submitted to MPNs or FWNs. The latency in a cloud arrangement is relatively significant due to multihop data transfer outside the network, which is the primary function of the FC. Arbitration time refers to the time limit for the MPN to respond to the gateway devices,

1 Inputs :  $SDT_i$   
 Output :  $RES_i$   
 True : Samples in training mode  
 2 True  $i = 1$  to  $M$  Obtain  $SDT_i$  Training  $DLA_i$  on  $SDT_i$  Bootstrap  $DLA_i$  using  $BCF_i$  Apply Majority Voting or Weighted Averaging Calculate  $PPR_i$  Generate an EDL Model

ALGORITHM 3: Training EDL model(s).

1 Inputs :  $TDT_i$   
 Output :  $RES_i$   
 True : Data in test mode  
 2 True  $j = 1$  to  $N$  Apply  $TDT_i$  to generated EDL Model Assign  $RES_i$  to the nearest outcome values  $\{0, 1\}$  Calculate predictive class ( $RES_i$ ) Return  $RES_i$

ALGORITHM 4: EDL model test cases.

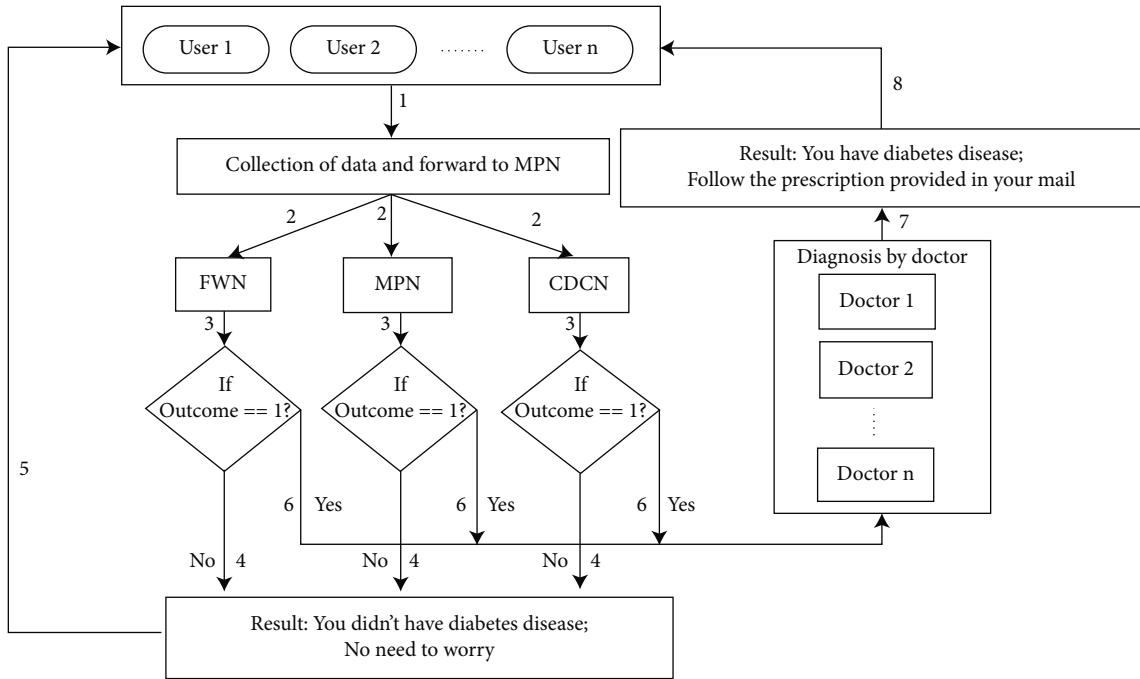


FIGURE 6: The flowchart of data communications in DiaFog.

TABLE 6: Observed results of various performance parameters.

Performance parameters	EDL models					
	Model 1	Model 2	Model 3	Model 4	Model 5	Model 6
Accuracy (in %)	81.6	90.2	94.5	83.5	93.4	98.6
Precision	0.72	0.91	0.96	0.81	0.95	0.99
Recall	0.69	0.88	0.94	0.76	0.93	0.96
F-measure	0.70	0.89	0.95	0.78	0.94	0.97

which might vary depending on the network setup. The arbitration time under different fog situations is shown in Figure 12. The incidence of arbitration is lower when assignments are routed directly to MPN or CDCNs. In other cases, time is spent balancing load between nodes, which reduces the arbitration rate. On the other hand, cloud processing is

exceptionally fast due to its superior capability. The processing time is longer because the nodes in FWNs have less processing power and a lower clock frequency. Processing time is the time it takes for a task to be started, processed, and returned to the users. It also changes with setups. The processing characteristics under varied fog conditions are

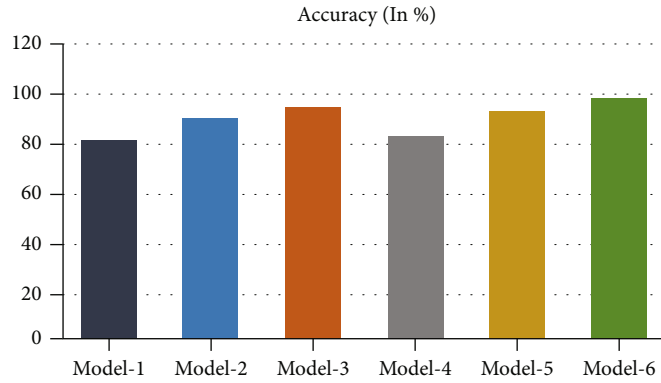


FIGURE 7: The accuracies of various models.

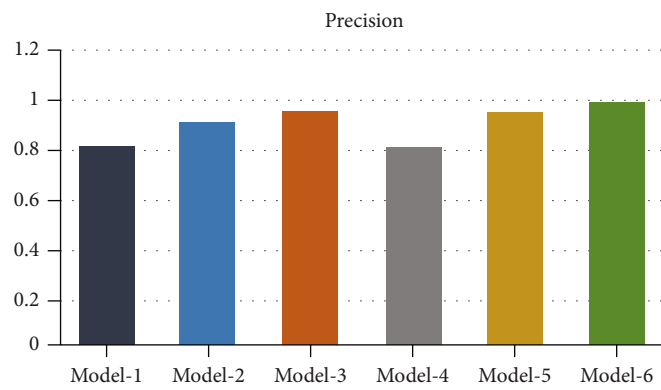


FIGURE 8: The precisions of various models.

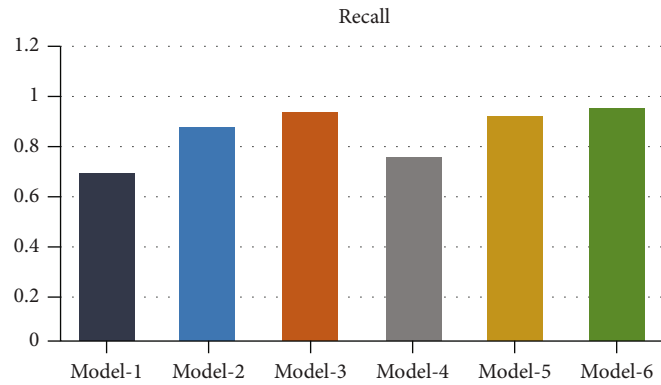


FIGURE 9: The recalls of various models.

shown in Figure 13 as well. One thing that may be seen is that the total processing time is considerably shorter in the case of cloud communications. Throughput is measured in bits per second, HTTP transactions per day, or millions of instructions per second. It is determined by the successful data packet delivery rate from any node to end users. Figure 14 shows a representation of the variation in throughputs, measured in megabits per second (Mbps), discovered for different configurations. Compared to the CDCN, the throughput numbers for MPN with FWNs are much greater than those for the CDCN. In order to compute the through-

put, it is necessary to determine the rate at which data packets are successfully sent from fog nodes to end users. Essentially, jitter is the temporal delay of changes in time. Jitter is the variation in response time between task requests. It is vital for many real-world applications, such as e-Healthcare data analysis. Figure 15 depicts the variation of jitter with different configurations. Because MPN additionally conducts other responsibilities such as arbitration, security checking, and resource management, jitter is more significant in the MPN-alone scenario than when tasks are transmitted to FWNs; nevertheless, jitter is significantly

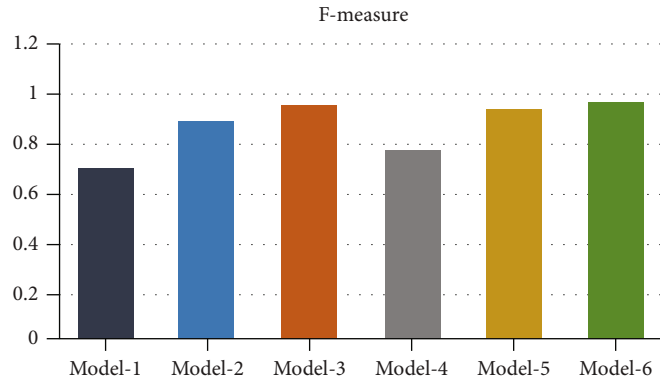


FIGURE 10: The *F*-measures of various models.

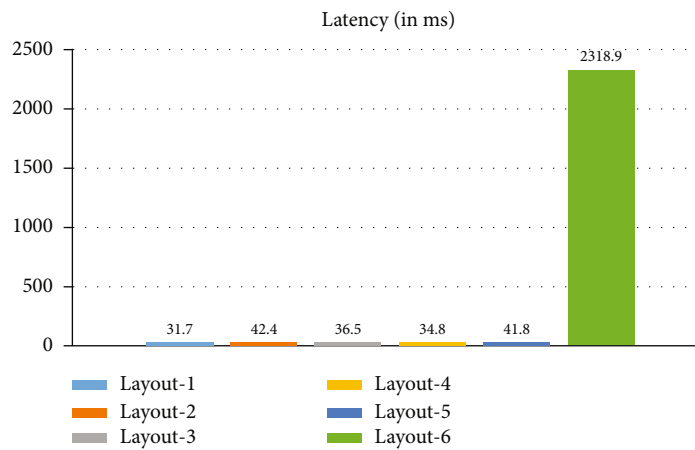


FIGURE 11: The latency of various configurations.

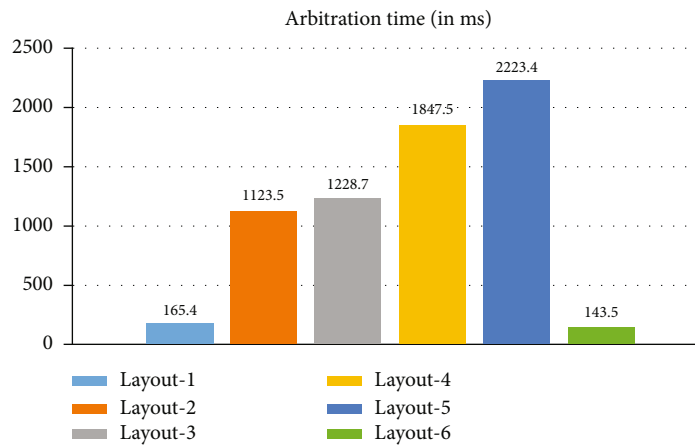


FIGURE 12: The arbitration time of various configurations.

higher when jobs are supplied to CDCN. Data transferred over an Internet connection is measured in bandwidth in a particular time period. It refers to the amount of data sent across a link in a specific time period (typically measured in kilobits per second (Kbps)). The circumstance, such as MPN alone, FWNs, or cloud, and the number of FWNs impact bandwidth consumption. Figure 16 demonstrates

the variation in bandwidth utilization across all FWNs in different configurations. Because of the high number of heartbeat packets, it is required to check for security vulnerabilities and transmit data (through the cloud). As the number of FWNs increases, the amount of bandwidth used increases. Network utilization is the average rate of successful data transmission across a communication link. A fog

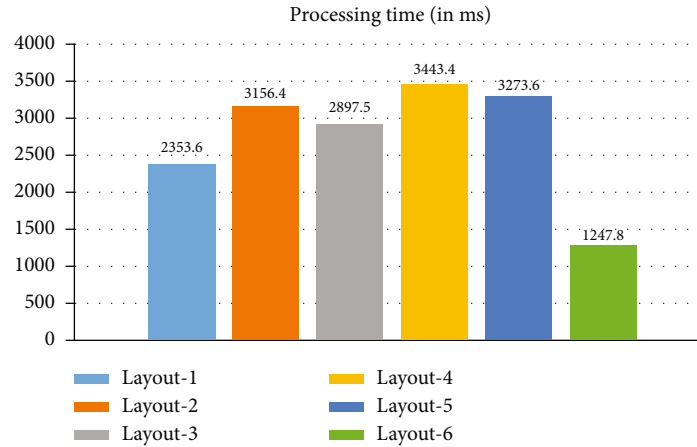


FIGURE 13: The total processing time of various configurations.

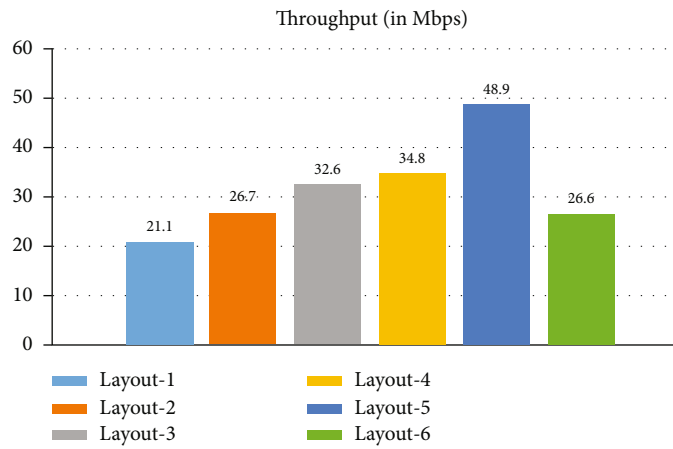


FIGURE 14: The throughput of various configurations.

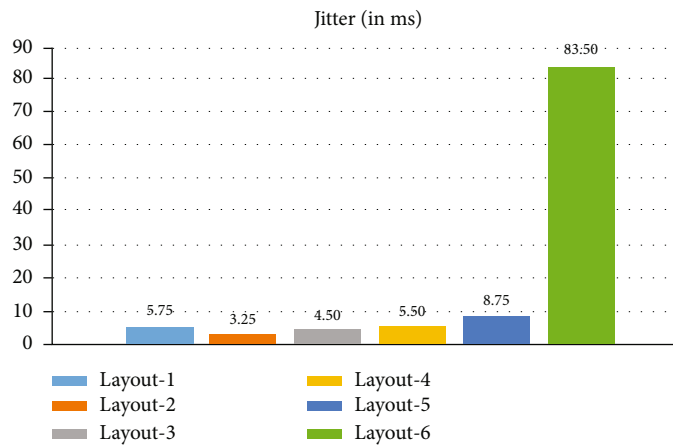


FIGURE 15: The jitter of various configurations.

computing design uses less network than a cloud computing system. The issue impacts the network utilization, including MPN alone, FWNs, or cloud, and the number of FWNs. Because the fog environment reduces the number of user requests routed to the cloud, as seen in Figure 17, network utilization time in the case of MPN and/or FWNs is much smaller than that of CDCNs.

Energy consumption is the total energy utilized by the system. Sensors and other system components need energy. The physical theorem uses the following formula to compute it [53]:

$$E = T \times p(X). \tag{14}$$

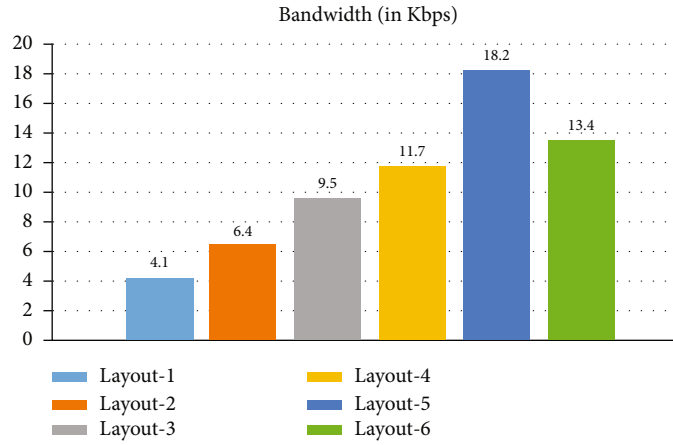


FIGURE 16: The bandwidth of various configurations.

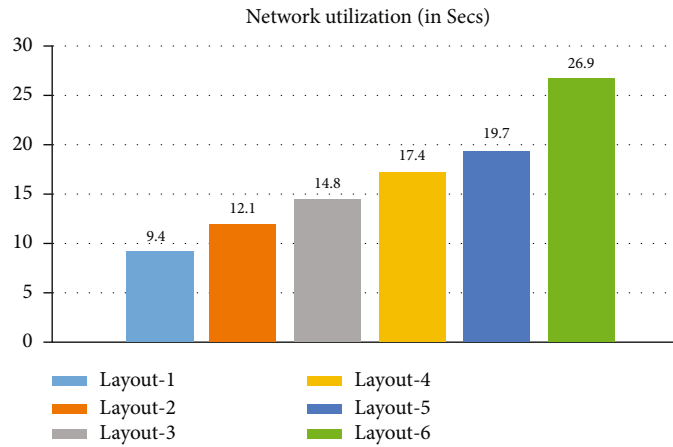


FIGURE 17: The total network utilization of various configurations.

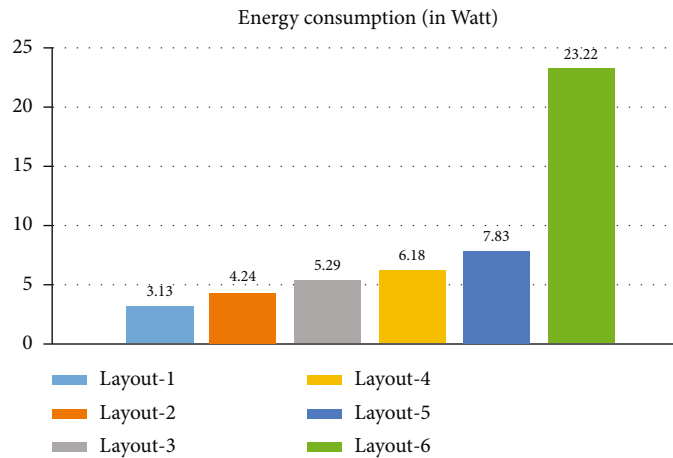


FIGURE 18: The energy consumption of various configurations.

Here,  $E$  is for the energy,  $p()$  is the power function,  $X$  is the parameter set that impacts power, and  $T$  is the task processing time. CDCN uses a significant amount of energy as compared to MPN or FWNs, as seen in Figure 18. CDCNs use a considerable amount of energy compared to FWNs

due to this. As the number of FWNs increases, the amount of energy used by the proposed task increases. Table 7 depicts the averages of observed outcomes of various network parameters corresponding to multiple configurations based on the data collected.



TABLE 7: Observed results of various network parameters.

Network parameters	Layouts					
	Layout 1	Layout 2	Layout 3	Layout 4	Layout 5	Layout 6
Latency (in ms)	32.3	41.3	36.8	35.7	43.2	2459.9
Arbitration time (in ms)	165.4	1123.5	1228.7	1847.5	2223.4	143.5
Processing time (in ms)	2353.6	3156.4	2897.5	3443.4	3273.6	1247.8
Throughput (in Mbps)	21.1	26.7	32.6	34.8	48.9	26.6
Jitter (in ms)	5.75	3.25	4.50	5.50	8.75	83.50
Bandwidth (in Kbps)	4.1	6.4	9.5	11.7	18.2	13.4
Network utilization (in sec)	9.4	12.1	14.8	17.4	19.7	26.9
Energy consumption (in watt)	3.13	4.24	5.29	6.18	7.83	23.22

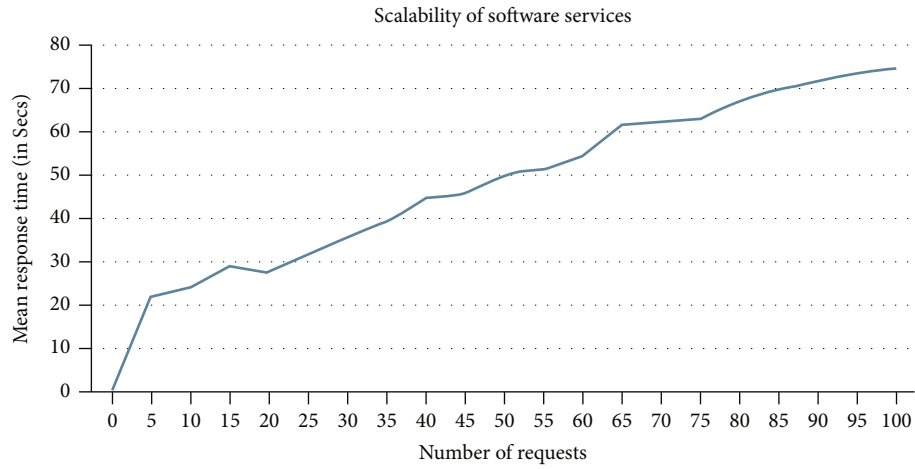


FIGURE 19: The mean response time concerning the number of requests.

TABLE 8: Comparison of the proposed work DiaFog with the considered existing works.

Work	IoT	CC	FC	ML	DL	EL	Network parameters								Evaluative parameters				
							AT	LT	PT	TP	EC	BW	JT	NU	SC	Acc	Pre	Rec	F-M
[22]	Y	Y	N	Y	Y	N	N	N	N	N	N	N	N	N	N	Y	N	Y	N
[15]	Y	Y	Y	NN	Y	N	N	N	N	N	N	N	N	N	N	Y	Y	Y	Y
[21]	Y	Y	Y	N	N	N	N	N	N	N	N	N	N	N	N	N	N	N	N
[23]	Y	Y	Y	Y	Y	N	N	N	N	N	N	N	N	N	N	Y	N	N	N
[6]	Y	Y	Y	N	N	N	N	N	Y	Y	Y	N	N	Y	Y	N	N	N	N
[24]	Y	Y	Y	Y	N	N	N	Y	N	N	Y	N	N	N	N	N	N	N	N
[25]	Y	Y	Y	Y	Y	N	N	N	N	N	N	Y	N	N	N	Y	Y	Y	Y
[26]	Y	Y	Y	N	N	N	N	N	Y	N	N	N	N	N	N	Y	N	N	N
[27]	N	N	N	Y	N	Y	N	N	Y	N	N	N	N	N	N	Y	N	N	N
[28]	N	N	N	Y	N	Y	N	N	N	N	N	N	N	N	N	Y	Y	Y	Y
[29]	N	N	N	Y	N	Y	N	N	N	N	N	N	N	N	N	Y	Y	Y	Y
[30]	Y	Y	Y	Y	N	N	N	N	Y	N	N	N	N	N	N	Y	N	N	N
[31]	N	N	N	Y	N	Y	N	N	N	N	N	N	N	N	N	Y	Y	Y	N
[32]	Y	Y	N	Y	N	N	N	N	N	N	N	N	N	N	N	Y	Y	Y	Y
DiaFog (proposed)	Y	Y	Y	N	Y	Y	Y	Y	Y	Y	Y	Y	Y	Y	Y	Y	Y	Y	Y

Scalability refers to the capacity of the IoT-fog-cloud-based system to raise the resources of software service delivery when higher revenue for the service is needed over time (i.e., a demand scenario) [54, 55]. A scalable infrastructure

may increase resources to meet changing application demands while maintaining the infrastructure’s constraints. As shown in Figure 19, our main worry is whether the system can scale up in quantity as consumers need it over time.

As the number of requests grows, the mean response time grows as well. The increase in mean reaction time is not exponential but relatively moderate. It is also noted that response times do not fluctuate with increased queries, indicating the research's scalability.

**4.3. Comparison.** The proposed framework is compared with some considered existing works involving various performance and network parameters. We included other aspects such as throughput, network usage, and scalability that were not evaluated before, demonstrating the work's uniqueness. Table 8 depicts a comparison of the proposed work, DiaFog, with several existing results employed in this research relevant to this suggested work. The following abbreviations are used in Table 8: yes (Y), no (N), latency (LT), arbitration time (AT), processing time (PT), throughput (TP), energy consumption (EC), bandwidth (BW), jitter (JT), network utilization (NU), accuracy (Acc), precision (Pre), recall (Rec), and  $F$ -measure (F-M) are some of the terms used.

## 5. Conclusion and Future Scope

To make an individual's life easier and more consistent, the FC idea with IoT implementations has played an important part in recent days. Because DMDs have a high mortality rate, it is beneficial if the patient may self-diagnose remotely by employing IoT applications. However, formal IoT implications only use CC for real-time data storage, analysis, etc., with several drawbacks like latency and network usage. To solve this problem, FC should be combined with IoT and CC. This research proposes DiaFog, a fog-enabled system for real-time diagnosis of diabetes patients utilizing EDL methods. The model is trained on the combined HFGDD and PIDD diabetes datasets from Kaggle and UCI-ML warehouses. The IDD is both cost-effective and sensitive to real-time diabetes patient diagnosis. Aspects of this study, DiaFog, are examined including accuracy, precision, recall,  $F$ -measure, latency, arbitration time, jitter, throughput, energy consumption, bandwidth use, network utilization, and scalability. This framework integrates IoT, CC, and FC ideas to guarantee low latency and high accuracy applications in patients' DMD diagnostics and remote prediction. The trials show that it is a viable and user-friendly platform for instantaneous remote DMD diagnosis.

DiaFog may be used to diagnose diabetes patients remotely, anywhere around the globe. This study work's combined IoT, FC, and CC strategy establishes low latency, high precision, etc. The research concluded that it is a robust and user-friendly framework for immediate remote DMD diagnostics. In terms of latency, network usage, energy usage, security, and privacy, the results support FC's appropriateness for real-time remote diabetic patient diagnostics. A person with a few sensors and a smartphone app can be diagnosed anywhere. Every study has its benefits and drawbacks. This study has certain disadvantages; for example, the general execution of the suggested work is difficult and expensive. The dataset we used in this study comprises 2768 instances, which looks little from a DL experiment perspective since more examples mean more accurate and exact

conclusions. This modular design relies on a single network platform, a work restriction.

Moreover, the suggested work may be improved by incorporating additional well-known DL principles. This work's expansions may be used to treat various chronic disorders. Also, alternative CC platforms such as edge computing, mist computing, and surge computing should be used to extend this suggested architecture. Another area where we should work in the future is the problem of a single network platform. Individuals must be made aware of the importance of IoT, cloud, fog, and edge computing and other related technologies and their worldwide consequences in recent days.

## Notations

USR <sub><i>i</i></sub> :	Users' data {USR <sub>1</sub> , USR <sub>2</sub> , USR <sub>3</sub> , ...}
GTW <sub><i>i</i></sub> :	Gateways {GTW <sub>1</sub> , GTW <sub>2</sub> , GTW <sub>3</sub> , ...}
IHD <sub><i>i</i></sub> :	IoT health devices {IHD <sub>1</sub> , IHD <sub>2</sub> , IHD <sub>3</sub> , ...}
ATB <sub><i>i</i></sub> :	Attributes/features/characteristics (ATB <sub>1</sub> for age, ATB <sub>2</sub> for blood pressure, ATB <sub>3</sub> for pregnancies, ATB <sub>4</sub> for glucose, ATB <sub>5</sub> for skin thickness, ATB <sub>6</sub> for DPF, ATB <sub>7</sub> for insulin, ATB <sub>8</sub> for BMI, and ATB <sub>9</sub> for outcome)
MPN:	Master PC node
FWN <sub><i>i</i></sub> :	Fog worker nodes {FWN <sub>1</sub> , FWN <sub>2</sub> , FWN <sub>3</sub> , ...}
CDCN <sub><i>i</i></sub> :	Cloud data center nodes {CDCN <sub>1</sub> , CDCN <sub>2</sub> , CDCN <sub>3</sub> , ...}
SDT <sub><i>i</i></sub> :	Training samples {SDT <sub>1</sub> , SDT <sub>2</sub> , SDT <sub>3</sub> , ...}
TDT <sub><i>i</i></sub> :	Test data {TDT <sub>1</sub> , TDT <sub>2</sub> , TDT <sub>3</sub> , ...}
BCF <sub><i>i</i></sub> :	Bagging classifier algorithms {BCF <sub>1</sub> , BCF <sub>2</sub> , BCF <sub>3</sub> , ...}
DLA <sub><i>i</i></sub> :	DL algorithms {DLA <sub>1</sub> , DLA <sub>2</sub> , DLA <sub>3</sub> , ...}
$M$ :	Maximum number of iterations in training EDL model(s)
$N$ :	Number of test data
PPR <sub><i>i</i></sub> :	Performance parameters (PPR <sub>1</sub> for accuracy, PPR <sub>2</sub> for blood precision, PPR <sub>3</sub> for recall, and PPR <sub>4</sub> for $F$ -measure)
RES <sub><i>i</i></sub> :	Results (RES <sub>D</sub> , i.e., diabetic when the value of outcome is 1, RES <sub>H</sub> , i.e., healthy when the value of outcome is 0).

## Data Availability

The IoT data used to support the findings of this study are available from the corresponding author upon request.

## Conflicts of Interest

The authors of this manuscript declared that they do not have any conflict of interest.

## Acknowledgments

This work is partially supported by DST/TDT/DDP-38/2021, Device Development Programme (DDP), by the Department of Science Technology (DST), Ministry of Science and Technology, Government of India. Sajal Biring

would like to thank Ministry of Science and Technology, Taiwan, under grant no. MOST 110-2221-E-131-019 for financial support.

## References

- [1] S. Dubravac and C. Ratti, *The Internet of Things: Evolution or Revolution?*, vol. 1, Wiley, Hoboken, NJ, USA, 2015.
- [2] A. Lakhan, M. A. Mohammed, S. Kozlov, and J. J. P. C. Rodrigues, "Mobile-fog-cloud assisted deep reinforcement learning and blockchain-enable IoMT system for healthcare workflows," *Transactions on Emerging Telecommunications Technologies*, vol. 1, 2021.
- [3] N. Matar and M. Alnabhan, "Evaluating E-health services and patients requirements in Jordanian hospitals," *International Arab Journal of e-Technology*, vol. 3, no. 4, pp. 250–257, 2014.
- [4] A. Haboush, M. N. Mohanty, B. K. Pattanayak, and M. Al-Tarazi, "A framework for wireless sensor network fault rectification," *International journal of multimedia and ubiquitous Engineering*, vol. 9, no. 1, pp. 133–142, 2014.
- [5] World Health Organization, *Global Status Report on Non-Communicable Diseases 2014*, WHO, 2014, March 2020, <https://apps.who.int/iris/handle/10665/148114>.
- [6] T. M. Fernández-Caramés, I. Froiz-Míguez, O. Blanco-Novoa, and P. Fraga-Lamas, "Enabling the Internet of mobile crowdsourcing health things: a mobile fog computing, blockchain and iot based continuous glucose monitoring system for diabetes mellitus research and care," *Sensors*, vol. 19, no. 15, p. 3319, 2019.
- [7] A. Pati, M. Parhi, and B. K. Pattanayak, "COVID-19 pandemic analysis and prediction using machine learning approaches in India," in *Advances in Intelligent Computing and Communication*, pp. 307–316, Springer, Singapore, 2021.
- [8] S. M. R. Islam, D. Kwak, M. H. Kabir, M. Hossain, and K. S. Kwak, "The Internet of things for health care: a comprehensive survey," *IEEE Access*, vol. 3, pp. 678–708, 2015.
- [9] S. Tuli, R. Mahmud, S. Tuli, and R. Buyya, "FogBus: a blockchain-based lightweight framework for edge and fog computing," *Journal of Systems and Software*, vol. 154, pp. 22–36, 2019.
- [10] A. M. Rahmani, T. N. Gia, B. Negash et al., "Exploiting smart e-Health gateways at the edge of healthcare Internet-of-Things: a fog computing approach," *Future Generation Computer Systems*, vol. 78, pp. 641–658, 2018.
- [11] A. A. Mutlag, M. K. Abd Ghani, N. Arunkumar, M. A. Mohammed, and O. Mohd, "Enabling technologies for fog computing in healthcare IoT systems," *Future Generation Computer Systems*, vol. 90, pp. 62–78, 2019.
- [12] S. Tuli, N. Basumatary, and R. Buyya, "EdgeLens: deep learning based object detection in integrated IoT, fog and cloud computing environments," in *2019 4th International Conference on Information Systems and Computer Networks, ISCON 2019*, pp. 496–502, Mathura, India, 2019.
- [13] S. S. Gill, R. C. Arya, G. S. Wander, and R. Buyya, "Fog-based smart healthcare as a big data and cloud service for heart patients using IoT," in *Lecture Notes on Data Engineering and Communications Technologies*, vol. 26, pp. 1376–1383, Springer Science and Business Media Deutschland GmbH, 2019.
- [14] D. C. Klonoff, "Fog computing and edge computing architectures for processing data from diabetes devices connected to the medical Internet of things," *Journal of Diabetes Science and Technology*, vol. 11, no. 4, pp. 647–652, 2017.
- [15] R. Priyadarshini, R. K. Barik, and H. Dubey, "DeepFog: fog computing-based deep neural architecture for prediction of stress types, diabetes and hypertension attacks," *Computation*, vol. 6, no. 4, p. 62, 2018.
- [16] R. O. Aburukba, M. AliKarrar, T. Landolsi, and K. El-Fakih, "Scheduling Internet of things requests to minimize latency in hybrid fog-cloud computing," *Future Generation Computer Systems*, vol. 111, pp. 539–551, 2020.
- [17] I. H. Laradji, M. Alshayeb, and L. Ghouti, "Software defect prediction using ensemble learning on selected features," *Information and Software Technology*, vol. 58, pp. 388–402, 2015.
- [18] G. Haixiang, L. Yijing, L. Yanan, L. Xiao, and L. Jinling, "BPSO-Adaboost-KNN ensemble learning algorithm for multi-class imbalanced data classification," *Engineering Applications of Artificial Intelligence*, vol. 49, pp. 176–193, 2016.
- [19] L. Tang, Y. Wu, and L. Yu, "A non-iterative decomposition-ensemble learning paradigm using RVFL network for crude oil price forecasting," *Applied Soft Computing Journal*, vol. 70, pp. 1097–1108, 2018.
- [20] S. El-Sappagh, M. Elmogy, F. Ali, T. Abuhmed, S. M. R. Islam, and S. K. Kwak, "A comprehensive medical decision-support framework based on a heterogeneous ensemble classifier for diabetes prediction," *Electronics*, vol. 8, no. 6, p. 635, 2019.
- [21] T. M. Fernández-Caramés and P. Fraga-Lamas, "Design of a fog computing, blockchain and IoT-based continuous glucose monitoring system for crowdsourcing mHealth," *Multidisciplinary Digital Publishing Institute Proceedings*, vol. 4, no. 1, p. 37, 2018.
- [22] P. Kaur, N. Sharma, A. Singh, and B. Gill, "CI-DPF: a cloud IoT based framework for diabetes prediction," in *2018 IEEE 9th annual information technology, Electronics and Mobile Communication Conference (IEMCON)*, pp. 654–660, Vancouver, BC, Canada, 2018.
- [23] R. K. Barik, R. Priyadarshini, H. Dubey, V. Kumar, and K. Mankodiya, "FogLearn," *International Journal of Fog Computing (IJFC)*, vol. 1, no. 1, pp. 15–34, 2018.
- [24] T. N. Gia, I. B. Dhaou, M. Ali et al., "Energy efficient fog-assisted IoT system for monitoring diabetic patients with cardiovascular disease," *Future Generation Computer Systems*, vol. 93, pp. 198–211, 2019.
- [25] M. Devarajan, V. Subramaniaswamy, V. Vijayakumar, and L. Ravi, "Fog-assisted personalized healthcare-support system for remote patients with diabetes," *Journal of Ambient Intelligence and Humanized Computing*, vol. 10, no. 10, pp. 3747–3760, 2019.
- [26] M. Abdel-Basset, G. Manogaran, A. Gamal, and V. Chang, "A novel intelligent medical decision support model based on soft computing and IoT," *IEEE Internet of Things Journal*, vol. 7, no. 5, pp. 4160–4170, 2019.
- [27] A. U. Haq, J. P. Li, J. Khan et al., "Intelligent machine learning approach for effective recognition of diabetes in E-healthcare using clinical data," *Sensors*, vol. 20, no. 9, p. 2649, 2020.
- [28] S. Kumari, D. Kumar, and M. Mittal, "An ensemble approach for classification and prediction of diabetes mellitus using soft voting classifier," *International Journal of Cognitive Computing in Engineering*, vol. 2, pp. 40–46, 2021.
- [29] G. Geetha and K. M. Prasad, "An hybrid ensemble machine learning approach to predict type 2 diabetes mellitus," *Webology*, vol. 18, no. Special Issue 02, pp. 311–331, 2021.

- [30] P. G. Shynu, V. G. Menon, R. L. Kumar, S. Kadry, and Y. Nam, "Blockchain-based secure healthcare application for diabetic-cardio disease prediction in fog computing," *IEEE Access*, vol. 9, pp. 45706–45720, 2021.
- [31] A. Singh, A. Dhillon, N. Kumar, M. S. Hossain, G. Muhammad, and M. Kumar, "eDiaPredict: an ensemble-based framework for diabetes prediction," *ACM Transactions on Multimedia Computing Communications and Applications*, vol. 17, no. 2s, pp. 1–26, 2021.
- [32] D. S. Rajput, S. M. Basha, Q. Xin et al., "Providing diagnosis on diabetes using cloud computing environment to the people living in rural areas of India," *Journal of ambient intelligence and humanized Computing*, vol. 13, no. 5, pp. 2829–2840, 2022.
- [33] H. F. Germany, *Diabetes Dataset*, Kaggle, 2020, October 2020, <https://www.kaggle.com/johndasilva/diabetes>.
- [34] Pima Indian Diabetes Dataset, "UCI-ML repository," 2020, March 2020, <https://archive.ics.uci.edu/ml/datasets/pima+indians+diabetes>.
- [35] B. Ihnaini, M. A. Khan, T. A. Khan et al., "A smart healthcare recommendation system for multidisciplinary diabetes patients with data fusion based on deep ensemble learning," *Computational Intelligence and Neuroscience*, vol. 2021, 11 pages, 2021.
- [36] B. Shickel, P. J. Tighe, A. Bihorac, and P. Rashidi, "Deep EHR: a survey of recent advances in deep learning techniques for electronic health record (EHR) analysis," *IEEE Journal of Biomedical and Health Informatics*, vol. 22, no. 5, pp. 1589–1604, 2018.
- [37] H. Yan, Y. Jiang, J. Zheng, C. Peng, and Q. Li, "A multilayer perceptron-based medical decision support system for heart disease diagnosis," *Expert Systems with Applications*, vol. 30, no. 2, pp. 272–281, 2006.
- [38] T. T. Hasan, M. H. Jasim, and I. A. Hashim, "Heart disease diagnosis system based on multi-layer perceptron neural network and support vector machine," *International Journal of Current Engineering and Technology*, vol. 77, no. 55, pp. 2277–4106, 2017.
- [39] V. Sharma, A. Rasool, and G. Hajela, "Prediction of heart disease using DNN," in *2020 Second International Conference on Inventive Research in Computing Applications (ICIRCA)*, pp. 554–562, Coimbatore, India, 2020.
- [40] P. Ramprakash, R. Sarumathi, R. Mowriya, and S. Nithyavishnupriya, "Heart disease prediction using deep neural network," in *2020 International Conference on Inventive Computation Technologies (ICICT)*, pp. 666–670, Coimbatore, India, 2020.
- [41] S. Sharma and M. Parmar, "Heart diseases prediction using deep learning neural network model," *International Journal of Innovative Technology and Exploring Engineering (IJITEE)*, vol. 9, no. 3, pp. 2244–2248, 2020.
- [42] S. Tuli, N. Basumatary, S. S. Gill et al., "HealthFog: an ensemble deep learning based smart healthcare system for automatic diagnosis of heart diseases in integrated IoT and fog computing environments," *Future Generation Computer Systems*, vol. 104, pp. 187–200, 2020.
- [43] I. E. Livieris, E. Pintelas, S. Stavroyiannis, and P. Pintelas, "Ensemble deep learning models for forecasting cryptocurrency time-series," *Algorithms*, vol. 13, no. 5, p. 121, 2020.
- [44] X. Y. Gao, A. A. Ali, H. Shaban Hassan, and E. M. Anwar, "Improving the accuracy for analyzing heart diseases prediction based on the ensemble method," *Complexity*, vol. 2021, 10 pages, 2021.
- [45] F. Ali, S. El-Sappagh, S. R. Islam et al., "A smart healthcare monitoring system for heart disease prediction based on ensemble deep learning and feature fusion," *Information Fusion*, vol. 63, pp. 208–222, 2020.
- [46] M. N. Uddin and R. K. Halder, "An ensemble method based multilayer dynamic system to predict cardiovascular disease using machine learning approach," *Informatics in Medicine Unlocked*, vol. 24, p. 100584, 2021.
- [47] H. Gupta, A. Vahid Dastjerdi, S. K. Ghosh, and R. Buyya, "iFogSim: a toolkit for modeling and simulation of resource management techniques in the Internet of things, edge and fog computing environments," *Software: Practice and Experience*, vol. 47, no. 9, pp. 1275–1296, 2017.
- [48] S. Narula and A. Jain, "Cloud computing security: Amazon web service," in *2015 Fifth International Conference on Advanced Computing & Communication Technologies*, pp. 501–505, Haryana, India, 2015.
- [49] C. Vecchiola, X. Chu, and R. Buyya, "Aneka: a software platform for .NET-based cloud computing," *High speed and large scale scientific computing*, vol. 18, pp. 267–295, 2009.
- [50] A. Pati, M. Parhi, and B. K. Pattanayak, "IDMS: an integrated decision making system for heart disease prediction," in *2021 1st Odisha International Conference on Electrical Power Engineering, Communication and Computing Technology (ODI-CON)*, pp. 1–6, Bhubaneswar, India, 2021.
- [51] A. Pati, M. Parhi, and B. K. Pattanayak, "IADP: an integrated approach for diabetes prediction using classification techniques," in *Advances in Distributed Computing and Machine Learning*, pp. 287–298, Springer, Singapore, 2022.
- [52] Explore MIT App Inventor, *MIT App Inventor* July 2020, <https://appinventor.mit.edu/>.
- [53] H. Liu, F. Yan, S. Zhang, T. Xiao, and J. Song, "Source-level energy consumption estimation for cloud computing tasks," *IEEE Access*, vol. 6, pp. 1321–1330, 2017.
- [54] S. Lehrig, H. Eikerling, and S. Becker, "Scalability, elasticity, and efficiency in cloud computing: a systematic literature review of definitions and metrics," in *Proceedings of the 11th International ACM SIGSOFT Conference on Quality of Software Architectures*, pp. 83–92, Montreal, Canada, 2015.
- [55] A. A. S. Ahmad and P. Andras, "Scalability analysis comparisons of cloud-based software services," *Journal of Cloud Computing*, vol. 8, no. 1, pp. 1–17, 2019.

15 December 2022

Dr. Amit Banerjee,  
Assistant Professor,  
Dept of Physics,  
Principal Investigator, Microsystem Design-Integration Lab,  
Bidhan Chandra College,  
Dist: Paschim Bardhaman,  
Asansol- 713304, INDIA

Dear Amit,

This is further to the recent discussions that Professor Bhanu Pratap Das, Director of the Centre for Quantum Engineering, Research and Education (CQuERE) of TCG CREST and a few other senior members of TCG CREST had with you. With great pleasure we are extending an invitation to you to join us as an Honorary Adjunct Faculty for a period of one year from 20 December 2022.

We will be much obliged if you could regularly find time to visit TCG CREST for interacting with our faculty members, research scholars and students for guiding and advising them in your domain of expertise and interest.

We will be looking forward to receiving a confirmatory note from you soon.

Thanking you,

Yours sincerely,



Joydeep Bhattacharya  
Chief Development Officer  
TCG Centres for Research and Education in Science and Technology





# A Study on the Mechanical Properties of Rare Earth-based Aluminium Composite

K. Balamurugan<sup>1</sup> · T. Deepthi<sup>1</sup> · Ananda Kumar Subramanian<sup>2</sup> · Amit Banerjee<sup>3</sup> · Daksh Agarwal<sup>4,5</sup> · Arindam Biswas<sup>6</sup> · Arijit Sinha<sup>7</sup> 

Received: 6 March 2022 / Accepted: 6 June 2022  
© The Institution of Engineers (India) 2022

**Abstract** The present investigation signifies the effect of incorporation of lanthanum phosphate nanopowder at different weight ratios in aluminium matrix. The lanthanum phosphate reinforcements in the 50–80 nm size range are synthesized through a cost-effective sol–gel process, without any subsequent secondary process. The composite is fabricated by the ultrasonic-assisted stir casting process, a low cost and a less defective manufacturing process. Various mechanical properties, viz. ultimate tensile strength, flexural strength, compressive strength and hardness, are examined. From the study, it is concluded that MMC with 15 wt% the lanthanum phosphate leads to the best tensile, compression and flexural properties as well as hardness. Blending the reinforcement in the matrix is a challenging task, besides the selection of suitable stirring conditions which greatly reduces the agglomerations. The higher bonding force between the reinforcement and the

matrix makes the reinforcement a suitable material in the aluminium matrix composite, and it is confirmed through density functional theory studies. The superior properties of the Al/LaPO<sub>4</sub> composite make it a suitable replacement material for aerospace and defence applications.

**Keywords** Al6061/LaPO<sub>4</sub> composite · Tensile testing · Flexural testing · Compressive testing · Surface topography · Density functionality theorem

## Introduction

According to Bodunrin et al. [1], Metal matrix composite (MMC) exhibits variable properties depending on the properties of reinforcement materials such as shape, thickness, absorption, interfacial wetting and dispersion rate in the matrix, and also with different weight and volume percentage. Kumar et al. [2] stated that the Al6061 composite has a wide range of applications in railing, marine, aeronautics and automobiles because of its high weldability, medium-quality machinability, etc. Manganese and silicon in Al6061 alloys enhance the properties of the composite for applications in a wide range of engineering applications, particularly in the areas of automotive components. Furthermore, the tempered aluminium series is proved to have high strength. Mummoorthi et al. [3] reported that the uniform distribution of Fe<sub>2</sub>O<sub>3</sub> and B<sub>4</sub>C in Al6061 tempered alloys will provide improved tensile strength. Kumar et al. [4] manufactured Al/SiC composite through the conventional stir casting process and attained improved tribological properties by increasing the wt.% of SiC reinforcement material. Bragaglia et al. [5] reported the effect of pitting (corrosion) in Al6061 by adding

✉ Arijit Sinha  
sinharijit@gmail.com

<sup>1</sup> Department of Mechanical Engineering, Vignana's Foundation for Science, Technology & Research, Guntur, Andhra Pradesh 522213, India  
<sup>2</sup> School of Computer Science and Engineering, Vellore Institute of Technology, Vellore, Tamil Nadu 632014, India  
<sup>3</sup> Physics Department, Bidhan Chandra College, Asansol, West Bengal 713 303, India  
<sup>4</sup> Department of Materials Science and Engineering, University of Pennsylvania, Philadelphia, PA 19104, USA  
<sup>5</sup> Lam Research Corporation, Fremont, CA 94538, USA  
<sup>6</sup> Department of Mining Engineering, Kazi Nazrul University, Asansol, West Bengal 713340, India  
<sup>7</sup> Department of Metallurgical Engineering, Kazi Nazrul University, Asansol, West Bengal 713340, India

alumina within the matrix as the progressive action of magnesium considerably reduces such effect.

Fenghong et al. [6] prepared Al/SiC/WC composites by stir casting process with excellent tensile, wear and compression properties. Murugan et al. [7] successfully manufactured Al/7%Al<sub>2</sub>O<sub>3</sub>/x% SiC through stir casting process and reported improvement in the mechanical properties of composite with an increase in the SiC content. Sivanathan et al. [8] manufactured Al-Al<sub>2</sub>O<sub>3</sub> composite through conventional stirring process and confirmed that uniform dispersion composite will improve the tensile, compression and hardness properties. Reddy et al. [9] prepared Al6061/2SiC/x% of Gr hybrid composite by the ultrasonic-assisted stir casting process and concluded that the appropriate composition percentage of reinforcement in the matrix alone would improve the dispersion rate, regardless of the use of ultrasonic probe sonicator. According to Luan et al. [10], several techniques such as spraying process, squeezing casting, stir casting and powder metallurgy are available. Kumar and Murugan [11] proposed that the stir casting process has proved to be a suitable technique for fabrication of MMC with advantages. Inegbenebor et al. [12] fabricated an aluminium composite with a varied SiC composition with uniform distribution of the particle through the stirring process. According to Kalra et al. [13], stir casting is the most preferable and practical technique, as this process leads to reduce agglomeration and clustering of particles. Eskin [14] reported the dendritic structures formed during the cementation, and further, agglomeration arrangement will reduce the mechanical properties of the prepared composite. Madhukar et al. [15] confirmed that the use of an ultrasonicator in the stir casting process will break the clusters of particles and reduces the potential for agglomeration. Idrisi and Mourada [16] have taken a comparative approach to ultrasonic aided and conventional stir casting and concluded that samples prepared by the ultrasonic probe technique exhibit uniform distribution of the SiC particles. Greil [17] reported that lanthanum phosphate (LaPO<sub>4</sub>) has low thermal conductivity, non-reactive at the high sintering temperature and machinable ceramic materials, as noted by Sujith et al. [18] irregular grain growth along the grain boundary is observed above 1400 °C sintering temperature. In the present case, however, the optimum temperature for curing the powder is 1200 °C and the sintering temperature is much lower than the curing temperature, so there is no risk of irregular grain boundaries in the prepared composite microstructure. Rajesh et al. [19] confirmed that the LaPO<sub>4</sub> in alumina composite is non-reactive at a temperature of 1600 °C with 5–7 nm crystallite size.

Generally, the addition of hard ceramic reinforcement in the metal matrix composite is to enhance the material

properties. Adversely it may affect the other properties of the material which are very good before the combination. The composite material has now replaced the traditional material because of its own advantages. However, the machining of these ceramic-reinforced metal matrix composites is always a challenging task for the manufacturers. Proper investigation is required towards the machining of composite because of the addition of hard reinforced ceramic particles. Through the literature, it can be confirmed that LaPO<sub>4</sub> ceramic particles are very soft in nature when compared to the other available ceramic materials [20, 21]. Certain investigations on machining of LaPO<sub>4</sub> ceramic material on the ceramic matrix composites are also reported [22]. Early studies clearly confirms that the addition of rare earth lanthanum phosphate particles improves the machinability characteristics of the sample [23]. The addition of the soft ceramic in the metal matrix composite will not affect the standard operating conditions, and the traditional machining operations can also be performed on the fabricated composite [24]. Most of the properties of fabricated composite and the available composite are found to be same. Hence, Al/LaPO<sub>4</sub> suits for all engineering applications and it can be a replacement material over the available composite materials. Further, the suitable mix of LaPO<sub>4</sub> in Al matrix can be used for structural and load bearing applications.

A limited study is available in LaPO<sub>4</sub> ceramic matrix composite. Further, earlier studies reported that the LaPO<sub>4</sub> is a suitable material in the ceramic matrix composite because of its monazite structure. Some work also conducted using LaPO<sub>4</sub> as reinforcement in the ceramic matrix composite. Because of the rare earth elements and its scarcity in availability of LaPO<sub>4</sub>, the available literature is very limited. Here in the present study, through chemical route, authors fabricated the LaPO<sub>4</sub> in nanopowder form and the same is used as the reinforcement in the metal matrix composite. So far, the commercial available ceramic materials such as SiC and TiC are used as reinforcement in the Al matrix. Authors has made an attempt to fabricate the soft and monazite structure LaPO<sub>4</sub> rare earth element in nanopowder form, and the significance of LaPO<sub>4</sub> in aluminium matrix composite is examined with the different weight percentages of LaPO<sub>4</sub>. Mechanical characterization is performed, and the suitable composition for the Al matrix is proposed.

## Materials and Methods

Initially, a stoichiometric quantity of lanthanum hexachloride is mixed with orthophosphoric acid in an ammonia atmosphere. 20% nitric acid is added to the reaction mixture to maintain a pH level of 2. The deposited



powder is separated, washed and dried to a temperature of 1200 °C. The powder is then ball-milled for 24 h to get a particle size of 20–40 nm. The method of preparation of LaPO<sub>4</sub> powder is furnished in Fig. 1a.

Commercially available Al6061 aluminium rod is procured, and a calculated quantity is melted in an electric furnace at a temperature of 750 °C. The synthesized LaPO<sub>4</sub> powder is preheated to a temperature of 200 °C to remove any excess oxygen content. Two teeth stainless steel stirrer is allowed to rotate into the molten mixture at a constant speed of 250 rpm. A calculated quantity of the reinforcement material is slowly added into the vortex of the molten material. The mixture is continuously stirred for 20 min at a temperature of 600 °C. A two-side open die is specially designed for the fabrication process which is made of Die steel with a geometry of dia 120 × 10 mm is used as a mould and it is preheated to a temperature of 200 °C to

avoid shrinking and other defects. The lower side of the die is locked and allowed to hold the poured molten mixture. Once the molten mixture is poured into the die through the top opening, the die is then subjected to a uniaxial compressed load of 80 kg/mm to reduce the casting defects and to develop improved microstructure. Five different samples with 0, 5, 10, 15 and 20% weight percentage LaPO<sub>4</sub> are fabricated by following the same procedures. The experimental set-up, fabrication condition and the fabricated composite samples are shown in Fig. 1b, c, d. The compressed samples are ejected from the die and the samples are sintered to a temperature of 400 °C for 2 h to reduce any developed internal stress and porosity. Hedayatian et al. [25] fabricated Al6061/graphene composite by casting, followed by hot rolling and it is confirmed that the porosity of the samples is greatly reduced as the result of hot rolling. Figure 1e displays the nanoparticle size LaPO<sub>4</sub>

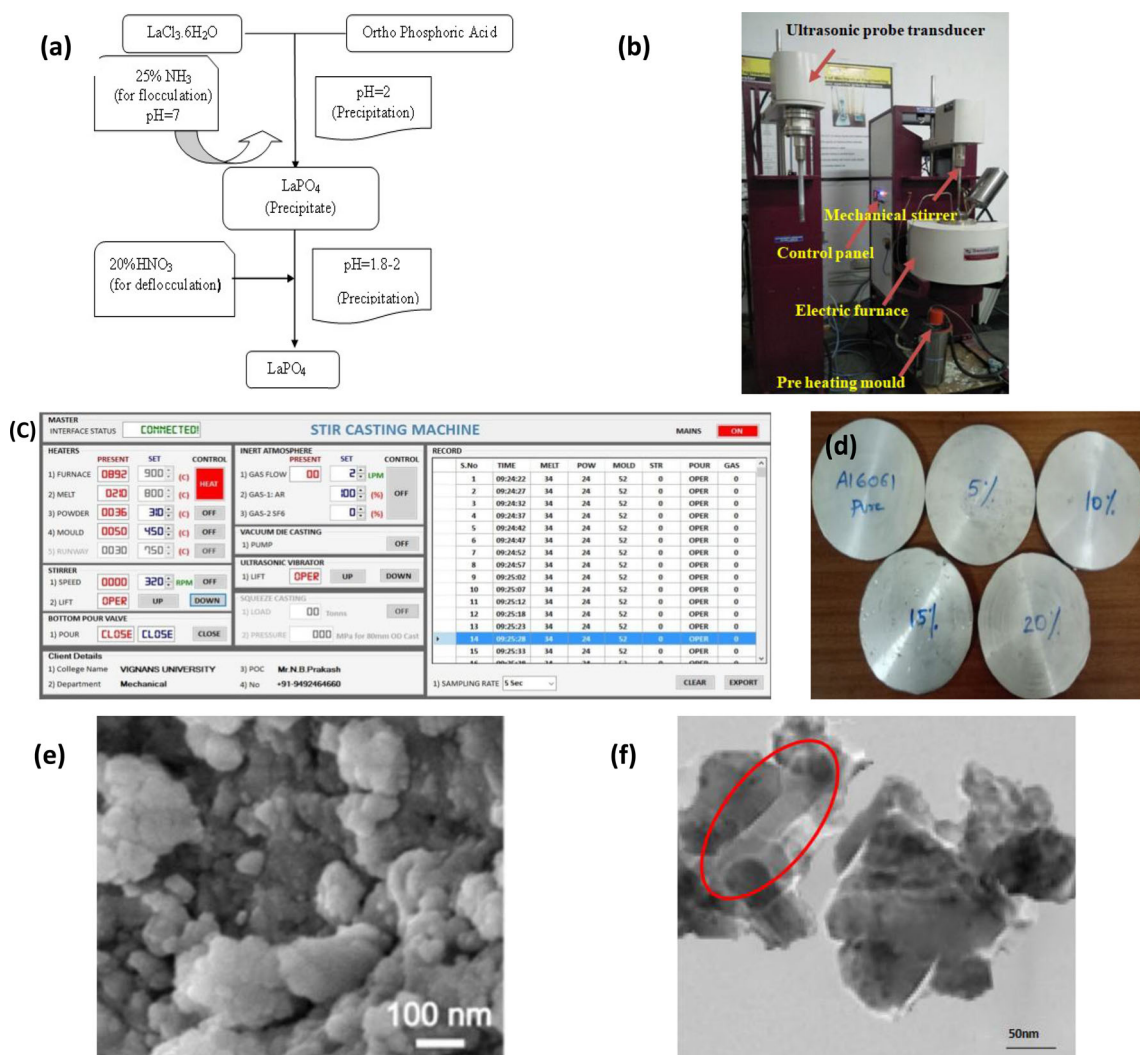


**Fig. 1** Material processing techniques. **a** Flow diagram of LaPO<sub>4</sub> preparation, **b** ultrasonic stir casting machine, **c** stir casting process parameters, **d** Al/x% LaPO<sub>4</sub> samples, **e** SEM of LaPO<sub>4</sub> particle, **f** TEM image of nano-LaPO<sub>4</sub>

powder, and Fig. 1f shows the transmission electron microscopy image of the composite surface. The survey report on  $\text{LaPO}_4$  confirms that the structure of the synthesized  $\text{LaPO}_4$  nanoparticles is in rod form; similar observations are noted on the composite surface. Energy-dispersive X-ray spectroscopy confirms the presence of all elemental composition in the composite and it is shown in Fig. 2.

The measurements of the mechanical properties of the fabricated composite is taken using the standard specimen as per the ASTM-B 557 for the tensile test, ASTM A370 for the flexural test with a dimension of  $100 \times 10 \times 10$  mm and ASTM E9-09 for the compression test with a dimension of  $25 \times 13$  mm and L/D ratio of 0.2. Four trial runs are conducted, and the average of the each test observations is reported. The specimens are cut to the required dimension using an abrasive water jet, and the schematic representation is shown in Fig. 3.

Universal test machines is used to make tensile observations at a cross head speed of 1.5 mm/min with a strain rate of 0.01 mm/mm and 0.2% proof stress. The three-point bend test is performed at room temperature with the UTM. An Instron universal hydraulic inspection equipment with a capacity of 100 kN built into a computer and data retrieval software is used for compression testing. A compression load with a continued frequency is applied to the load control system. The load distribution curves are plotted according to the test condition applied to the tension and compression load. The Vickers microhardness is measured using Mituto hardness tester as per ASTM E384. The applied load is 500 g for a dwell period of 15 s. The test piece measured 70 mm long, 25 mm wide and 20 mm thick. To prevent errors, failed samples with significant deviations in test conditions are removed.

## Results and Discussion

### Ultimate Tensile Strength

The tensile strength observation of  $\text{Al}/x\%\text{LaPO}_4$  is shown in Table 1, and an increasing trend with the increase in the  $\text{LaPO}_4$  content up to 15% is noted and then decreases, irrespective of break load and displacement conditions. Errandonea and Manjon [26] studied the bonding behaviour of different elements in the matrix and concluded that three of the phosphate–oxygen bonds are strong and hold rigid, but the remaining one oxygen bond is likely loosely bonded and can undergo deformation. The aluminium–oxygen bond with monazite elements such as  $\text{LaPO}_4$  has four strong bonds and five loosely packed elements, which can lead to deformation, which is validated through the density functionality theorem. Applying the same concept, it can be stated that the excess composition of  $\text{LaPO}_4$ , a monazite structure, in the Al6061 progresses to materials deformation due to increment in the weak bond regions. However, one-third of the strong bonds of  $\text{LaPO}_4$  are believed to yield high tensile strength irrespective of breaking load.

The bond that exists between aluminium alone can cause variation in the break load. The excess amount of loose bonded elements between aluminium and oxygen initiates deformation, and with an increase in the applied load condition, the bonds between the reinforcements are weakened and lead to failure. According to Wang [27], the addition of  $\text{LaPO}_4$  in the alumina creates unstable bonds and tends to have deformation. The study of  $\text{LaPO}_4$  in the aluminium metal matrix composite is nowhere reported; hence, an extensive study on the debonding mechanism is to be done.

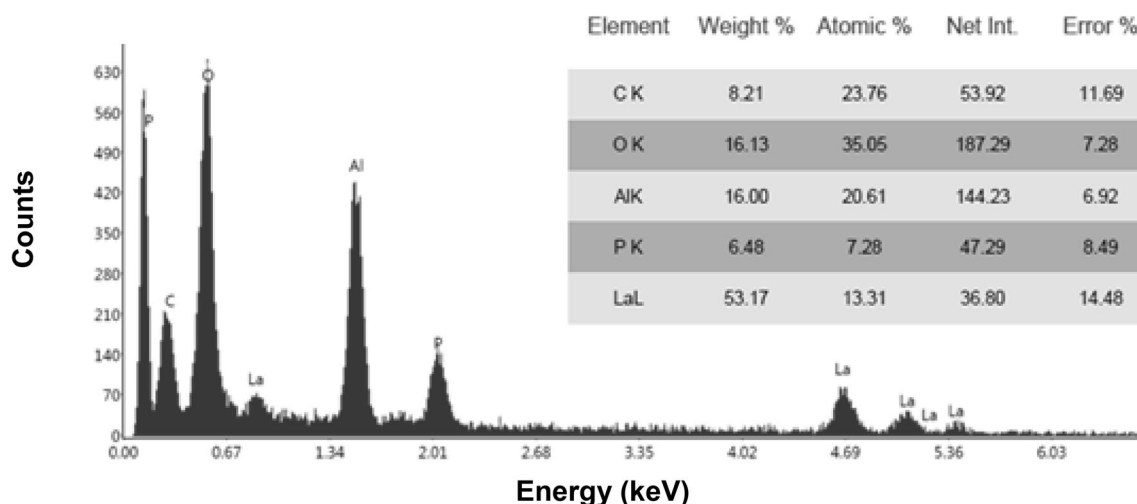
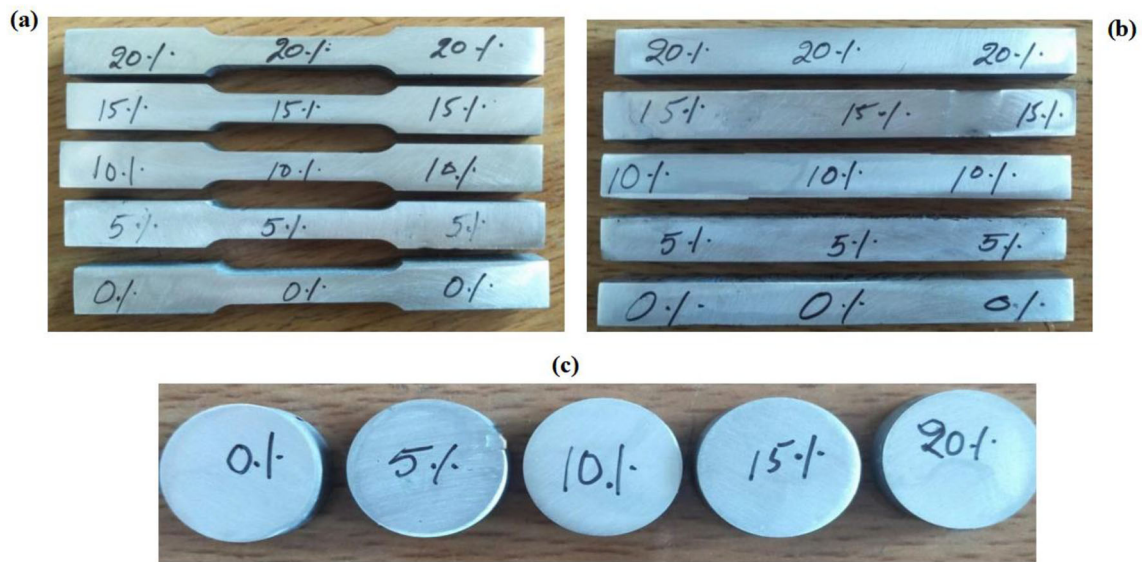


Fig. 2 Energy-Dispersive Spectra of Al/ $\text{LaPO}_4$  sample



**Fig. 3** Schematic representation of the specimens for **a** Tensile, **b** flexural and **c** compression test

**Table 1** Tensile properties of Al/LAP

Sample name	Break load (kN)	Displacement (mm)	Tensile strength (MPa)
Al	7.16	5.4	139.44
Al/5%LAP	7.64	8.17	160.55
Al/10%LAP	6.8	7.8	190.75
Al/15%LAP	5.96	6.9	204.15
Al/20%LAP	4.08	6.32	193.95

Figure 4a displays the trends of load versus displacement plot of the tensile test. Till 15% of LaPO<sub>4</sub> composition, the composite shows the same failure trend irrespective of break load. The sudden drop in the peak occurs due to the bond failure caused within the matrix and reinforcements. As an excess quantity of nanopowder LaPO<sub>4</sub> causes agglomeration, the reduction of 16.75% of tensile strength from the nascent sample can be compromised. On considering the maximum strength, it is proposed that the addition of 15% of rare earth LaPO<sub>4</sub> will be much suitable composition in the Al6061 matrix. Similar observations are noticed by Aynalem [28] as a 12% increment in UTS with 15% of TiC and WC when added as reinforcements in aluminium matrix.

**Flexural Strength**

The flexural strength of the composite observations is shown in Table 2. Maximum flexural strength of 215 MPa

is recorded at 15% of LaPO<sub>4</sub> reinforcement. The gradual increment in the flexural strength is observed until 15% of LaPO<sub>4</sub>, and the addition of an excess quantity of LaPO<sub>4</sub> in the Al6061 matrix gives rise to the particle deformation. Sha et al. [29] reported that operating temperature will greatly influence the property of materials, for instance 47% increment is noted on flexural strength with the change in operating conditions. Unlike other ceramic reinforcements, LaPO<sub>4</sub> has an irregular surface boundary which is verified through SEM and TEM images (refer Fig. 1e, f) which enhances bonding in the matrix.

Majeed et al. [23] confirmed that LaPO<sub>4</sub>-reinforced alumina composite can be machined using a conventional machining process, as the soft phase of LaPO<sub>4</sub> improve the toughness property of the materials and enhance machinability. The same phenomenon is observed in a three-point bending test. At three-point load test conditions, increment in the breaking load capacity and displacement concerning the reinforcement is due to the resistance offered by the irregular shape of LaPO<sub>4</sub> at the applied load. The higher composition of LaPO<sub>4</sub> in the matrix improves the sliding property and has material deformation. With the increment of the applied load, the fabricated composite material deflection with the propagation of crack on the surface of the test sample. Microstructural examination of the fracture surface revealed the presence of transgranular and intergranular fractures. The particle pull-out and the dimples are not visible on the fracture surface indicates that the soft ceramic lanthanum phosphate element also deflects along with the aluminium and the irregular shape of the reinforcement provides better bonding capability and improves the flexural property of the composite. The test sample image superimposed in Fig. 4b shows the impact of the

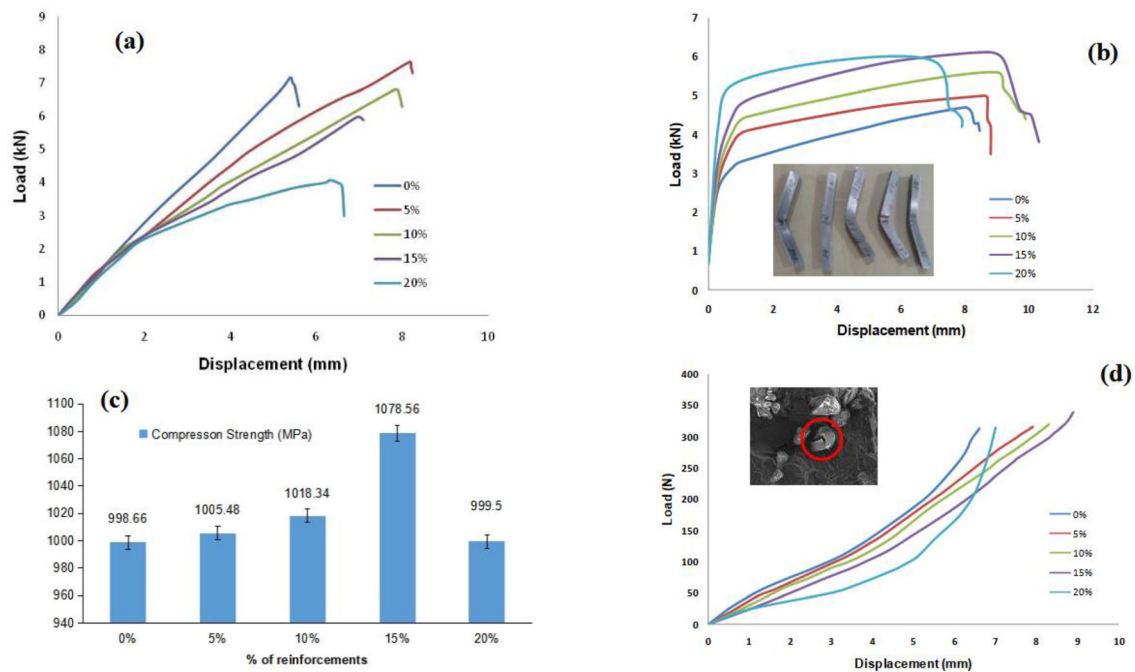


**Fig. 4** **a** Tensile behaviour of Al/x%LaPO<sub>4</sub>, **b** flexural strength of Al/x%LaPO<sub>4</sub>, **c** compression strength of Al/x%LaPO<sub>4</sub> and **(d)** load versus displacement plot of Al/x%LaPO<sub>4</sub>

**Table 2** Flexural properties of Al/LAP

Sample name	Break load (kN)	Displacement (mm)	Flexural strength (MPa)
Al	4.68	8	146.92
Al/5%LAP	5	8.6	170.28
Al/10%LAP	5.6	9	210.59
Al/15%LAP	6.1	8.7	215.27
Al/20%LAP	4.7	7.5	200.46

applied load. Among the five test samples, Al/20%LaPO<sub>4</sub> has undergone severe deformation which can be measured from the angle created at the flexural load condition.

Figure 4b also shows the deflection of the test sample for the test load condition. The primary deformation of the particles inside the composite structure for all the samples at different load conditions starts at 0.8 mm. The load range starts from 3.2 to 5.3 MPa with reinforcements. Bhasa and Balamurugan [30] reported that an increase in reinforcements significantly reduces the dislocation of the particles in the aluminium matrix and progresses to deflection. Among the developed composite samples, Al/20% LaPO<sub>4</sub> shows less deflection than nascent samples and a superior withstanding load of 5.3 MPa conveys that the presence of an excess quantity of LaPO<sub>4</sub> causes dislocation plane.

### Compressive Strength

A uniaxial compression load of 80 kg/mm is applied at the time of preparation of the composite itself. The maximum compressive load capacity of Al/LaPO<sub>4</sub> is shown in Table 3.

The compressive strength and the load–displacement curve of the fabricated composite are shown in Fig. 4c and d, respectively. Figure 4c shows that except for 20% of LaPO<sub>4</sub>, the remaining composition provides an incremental rate of compressive strength. A maximum compressive property of 1078 MPa is observed at 15% reinforcement. Imran and Khan [31] stated that the addition of ceramic particles in the soft matrix will increase the compressive property as the ceramic particle surface area significantly enhances the load withstanding capacity and has improved hardness. Further increase in reinforcements will have to increase the compressive strength, but at 20% a decrement is observed. Balamurugan et al. [32] stated that monazite LaPO<sub>4</sub> is proved to be the soft ceramic among the available materials. Each LaPO<sub>4</sub> particle has its surface area and it resists the applied load to a certain limit. When the load exceeds the threshold limit, i.e. as it exceeds the particle breaking force, material deformation takes place.

A higher reinforcement percentage will enhance the load withstanding capacity and may cause the slippery of the particles and progress to have large cracks on the surface of



**Table 3** Compressive properties of Al/LAP

Sample name	Load ( <i>N</i> )	Displacement (mm)	Compressive strength (MPa)
Al	6.6	313.74	998.66
Al/5%LAP	7.9	314.21	1005.48
Al/10%LAP	8.3	319.92	1018.34
Al/15%LAP	8.9	338.84	1078.56
Al/20%LAP	7	314.08	999.50

the test samples. At the same time, as reported by Balamurugan et al. [33] LaPO<sub>4</sub> particle will break at the working load condition, similar observation is noted for the fabricated composite. A higher percentage of reinforcement will lead to sudden failure of composite and this can be verified from the 20% LaPO<sub>4</sub> plot. Figure 4d displays the load withstanding ability of the composite. Agglomeration of the particles improves the compression load capacity but being a soft ceramic the sudden deformation reported for a 20% sample. It is further noted that the distribution of the reinforcements greatly determines the load withstanding ability. The increase in reinforcement gradually improves the compressive property of the composite. The SEM image of the LaPO<sub>4</sub> particle that appeared on the surface of the fractured surface is superimposed in Fig. 4d which shows the effect of the applied load.

### Hardness

The hardness values for different proposition composite is measured in the Vickers hardness number and it is shown in Fig. 5a. Cast samples have undergone uniaxial compression load immediately after casting, causing the increase in the residual stress, and each molecule in the composite will have undergone severe compression and tries to regain its original shape. The intense compression load is to provide enough support from the neighbouring particles with the reinforcements to improve the bonding property with the LaPO<sub>4</sub> particle. However, sintering after compression action will reduce the internal stress.

The optical image of the samples in Fig. 5b shows the indentation mark experienced by different composition composites. No Palmqvist cracks are visible on the loaded surface. While observing the impressions produced by the intender at different compositions, the impression depth is significantly reduced with the increase in composition. Deepthi and Balamurugan [34] reported that the hardness of nascent LaPO<sub>4</sub> samples is 5GPa, on the addition of this material as reinforcement usually improves the hardness of the sample. A gradual increment of 3% in hardness is observed with the increase of 5 weight per cent of LaPO<sub>4</sub> in

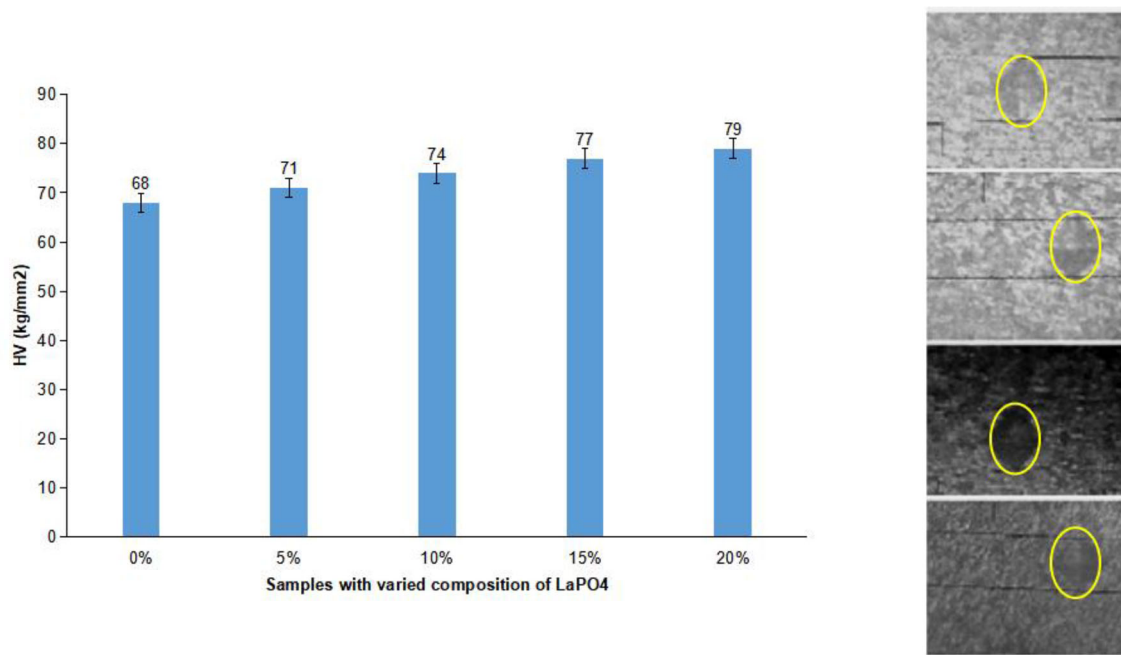
the composition. As per metweb.com data on aluminium 6061-T6, 6061-T651, it is displayed that the component possesses a hardness of 107 VHN, whereas the maximum hardness observed with 20% of LaPO<sub>4</sub> composite is recorded to be 79VHN. The lower the hardness means the higher the ductility. The materials fabrication process predominantly determines the property of the end product as it has yielded to get observations.

### Morphological Features

Typical surface topography on the fracture region of the test sample is shown in Fig. 6. The uniform dispersion of the reinforcement particles along the Al6061 grain boundary is shown in Fig. 6a. Warcholinski et al. [35] reported that the uniform dispersion of the micro and macroparticles will improve the surface quality and reduce the wear rate. The particle deformation occurring on the aluminium grain is limited by LaPO<sub>4</sub>. Upon closer inspection, many cracks seen on the aluminium grain boundary are formed during a uniaxial compression load applied during the composite manufacturing operation and also by thermal distortion. Adnan et al. [36] stated that the application of the uniaxial compression load at the time of fabrication will improve the UTS and the hard of the sample. Besides, the defects like voids will disappear and enhance the grain boundary diffusion and the load at the red hot condition will progress to have thermal distortion with surface microcracks. The increase in weight percentage of reinforcement results in particle clustering independent of the ultrasonic phase fabrication, and it is shown in Fig. 6b, c. Particle deformation occurs in the form of an intergranular and transgranular fracture mechanism. The bulk deformation of materials with the formation of the crater at the applying load condition infers the reinforcement soft nature and is shown in Fig. 6d.

### Density Functional Theory Study

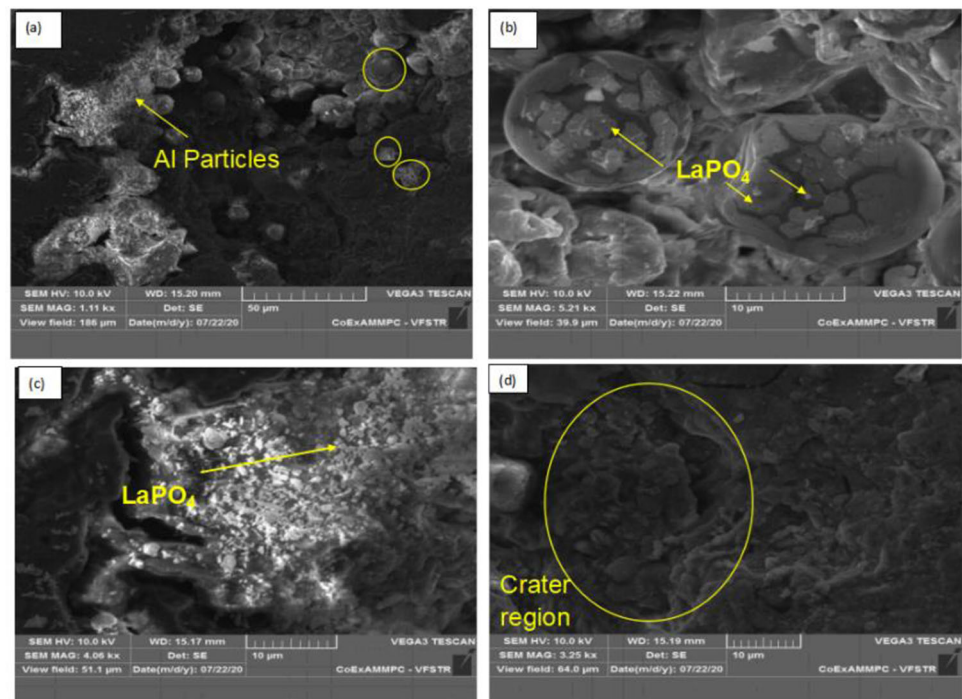
To understand the binding nature that exists between the elements, the density functionality theorem study is conducted. All the optimization is employed at the B3LYP/LANL2DZ [37] level in the gas phase. Initially, the aluminium clusters are prepared and optimized as stated by Frisch [38] using the Gaussian 09 suit. The surface of aluminium cluster is allowed to interact with LaPO<sub>4</sub>, and the complex is also optimized at the B3LYP level of theory. Figure 7a shows that the lanthanum and oxygen molecules interact with aluminium surface with strong to weak interaction. According to Warcholinski et al. [39], an increase in oxygen content will reduce the particle grain size and improve the surface texture. Metal–metal interaction is weak as compared to metal–oxygen interaction.



**Fig. 5** VHN of Al/x%LaPO<sub>4</sub>. **a** 5% of LAP, **b** 10% of LAP, **c** 15% of LAP, **d** 20% of LAP

**Fig. 6** Microstructure of the Al/x% LaPO<sub>4</sub> fracture surface.

**a** Uniform dispersion of LAP, **b** LaPO<sub>4</sub> resists dislocation, **c** agglomeration of LaPO<sub>4</sub> in the matrix, **d** bulk removal of LaPO<sub>4</sub>



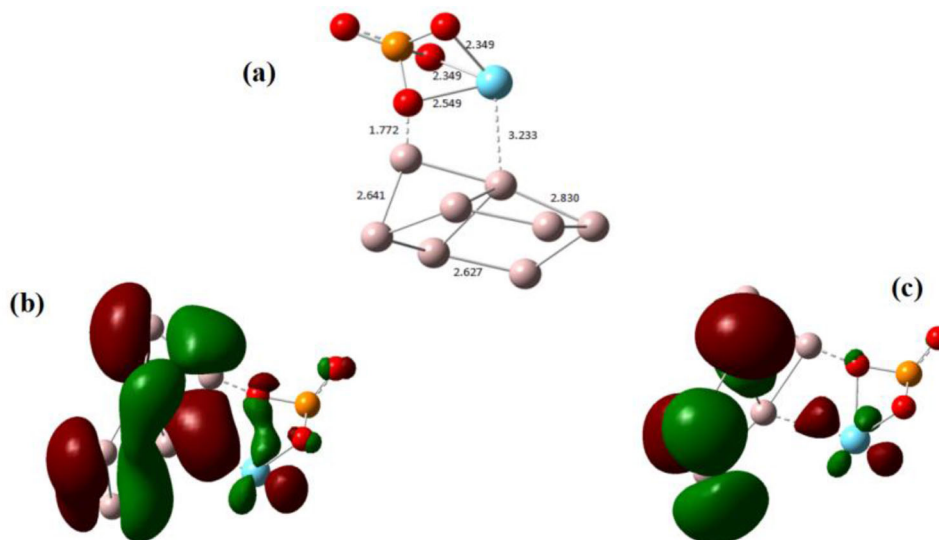
LaPO<sub>4</sub> has been observed to exist as a tetrahedral shape. The three oxygen of phosphorus (PO<sub>4</sub>) group strongly interacted and bonded with the lanthanum atom.

Figure 7a shows that there is no force of attraction that exists between the phosphorous and aluminium as well as lanthanum. Under the initial test load condition, the hydrogen bond between aluminium alloy and LaPO<sub>4</sub>, i.e.

metal–metal bond, has started to weaken and get separated. Upon increasing the load, the hydrogen bond between oxygen and aluminium starts to break. Hence, it can be stated that the sliding energy obtained due to the test load allows aluminium to deform rather than LaPO<sub>4</sub>.



**Fig. 7** **a** Optimized structure of Al/x%LaPO<sub>4</sub> complex at the B3LYP/LANL2DZ level in the gas phase and **b** frontier molecular orbital structure of Al/x%LaPO<sub>4</sub> complex employed at B3LYP/LANL2DZ level in the gas phase. **c** HOMO. (d) LUMO



The highest occupied molecular orbital and the lowest molecular orbital (HOMO–LUMO) pictures are depicted in Fig. 7b, c which shows that the electron localization. At HOMO, the electronic clouds are observed on the aluminium cluster and LaPO<sub>4</sub>. However, when shifting to the LUMO level, the electron clouds are localized on the aluminium cluster alone. The bandgap of HOMO–LUMO is 1.91 eV.

The presence of excess quantity of monazite LaPO<sub>4</sub> in the matrix causes deflection and a slip of particles at the time of test load conditions. Irrespective of the ultrasonication process, the clustering of nano-LaPO<sub>4</sub> cannot be avoided with the increase in reinforcements. However, the uniaxial compression load at the time of sample preparation greatly reduces the porous microstructure. Excellent bonding is obtained between the lanthanum, oxygen, phosphate and aluminium elements inside the matrix.

## Conclusions

By sol–gel process, nano-LaPO<sub>4</sub> powder with a size range from 50 to 80 nm is prepared and used as the reinforcement in the preparation of Al matrix composite with different weight per cents of 0–20 with an increment of 5%. Maximum tensile strength of 204 MPa with an increase of 31.7% is recorded for Al/15%LAP. Four strong bonds that exist between the aluminium–oxygen–LAP progress to have excess tensile strength. Further, it can be conveyed that the five weak bonds that exist within the LAP may lead to have early failure. This happens with the increment of LaPO<sub>4</sub> in the matrix. During the flexural test, the irregular shape LaPO<sub>4</sub> may resist the applied load and cause excellent displacement. The deformation of Al/LAP samples showed

at least 1 mm deformation at different work load conditions. A 31.7% increment in flexural property is observed on Al/15%LAP sample; this is because of the excellent bond and the LAP particle shape with the Al matrix. The highest observation on the compressive strength of 1078 MPa with an increase of 7.4% is reported for Al/15%LAP. Excess amount of availability of soft LaPO<sub>4</sub> ceramic elements may progress to sudden rupture. A gradual increment of 5% is observed with increase of LaPO<sub>4</sub> in the matrix. The compressive force applied at the fabrication of the composite improved the microstructural property of the composite. From the conducted test, it can be inferred that 15% of LaPO<sub>4</sub> in the Al6061 matrix is an adequate composition. The presence of transgranular and intergranular fracture on the test surface reveals that the introduction of LaPO<sub>4</sub> as reinforcements will create least machining defects. Further, through density functionality theory it can be stated that the deformation or the failure in the composite is mainly due to the metal to metal bond failure. The estimated energy of 1.91 eV is required to debond the elements that are present inside the Al/LAP composite.

**Funding** This work is partially supported by DST/TDT/DDP-38/2021, Device Development Programme (DDP), by the Department of Science and Technology (DST), Ministry of Science and Technology, Government of India.

## Declarations

**Conflict of interest** The authors declare that they have no conflict of interest.

## References

- M.O. Bodunrin, K.K. Alaneme, L.H. Chown, Aluminium matrix hybrid composites: a review of reinforcement philosophies; mechanical, corrosion, and tribological characteristics. *J. Mark. Res.* **4**(4), 434–445 (2015)
- S. Kumar, S.R. Hashmi, M.S.J., Metal matrix composite: a methodological review. *Adv. Mater. Process. Technol.* **6**(1), 13–24 (2020)
- D. Mummoorthi, M. Rajkumar, S. Kumar, G: Advancement and characterization of Al-Mg-Si alloy using reinforcing materials of Fe<sub>2</sub>O<sub>3</sub> and B<sub>4</sub>C composite produced by stir casting method. *J. Mech. Sci. Technol.* **33**(7), 3213–3222 (2019)
- G.V. Kumar, P.P. Panigrahy, S. Nithika, R. Pramod, C.S.P. Rao, Assessment of mechanical and tribological characteristics of Silicon Nitride reinforced aluminium metal matrix composites. *Compos. B Eng.* **175**, 107138 (2019)
- M. Bragaglia, R. Montanari, G. Montesperelli, Effect of Al<sub>2</sub>O<sub>3</sub> reinforcement and precipitates on corrosion behaviour of 2618 and 6061 aluminium MMCs. *Corros. Eng. Sci. Technol.* **54**(7), 601–613 (2019)
- C. Fenghong, C. Chang, W. Zhenyu, T. Muthuramalingam, G. Anbuhezhiyan, Effects of silicon carbide and tungsten carbide in aluminium metal matrix composites. *Silicon* **11**(6), 2625–2632 (2019). <https://doi.org/10.1007/s12633-018-0051-6>
- S.S. Murugan, V. Jegan, M. Velmurugan, Mechanical properties of SiC, Al<sub>2</sub>O<sub>3</sub> reinforced aluminium 6061-T6 hybrid matrix composite. *J. Inst. Eng. India Ser. D* **99**(1), 71–77 (2018). <https://doi.org/10.1007/s40033-017-0142-3>
- S. Sivananthan, V.R. Reddy, C.S.J. Samuel, Preparation and evaluation of mechanical properties of 6061Al-Al<sub>2</sub>O<sub>3</sub> metal matrix composites by stir casting process. *Mater. Today Proc.* **21**, 713–716 (2020)
- A.P. Reddy, P.V. Krishna, R.N. Rao, Tribological behaviour of Al6061–2SiC-xGr hybrid metal matrix nanocomposites fabricated through ultrasonically assisted stir casting technique. *Silicon* **11**(6), 2853–2871 (2019). <https://doi.org/10.1007/s12633-019-0072-9>
- B.F. Luan, N. Hansen, A. Godfrey, G.H. Wu, Q. Liu, High strength Al–Al<sub>2</sub>O<sub>3</sub>p composites: optimization of extrusion parameters. *Mater. Des.* **32**, 3810–3817 (2011)
- B.A. Kumar, N. Murugan, Metallurgical and mechanical characterization of stir cast AA6061-T6–AlNp composite. *Mater. Des.* **40**, 52–58 (2012)
- A.O. Inegbenebor, C.A. Bolu, P.O. Babalola, A.I. Inegbenebor, O.S.I. Fayomi, Aluminium silicon carbide particulate metal matrix composite development via stir casting processing. *Silicon* **10**(2), 343–347 (2018)
- C.S. Kalra, V. Kumar, A. Manna, The wear behavior of Al/(Al<sub>2</sub>O<sub>3</sub>+ SiC+ C) hybrid composites fabricated stir casting assisted squeeze. *Part. Sci. Technol.* **37**(3), 303–313 (2019)
- DG Eskin Basics of solidification processing of metallic alloys. In: Solidification processing of metallic alloys under external fields (Springer Cham, 2018) pp 1–17. [https://doi.org/10.1007/978-3-319-94842-3\\_1](https://doi.org/10.1007/978-3-319-94842-3_1)
- P. Madhukar, N. Selvaraj, C.S.P. Rao, G.V. Kumar, Fabrication and characterization two step stir casting with ultrasonic assisted novel AA7150-hBN nanocomposites. *J. Alloy. Compd.* **815**, 152464 (2020)
- A.H. Idrisi, A.H.I. Mourad, Conventional stir casting versus ultrasonic assisted stir casting process: Mechanical and physical characteristics of AMCs. *J. Alloy. Compd.* **805**, 502–508 (2019). <https://doi.org/10.1016/j.jallcom.2019.07.076>
- P. Greil, Generic principles of crack-healing ceramics. *J. Adv. Ceram.* **1**(4), 249–267 (2012)
- S.S. Sujith, S.A. Kumar, R.V. Mangalaraja, A.P. Mohamed, S. Ananthakumar, Porous to dense LaPO<sub>4</sub> sintered ceramics for advanced refractories. *Ceram. Int.* **40**(9), 15121–15129 (2014). <https://doi.org/10.1016/j.ceramint.2014.06.125>
- K. Rajesh, K.V. Baiju, M. Jayasankar, K.G.K. Warriar, A facile aqueous sol–gel process for the synthesis of alumina–lanthanum phosphate nanocomposite. *J. Am. Ceram. Soc.* **91**(7), 2415–2418 (2018). <https://doi.org/10.1111/j.1551-2916.2008.02453.x>
- L.P. Mezentseva, A.V. Osipov, A.A. Akatov, V.A. Doil'nitsyn, K.E. Pugachev, L.A. Koptelova, Ceramic matrix composites based on lanthanum orthophosphate for disposal of high-level radioactive waste. *Glass Phy. Chem.* **45**(6), 565–572 (2019)
- L.P. Mezentseva, A.V. Osipov, V.L. Ugolkov, A.A. Akatov, L.A. Koptelova, Ceramic composite matrices based on the LaPO<sub>4</sub>–ZrO<sub>2</sub> system: preparation and properties. *Glass Phys. Chem.* **47**(6), 665–670 (2021)
- Y. Yang, D.R. Mumm, M.L. Mecartney, Flash sintering produces eutectic microstructures in Al<sub>2</sub>O<sub>3</sub>–LaPO<sub>4</sub> versus conventional microstructures in 8YSZ–LaPO<sub>4</sub>. *J. Am. Ceram. Soc.* **104**(8), 3895–3909 (2021)
- M.A. Majeed, L. Vijayaraghavan, S.K. Malhotra, R. Krishnamurthy, Ultrasonic machining of Al<sub>2</sub>O<sub>3</sub>/LaPO<sub>4</sub> composites. *Int. J. Mach. Tools Manuf.* **48**(1), 40–46 (2008)
- T. Deepthi, K. Balamurugan, P. Balamurugan, Parametric studies of abrasive waterjet machining parameters on Al/LaPO<sub>4</sub> using response surface method. *IOP Conf. Ser. Mater. Sci. Eng.* **988**(1), 012018 (2020). <https://doi.org/10.1088/1757-899X/988/1/012018>
- M. Hedayatian, K. Vahedi, A. Nezamabadi, A. Momeni, Microstructural and mechanical behavior of Al6061-graphene oxide nanocomposites. *Met. Mater. Int.* **26**(6), 760–772 (2020). <https://doi.org/10.1007/s12540-019-00361-9>
- D. Errandonea, F.J. Manjon, Pressure effects on the structural and electronic properties of ABX<sub>4</sub> scintillating crystals. *Prog. Mater. Sci.* **53**(4), 711–773 (2008)
- R. Wang, W. Pan, J. Chen, M. Fang, J. Meng, Effect of LaPO<sub>4</sub> content on the microstructure and machinability of Al<sub>2</sub>O<sub>3</sub>/LaPO<sub>4</sub> composites. *Mater. Lett.* **57**(4), 822–827 (2002). [https://doi.org/10.1016/S0167-577X\(02\)00880-7](https://doi.org/10.1016/S0167-577X(02)00880-7)
- G.F. Aynalem, Processing methods and mechanical properties of aluminium matrix composites. *Adv. Mater. Sci. Eng.* (2020). <https://doi.org/10.1155/2020/3765791>
- J. Sha, S. Wang, J. Dai, Y. Zu, W. Li, R. Sha, High-temperature mechanical properties and their influence mechanisms of ZrC-modified C–SiC ceramic matrix composites up to 1600°C. *Materials* **13**(7), 1581–1589 (2020)
- A.C. Bhasha, K. Balamurugan, Fabrication and property evaluation of Al 6061 + x% (RHA + TiC) hybrid metal matrix composite. *SN Appl. Sci.* **1**(9), 977 (2019)
- M. Imran, A.A. Khan, Characterization of Al-7075 metal matrix composites: a review. *J. Mark. Res.* **8**(3), 3347–3356 (2019)
- K. Balamurugan, M. Uthayakumar, S. Sankar, U.S. Hareesh, K.G.K. Warriar, Predicting correlations in abrasive waterjet cutting parameters of Lanthanum phosphate/Yttria composite by response surface methodology. *Measurement* **131**, 309–318 (2019)
- K. Balamurugan, M. Uthayakumar, S. Sankar, U.S. Hareesh, K.G.K. Warriar, Modeling and surface texturing on surface roughness in machining LaPO<sub>4</sub>–Y<sub>2</sub>O<sub>3</sub> composite. *Mater. Manuf. Process.* **33**(4), 405–413 (2018)
- T. Deepthi, K. Balamurugan, Effect of Yttrium (20%) doping on mechanical properties of rare earth nano lanthanum phosphate (LaPO<sub>4</sub>) synthesized by aqueous sol-gel process. *Ceram. Int.* **45**(15), 18229–18235 (2019)
- B. Warcholinski, A. Gilewicz, T.A. Kuznetsova, T.I. Zubar, S.A. Chizhik, S.O. Abetkovskaia, V. Lapitskaya, A: Mechanical

- properties of Mo (C) N coatings deposited using cathodic arc evaporation. *Surf. Coat. Technol.* **319**, 117–128 (2017)
36. F. Adnan, Z. Sajuri, A.H. Baghdadi, M.Z. Omar, Effects of rapid heating and uniaxial loading on the phase transformation and mechanical properties of direct partial remelted butt joint of AISI D2 tool steel. *Mater. Sci. Eng. A* **797**, 140250 (2017)
37. A.D. Becke, Perspective: fifty years of density-functional theory in chemical physics. *J. Chem. Phys.* **140**(18), 18A301 (2014)
38. A. Frisch, *Gaussian 09W reference* (Wallingford, USA, 2009), p. 25
39. B. Warcholinski, A. Gilewicz, O. Lupicka, A.S. Kuprin, G.N. Tolmachova, V.D. Ovcharenko, T.A. Kuznetsova, Structure of CrON coatings formed in vacuum arc plasma fluxes. *Surf. Coat. Technol.* **309**, 920–930 (2017)

**Publisher's Note** Springer Nature remains neutral with regard to jurisdictional claims in published maps and institutional affiliations.

## Research Article

# Metaheuristic Load-Balancing-Based Clustering Technique in Wireless Sensor Networks

Sandip K. Chaurasiya,<sup>1</sup> Arindam Biswas ,<sup>2</sup> Prasit Kumar Bandyopadhyay,<sup>3</sup> Amit Banerjee ,<sup>4</sup> and Rajib Banerjee<sup>5</sup>

<sup>1</sup>University of Petroleum & Energy Studies (UPES), Department of Cybernetics, School of Computer Science, Energy Acres Building Bidholi, Dehradun-248007, Uttarakhand, India

<sup>2</sup>School of Mines, Kazi Nazrul University, Asansol, West Bengal, India

<sup>3</sup>Department of Electronics & Communication Engineering, School of Engineering, Sister Nivedita University, DG 1/2, New Town, Action Area 1, Kolkata, West Bengal, India

<sup>4</sup>Physics Department, Bidhan Chandra College, Asansol, 713303 West Bengal, India

<sup>5</sup>Department of Electronics & Communication Engineering, Dr. B. C. Roy Engineering College, Durgapur, West Bengal, India

Correspondence should be addressed to Arindam Biswas; [mailarindambiswas@yahoo.co.in](mailto:mailarindambiswas@yahoo.co.in) and Amit Banerjee; [amitbanerjee.nus@gmail.com](mailto:amitbanerjee.nus@gmail.com)

Received 11 August 2021; Accepted 6 December 2021; Published 21 January 2022

Academic Editor: Rajesh Kaluri

Copyright © 2022 Sandip K. Chaurasiya et al. This is an open access article distributed under the Creative Commons Attribution License, which permits unrestricted use, distribution, and reproduction in any medium, provided the original work is properly cited.

The resource-constrained nature of wireless sensor networks engenders the development of energy-efficient network operations. To mitigate the prime concern of developing an energy-efficient network, clustering of the nodes has emerged as a very effective tool. If executed intelligently, clustering can not only help in obtaining even load distribution among the network nodes but also help in having the enhanced network lifetime and scalability. In this work, a Metaheuristic Load-Balancing-Based Clustering Technique (MLBCT) in wireless sensor networks has been proposed which formulates the energy-balanced clusters based on the differential evolution technique to improve the network lifetime. To ensure the formation of balanced clusters, several metrics like nodes' proximity, nodes' distribution, and energy distribution across the sensing field have been considered. Moreover, to facilitate the even load distribution among the cluster members, a randomized rotation of cluster head is implemented. The supremacy of the proposed scheme is confirmed through an extensive set of simulations against the state-of-art schemes. Simulation results reflect an average gain of 51.85% in network lifetime under the variable network configurations in an ideal environment. Moreover, a thorough statistical analysis is performed to prove the efficacy of the proposed fitness function by obtaining confidence intervals under two different network scenarios with variable node counts.

## 1. Introduction

A wireless sensor network (WSN) comprises a large number of tiny devices capable of sensing the surrounding, processing the collected data as per the application, and communicating the processed field information to the centralized base station (BS) [1]. However, the sensor nodes deployed (either randomly or deterministically) in the sensing field suffer from several constraints. They are limited in processing abilities, storage abilities, power, and other allied restrictions [2]. Among all these restrictions, limited power is the most

severe one as the node drained of all the energy and frequent recharging and replacement cannot be facilitated, especially in remote applications of WSN like habitat monitoring, environmental monitoring, industrial monitoring, and military surveillance systems [3, 4].

Typically, transmission and route allocation consume most of the nodes' energy and are very much responsible for the power drainage of the sensor nodes. Thus, to solve this issue, energy-efficient network layer operations have been targeted by researchers for many years. Routing is the main functionality of the network layer, and hence,

designing an energy-efficient routing protocol is consistently captivating the attention of the community. To the aforementioned, clustering has evolved as a very significant tool that not only eases the task of routing and distributes the load evenly within a cluster but also, through the use of data aggregation, results in substantial saving of nodes' energy to be consumed in other significant network operations.

Clustering has been defined as the grouping of nodes based on some common attributes. In a clustering-based architecture, the network nodes are partitioned into some groups termed clusters. Within the cluster, a node is designated as cluster head (CH) which carries out more energy heavy tasks such as data aggregation and long-distance communication to the sink on behalf of the entire cluster. The rest of the nodes, called cluster members, perform the basic task of sensing and short-distance communication to the CH [5]. To effectively improve the WSN performance, balancing the clusters is a prerequisite. Thus, the formation of clusters in the WSN can be seen as an optimization problem involving multiple variables to be brought into consideration like nodes' proximity, nodes' residual energy, and size of the tentative clusters. The optimization problems can be classified into two major categories—*heuristic* and *metaheuristic*.

The primary motivation behind this work is to pursue the problem of clustering through metaheuristic algorithms. As mentioned above, since the formation of balanced clusters leading to the energy-efficient network operation requires the adequate consideration of various parameters such as nodes' proximity and cluster size, optimization techniques can help a lot in having a suitable solution. With the obtainment of balanced clusters and rotation of cluster head's role among the nodes over the network rounds, the foremost goal of network lifetime improvement can be achieved effectively. In this paper, a novel energy-efficient clustering protocol, *Metaheuristic Load-Balancing-Based Clustering Technique (MLBCT)*, is proposed for the wireless sensor networks based on the idea of differential evolution, a metaheuristic technique. The proposed scheme defines a suitable fitness function to formulate the balanced network partitioning. Once the clusters are finalized, the scheme freezes those and enables the CH-role rotation among the cluster members. To prove the scheme's efficacy, an extensive set of simulations demonstrate the showcasing of the improved network lifetime and network energy consumption.

*1.1. Major Contributions and Organization of the Paper.* The major contributions of the proposed MLBCT are as follows:

- (i) Design of an appropriate fitness function leading to
  - (a) balanced cluster formation
  - (b) reduced intracluster communication cost
- (ii) Development of a differential evolution-based energy-efficient clustering scheme on the basis of the devised fitness function
- (iii) Performance analysis of the proposed scheme, MLBCT

- (a) under varying network configurations to showcase its adaptability and scalability
- (b) with comparison to the state-of-art schemes in terms of network performance
- (c) with statistically justified results

The rest of the paper is organized into five descriptive sections. Section 2 outlines the literature review of the existing works in the same context to identify the technical gaps. Section 3 presents the adopted network model, an introductory discussion on differential evolution, and the terminology to be used throughout the work. Section 4 describes the proposed scheme detailing each of its constituent phases. Section 5 discusses the performance in detail to confirm the supremacy and efficacy of the MLBCT, and finally, Section 6 concludes the work by mentioning the future scope for the same.

## 2. Literature Review

As mentioned in Section 1, the optimization techniques can be majorly categorized as *heuristic* and *metaheuristic* schemes. *Heuristic* techniques utilize the complete set of particulars of a given problem and, being greedy in nature, generate solutions that might get trapped into local maxima/minima instead of producing the global maxima/minima.

On the other hand, *metaheuristic* techniques, also termed *guided random search* algorithms, are problem-independent, providing the optimal solution without getting stuck into the local maxima/minima. *Metaheuristic* algorithms compute the optimal solution by thoroughly exploring and exploiting the available search space in multiple iterations. The general working of the metaheuristic techniques is summarized in Figure 1.

The metaheuristic scheme starts working with a randomly selected set of solution vectors that improve over the iteration. Once the application-specific parameters such as scaling factor and crossover rate are defined, the fitness of the current solution set is evaluated through a carefully designed fitness function. Then, the counter which keeps track of the iterations is initialized. Afterward, a selection from the population chosen is made, and the selected vectors undergo a variation phase (*mutation/crossover*). Thus, updated vectors are again evaluated for their current fitness, and through a survivor function, a greedy selection strategy, the population for the next generation is finalized. The process of updating the set of solutions is repeated for a predefined number of iteration, and at last, the most recent population is selected as the final solution. An intelligently and carefully designed fitness function plays the most significant role in obtaining further improved offspring in metaheuristic techniques.

Here, we present a brief review of such schemes based on the approaches known as *heuristic* and *metaheuristic*.

*2.1. Heuristic Schemes.* In one work [6], the authors proposed the most popular clustering-based routing protocol, *Low-Energy Adaptive Clustering Hierarchy (LEACH)*, for the wireless sensor networks, which features a probabilistic



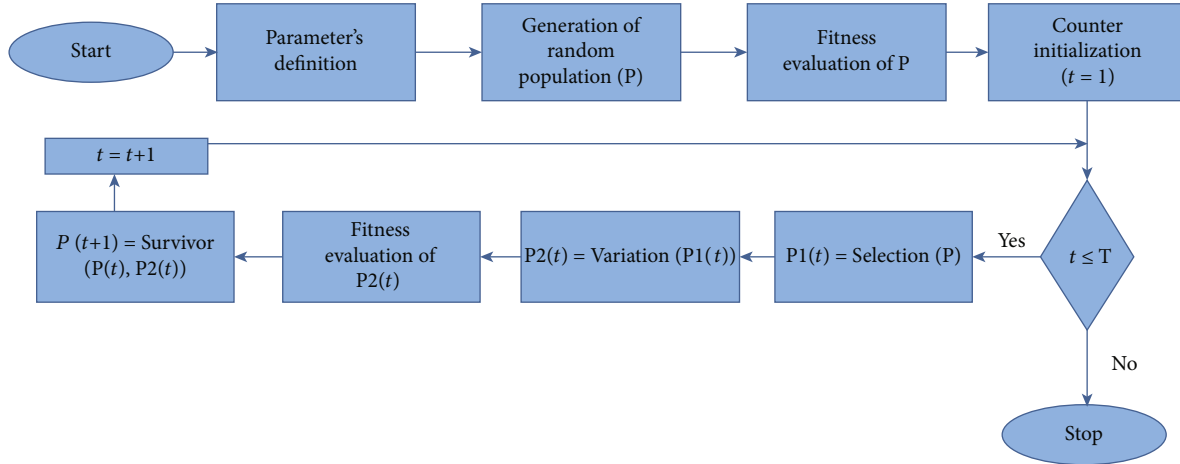


FIGURE 1: General scheme of metaheuristic techniques.

selection of cluster heads. It implements the localized coordination for various network operations and randomized rotation of the role of the cluster heads for load balancing among the nodes. However, since the selection of cluster heads does not count the residual energy of the nodes, nodes with low residual energy might suffer from early death if frequently selected as cluster heads.

In another work [7], the authors of the LEACH proposed an extension of the [6] requiring the nodes to send their location and energy status to the base station for the selection of cluster heads in a centralized manner and the formation of appropriate clusters via the application of simulated annealing algorithm.

The authors proposed a chain-based scheme in which, instead of forming multiple clusters [8], the nodes were provisioned to develop chains in a way that each sensor could exchange data with the neighbor nodes. At last, the chain leader concludes the entire data flow and forwards it to the base station. However, the scheme proved to be more energy-efficient than LEACH, but the significant delay in the delivery and dynamic topological adjustments appeared as the major issues of the scheme.

In [9], the authors proposed a static clustering scheme that eradicated the energy costing of the dynamic cluster formation in every round of the network operation as in LEACH, etc. In this scheme, distance-based clustering is executed via the base station. Once the clusters are decided, two important parameters—residual energy of the nodes and the nodes' spatial distribution—are considered to select cluster heads. However, the scheme only targeted energy consumption minimization.

In one scheme [10], the authors proposed a centralized scheme that treated coverage in the sensing field as equally important as the energy efficiency. The scheme starts with the distance-based clustering as in the [9]. It selects the cluster heads based on the weighted mean of the contribution factor of the nodes, where the contribution factor is defined as the ratio of the node's residual energy to that of the native grid in the sensing field. The main objective of the scheme is to assure network-wide coverage for the maximum network operation time.

In [11], the authors proposed a LEACH-based clustering protocol that mainly targets the energy efficiency and the fault tolerance in the network. To improve the network lifetime, the network nodes are provisioned to send their data to their respective cluster heads only when the current data is distinct from the previous data. At the end of every network round, noncluster head nodes forward their current energy status to the respective cluster heads to get classified as faulty (nodes with lower residual energy level) and live nodes (nodes with sufficient residual energy). The identification of faulty nodes facilitates the fault tolerance in the network.

In [12], the authors proposed a Fault-Tolerant Clustering-based Multipath algorithm (FTCM) to address the problems of energy efficiency and fault tolerance in the wireless sensor networks. The scheme calls the hybrid energy-efficient distributed clustering (HEED) [13] scheme to partition the network into an appropriate number of clusters. It also appoints a backup CH (BCH) for a cluster head to improve the fault tolerance. The BCH consistently monitors the performance of CH and keeps a copy of CH's data until delivered to the base station. In case of any mishap at the CH end, the BCH can instantly transmit data to the base station without asking the member nodes to send their data again. In addition to the regular responsibilities of CH, the CH is also responsible for the removal of the majority of faulty nodes via hypothesis testing and majority voting. The proposed scheme enables three paths to transfer data from the source node to the base station based on the parameters—residual energy of the nodes, number of hops, propagation speed, and path reliability.

In [14], the authors proposed a clustering-based Hierarchical Fault-Management Framework (HFMF) to address energy management and fault management jointly. For the minimization of energy consumption, the sleep/active method is used. For the management of faults, that is, faults' detection and recovery, backup CH (BCH) is appointed along with every CH to take care of acting CH in the event of its malfunctioning or failure. Later by measuring the data correlation among the cluster members, nodes are grouped virtually to further achieve the energy and fault



management. The authors have successfully demonstrated that the proposed scheme not only manages the transient faults, intermittent faults, and permanent hardware faults but also the link faults are detected.

*2.2. Metaheuristic Schemes.* A wide variety of metaheuristic techniques such as genetic algorithm (GA), genetic programming (GP), evolutionary programming (EP), evolution strategies (ES), differential evolution (DE), particle swarm optimization (PSO), ant colony optimization (ACO), and teaching-learning-based optimization (TLBO) exist in the literature. Such metaheuristic techniques with the virtue of being problem-independent have already imparted a lot in almost every field of engineering like [15]. In the context of wireless sensor networks, some contributions are noticed especially for the selection of cluster heads and the effective formulation of the clusters like in [16–25].

Due to its simplicity, robustness, and fast convergence, differential evolution has proved its worth over the algorithms like GA and PSO [26]. Several contributions have already been proposed based on this outstanding differential evolution technique in search of suitable clusters of the nodes in WSN. This subsection discusses some of the prime contributions in this regard as follows:

In one work [27], a differential evolution-based routing scheme, DE-LEACH, is proposed for environmental monitoring wireless sensor networks. DE-LEACH applies the fast and straightforward converging search technique of differential evolution to produce the clusters by considering the nodes' residual energy status and spatial distribution. The scheme consists of four phases: partitioning initial clusters, collecting status information of the nodes within the clusters through the auxiliary cluster heads, determining optimized cluster heads with differential evolution, and forming optimized clusters. The phases are to be executed in every round of the network operation. The scheme outperforms the traditional LEACH, and LEACH-C [7]. However, the nodes are burdened with heavy computational responsibilities.

In another work [28], a differential evolution-based clustering algorithm (DECA) is proposed, which provisions specialized nodes enriched with the additional amount of initial energy to act as cluster heads. These specialized nodes are called relay nodes or gateways. In DECA, besides providing a suitable fitness function (to measure the health of the tentative clusters), a new local improvement phase has also been proposed that carefully prevents early death of the gateways. DECA utilizes the DE/best/1/bin scheme for the differential evolution. In addition to a novel scheme for the vector representation, a fitness function is designed by considering the standard deviation of the lifetime of gateways and average cluster distance. The scheme outperforms the [29–31] traditional differential evolution and genetic algorithm-based scheme in terms of network lifetime; however, the scheme gives only a little attention to the cluster balancing via its local improvement phase.

A hybrid differential evolution and simulated annealing (DESA) scheme for the improvement of network lifetime in wireless sensor networks is proposed in [32]. The scheme utilizes a hybrid of differential evolution and simulated

annealing for local and global optimal solutions, respectively. There are four phases in the scheme—population vector initialization, mutation, crossover, and selection as in the traditional differential evolution. However, instead of using a random selection of population vectors, a more effective, “opposite point method” [33] technique is used for the initialization of population vectors. The mutation scheme is decided randomly at run time based on a chosen threshold value (here, it is 0.5) in such a way that a random number belonging to (0, 1) is observed, and if it is below the threshold, the mutation scheme is DE/rand/1; otherwise, it is DE/target – to – best/1. The fitness function is designed by considering the ratio of nodes' energy to that of the respective clusters. And for crossover, a blending rate based on Gaussian distribution is used. The scheme outperforms the traditional differential evolution scheme in terms of network lifetime, energy consumption, throughput, etc.; however, it converges slowly.

In [34], the authors proposed Multiobjective Load-Balancing Clustering (MLBC) which is a multiobjective optimization technique that addresses two significant problems in WSN—energy efficiency and reliability. It utilizes the Multiobjective Particle Swarm Optimization (MOPSO). MLBC targets energy efficiency by appropriately considering the average residual energy of the cluster heads and reliability by reducing the intercluster communication cost among the nodes in a cluster. It also provisions the load balancing via shuffling the roles of the next-hop node and CH in every iteration. However, it considers only the average residual energy of cluster heads in formulating the objective function for energy efficiency.

In a scheme [35], efficient energy consumption in wireless sensor networks using an improved differential evolution algorithm is highlighted. The scheme is an improvement of [28], in which the mutation strategy has been updated to accommodate the target vector along with the prior best and two random population vectors. Also, the fitness function has been upgraded to accommodate the total energy of the gateways and nodes in addition to the existing network lifetime standard deviation component. However, nothing has been mentioned concerning the load balancing among the clusters.

In one work [36], the authors proposed a hybrid metaheuristic clustering algorithm that exploits the best of Artificial Bee Colony and differential evolution optimization techniques. In their proposed Artificial Bee Colony (ABC) with differential evolution (DE) scheme, known as ABC-DE-based clustering scheme, the objective function is designed by taking into account the three network parameters—average intracluster distance, average energy of cluster heads, and data transmission delay to ensure the load-balanced cluster heads. In addition to this, an ABC-based metaheuristic algorithm has also been proposed to facilitate the dynamic repositioning of the mobile sink within the cluster-based network to achieve further energy efficiency.

In [37], the authors have addressed the problem of energy optimization in an Internet-of-Thing-based WSN (IoT-based WSN). In pursuance of the problem, as mentioned earlier, a hybrid of the Whale Optimization

Algorithm (WOA) and simulated annealing (SA) metaheuristic algorithms have been employed to select the most suitable cluster heads in their respective clusters. For choosing the most appropriate cluster heads, the fitness function of the proposed scheme considers a set of five node-specific parameters: residual energy, load, delay, distance, and temperature. The fitness function ensures that the node with the highest residual energy but the least load, delay, distance, and temperature is selected as the cluster heads in every network round.

In one work [38], the authors proposed an Artificial Intelligence- (AI-) based quorum system to address the issue of energy conservation in the wireless sensor networks. The primary motivation behind the proposed AI-based was to fasten the neighbor discovery process in order to minimize the network latency. Moreover, the scheme facilitates a quorum-based grid system that allows a substantial increase in the number of nodes in the quorum without mandating the increase in the number of quorums to reduce the effective network delay. In addition to the aforesaid, the feature of weighted load balancing reduces the network energy consumption to improve the network lifetime. Through the various experimentation, the authors have established the outperformance of their proposed scheme over the state-of-the-art quorum algorithms in terms of latency, improved coverage, energy efficiency, and network lifetime.

In [39], the authors proposed a genetic algorithm- (GA-) inspired clustering-based approach to address the problem of node's localization in wireless sensor networks. To find the accurate position of unknown nodes with respect to the anchors or known nodes, the authors used the Euclidean distance objective function in their proposed scheme. Through various simulation results, the supremacy of the GA-based localization scheme with an extended clustering approach has been established over the state-of-the-art schemes like Centroid and Distance Vector-Hop (DV-Hop) in terms of improved location accuracy.

In a scheme [40], the author proposed a genetic algorithm-based energy-efficient clustering scheme which addressed the localization problems in wireless sensor networks. The authors utilized parameters like node's residual energy, distance estimation, and coverage connection in the formulation of fitness function for their proposed scheme, Energy-Efficient Clustering in Genetic Algorithm Localization (EECGL). Through various experimentation, the authors have shown that EECGL approximates the unknown node's location with the least localization error and extends the effective network lifetime by minimizing the overall network energy consumption.

In a work [41], the authors proposed a metaheuristic energy-efficient clustering technique which is inspired by the Brain Storm Optimization (BSO). The BSO is a swarm-based metaheuristic technique exploiting the human brainstorming process in search of the best possible solutions. In their proposed scheme, Energy-Efficient Clustering-Brain Storm Optimization (EEC-BSO), the authors have focused on deciding energy-efficient clusters in a way that nonparticipating nodes in the information transmission process are sent to sleep mode minimizing the overall network

consumption. In the formulation of such clusters, the fitness function is designed by considering the parameters like node's residual energy, coverage, and packet data rate. Moreover, the outperformance of EEC-BSO has been established over the state-of-the-art schemes such as LEACH, LEACH-Centralized, Energy-Efficient Clustering Scheme (EECS), and LEACH-BSO in terms of reduced energy consumption, improved coverage, and data packet rate.

In a proposed scheme [42], a differential evolution-based clustering routing protocol (DEBCRP) for wireless sensor networks. DEBCRP is a base station-dependent scheme that applies DE/best/1/bin scheme for the network partitioning into some clusters. The fitness function devised by the authors considers the nodes' residual energies with respect to the probable cluster heads and the distance between the nodes and the cluster heads for the formulation of clusters. At last, to communicate the data from the sensing field to the base station, a PEGASIS [8] like a chain of the cluster heads is formed. The scheme DEBCRP is reported to outperform the S-DE [43] in terms of network lifetime. However, no adequate consideration is given for the formulation of load-balanced clusters, which is the most prime key to network lifetime improvement. Also, PEGASIS like chain of the cluster heads suffers from similar problems as in [8], for example, delayed communication, and since data from one CH is to be aggregated with that of the others in the direction to the sink, there might be introduced some inaccuracy in the information being sent to the base station.

From the aforementioned analysis, it can be easily concluded that despite being the most important factor for the formulation of clusters in the network, cluster balancing has been addressed the least. Thus, the work being presented here serves the following objectives:

- (i) Balanced cluster formulation to contribute effectively towards the enhancement of network lifetime
- (ii) Adaptable clustering solution to perform consistently well in any network configuration

### 3. Preliminaries

This section describes the network model for the scheme. In addition to this, it also discusses the basics of the differential evolution metaheuristic technique and the entire set of notations used throughout the work.

*3.1. Network Model.* MLBCT assumes the wireless sensor network with the following characteristics:

- (1) All the sensor nodes are deployed randomly across the sensing field and are static. More illustratively, nodes once deployed cannot change their location
- (2) The sensor nodes are homogeneous and equipped with a definite amount of initial energy
- (3) The sensor nodes are facilitated with the power control features to introduce variations in the transmission power as and when needed

- (4) The base station is also static and can be placed at any point in the network accordingly
- (5) The continuous data flow model is used here to define the working mode of the sensor nodes

**3.2. Differential Evolution: An Overview.** The differential evolution has evolved as a prevalent stochastic metaheuristic multimodal optimization technique over the continuous search space. Similar to the general scheme of metaheuristic techniques as discussed in Section 1, it starts with the definition of the initial parameters where the values of scaling factor and crossover rate are defined along with the randomized set of initial solutions (initial population) and the number of iterations. Here, each solution vector (equivalently known as chromosome or genome) termed as a target vector undergoes the mutation phase followed by the recombination. This mutation followed by the recombination is nothing but the variation phase of Figure 1. As depicted in Figure 2, the target vector, once it passes through the mutation phase, becomes the donor/mutant vector. After the recombination or crossover phase, the donor vector is known as the trial vector.

In the differential evolution scheme, obtainment of the next-generation solutions is performed only after the generation of all trail vectors when compared to particle swarm optimization, and teaching-learning-based optimization [44, 45]. In other words, the greedy selection towards the next-generation solution is performed between the pair of target and trial vectors once all the target vectors have been converted into trial vectors. A variety of mutation strategies exist, such as random, best, and target-to-best, along with the two types of crossover techniques—binomial and exponential crossovers. The binomial and exponential crossover can be defined as follows:

### 3.2.1. Binomial Crossover.

$$u_j = \begin{cases} v_j & \text{if } r \leq C_p \text{ OR } j = \delta, \\ x_j & \text{if } r > C_p \text{ AND } j \neq \delta, \end{cases} \quad (1)$$

where  $C_p$  is the crossover probability,  $\delta$  is the randomly selected variable location from the set  $\{1, 2, 3, \dots, |\text{decision variable}|\}$ ,  $r$  is the random number between 0 and 1,  $u_j$  refers to the  $j^{\text{th}}$  variable of the trial vector,  $v_j$  refers to the  $j^{\text{th}}$  variable of donor/mutant vector, and  $x_j$  refers to the  $j^{\text{th}}$  variable of the target vector.

**3.2.2. Exponential Crossover.** In the exponential crossover, at very first, the  $n^{\text{th}}$  variable from the donor vector is copied into the trial vector. Afterward, every subsequent variable from the donor vector is copied into the trial vector as long as the  $r < C_p$ . Once  $r > C_p$ , variables from the target vector are copied into the trial vector.

Based on the adapted mutation strategy and crossover type, various schemes have been proposed for differential evolution, and to discriminate among them, a standard notation, **DE/x/y/z**, is used. Here, **DE** refers to the differential evolution,

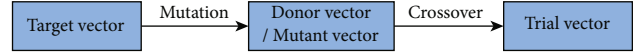


FIGURE 2: Vector transformation in differential evolution.

$\mathbf{x}$  denotes the mutation strategy,  $\mathbf{y}$  denotes the number of difference vectors to be used in the mutation operation, and  $\mathbf{z}$  refers to the crossover scheme selected. Some of the variants of the DE schemes are listed here in Table 1.

Here, in Table 1,  $V$  is the donor vector,  $F$  is the scaling factor such that  $F \in (0, 2)$ ,  $X_{\text{best}}$  is the target vector with best fitness value,  $X_i$  is the  $i^{\text{th}}$  target vector, and  $X_{r_j}$  is the  $j^{\text{th}}$  target vector chosen randomly where  $j \in [1, N]$ ,  $N$  being the number of target vectors in the population. Once the trail vectors are generated for all the target vectors of current generation, say  $G$ , offsprings are chosen based on the fitness value of the corresponding pairs of target and trial vectors, i.e.,  $\langle X_{i,G}, U_{i,G} \rangle$  for  $i \in [1, N]$  as follows:

$$X_{i,G+1} = \begin{cases} U_i & \text{if } \text{fitness}(U_{i,G}) \geq \text{fitness}(X_{i,G}), \\ X_i & \text{otherwise.} \end{cases} \quad (2)$$

**3.3. Terminology.** The notations used throughout the work have been listed as follows:

- (i)  $S$  denotes the set of sensor nodes such that  $S = \{s_1, s_2, s_3, \dots, s_N\}$  where  $N$  is the number of nodes deployed in the sensing field
- (ii)  $\Theta$  denotes the set of cluster heads such that  $\Theta = \{CH_1, CH_2, CH_3, \dots, CH_k\}$  where  $k$  is the number of cluster heads
- (iii)  $RE_i$  denotes the residual energy of the  $i^{\text{th}}$  node in the network
- (iv)  $\text{Cluster}_{RE}^i$  denotes the residual energy of the  $i^{\text{th}}$  cluster such that  $\text{Cluster}_{RE}^i = \sum_{j=1}^m RE_j$  where  $m$  refers to the cluster size
- (v)  $CS_i$  denotes the cluster size of the  $i^{\text{th}}$  cluster
- (vi)  $\text{AvgCS}$  refers to the average cluster size, i.e., average number of nodes in a cluster
- (vii)  $\text{ACE}$  refers to the average cluster energy such that  $\text{ACE} = \sum_{i=1}^N RE_i/k$
- (viii)  $d(i, j)$  denotes the Euclidean distance between the  $i^{\text{th}}$  and  $j^{\text{th}}$  nodes in the network
- (ix)  $\text{dist}_m(i, j)$  denotes the Euclidean distance between the  $i^{\text{th}}$  and  $j^{\text{th}}$  members of the  $m^{\text{th}}$  cluster. This parameter is basically used to measure the nodes' proximity
- (x)  $R_C$  denotes the communication range of the nodes
- (xi)  $\text{ComCH}(s_i)$  refers to the set of cluster heads within the communication range of the node  $s_i$ , i.e.,  $\text{ComCH}(s_i) = \{CH_j \mid d(s_i, CH_j) \leq R_C\}$

TABLE 1: Differential evolution schemes.

DE scheme	Mutation strategy	Mutation expression	Crossover type
DE/rand/1/bin	Random	$V = X_{r_1} + F(X_{r_2} - X_{r_3})$	Binomial
DE/rand/2/exp	Random	$V = X_{r_1} + F(X_{r_2} - X_{r_3}) + F(X_{r_4} - X_{r_5})$	Exponential
DE/best/1/bin	Best	$V = X_{\text{best}} + F(X_{r_1} - X_{r_2})$	Binomial
DE/best/2/bin	Best	$V = X_{\text{best}} + F(X_{r_1} - X_{r_2}) + F(X_{r_3} - X_{r_4})$	Binomial
DE/target-to-best/1/exp	Target-to-best	$V = X_i + F(X_{\text{best}} - X_i) + F(X_{r_1} - X_{r_2})$	Exponential
DE/target-to-best/2/exp	Target-to-best	$V = X_i + F(X_{\text{best}} - X_i) + F(X_{r_1} - X_{r_2}) + F(X_{r_3} - X_{r_4})$	Exponential

The main objective of the present work is to formulate the balanced clusters within the network for the even distribution of load among the nodes. To ensure this, it is attempted that the clusters are equipped with an almost similar count of member nodes situated close to one another. Also, the clusters are left with an approximately equal amount of residual energy at the end of every network round.

#### 4. Proposed Scheme: Metaheuristic Load-Balancing-Based Clustering Technique (MLBCT)

This section describes the proposed scheme, Metaheuristic Load-Balancing-Based Clustering Technique (MLBCT) in wireless sensor network. The MLBCT is a base station-(BS-) assisted scheme which calls the BS for the differential evolution-based cluster formation. Once the optimized and balanced clusters come into existence, it hands over the responsibility of further network operations to the network nodes.

The scheme starts with a bootstrapping phase in which all the nodes are assigned unique IDs, which in turn communicate their IDs and location information to the BS. The BS then applies the differential evolution with a well-established fitness function (detailed below) and formulates the balanced clusters. The selected cluster heads are then informed of their specific roles and their members' information by the base station. Thus, selected cluster heads then provide their IDs to the respective members along with the TDMA schedules. Afterward, the overall network operation is divided into rounds where each round consists of the steady-state phase and the responsible node selection phase. In the steady-state phase, cluster members send their data to their respective cluster heads, which aggregate the received data and forward it to the base station. In the responsible node selection phase, the current cluster head in a cluster, select a node randomly to act as head for the next round and broadcast into the concerned cluster. The entire workflow is summarized in Figure 3 and has been detailed into the subsequent subsections and algorithm as follows:

*4.1. Bootstrapping.* In bootstrapping, differential evolution is applied by the base station to divide the entire network into  $k$  number of balanced clusters where  $k$  is a user-defined

parameter. It starts with the sharing of node-specific information such as identity, residual energy, and location information to the base station by the nodes deployed. Based on the information received, BS performs the following to determine the required partitioning.

*4.1.1. Generation of the Random Population.* The population vectors are generated as per the [28]. Each population vector is chosen in such a way that it indicates the assignment of every network node to one of the cluster heads. The notation adopted to represent the  $i^{\text{th}}$  population vector of the  $G^{\text{th}}$  generation is as follows:

$$\vec{X}_{i,G} = [x_{1,i,G}, x_{2,i,G}, x_{3,i,G}, \dots, x_{N,i,G}], \quad (3)$$

where  $x_{1,i,G}, x_{2,i,G}, x_{3,i,G}, \dots, x_{N,i,G}$  are the random numbers between 0 and 1.  $x_{j,i,G}$  denotes the assignment of the node  $s_j$  to one of cluster heads, say  $k$ , as follows:

$$l = \text{ceiling}(x_{j,i,G} * |\text{ComCH}(s_j)|), \quad (4)$$

$$\text{CH}_k = \text{index}(\text{ComCH}(s_j), l). \quad (5)$$

Here, the length of the population vectors is definite and determined by the number of nodes deployed in the field.

Thus, corresponding to every population vector, say  $\vec{X}_{i,G} = [x_{1,i,G}, x_{2,i,G}, x_{3,i,G}, \dots, x_{N,i,G}]$ , we have another vector, say  $\vec{Y}_{i,G} = [y_{1,i,G}, y_{2,i,G}, y_{3,i,G}, \dots, y_{N,i,G}]$  such that

$$f(x_{j,i,G}) = y_{k,i,G}, \quad (6)$$

where  $y_k \in \Theta$  is assigned to the node  $x_j$  in the  $i^{\text{th}}$  vector of  $G^{\text{th}}$  generation as per equations (4) and (5).

*4.1.2. Fitness Function.* It can be easily intuited that if the clusters are balanced in the clustered network architecture, they might have an almost similar level of residual energy and a similar count of member nodes. With this conception, to meet our primary objective of network partitioning into some balanced clusters, nodes' residual energy and cluster size have been taken as the decision parameters. In addition to this, nodes' proximity has also been taken into account, ensuring the reduced energy consumption in intracommunication.



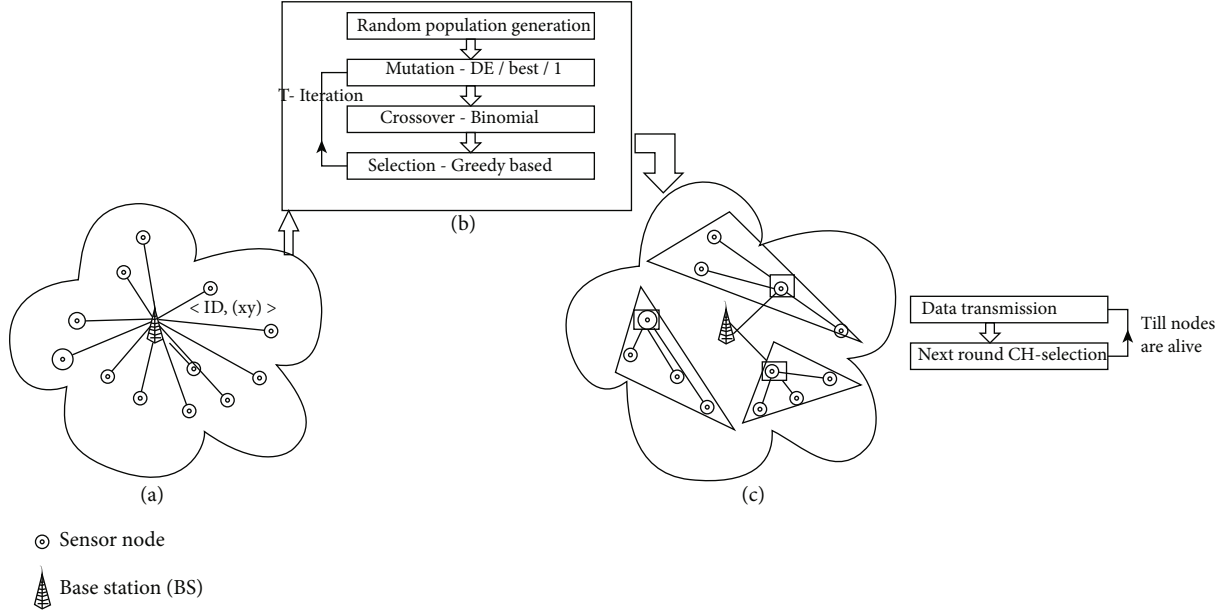


FIGURE 3: MLBCT: operation.

A suitable fitness function always contributes the most to the differential evolution to converge. Thus, the fitness function has been derived in such a way that it characterizes all the aforementioned requirements as follows:

(i) Standard deviation of average cluster energy

If the clusters have been formed in an optimized way, ensuring the entire network energy is distributed evenly across the clusters formed in the network, each cluster is supposed to have an almost similar level of residual energy. In other words, it can be said that in terms of average cluster energy (ACE), each cluster should have the approximately same amount of energy, and hence, the standard deviation accords to the following:

$$\sigma_{CE} = \sqrt{\frac{1}{k} * \sum_{i=1}^k (ACE - \text{Cluster}_{RE}^i)^2}, \quad (7)$$

where  $k$  is the number of clusters. It is quite obvious that the lower the value of  $\sigma_{CE}$ , the higher the value of fitness, i.e.,

$$\text{Fitness Value} \propto \frac{1}{\sigma_{CE}}. \quad (8)$$

(ii) Standard deviation of average cluster size

The balanced clusters must have an approximately equal number of members. In other words, it can be said that the average cluster size (AvgCS) of each cluster should have the almost same count of cluster members.

With this, the standard deviation and the fitness value accord to equations (9) and (10), respectively.

$$\sigma_{CS} = \sqrt{\frac{1}{k} * \sum_{i=1}^k (\text{AvgCS} - CS_i)^2}, \quad (9)$$

where  $k$  is the number of clusters. It can be intuited again that the lower the value of  $\sigma_{CS}$ , the higher the value of fitness, i.e.,

$$\text{Fitness Value} \propto \frac{1}{\sigma_{CS}}. \quad (10)$$

(iii) Nodes' proximity within the cluster

This is the metric that ensures that when there comes to decide on the nodes to be a part of a cluster, the one who is located at a shorter distance from the other members gets priority. The central idea behind having this metric is to reduce the cost of communication within the cluster. The lower the value of this metric, the higher the value of fitness. More illustratively,

$$\text{Fitness Value} \propto \frac{1}{\sum_{m=1}^k \text{dist}_m(i, j)}. \quad (11)$$

From equations (8), (10), and (11), we can have the following:

$$\text{Fitness Value} \propto \frac{1}{\sigma_{CE}} * \frac{1}{\sigma_{CS}} * \frac{1}{\sum_{m=1}^k \text{dist}_m(i, j)}, \quad (12)$$

i.e.,

$$\text{Fitness Value} = \frac{K}{\sigma_{\text{CE}} * \sigma_{\text{CS}} * \sum_{m=1}^k \text{dist}_m(i, j)}, \quad (13)$$

where “ $K$ ” is proportionality constant which can be set as  $K = 1$  without loss of generality.

And, hence,

$$\text{Fitness Value} = \frac{1}{\sqrt{1/k * \sum_{i=1}^k (\text{ACE} - \text{Cluster}_{\text{RE}}^i)^2} * \sqrt{1/k * \sum_{i=1}^k (\text{AvgCS} - \text{CS}_i)^2} * \sum_{m=1}^k \text{dist}_m(i, j)} \quad (14)$$

or

$$\text{Fitness Value} = \frac{k}{\sqrt{\sum_{i=1}^k (\text{ACE} - \text{Cluster}_{\text{RE}}^i)^2} * \sqrt{\sum_{i=1}^k (\text{AvgCS} - \text{CS}_i)^2} * \sum_{m=1}^k \text{dist}_m(i, j)}. \quad (15)$$

**4.1.3. Mutation Strategy.** Like in [28, 42], **DE/best/1/bin** scheme is adapted here in this work which refers to the application of the **DE/best/1** mutation strategy. As depicted in Figure 2, each target vector of the population (say, of the size  $P$ ) will go through this scheme to get transformed into a donor vector. From Table 1, the mutation expression for the selected strategy is

$$\vec{V}_{i,G} = \vec{X}_{\text{best},G} + F(\vec{X}_{r_1,G} - \vec{X}_{r_2,G}), \quad (16)$$

where  $\vec{X}_{\text{best},G}$  and  $\vec{X}_{r_1,G}$ ,  $\vec{X}_{r_2,G}$  refer to the best vector, and any two randomly selected vectors from the  $G^{\text{th}}$  generation of the population such that  $i$ ,  $r_1$ , and  $r_2$  are the three random integers  $\in [1, P]$  and  $i \neq r_1 \neq r_2$ , respectively.  $F$  is the scaling factor that may have any value between  $(0, 2)$ .

From equation (3), it is quite obvious that the components of the vectors in equation (16)— $\vec{X}_{\text{best},G}$ ,  $\vec{X}_{r_1,G}$ , and  $\vec{X}_{r_2,G}$ —are the random values  $\in (0, 1)$ . In order to ensure that the components of the vector  $\vec{V}_{i,G}$  are also the values  $\in (0, 1)$ , a few amendments are being introduced as in [28].

Let

$$\vec{D}_{i,G} = \vec{X}_{r_1,G} - \vec{X}_{r_2,G}, \quad (17)$$

then,

$$d_{j,i,G} = \begin{cases} 1 + (x_{j,r_1,G} - x_{j,r_2,G}) & \text{if } (x_{j,r_1,G} - x_{j,r_2,G}) \leq 0, \\ (x_{j,r_1,G} - x_{j,r_2,G}), & \text{otherwise.} \end{cases} \quad (18)$$

Also, for the computation of  $v_{j,i,G}$  contributing to  $\vec{V}_{i,G}$ , the following can be referred to

$$v_{j,i,G} = \begin{cases} (x_{j,\text{best},G} + F * d_{j,i,G}) - 1, & \text{if } (x_{j,\text{best},G} + F * d_{j,i,G}) > 1, \\ x_{j,\text{best},G} + F * d_{j,i,G}, & \text{otherwise.} \end{cases} \quad (19)$$

**4.1.4. Crossover Scheme.** The crossover schemes in terms of the binomial and exponential crossover are already described in Section 3. A binomial crossover scheme is used in this work to convert the donor vector into the trial vector.

**4.1.5. Selection or Offspring Generation.** Once all the trial vectors are generated following the above-mentioned steps, the next generation can be obtained on basis of the comparison of fitness values of the corresponding pair of target and trial vectors as given in

$$\vec{X}_{i,G+1} = \begin{cases} \vec{U}_{i,G} & \text{if } \text{fitness}(\vec{U}_{i,G}) \geq \text{fitness}(\vec{X}_{i,G}), \\ \vec{X}_{i,G}, & \text{otherwise.} \end{cases} \quad (20)$$

**4.1.6. Complexity Analysis.** Throughout the proposed scheme, fitness function would be evaluated for  $N_p + N_p * T$  times where  $N_p$  refers to the size of population and  $T$  refers to the number of iterations known a priori.

Moreover, exploiting solution space in search of the most optimal solution is a continuous process in the meta-heuristic scheme. For this reason, even in the best case, the complexity of the fitness function will be  $O(n^2)$  as each newly generated solution has to be compared with its predecessor in terms of its fitness value. Similarly, complexity of the fitness function in the worst case will be  $O(n^2)$  due to successive fitness value computation and comparison. Thus, the average-case complexity for the fitness function can be concluded as  $O(n^2)$ .

As explained at the beginning of this section, once the clusters are formed, and members are notified of their respective initial heads, further network operations can be



divided into two rounds—the steady-state phase and the responsible node selection phase.

**4.2. Steady-State Phase.** This phase refers to the data transmission in which cluster members send their data to their respective cluster heads in the designated time slots. After receiving the data from its members, cluster heads aggregate the collected data and forward it to the base station on behalf of their entire cluster.

**4.3. Responsible Node Selection Phase.** After executing the steady-state phase, a cluster head in its respective cluster selects a node randomly as the head for the next round and communicates the same to its members. The members note the same and communicate their data to that newly selected cluster head in the upcoming round accordingly. The process is carried out in each of the clusters in the network.

## 5. Performance Analysis

This section deals with the various experimental processes conducted throughout the work and analyses the obtained results thoroughly.

**5.1. Experimental Environment.** In conducting the experiments, different network configurations with varying node densities have been examined. More illustratively, experiments have been performed with the different number of nodes, say 50, 100, 150, and 200 in an area of  $100 \times 100 \text{ m}^2$  with two different sink placements—one at the center of the sensing field (50 m, 50 m) and another beyond the network precisely at (50 m, 150 m). An instance of clustering with 50 nodes and 5 and 10 cluster heads, respectively, is demonstrated in Figure 4. The base station is situated at (50 m, 150 m) in this exemplary instance.

An extensive set of experiments have been performed for the proposed scheme using MATLAB.

Mainly, the experiments have been performed to

- (1) Prove the efficacy of the proposed fitness function

In this set of experiments, the proposed fitness function as in equation (15) has been tested for the quality of clusters being produced. It has been verified that the proposed fitness function yields balanced clusters in terms of cluster size. The clusters generated as per equation (15) have been compared with the clusters produced by the fitness function given in [42] under two different clustering scenarios. The network is divided into 5 clusters and 10 clusters, respectively.

- (2) Prove the supremacy of the proposed scheme, MLBCT in terms of network lifetime and network stability

In the second set of experiments, the performance of MLBCT is compared to that of DEBCRP [42] and improved differential evolution-LEACH (ImDE-LEACH) [46], majorly in terms of network lifetime and network stability with respect to the number of alive nodes in the network, network energy

consumption, average residual energy per network nodes over the network rounds, and data packets delivered to the base station under the variable network configurations. Moreover, for the sake of experimentation, the performance of the LEACH [6] has also been recorded into the same context as that of MLBCT, DEBCRP, and ImDE-LEACH.

**5.2. Simulation Parameters.** To compare the performance of the proposed scheme, MLBCT, with that of DEBCRP and ImDE-LEACH, simulation parameters have been adopted here as listed in Table 2. However, to prove the scalability and adaptability of the proposed scheme, the performance has also been tested under variable network configurations.

In addition to the parameters listed in Table 2, the following performance criteria have been used for the evaluation of schemes:

- (i) Network lifetime: the network lifetime is generally measured as the time when the first node dies, or when the last node dies in the network [28–31, 42]. In this work, both definitions have been considered to demonstrate the supremacy of the MLBCT over DEBCRP, and ImDE-LEACH
- (ii) Network stability: network stability refers to how smoothly the network operations are going on. It can be measured in terms of the rate of the network energy consumption and the average residual energy per network node. The lower the rate of energy consumption, the more stable the network is, resulting in improved network lifetime. Similarly, the higher the value of average residual energy per network node, the more stable and durable the network is

To further compare the performance of the schemes—MLBCT, DEBCRP, and ImDE-LEACH, packet delivery at the base station can also be considered as a criterion.

The success in this regard can be judged by the higher number of successfully delivered packets to the base station.

To find the energy consumption by the nodes in the network operation, the widely adopted first-order radio model [13, 28, 42, 46–52] has been used here in this work.

**5.3. Results and Discussion.** As stated in point 1 of Section 5.1, the suitability of the proposed fitness function equation (15) is manifested in the first set of experiments. Since the scheme is a metaheuristic one, a suitable fitness function might contribute a lot to decide the best possible clusters. The main objective of this work is to formulate the clusters which are balanced in the sense that the clusters are having an almost similar count of member nodes and the member nodes are located close to one another to have minimized intracluster communication.

In this experimentation, variable node counts as in Table 2 have been considered for two instances of clustering such as 5 clusters and 10 clusters as shown in Figure 5.

The success of the fitness proposal mentioned above is evident in Figure 5. When implemented in the scheme DEBCRP, the proposed fitness function has been found more effective in having more balanced clusters. In other

**Input:**

\* N: No. of randomly deployed sensor nodes.

\*  $ff^n()$ : Fitness function.

\* F: Mutation/Scaling factor.

\* T: No. of iteration

\* k: No. of user-specified clusters

\*  $C_r$ : Crossover rate

◇ BEGIN

%% BOOTSTRAPPING PHASE %%.

◇ for  $i \leftarrow 1$ : N

◇ Status Transmission( $Node_i \rightarrow BS$ )

◇ end for

◇ Random population generation (P) where each vector ( $X_i$ ) refers to the complete assignment of all the nodes to the  $k$  cluster heads

◇ for  $i \leftarrow 1$ : size(P)

◇  $ff^n(X_i)$

◇ end for

◇ for  $i \leftarrow 1$ : T

◇ for  $j \leftarrow 1$ : size(P)

◇  $V_j = X_{best} + F(X_{r_1} - X_{r_2})$

%%  $V_j$  is the  $j^{th}$  donor vector

◇  $U_j = [u_j^l]$  where  $u_j^l$  is the  $l^{th}$  component of  $U_j$  defined as follows:

$$u_j^l = \begin{cases} v_j^l & \text{if } r \leq C_r \text{ OR } l = \delta \\ x_j^l & \text{if } r > C_r \text{ AND } l \neq \delta \end{cases}$$

%%  $U_j$  is the  $j^{th}$  trial vector

◇ end for (inner loop)

◇ for  $j \leftarrow 1$ : size(P)

◇  $ff^n(U_j)$

%% i.e. fitness function evaluation of the  $j^{th}$  trial vector

◇ if ( $ff^n(U_j) > ff^n(X_j)$ )

◇ Update P

%% Greedy approach for the update of population vector

◇ end if

◇ end for (inner loop)

◇ end for (outer loop)

%% STEADY STATE PHASE %%

◇ while(nodes are alive)

◇ for  $i \leftarrow 1$ :

%% i.e. for every cluster

◇ for  $j \leftarrow 1$ :

%%  $m \rightarrow$  no. of members in the  $i^{th}$  cluster

◇ DataTransmission( $Node_j^i \rightarrow CH^i$ )

◇ end for (inner loop)

◇ DataTransmission( $CH^i \rightarrow BS$ )

%% here, aggregated data by the  $CH^i$  to the base station

◇ end for (outer loop)

%% RESPONSIBLE NODE SELECTION PHASE %%

◇ for  $i \leftarrow 1$ : k

◇ Random selection of  $CH_{next}^i$  from within the  $i^{th}$  cluster by  $CH^i$ .

◇ New CH's Information dissemination by the  $CH^i$

◇ end for

◇ end while

◇ END

ALGORITHM 1: MLBCT.

words, clusters are obtained with an approximately similar count of member nodes, leading to the even distribution of load throughout the network nodes. In Figure 5(a), the efficacy of the proposed scheme is demonstrated with five clus-

ters being formed in the network, whereas Figure 5(b) presents the same while partitioning the network into 10 clusters. It can be easily observed from the figure that the members recorded in the clusters do not vary to the extent

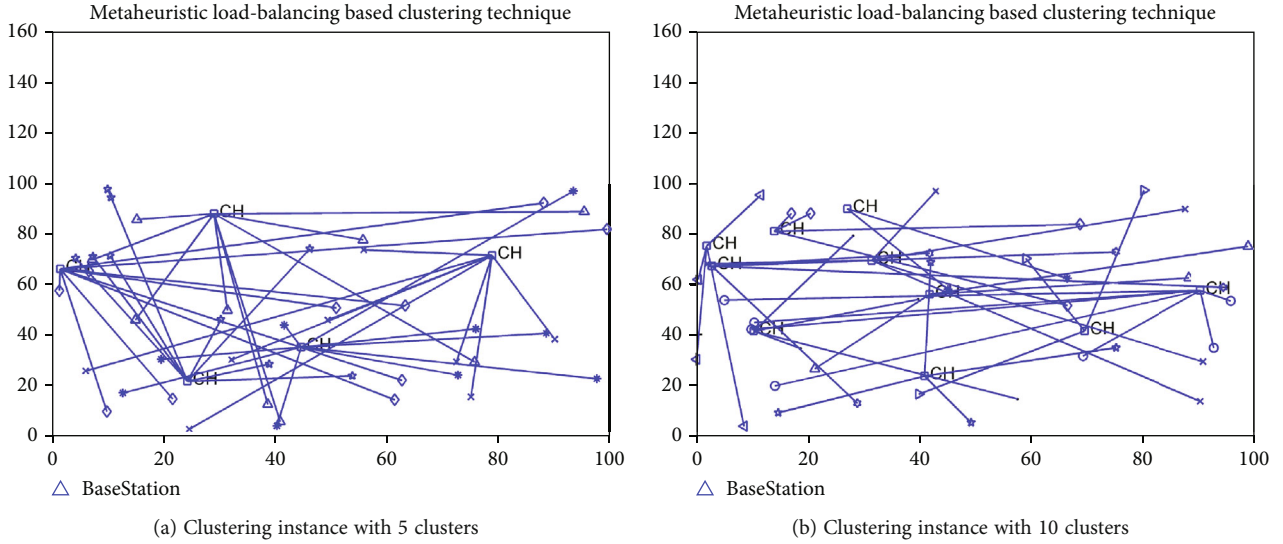


FIGURE 4: Simulation interface for network operation.

TABLE 2: Parameters used in the simulation.

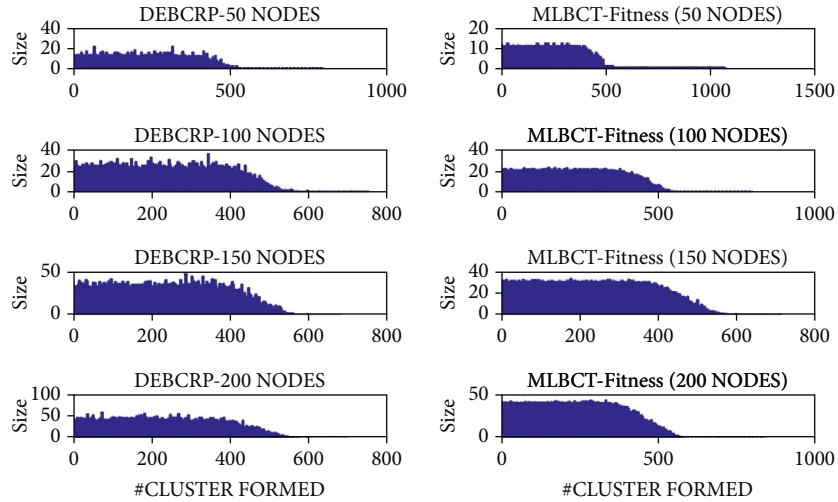
Parameter	Parameter's value
Network area	$100 \times 100 \text{ m}^2$
Base station's position	$\{(50 \text{ m}, 50 \text{ m}), (50 \text{ m}, 150 \text{ m})\}$
Node deployment strategy	Random deployment
Number of nodes deployed in the network	$\{50, 100, 150, 200\}$
Initial energy of the normal nodes	0.1 J
Size of data packet	4000 bits
Size of data packet header	200 bits
Energy consumed in data aggregation ( $\epsilon_{da}$ )	5 nJ/bits/signal
Energy consumed in the transceivers' circuitry ( $E_{elec}$ )	50 nJ/bit
Amplification factor in free space model ( $\epsilon_{fs}$ )	10 pJ/bit/m <sup>2</sup>
Amplification factor in multipath fading model ( $\epsilon_{mp}$ )	0.0013 pJ/bit/m <sup>4</sup>
Population size	10
Mutation factor	0.5
Crossover rate	0.7

as it is there in DEBCRP over the network rounds. Also, it has been verified that the scheme for the fitness evaluation of the clusters works invariably well irrespective of node density present in the network.

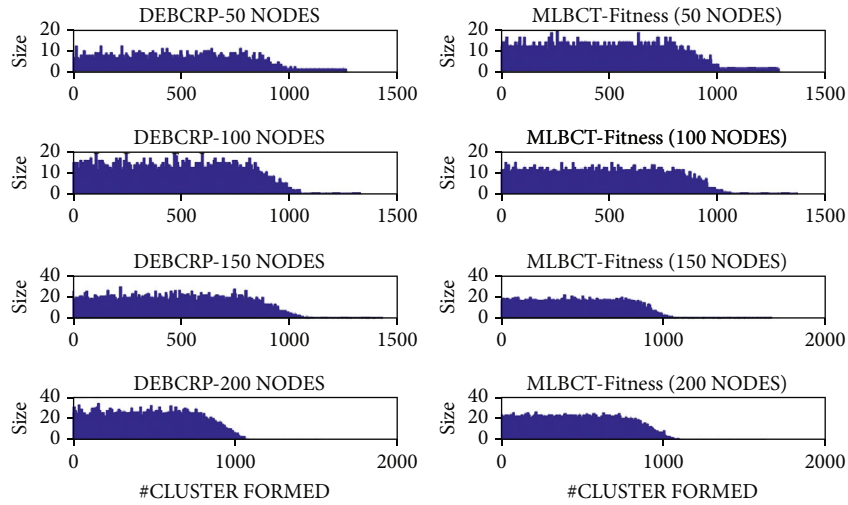
**5.3.1. Statistical Analysis.** Statistical analysis is performed to further explain the efficacy of the proposed fitness function (MLBCT-fitness) as in equation (15) in producing the balanced clusters. This is done by finding out the standard deviation of average cluster size,  $\sigma_{CS}$  following equation (9) along with the confidence interval. Standard deviation is defined as the measurement of how the clusters being produced deviate from the ideal distribution of the nodes among the specified number of clusters. The ideal distribution refers to the clusters with  $(N/k)$  nodes if  $N$  nodes are to be distributed among  $k$  clusters.

For this very purpose, as explained above, the proposed fitness function is fitted into the scheme of DEBCRP, and the performance of such a modified scheme is compared with that of DEBCRP with respect to the formation of clusters. This is achieved by recording the clusters' length in both cases until the first node dies. Afterward, standard deviations of the average cluster size are measured in both of the cases—with its own fitness function ( $\sigma_{D-Fitness}$ ) and MLBCT-fitness function ( $\sigma_{M-Fitness}$ ).

Figures 6(a) and 6(b) demonstrate the standard deviations of the average cluster size for the different network deployments with 50, 100, 150, and 200 nodes with the requirements mentioned above of having 5 clusters and 10 clusters, respectively. It can be explicitly observed that the standard deviations and the MLBCT-fitness function are quite low compared to the standard deviations obtained via



(a) Cluster formation with the 5 clusters



(b) Cluster formation with the 10 clusters

FIGURE 5: Efficacy of the proposed fitness function.

the application of the DEBCRP-fitness function for all the node deployments under both the specified requirements of 5 clusters and 10 clusters. This also justifies the efficacy of the scheme.

Another statistical analysis known as confidence interval justifies the probability of the deployment of the nodes within a range of the values of the cluster. In this case, the confidence intervals with the confidence levels 95% and 99%, respectively, are measured for both cases of the clustering scenarios with variable node counts. Table 3 clearly explains the efficacy of the MLBCT-fitness function over the fitness function used in DEBCRP in every possible network configuration. For example, when 100 nodes are deployed to be distributed among 5 clusters, ideally, each cluster should have 20 nodes. Here, the proposed fitness function ensures that each cluster has a node count in the range [18.8245, 21.1755] with 95% confidence and in the range [18.4526, 21.5474] with 99% confidence, whereas the fitness function of DEBCRP finds the same as in the ranges [15.2210, 24.7790] and [13.7093, 26.2907] with 95% and

99% confidences, respectively. It can be easily intuited that the node count in each cluster is much closer to the ideal node count (20 here) with the MLBCT-fitness function when compared to that with the DEBCRP-fitness function. The consistency of the MLBCT-fitness function in terms of balanced clusters' formation can be seen in Table 3.

**5.3.2. Experimental Analysis.** In this second set of experiments, as stated in point 2 of Section 5.1, MLBCT is compared to DEBCRP, ImDE-LEACH, and LEACH concerning the metrics—network lifetime, network energy consumption rate, and average residual energy per network node under two different network configurations, say WSN#1 and WSN#2. In WSN#1, the sink has been placed at the center of the  $100 \times 100 \text{ m}^2$  sensing field, precisely at (50 m, 50 m) whereas, in WSN#2, the sink is located outside the sensing field at (50 m, 150 m). Moreover, to validate the adaptability of the scheme, simulations have been conducted with variable node deployments, say with 50 nodes, 100 nodes, 150 nodes, and 200 nodes.

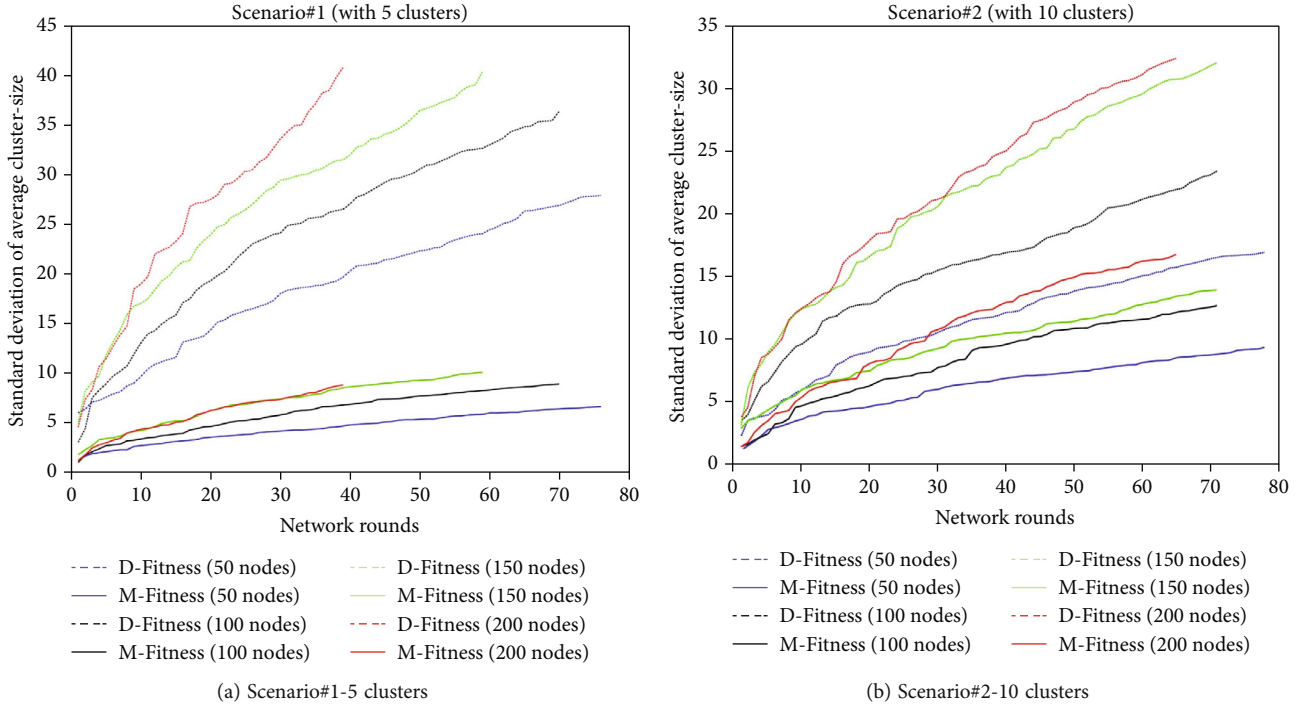


FIGURE 6: Standard deviation of average cluster size for the clusters formed over the network rounds.

TABLE 3: Mean of standard deviations and confidence intervals for the clusters generated.

Clustering scenario	#nodes	Mean $_{\sigma D-Fitness}$	Mean $_{\sigma M-Fitness}$	Interval estimate with 95% confidence		Interval estimate with 99% confidence	
				With <i>D</i> -fitness	With <i>M</i> -fitness	With <i>D</i> -fitness	With <i>M</i> -fitness
Scenario#1 (with 5 clusters)	50	18.9254	4.4628	[4.7541, 15.2459]	[8.7630, 11.2370]	[3.0947, 16.9053]	[8.3717, 11.6283]
	100	24.3826	5.9975	[15.2210, 24.7790]	[18.8245, 21.1755]	[13.7093, 26.2907]	[18.4526, 21.5474]
	150	27.1672	6.9578	[25.6523, 34.3477]	[28.8865, 31.1135]	[24.2771, 35.7229]	[28.5343, 31.4657]
	200	25.9534	5.7280	[36.4030, 43.5970]	[39.2061, 40.79939]	[35.2652, 44.7348]	[38.9550, 41.0450]
Scenario#2 (with 10 clusters)	50	11.6163	6.3429	[1.7801, 8.2199]	[3.2419, 6.7581]	[0.7616, 9.2384]	[2.6857, 7.3143]
	100	15.8541	8.4076	[6.8926, 13.1074]	[8.3521, 11.6479]	[5.9096, 14.0904]	[7.8308, 12.1692]
	150	21.6239	9.5944	[11.5395, 18.4605]	[13.4646, 16.5354]	[10.4448, 19.5552]	[12.9789, 17.0211]
	200	21.7987	10.7536	[16.9789, 23.0211]	[18.5096, 21.4904]	[16.0232, 23.9768]	[18.0382, 21.9618]

(1) *Network Lifetime*. As mentioned earlier in this section that the network lifetime can be defined as the time when the first node dies in the network or the time when the last node dies in the network. In Figures 7 and 8, both strategies have been followed separately.

Figures 7(a) and 7(b) describe the death of the first node that is FND (first node death) in the schemes MLBCT,

DEBCRP, ImDE-LEACH, and LEACH under the network scenarios WSN#1 and WSN#2.

In WSN#1 (Figure 7(a)), when the number of nodes deployed are 50, 100, 150, and 200, the events of the first node's death (FND) occur at the round no. 115, 106, 99, and 82 in the proposed scheme; at 84, 72, 63, and 49 in DEBCRP; at 76, 75, 68, and 58 in ImDE-LEACH; and 33, 36, 35, and 33 in LEACH, respectively. Similarly, in

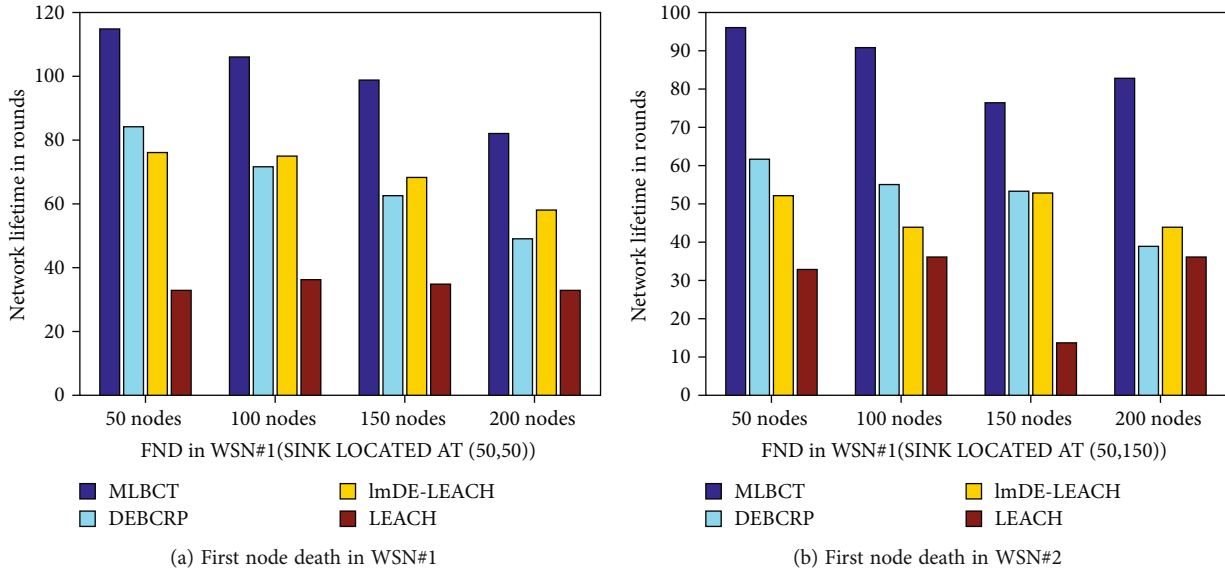


FIGURE 7: Network lifetime comparison in terms of FND.

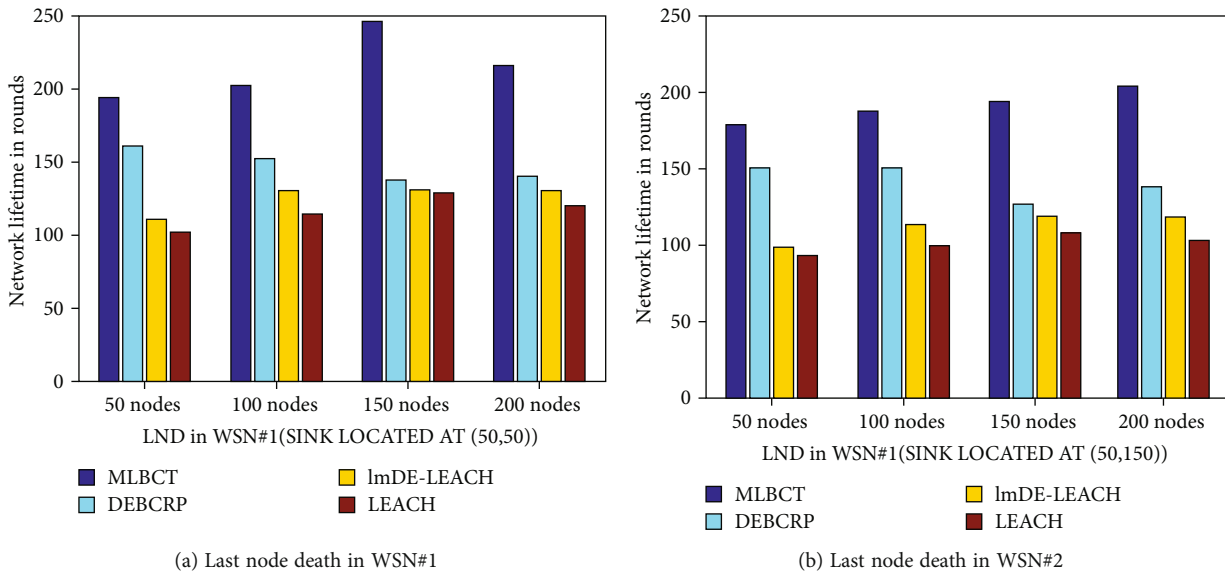


FIGURE 8: Network lifetime comparison in terms of LND.

WSN#2 (Figure 7(b)), FNDs occur at round no. 96, 91, 77, and 83 in MLBCT; at 62, 55, 53, and 59 in DEBCRP; at 52, 44, 53, and 44 in ImDE-LEACH; and at 33, 36, 14, and 36 in LEACH, respectively, for the aforementioned nodes' count.

On the other hand, if the network lifetime is taken as the time when the last node dies that is LND (last node death) in the network, Figures 7(a) and 7(b) describe the outcomes of experiments conducted in this regard with the variable number of nodes as above, say 50, 100, 150, and 200, respectively.

In WSN#1 (Figure 8(a)), the last node's death events occur at round no. 194, 202, 246, and 216 in the MLBCT; at 161, 152, 138, and 141 in DEBCRP; at 111, 131, 131,

and 130 in ImDE-LEACH; and at 102, 114, 129, and 119 in LEACH, respectively. Likewise, in WSN#2 (Figure 8(b)), LNDs occur at round no. 178, 187, 193, and 203 in MLBCT; at 150, 151, 126, and 138 in DEBCRP; at 98, 113, 119, and 118; and at 93, 99, 108, and 103 in LEACH, respectively, for the aforementioned nodes' count. The appreciable results due to FND and LND calculation state the supremacy of using the proposed MLBCT over other schemes.

Moreover, the comparative performance of the schemes MLBCT, DEBCRP, ImDE-LEACH, and LEACH with respect to the nodes' death rate can also be observed from Figure 9.

Figure 9(a) describes the performance of the MLBCT against that of DEBCRP, ImDE-LEACH, and LEACH in



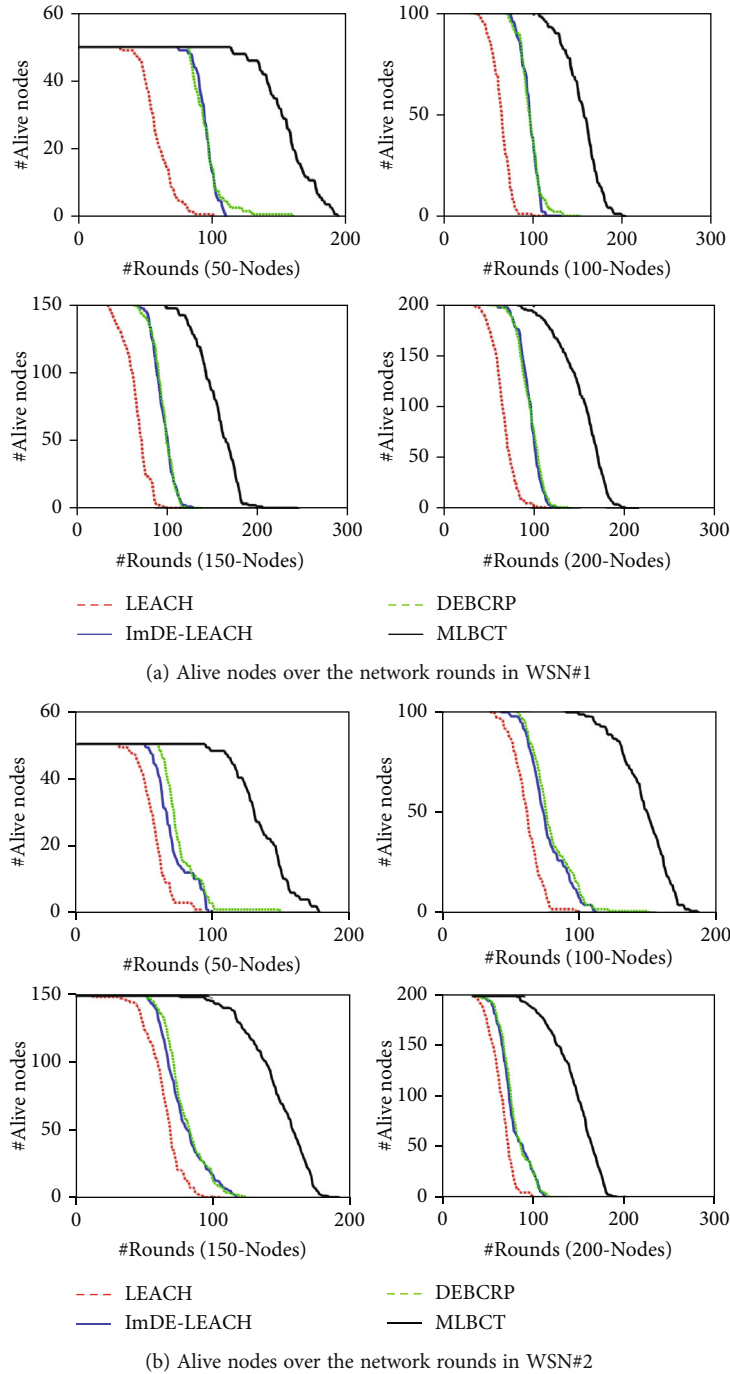


FIGURE 9: Network lifetime comparison in terms of alive nodes/round.

variable node population under the first network scenario WSN#1. Similarly, Figure 9(b) describes the same but for WSN#2. It is evident from Figure 9 that irrespective of the network configuration and nodes' population in the sensing field, MLBCT performs consistently well as the nodes' death rate is low in MLBCT, and hence, the number of alive nodes is high at any point of network operation in MLBCT when compared to DEBCRP, ImDE-LEACH, and LEACH. Thus, it can be concluded here

that the MLBCT outperforms DEBCRP, ImDE-LEACH, and LEACH in terms of the first performance criterion—network lifetime.

(2) *Network Energy Consumption.* From Figure 10, it can be concluded that at any point of the network operation, the energy consumption in MLBCT is less than that in DEBCRP, ImDE-LEACH, and LEACH in both of the scenarios implemented that is in WSN#1 (Figure 10(a)) and

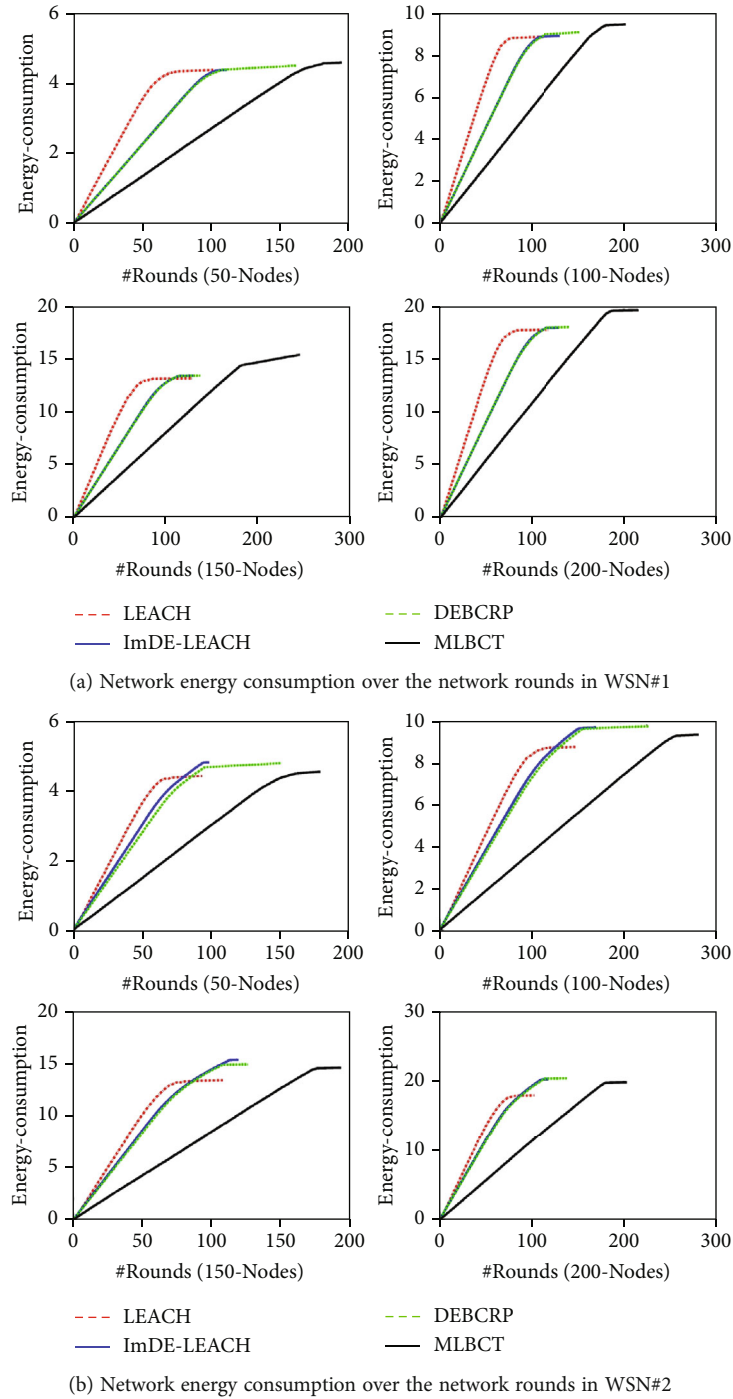


FIGURE 10: Comparison of network energy consumption over the network rounds.

WSN#2 (Figure 10(b)). Moreover, to demonstrate the consistency in the performance, variable counts of sensor nodes have been deployed here too.

(3) *Average Residual Energy/Node.* In this next set of experiments, the performance of MLBCT is measured in terms of the average residual energy that a network node has at any point in the network operation for the schemes DEBCRP,

ImDE-LEACH, and LEACH. It can be explicitly observed that the nodes are always equipped with a larger amount of residual energy if being operated with MLBCT in comparison to DEBCRP, ImDE-LEACH, and LEACH (Figure 11). It is noticed not only in WSN#1 (Figure 11(a)) but also in WSN#2 (Figure 11(b)); average residual energy for a network node is higher at any point in network operation if implemented with MLBCT.

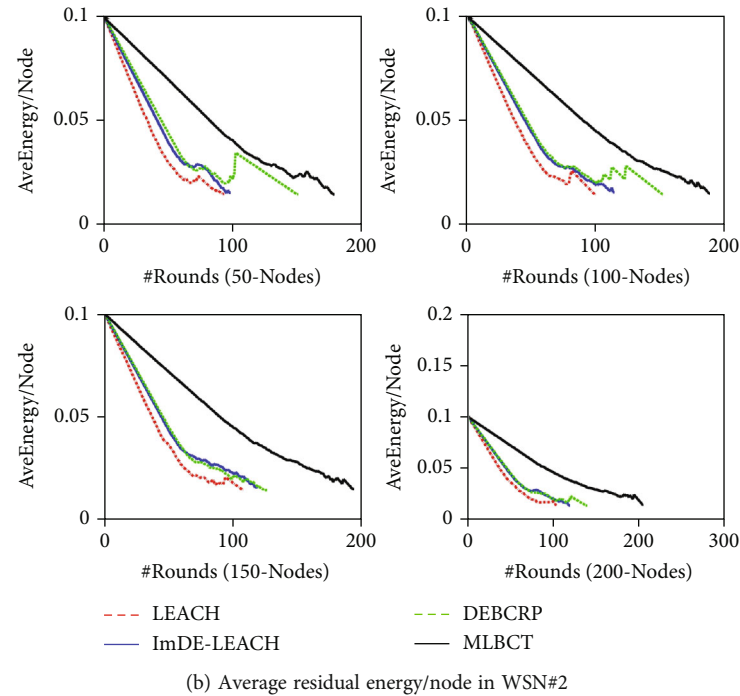
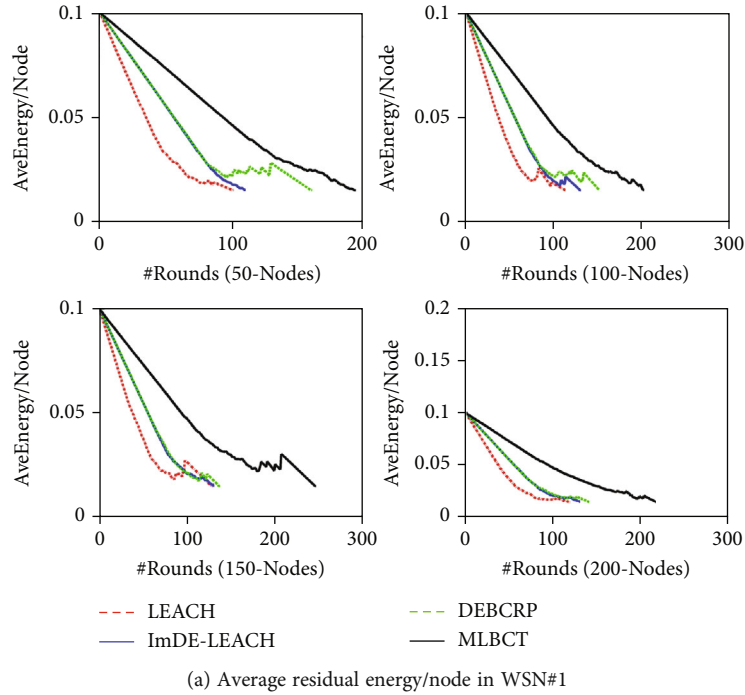


FIGURE 11: Comparison of average energy/node over the network rounds.

This depicts that a network utilizing MLBCT saves energy and keeps its resource intact for future usage, which is the desired criteria for sensor networks.

(4) *Data Packet Delivery at Base Station.* In the final set of experiments, the performance of MLBCT against the DEBCRP, ImDE-LEACH, and LEACH with respect to the number of data packets delivered to the base station is com-

pared. The predominance of the proposed scheme, MLBCT, can be read for both the network scenarios WSN#1 and WSN#2 in Figures 12(a) and 12(b), respectively. For the 50, 100, 150, and 200 nodes, MLBCT enriches the base station with 915, 969, 1221, and 1054 data packets, respectively. However, DEBCRP results into 800, 755, 685, and 700 data packets, ImDE-LEACH results into 550, 650, 650, and 645 data packets, and LEACH results into 416, 477, 533, and

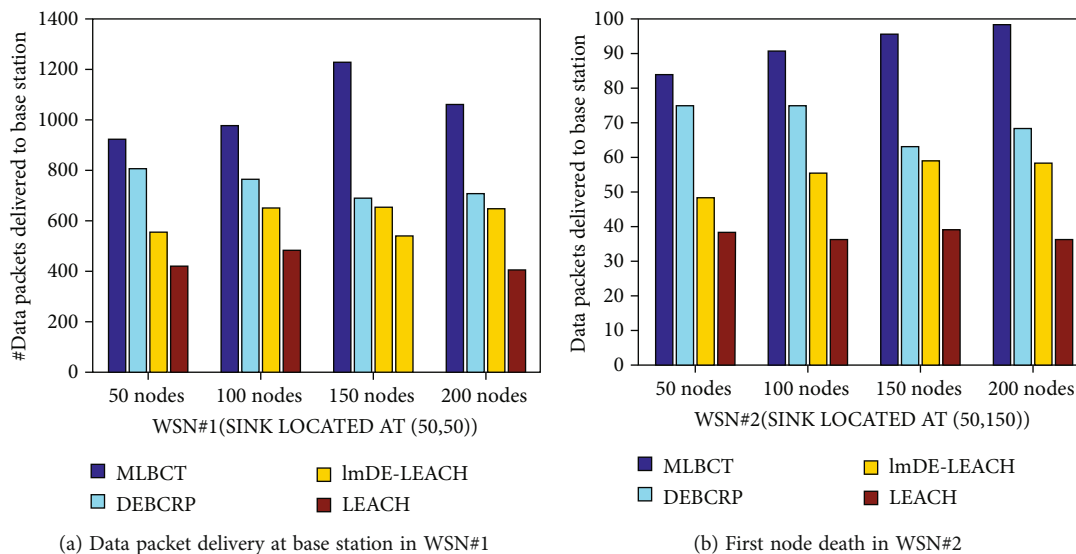


FIGURE 12: Data packet delivery at base station.

401 data packets, respectively, for the aforesaid network nodes into WSN#1. Similarly, for the WSN#2, in comparison to 745, 750, 625, and 685 data packets due to DEBCRP, 98, 113, 119, and 118 data packets through ImDE-LEACH, and 382, 360, 388, and 372 data packets via LEACH, MLBCT results into 838, 903, 950, and 983 data packets at the base station, respectively, for the node deployment mentioned above. This suggests that MLBCT successfully transmits more packets depicting its dominance in terms of successful transmission.

Based on the outcomes of the various simulations conducted so far, it can be concluded that the MLBCT outperforms the DEBCRP, ImDE-LEACH, and LEACH in terms of the chosen criteria of network lifetime, network stability, average residual energy, and data packet delivery.

## 6. Conclusion and Future Works

In this work, a Metaheuristic Load-Balancing-Based Clustering Technique has been proposed for wireless sensor networks. To achieve the prime objective of load-balanced clusters, a fitness function has been proposed that offers balanced clusters in terms of their size and energy and ensures the members to be in close proximity to one another reducing the cost of intracluster communication. Through an extensive set of simulations and experimentation, the supremacy of the proposed scheme MLBCT has been proved over the existing ones DEBCRP, and ImDE-LEACH in terms of improved network lifetime and network stability, average residual energy, and data packet delivery.

Statistical analysis also justifies and supports the feasibility of the scheme. Moreover, the scheme's adaptability and scalability have also been established by varying the network configuration with the different number of nodes and different placement of the base station.

As a future extension of this work, a heterogeneous wireless sensor network (HWSN) would be investigated to device

a clustering-based scheme induced by metaheuristic techniques to consistently contribute to the network operations without being affected by the heterogeneity present in the network.

## Data Availability

Extensive analysis, method, and result data has been fully provided.

## Conflicts of Interest

The authors declare that they have no competing interests.

## Acknowledgments

This work is partially supported by DST/TDT/DDP-38/2021, Device Development Programme (DDP), by the Department of Science & Technology (DST), Ministry of Science and Technology, Government of India.

## References

- [1] I. F. Akyildiz, Weilian Su, Y. Sankarasubramaniam, and E. Cayirci, "A survey on sensor networks," *IEEE Communication Magazine*, vol. 40, no. 8, pp. 102–114, 2002.
- [2] C. O. Iwendi and A. R. Allen, "Enhanced security technique for wireless sensor network nodes," in *IET Conference on Wireless Sensor Systems (WSS 2012)*, pp. 1–5, London, 2012.
- [3] A. Dumka, S. K. Chaurasiya, A. Biswas, and H. L. Mandoria, *A Complete Guide to Wireless Sensor Networks: From Inception to Current Trends*, CRC Press, Boca Raton, Florida, USA, 1st edition, 2019.
- [4] S. J. Ramson and D. J. Moni, "Applications of wireless sensor networks –survey," in *2017 International Conference on Innovations in Electrical, Electronics, Instrumentation and Media Technology (ICEEIMT)*, pp. 325–329, Coimbatore, India, 2017.

- [5] S. Ghiasi, A. Srivastava, X. Yang, and M. Sarrafzadeh, "Optimal energy aware clustering in sensor networks," *Sensors Journal*, vol. 2, no. 7, pp. 258–269, 2002.
- [6] W. R. Heinzelman, A. Chandrakasan, and H. Balkrishnan, "Energy-efficient communication protocol for wireless micro-sensor networks," in *Proceedings of 33rd Hawaii international conference on system science*, pp. 1–10, Maui, HI, USA, 2000.
- [7] W. R. Heinzelman, A. Chandrakasan, and H. Balkrishnan, "An application -specific protocol architecture for wireless micro-sensor networks," *IEEE Transactions on wireless communications*, vol. 1, no. 4, pp. 660–670, 2002.
- [8] S. Lindsey and C. S. Raghavendra, "PEGASIS: power-efficient gathering in sensor information systems," in *Proceedings, IEEE Aerospace Conference*, pp. 1125–1130, Big Sky, MT, USA, 2002.
- [9] S. K. Chaurasiya, T. Pal, and S. D. Bit, "An enhanced energy-efficient protocol with static clustering for WSN," in *The International Conference on Information Networking 2011 (ICOIN2011)*, pp. 58–63, Kuala Lumpur, Malaysia, 2011.
- [10] S. K. Chaurasiya, J. Sen, S. Chatterjee, and S. D. Bit, "EBLEC: an energy-balanced lifetime enhancing clustering for WSN," in *2012 14th International Conference on Advanced Communication Technology (ICACT)*, pp. 189–194, PyeongChang, Korea (South), 2012.
- [11] M. N. Cheraghloou and M. Haghparast, "A novel fault-tolerant leach clustering protocol for wireless sensor networks," *Journal of Circuits, Systems and Computers*, vol. 23, no. 3, article 1450041, 2014.
- [12] E. Moridi, M. Haghparast, M. Hosseinzadeh, and S. Jafarali Jassbi, "Novel fault-tolerant clustering-based multipath algorithm (FTCM) for wireless sensor networks," *Telecommunication Systems*, vol. 74, no. 4, pp. 411–424, 2020.
- [13] O. Younis and S. Fahmy, "HEED: a hybrid energy-efficient distributed clustering approach for ad hoc sensor networks," *IEEE Transaction on Mobile Computing*, vol. 3, no. 4, pp. 366–379, 2004.
- [14] E. Moridi, M. Haghparast, M. Hosseinzadeh, and S. Jafarali Jassbi, "A novel hierarchical fault management framework for wireless sensor networks: HFMF," *Peer-to-Peer Networking and Applications*, vol. 85, 2021.
- [15] T. R. Gadekallu, M. Alazab, R. Kaluri et al., "Hand gesture classification using a novel CNN-crow search algorithm," *Complex & Intelligent Systems*, vol. 7, no. 4, pp. 1855–1868, 2021.
- [16] T. Shankar, S. Shanmugavel, A. Karthikeyan, A. M. Gupte, and S. Sarkar, "Load balancing and optimization of network lifetime by use of double cluster head clustering algorithm and its comparison with various extended LEACH versions," *International Review on Computers and Software*, vol. 8, no. 3, pp. 795–803, 2013.
- [17] T. Shankar and S. Shanmugavel, "Energy optimization in cluster based wireless sensor networks," *Journal of Engineering Science and Technology*, vol. 9, no. 2, pp. 246–260, 2014.
- [18] A. M. Zungeru, L. M. Ang, and K. P. Seng, "Classical and swarm intelligence based routing protocols for wireless sensor networks: a survey and comparison," *Journal of Network and Computer Applications*, vol. 35, no. 5, pp. 1508–1536, 2012.
- [19] M. Saleem, A. Gianni, and M. F. Di Caro, "Swarm intelligence based routing protocol for wireless sensor networks: survey and future directions," *Information Sciences*, vol. 181, no. 20, pp. 4597–4624, 2011.
- [20] R. V. Kulkarni and G. K. Venayagamoorthy, "Particle swarm optimization in wireless-sensor networks: a brief survey," *IEEE Transactions on Systems, Man, and Cybernetics, Part C (Applications and Reviews)*, vol. 41, no. 2, pp. 262–267, 2011.
- [21] R. Mukherjee, S. Debchoudhury, R. Kundu, S. Das, and P. Suganthan, "Adaptive differential evolution with locality based crossover for dynamic optimization," in *2013 IEEE Congress on Evolutionary Computation*, pp. 63–70, Cancun, Mexico, 2013.
- [22] S. Das, A. Konar, and U. K. Chakraborty, "Annealed differential evolution," in *2007 IEEE Congress on Evolutionary Computation*, pp. 1926–1933, Singapore, 2007.
- [23] P. Kuila, S. K. Gupta, and P. K. Jana, "A novel evolutionary approach for load balanced clustering problem for wireless sensor networks," *Evolutionary Computation*, vol. 12, pp. 48–56, 2013.
- [24] P. Kuila and P. K. Jana, "Energy efficient clustering and routing algorithms for wireless sensor networks: particle swarm optimization approach," *Engineering Applications of Artificial Intelligence*, vol. 33, pp. 127–140, 2014.
- [25] D. Kim, S. Song, and B. Y. Choi, "Energy-efficient adaptive geosource multicast routing for wireless sensor networks," *Journal of Sensors*, vol. 2013, 14 pages, 2013.
- [26] J. Vesterstrom and R. Thomsen, "A comparative study of differential evolution, particle swarm optimization, and evolutionary algorithms on numerical benchmark problems," in *Proceedings of the 2004 Congress on Evolutionary Computation (IEEE Cat. No.04TH8753)*, pp. 1980–1987, Portland, OR, USA, 2004.
- [27] X. Li, L. Xu, H. Wang, J. Song, and S. X. Yang, "A differential evolution-based routing algorithm for environmental monitoring wireless sensor networks," *Sensors*, vol. 10, no. 6, pp. 5425–5442, 2010.
- [28] P. Kuila and P. K. Jana, "A novel differential evolution based clustering algorithm for wireless sensor networks," *Applied Soft Computing*, vol. 25, pp. 414–425, 2014.
- [29] C. P. Low, C. Fang, J. M. Ng, and Y. H. Ang, "Efficient load-balanced clustering algorithms for wireless sensor networks," *Computer Communications*, vol. 31, no. 4, pp. 750–759, 2008.
- [30] G. Gupta and M. Younis, "Load-balanced clustering of wireless sensor networks," in *IEEE International Conference on Communications, 2003. ICC '03*, vol. 3, pp. 1848–1852, Anchorage, AK, USA, 2003.
- [31] K. Pratyay and P. K. Jana, "Energy efficient load-balanced clustering algorithm for wireless sensor networks," *Procedia Technology*, vol. 6, pp. 771–777, 2012.
- [32] T. Sweta Potthuri and A. R. Shankar, "Lifetime improvement in wireless sensor networks using hybrid differential evolution and simulated annealing (DESA)," *Ain Shams Engineering Journal*, vol. 9, no. 4, pp. 655–663, 2018.
- [33] J. Brest, S. Greiner, B. Boskovic, M. Mernik, and V. Zumer, "Self-adapting control parameters in differential evolution: a comparative study on numerical benchmark problems," *IEEE Transactions on Evolutionary Computation*, vol. 10, no. 6, pp. 646–657, 2006.
- [34] S. Randhawa and S. Jain, "MLBC: multi-objective load balancing clustering technique in wireless sensor networks," *Applied Soft Computing*, vol. 74, pp. 66–89, 2019.
- [35] M. Ghahramani and A. Laakdashti, "Efficient energy consumption in wireless sensor networks using an improved differential evolution algorithm," in *2020 10th International Conference on Computer and Knowledge Engineering (ICCCKE)*, pp. 18–23, Mashhad, Iran, 2020.

- [36] G. P. Gupta and B. Saha, "Load balanced clustering scheme using hybrid metaheuristic technique for mobile sink based wireless sensor networks," *Journal of Ambient Intelligence and Humanized Computing*, vol. 2020, 2020.
- [37] C. Iwendi, P. K. R. Maddikunta, T. R. Gadekallu, K. Lakshmana, A. K. Bashir, and M. J. Piran, "A metaheuristic optimization approach for energy efficiency in the IoT networks," *Software: Practice and Experience*, vol. 51, pp. 1–14, 2021.
- [38] S. Ponnann, A. K. Saravanan, C. Iwendi, E. Ibeke, and G. Srivastava, "An artificial intelligence-based quorum system for the improvement of the lifespan of sensor networks," *IEEE Sensors Journal*, vol. 21, no. 15, pp. 17373–17385, 2021.
- [39] S. H. Sackey, J. Chen, A. J. Henry, and X. Zhang, "A clustering approach based on genetic algorithm for wireless sensor network localization," in *2019 15th International Conference on Computational Intelligence and Security (CIS)*, pp. 54–58, Macao, China, 2019.
- [40] J. Chen, S. H. Sackey, J. H. Anajemba, X. Zhang, and Y. He, "Energy-efficient clustering and localization technique using genetic algorithm in wireless sensor networks," *Complexity*, vol. 2021, 12 pages, 2021.
- [41] S. H. Sackey, J. A. Ansere, J. H. Anajemba, M. Kamal, and C. Iwendi, "Energy efficient clustering based routing technique in WSN using brain storm optimization," in *2019 15th International Conference on Emerging Technologies (ICET)*, Peshawar, Pakistan, 2019.
- [42] M. Kaddi, Z. Khalili, and M. Bouchra, "A differential evolution based clustering and routing protocol for WSN," in *2020 International conference on mathematics and information technology*, pp. 190–195, Adrar, Algeria, 2020.
- [43] A. Gaur and T. Kumar, "Switching-differential evolution (S-DE) for cluster head election in wireless sensor network," *IJARIIIE*, vol. 2, no. 5, pp. 2395–4396, 2016.
- [44] R. V. Rao, V. J. Savsani, and D. P. Vakharia, "Teaching-learning-based optimization: a novel method for constrained mechanical design optimization problems," *Computer-Aided Design*, vol. 43, no. 3, pp. 303–315, 2011.
- [45] R. V. Rao, V. J. Savsani, and D. P. Vakharia, "Teaching-learning-based optimization: an optimization method for continuous non-linear large scale problems," *Information Sciences*, vol. 183, no. 1, pp. 1–15, 2012.
- [46] M. Ramadas and A. Abraham, "Clustering wireless sensor networks using ImDE algorithm with LEACH protocol," in *2019 2nd IEEE Middle East and North Africa COMMUNICATIONS Conference (MENACOMM)*, pp. 1–4, Manama, Bahrain, 2019.
- [47] S. K. Chaurasiya, J. Mondal, and S. Datta, "Field-of-view based hierarchical clustering to prolong network lifetime of WMSN with obstacles," in *2014 International Conference on Electronics, Communication and Computational Engineering (ICECCE)*, pp. 72–77, Hosur, India, 2014.
- [48] S. K. Singh, P. Kumar, and J. P. Singh, "A survey on successors of LEACH protocol," *IEEE Access*, vol. 5, pp. 4298–4328, 2017.
- [49] A. Mehmood, S. Khan, B. Shams, and J. Lloret, "Energy-efficient multi-level and distance-aware clustering mechanism for WSNs," *International Journal of Communication Systems*, vol. 28, no. 5, pp. 972–989, 2015.
- [50] R. Banerjee, S. Chatterjee, and S. Das Bit, "An energy saving audio compression scheme for wireless multimedia sensor networks using spatio-temporal partial discrete wavelet transform," *Computers and Electrical Engineering*, vol. 48, pp. 389–404, 2015.
- [51] R. Banerjee and S. Das Bit, "Low-overhead video compression combining partial discrete cosine transform and compressed sensing in WMSNs," *Wireless Networks*, vol. 25, no. 8, pp. 5113–5135, 2019.
- [52] R. Banerjee and S. Das Bit, "An energy efficient image compression scheme for wireless multimedia sensor network using curve fitting technique," *Wireless Networks*, vol. 25, no. 1, pp. 167–183, 2019.





September 2, 2022

To the person in charge of International Bilateral Cooperation,  
Department of Science and Technology (DST), India

I agree to participate in the following DST-JSPS Bilateral Joint Research Project as a principal investigator on the Japan side.

1. Title of the research  
Design and Development of Photo-controlled Memristive Graphene/Diamond Heterojunction Devices for Ultralow-energy Microelectronics and Computing
2. Principal investigators  
India side:  
(PI)Dr. Amit Banerjee, Assistant Professor, Microsystem Design-Integration Lab, Physics Dept., Bidhan Chandra College  
Dr. Tanmoy Basu, Research Scientist, Centre for Quantum Engineering, Research and Education (CQuERE), TCG Centres for Research and Education in Science and Technology (TCG CREST)  
Prof. Dr. Partha Pratim Sarkar, Professor, Department of Engineering and Technological Studies (DETS), University of Kalyani  
Japan side:  
(PI)Dr. Tomoaki Masuzawa, Lecturer, Research Institute of Electronics, Shizuoka University  
Prof. Dr. Toru Aoki, Professor, Research Institute of Electronics, Shizuoka University
3. Research Period  
From June 1, 2023 to May 31, 2025 (2 years)
4. Brief description of the work plan  
In order to develop a novel photo-controlled memristive device, we shall fabricate carbon based hetero structures and characterize their structural, electronic, and optical properties. By making use of graphene/diamond structure, ultrafast switching of THz frequency and unified switching device and memory will be realized. The work will be performed by combining the experience and expertise in designing and simulation on the India side and fabrication and testing on the Japan side through the visits from both sides, i.e. 4 visits x 30 day/visit from India to Japan, and 4 visits x 7 day/visit from Japan to India.

Sincerely yours,

Tomoaki Masuzawa, Ph.D.  
Lecturer, Faculty of Infomatics / Research Institute of Electronics  
Shizuoka University  
3-5-1, Johoku, Naka-ku, Hamamatsu 432-8011, Japan  
TEL: +81-53-478-1347  
EMAIL: [masuzawa.tomoaki@shizuoka.ac.jp](mailto:masuzawa.tomoaki@shizuoka.ac.jp)

*Carbon Quantum Dots for Sustainable Energy and Optoelectronics* reviews the synthesis, properties, and applications of carbon nanodots. This book provides readers with an overview of the key advances in the development of carbon quantum dots including synthesis and surface engineering strategies such as pyrolysis-based synthesis, biomass-based synthesis, functionalization, and other methods toward large-scale development of these carbon nanomaterials. The emerging applications of carbon quantum dots in different fields, such as energy harvesting, energy storage, and biomedical applications, are thoroughly reviewed, emphasizing the impact of enhanced properties of carbon quantum dots for these applications.

*Carbon Quantum Dots for Sustainable Energy and Optoelectronics* is suitable for graduate students, materials scientists, and engineers working in academia and industry. This book is also beneficial for the interdisciplinary community of researchers and practitioners working in the field of nanotechnology.

**Key features**

- Introduces the recent advances in the understanding of carbon quantum dots, including relevant synthesis and surface engineering strategies for their large-scale development
- Provides an overview of the most relevant applications of carbon quantum dots for the development of sustainable technologies in optoelectronics, energy, and biomedical applications
- Discusses future research directions and remaining challenges toward the commercial translation of carbon quantum dots

**About the editors**

**Dr. Sudip Kumar Batabyal** is an associate professor in the Department of Science and senior research scientist in the ACIRI, Amrita School of Engineering, Amrita Vishwa Vidyapeetham, Coimbatore, Tamil Nadu, India.

**Dr. Basudev Pradhan** is an assistant professor at the Department of Energy Engineering, Centre of Excellence (CoE) in Green and Efficient Energy Technology (GEET), Central University of Jharkhand, Ranchi, Jharkhand, India.

**Dr. Kallol Mohanta** is an assistant professor at the PSG Institute of Advanced Studies, Coimbatore, Tamil Nadu, India.

**Dr. Rama Ranjan Bhattacharjee** is an associate professor and head of the department at the Amity Institute of Nanotechnology and also a university research coordinator in Kolkata, West Bengal, India.

**Dr. Amit Banerjee** is an assistant professor and group leader at the Microsystem Design-Integration Lab, Physics Department, Bidhan Chandra College, Asansol, West Bengal, India.



ISBN 978-0-323-90895-5

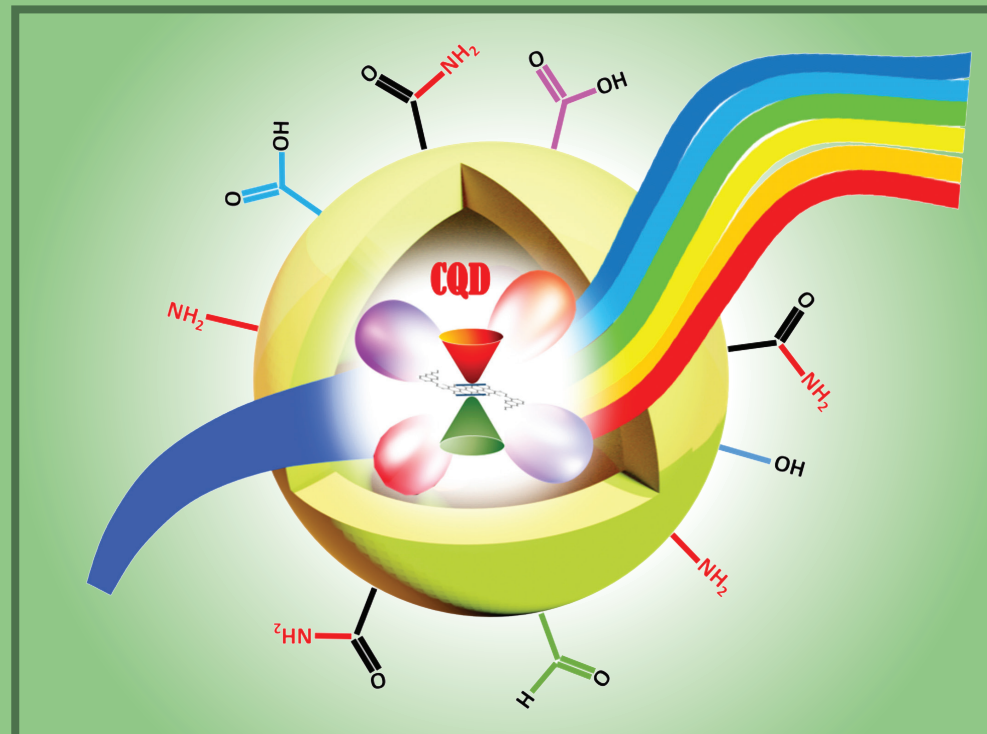


9 780323 908955



BATABYAL, PRADHAN,  
MOHANTA, BHATTACHARJEE,  
BANERJEE

CARBON QUANTUM DOTS FOR  
SUSTAINABLE ENERGY AND OPTOELECTRONICS



# CARBON QUANTUM DOTS FOR SUSTAINABLE ENERGY AND OPTOELECTRONICS

Edited by  
SUDIP KUMAR BATABYAL  
BASUDEV PRADHAN  
KALLOL MOHANTA  
RAMA RANJAN BHATTACHARJEE  
AMIT BANERJEE





# Carbon Quantum Dots for Sustainable Energy and Optoelectronics

Woodhead Publishing Series in Electronic and Optical Materials

2023, Pages 473-479

## 20 - Future perspectives of carbon quantum dots

[Amit Banerjee](#)<sup>1</sup>, [Sudip K. Batabyal](#)<sup>2</sup>, [Basudev Pradhan](#)<sup>3,4</sup>, [Kallol Mohanta](#)<sup>5</sup>, [Rama Ranjan Bhattacharjee](#)<sup>6</sup>

[Show more](#) ▾

[Outline](#) | [Share](#) [Cite](#)

<https://doi.org/10.1016/B978-0-323-90895-5.00019-9> ↗

[Get rights and content](#) ↗

### Abstract

A perspective on current and emerging applications of carbon quantum dots (CQDs), with critical review of few specific areas, expected to change our day to day outlook has been discussed here: luminescent CQDs for optical sensing; biogreen CQDs for biotechnology and nanomedicines, CQDs as contrast agent in advanced imaging; colloidal CQDs for green optoelectronics to name a few.

[Recommended articles](#)

### References (0)

### Cited by (1)

[An Overview on Carbon Quantum Dots Optical and Chemical Features](#) ↗

2023, Molecules

[View full text](#)

Copyright © 2023 Elsevier Ltd. All rights reserved.

---

**Invitation Letter**

1 message

---

**T. Som** <tsomiop@gmail.com>  
To: "Dr. Amit Banerjee" <amitbanerjee.nus@gmail.com>

Mon, Mar 6, 2023 at 1:44 PM

To

Dr. Amit BANERJEE, Ph.D.,  
Principal Investigator, Microsystem Design-Integration Lab;  
Assistant Professor, Dept. of Physics, Bidhan Chandra College, West Bengal;

Subject: Invitation to attend collaboration meeting at Institute of Physics, Bhubaneswar

Dear Dr. Banerjee,

Further to our detailed discussion, it is my pleasure to invite you to visit my laboratory at the Institute of Physics, Bhubaneswar from 15th to 17th March 2023, for intense interactive sessions with our group on scope of future collaboration with your Microsystem Design-Integration Lab.

Below is the brief meeting agenda :

**Venue:** Institute of Physics, Bhubaneswar

**Members:**

1. **Prof. Tapobrata Som**, Institute of Physics, Bhubaneswar;
2. **Dr. Tanmoy Basu**, Centre for Quantum Engineering, Research and Education, TCG Crest;
3. **Dr. Amit Banerjee**, Microsystem Design-Integration Lab, Bidhan Chandra College;

**Possible Agenda:**

- Presentation, discussion on your on-going project "Design and Development of Thermal Screening and Surveillance Device Prototype with On-chip Integrated Terahertz Detector Arrays".
- Integrated Photonics and micro-fabrication-related discussions, collaboration with RIE Japan on photonics devices.
- Collaboration capacity and usage of Microsystem Design-Integration Lab e.g. COMSOL Multiphysics (Wave Optics Module, Ray Optics Module, RF Module, AC/DC Module, Semiconductors Module, MEMS Module, Heat Transfer Module, Design Module, Particle Tracing Module); Siemens Solid Edge, NI Multisim, NI Ultiboard, NI LabVIEW and DAQs; MW Source 40 GHz; VNA 40 GHz; Power Meter and Power Sensor 40 GHz, any other.
- Scope of collaboration with Institute of Physics.

We look forward to hearing from you.

With regards,

Tapobrata Som



## Article

# Development and Analysis of Graphene-Sheet-Based GaAs Schottky Solar Cell for Enriched Efficiency

L. Kholee Phimu <sup>1</sup>, Rudra Sankar Dhar <sup>1,\*</sup>, Khomdram Jolson Singh <sup>2</sup> and Amit Banerjee <sup>3,\*</sup>

<sup>1</sup> Department of Electronics and Communication Engineering, National Institute of Technology Mizoram, Aizawl 796012, India

<sup>2</sup> Department of Electronics and Communication Engineering, Manipur Institute of Technology, Canchipur, Imphal 795003, India

<sup>3</sup> Microsystem Design-Integration Lab, Physics Department, Bidhan Chandra College, Asansol 713303, India

\* Correspondence: rudra.ece@nitmz.ac.in (R.S.D.); amitbanerjee.nus@gmail.com (A.B.)

**Abstract:** Comparative studies of the 2D numerical modelling and simulation of graphene-based gallium arsenide and silicon Schottky junction solar cell are studied using TCAD tools. The performance of photovoltaic cells was examined while taking parameters, such as substrate thickness, relationship between transmittance and work function of graphene, and n-type doping concentration of substrate semiconduction. The area with the highest efficiency for photogenerated carriers was found to be located near the interface region under light illumination. The significant enhancement of power conversion efficiency was shown in the cell with a thicker carrier absorption Si substrate layer, larger graphene work function, and average doping in a silicon substrate. Thus, for improved cell structure, the maximum  $J_{SC} = 4.7 \text{ mA/cm}^2$ ,  $V_{OC} = 0.19 \text{ V}$ , and fill factor = 59.73% are found under AM1.5G, exhibiting maximum efficiency of 6.5% (1 sun). The EQE of the cell is well above 60%. This work reports the influence of different substrate thickness, work function, and N-type doping on the efficiency and characteristics of graphene-based Schottky solar cells.

**Keywords:** external quantum efficiency; graphene; power conversion efficiency; Schottky barrier solar cell (SBSC); TCAD



**Citation:** Phimu, L.K.; Dhar, R.S.; Singh, K.J.; Banerjee, A. Development and Analysis of Graphene-Sheet-Based GaAs Schottky Solar Cell for Enriched Efficiency. *Micromachines* **2023**, *14*, 1226. <https://doi.org/10.3390/mi14061226>

Academic Editor: Hugo Aguas

Received: 11 March 2023

Revised: 16 May 2023

Accepted: 19 May 2023

Published: 10 June 2023



**Copyright:** © 2023 by the authors. Licensee MDPI, Basel, Switzerland. This article is an open access article distributed under the terms and conditions of the Creative Commons Attribution (CC BY) license (<https://creativecommons.org/licenses/by/4.0/>).

## 1. Introduction

Due to graphene's unique structure and characteristics, a single atomic layer has attracted significant attention, such as high mobility, low resistivity, and band gap [1]. Graphene has been created as ultrathin sheets made of a few atomic layers through mechanical exfoliation or CVD (chemical vapour deposition) and can be shifted to many substrates; thus, it will open up a large range of potential applications, including smart composites, photo sensors, and high-performance electronic devices [2]. Specifically, the graphene layer is a major material for use in the production of effective solar cells due to its exceptional combination of optical transparency and high electrical conductivity in the visible and near-infrared spectrum [3,4]. On various substrates, such as Si [5], CdS [6], CdSe [7], and GaAs [8], graphene-based Schottky junction solar cells have been produced in recent years. A Schottky junction was successfully formed on n-type GaAs by Wenjing et al., producing a power conversion efficiency of 1.95% [9]. GaAs has more radiation resistance [10] than the Si substrate, which is most frequently used, and has a direct band gap [11], which makes it suitable for highly efficient solar cells for both terrestrial and space applications. However, in order to increase solar cell efficiency, the band parameter must be studied, and various thicknesses of the structure must be optimised. We, therefore, optimised the thickness of the GaAs substrate with a graphene layer in SILVACO TCAD in this paper, and the results were confirmed using published experimental data.

The proposed graphene structure is shown in Figure 1. It consists of three regions. The ability to create graphene-on-silicon Schottky solar cells at room temperature opens up a wide

range of applications for light gathering and conversion with the benefits of environmental friendliness and lower cost [12]. In this design, the graphene sheet performs dual roles for separation of holes/electrons as an active layer and as a carrier medium for transportation, in addition to acting as a transparent electrode for the transmission of light [13]. Despite the fact that the initial energy conversion efficiency is only 1.65% [14], the performance of graphene silicon Schottky cells was improved using silicon nano-array substrate adoption [15], chemical doping [5], and a graphene/P3HT/silicon configuration [16], ranging from 1.96% up to 10.3%. Some of the critical parameters, such as surface charge recombination, work function, and graphene conductivity, played a key role in establishing the performance of the device. Still, there has not been much research conducted on Schottky barriers. Thus, considerably more consideration and study are needed for the use of graphene in Schottky solar cells. Figure 2 shows an energy band diagram of graphene solar cells.

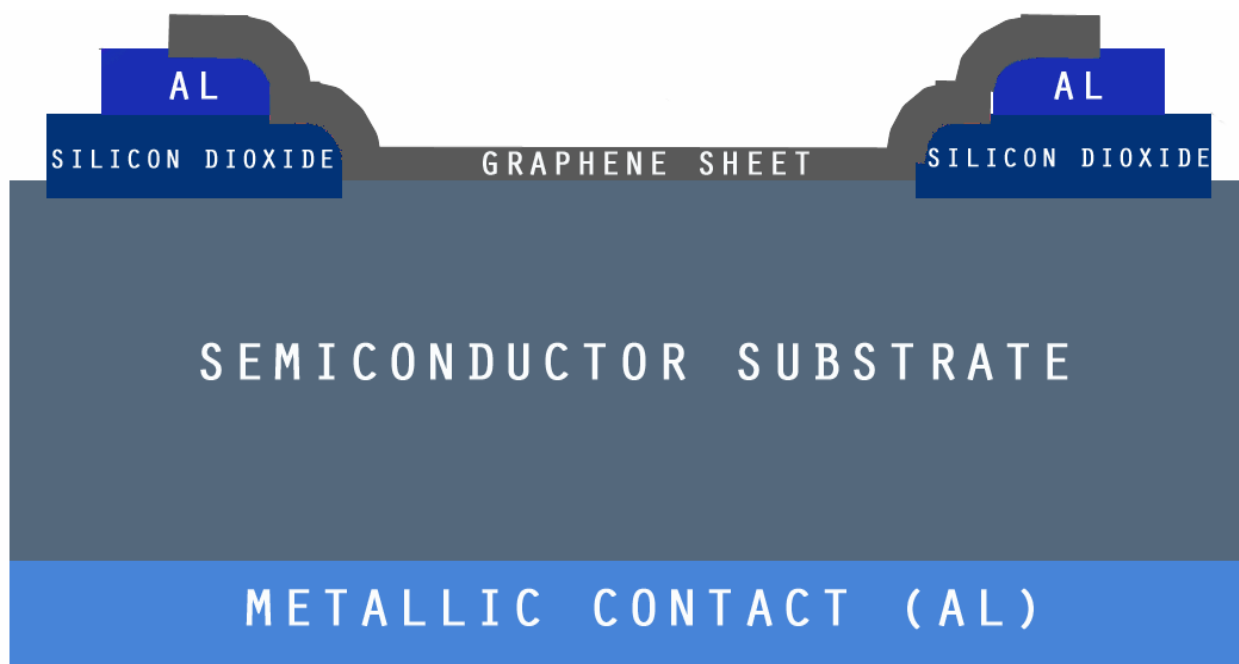


Figure 1. Proposed structure of Schottky graphene solar cell.

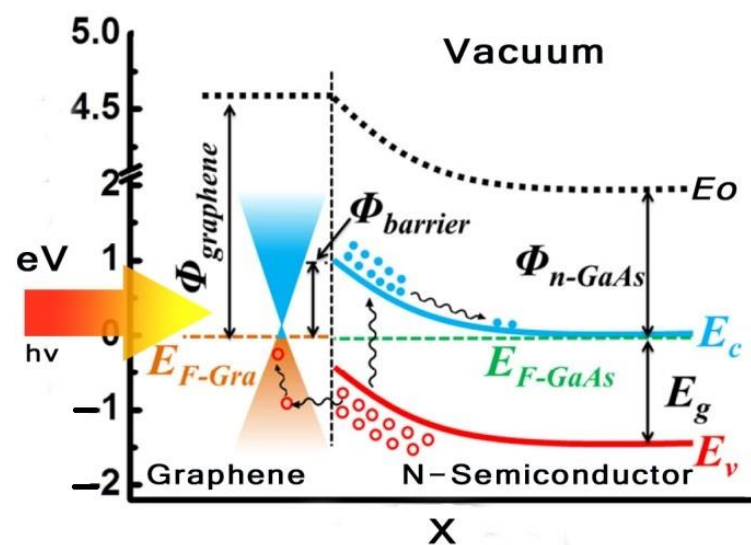


Figure 2. Energy band diagram of graphene solar cell.



The graphene GaAs and silicon junction solar cell are numerically simulated in this work using standard TCAD tools. It uses a typical method for materials such as amorphous, including state model of continuous density, auger recombination mechanisms, and Schottky, to solve continuity, Poisson, and current density equations. The dependence of these optical parameters with the photon energy has been included, taking into account the thickness of the substrate, work function of graphene, doping level, and their impact on cell efficiency.

## 2. Modelling Semi-Transparent Top-Layer Graphene in Atlas

Due to the fact that graphene is a novel material, it is not yet included in the SILVACO Atlas material library. As a result, in order to develop a reliable and exact model of the graphene film, the initial definition of the layer used 4H-SiC as the base material, which was then modified to give the metallic material properties and match experimental sheet resistance values [17]. First, the material 4H-SiC model was made entirely transparent without changing its optical characteristics. Next, the graphene transmittance was entered by creating an .nk file for graphene from the obtained value [18]. With 15,000 cm<sup>2</sup>/Vs of carrier mobility [19], graphene is described as the Fermi distribution, and band gap, effective masses, and thickness values of 10 nm were changed to make sure they matched the experimental findings. Table 1 is a list of the simulation parameters that the Atlas tool utilized for this cell [20].

**Table 1.** Material utilized in this numerical simulation.

Essential Layer Properties	ATLAS Identifier	Material Layer		
		Graphene	Substrate	
		4H-SiC	GaAs	Silicon
Band gap layer $E_g$ (eV)	$E_G$	0.0	1.42	1.08
Relative permittivity, $\epsilon_r$ (F cm <sup>-1</sup> )	Permittivity	25	13.1	13.5
Electron affinity $X_e$ (eV)	Affinity	5.8	4.07	4.17
Mobility, $\mu_p$ (cm <sup>2</sup> /V s)	MUP	15,000	400	500
Mobility, $\mu_n$ (cm <sup>2</sup> /V s)	MUN	15,000	8000	1000
Effective density of states $N_c$ (cm <sup>-3</sup> )	NC300	$3 \times 10^{17}$	$4 \times 10^{17}$	$2.8 \times 10^{19}$
Effective density of states $N_v$ (cm <sup>-3</sup> )	NV300	$3 \times 10^{17}$	$7 \times 10^{18}$	$1.0 \times 10^{19}$

## 3. Modelling Graphene-Based Solar Cells

With the use of TCAD, including the optical intensity, as shown in Figure 3, and using parameters from Table 1, the user of ATLAS can choose from a number of physics models to compute recombination and carrier mobility. We utilized the following models in our design for our analysis. The doping-dependent low-field mobilities of holes/electrons in the cell at 300 K were modelled. The recombination models utilized were the Optical Recombination (OPTR) and the Schottky–Read–Hall (SRH) recombination models. As already stated, Figure 4 shows the cross section of a graphene Si solar cell that was modelled in TCAD software. The device is made up of three areas, from bottom to top, namely the silicon substrate, the SiO<sub>2</sub> window, and the graphene layer. Here, an oxide window was used to coat the silicon substrate with a 10 nm thick layer of graphene. Figure 5 shows the detailed top layer of the cell.

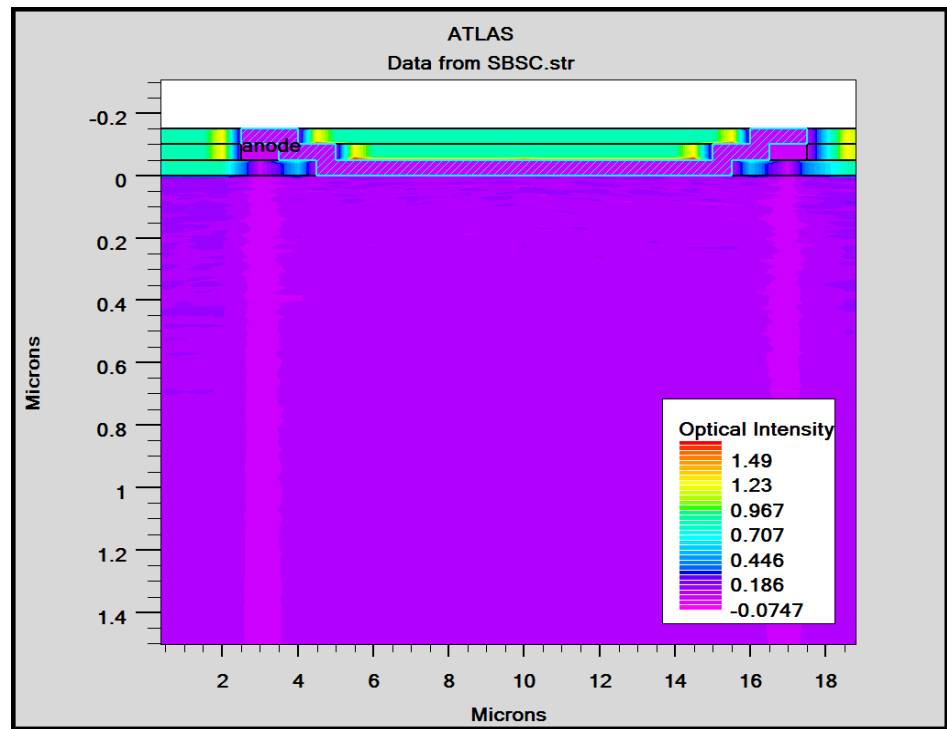


Figure 3. Optimized optical intensity in Si solar cell.

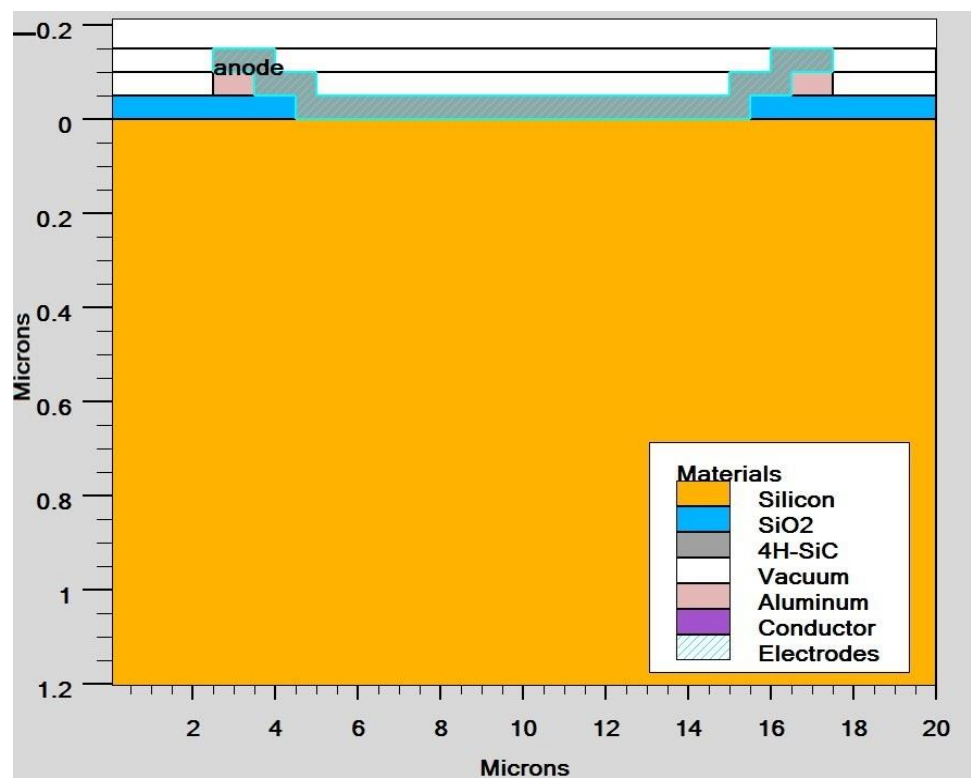


Figure 4. Solar cell cross-section view of graphene Si.

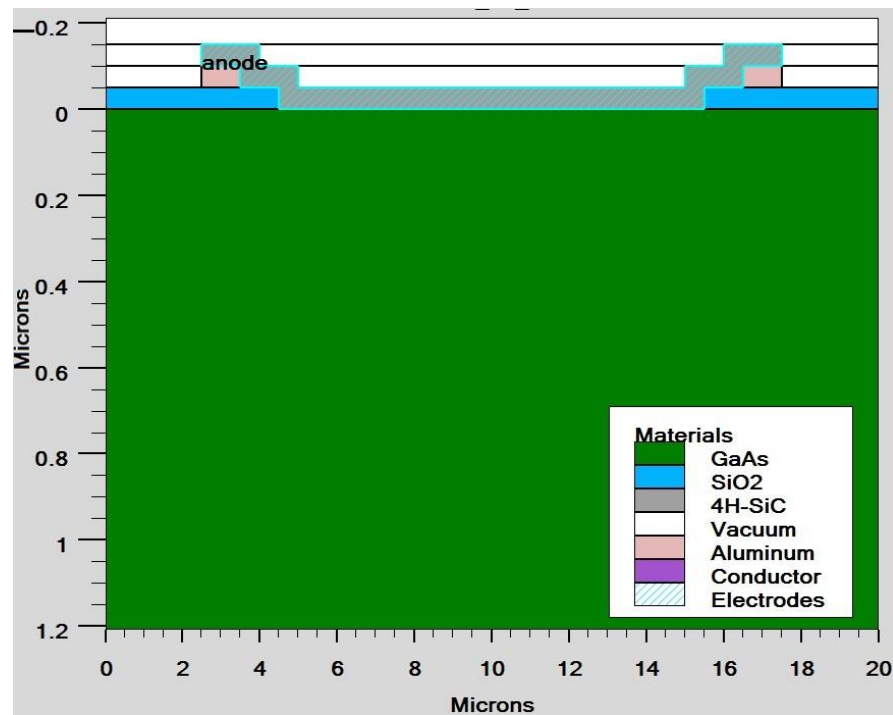


Figure 5. Solar cell cross-section view of graphene GaAs.

Most studies show that the heterojunction device for this structure is fabricated from a transferred chemical vapour deposition graphene layer on silicon in order to avoid expensive deposition methods and complicated processing [21,22]. In essence, the Schottky junction can be created using any semiconductor with a specific metal, provided the work function differences are sufficiently large and the carrier densities are moderate. The calculations show that graphene sheets and silicon create a Schottky junction, which is advantageous for creating a sizable built-in field [14]. The photoexcited holes and electrons are produced in the silicon substrate when it is illuminated, and they are subsequently separated at the Schottky junction through the built-in electric field. The bottom electrodes gather electrons/holes, leading to a photovoltaic reaction. The thermionic emission model can be used to describe the Schottky junction’s non-linear I-V property [23]:

$$I_o = \alpha B^* T^2 \exp(-e\phi_{Bn}/kT) \tag{1}$$

where  $\alpha$  is area cell,  $B^*$  is effective Richardson constant,  $\phi_{Bn}$  is metal–semiconductor (n-type),  $k$  is Boltzmann’s constant, and  $T$  absolute temperature.

$$\phi_B = \phi_G - \chi, \text{ for n-type semiconductor} \tag{2}$$

Additionally,

$$\phi_B = E_G - \phi_G + \chi, \text{ for p-type semiconductor} \tag{3}$$

where  $\phi_G$  = graphene work function,  $\chi$  = electron affinity,  $E_G$  = energy gap semiconductor.

#### 4. Results and Discussion

In order to mimic the global terrestrial sunshine, the modelled device was illuminated with AM1.5G solar spectrum, which is taken into account by LUMINOUS 3D for modelling sunlight in SILVACO Atlas [24]. The light could be absorbed in the barrier layer and inside the semiconductor. The photogeneration rate is provided by  $G = \eta_0 \frac{P\lambda}{hc} \alpha e^{-\alpha y}$ , where  $P$  represents the total effect of the ray path’s absorption, reflection, and transmission losses,  $y$

is the ray for the provided relative distance,  $\alpha$  is the computed absorption coefficient for every combination value of  $(n, k)$ ,  $\lambda$  is wavelength,  $h$  is Planck's constant,  $c$  is the speed of light, and  $\eta_0$  is the internal quantum efficiency, denoting the carrier number produced per photon per pair. It can be seen from Figure 6 that the highest efficient absorption area is around 0.1  $\mu\text{m}$  from the surface connection and it not only increases the light absorption length but is also concentrated to the light field, which results in enhanced excitation of photon-induced carriers. The recombination rate is also higher at the interface region, as indicated by the result shown in Figure 7. Figure 8 shows the potential developed inside the cell, indicating that maximum potential is developed in the anode vicinity and that there is a greater collection of charge. Figures 9–11 show a comparison of different thicknesses for the photogeneration rate, electric field, and potential, respectively. Figure 9a–c show the photogeneration rate of Si cells under AM1.5 (sun) with depths of absorption, which were examined at 5  $\mu\text{m}$ , 10  $\mu\text{m}$ , and 20  $\mu\text{m}$ . The semiconductor and barrier could both absorb the light. Figure 9c shows that 20  $\mu\text{m}$  thickness is more than sufficient for full-spectrum absorption because the intensity of the photogenerated carrier suddenly reduces in the deep area of the Si substrate. In Figure 10, as the number of solar cells rises, the electrical field also rises. In fact, an increase in the number of solar cells leads to an increase in the open-circuit photovoltage. The main aim of this paper is to enhance the conversion efficiency through a reduction in silicon matter. As a result, fewer solar cells must be utilised to generate the electrical field, which lowers the amount of semiconductor materials needed to make solar cells. Figure 10 gives the evolution of the electric field as a function of the solar cells. Figure 11 shows the potential developed inside the cell, showing that maximum potential is developed in the anode vicinity, indicating a greater collection of charge.

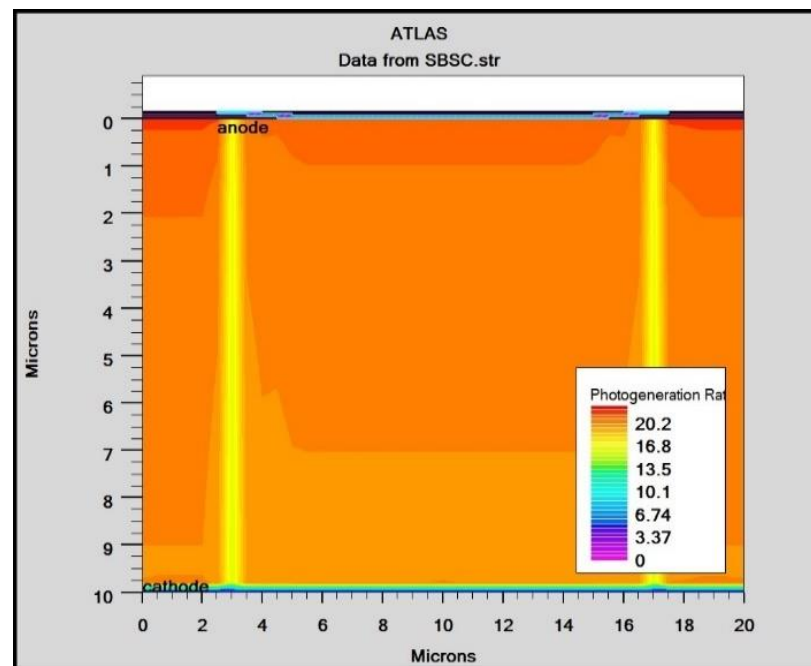


Figure 6. Photogeneration rate in Si solar cell.

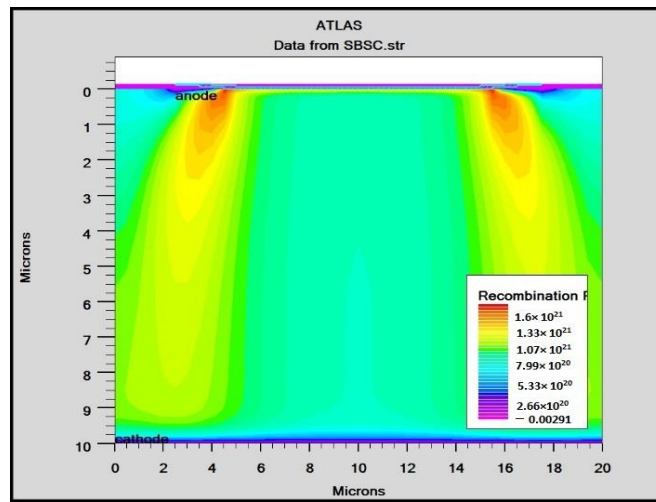


Figure 7. Recombination rate in Si Solar cell.

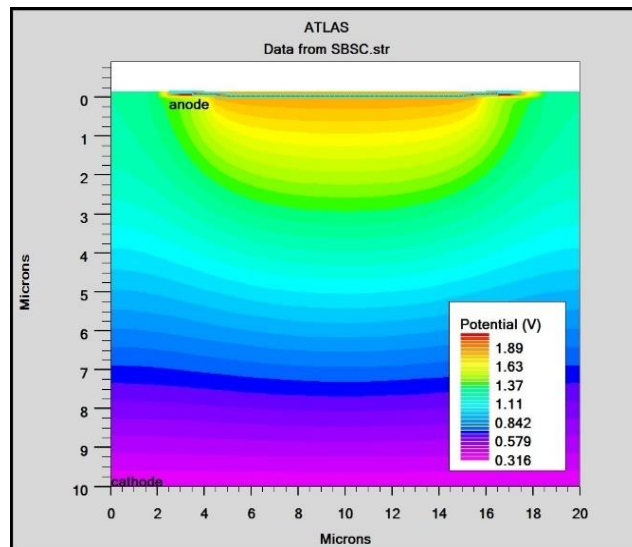


Figure 8. Potential of Si solar cell.

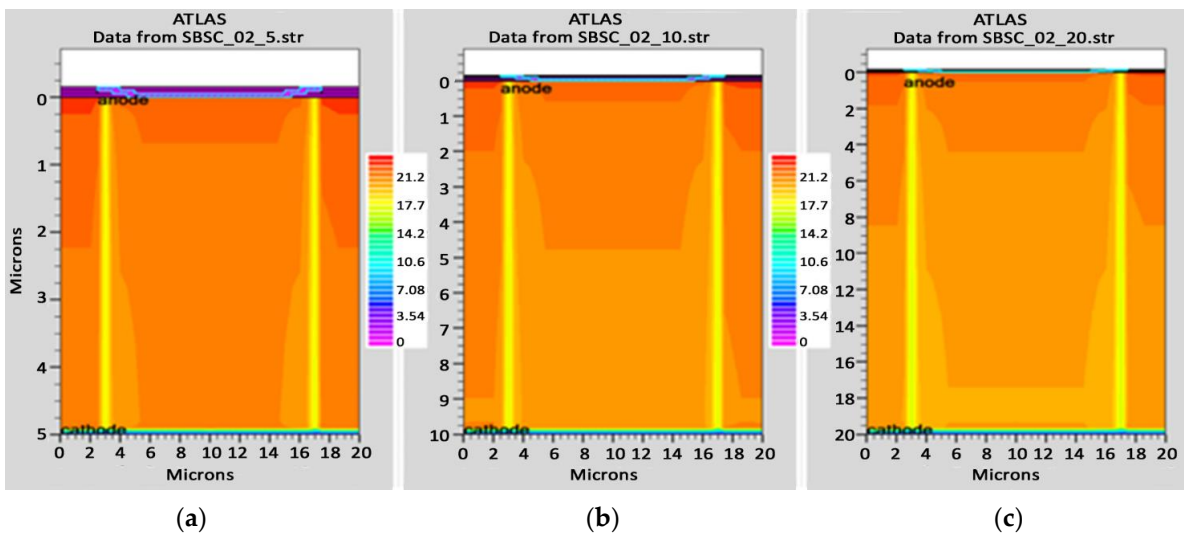


Figure 9. Photogeneration rate of Si cell: (a) 5  $\mu\text{m}$ , (b) 10  $\mu\text{m}$ , (c) 20  $\mu\text{m}$ .

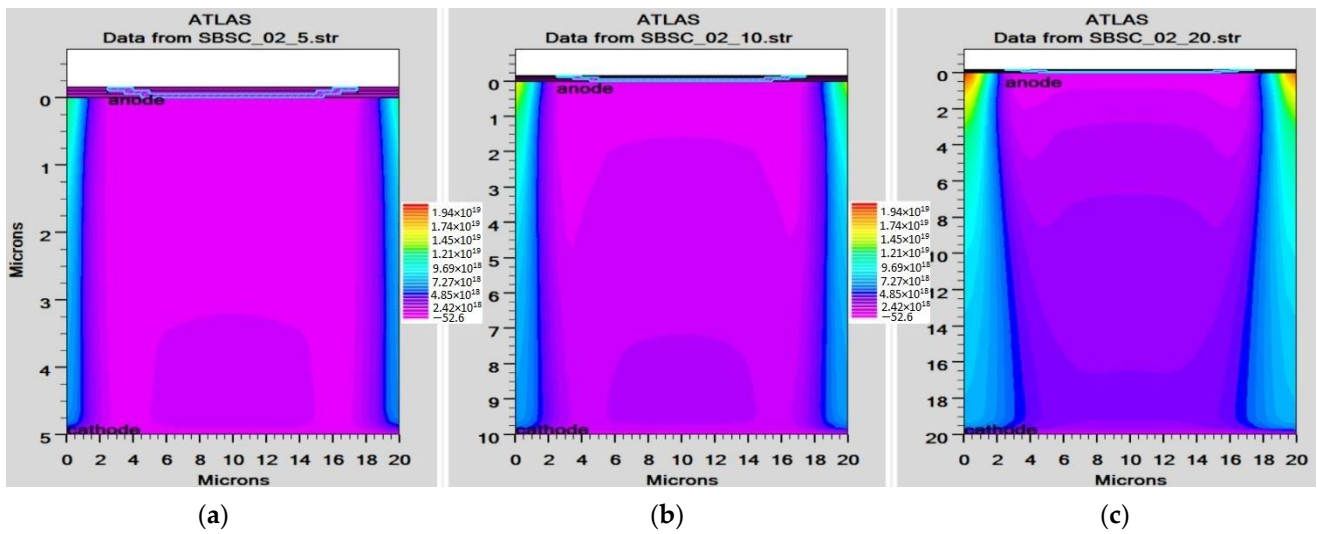


Figure 10. Electric field of Si cell: (a) 5 μm, (b) 10 μm, (c) 20 μm.

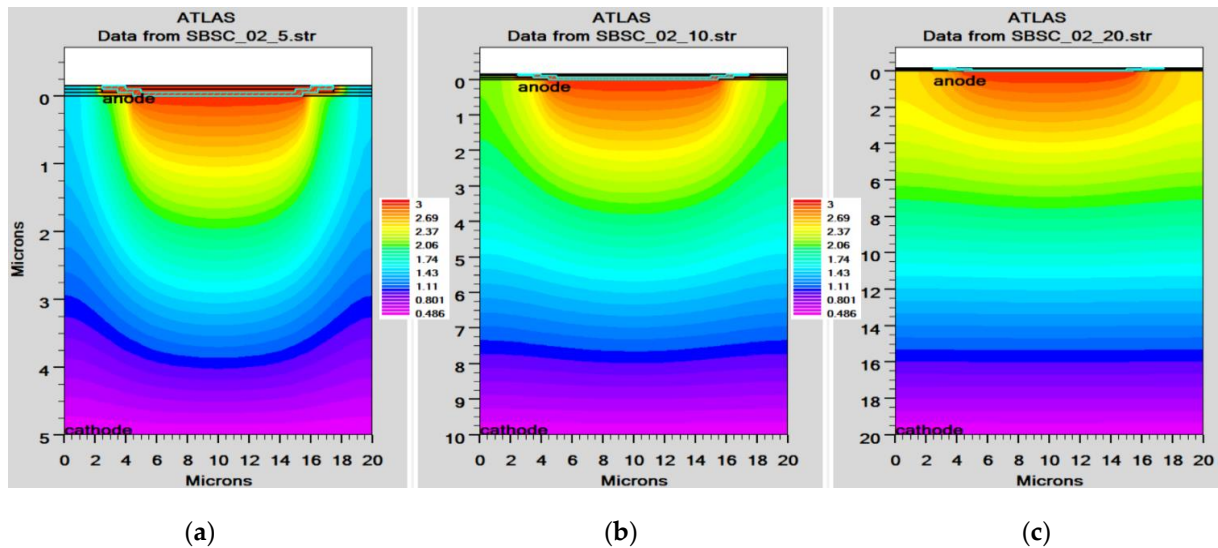


Figure 11. Potential of Si cell: (a) 5 μm, (b) 10 μm, (c) 20 μm.

It is crucial to utilize  $I_{SC}$  and  $V_{OC}$  to establish how well a solar cell works because they affect how much power it can produce.

$$V_{OC} = \frac{nKT}{q} \ln\left(\frac{I_L}{I_0} + 1\right) \tag{4}$$

$$FF = \frac{V_{OC} - \ln(V_{OC} + 0.72)}{V_{OC} + 1} = \frac{I_m V_m}{I_{SC} V_{OC}} \tag{5}$$

$I_{SC}$  and  $V_{OC}$  utilisation at maximum power is measured via the fill factor. The efficiency can be expressed using  $FF$  as:

$$\eta = \frac{V_{OC} I_{SC} FF}{P_{in}} = \frac{P_{max}}{1000 [Wm^{-2}] \times CellArea [m^2]} \tag{6}$$

These are the performance metrics that we employed in our research for evaluating solar cells.



#### 4.1. GaAs and Si Thickness Effect

The Si crystal substrate is illuminated with an orientation <100>. For photogenerated carrier intensity, graphene functions as a transparent electrode. The difference between the work functions was built using a Schottky junction. We computed the I-V curves and external quantum efficiency (EQE), as illustrated in Figures 12 and 13, respectively, to examine the impact of silicon thickness on solar cell performance. Since silicon has an indirect band gap, it works with longer wavelengths and results in higher quantum efficiency. When silicon crystal thickness decreases, long-wavelength light passes through the device and lowers the IQE. On the other hand, the enhanced recombination carrier rate on the back electrode causes a significant increase in the dark current. Because the silicon substrate is thicker, it is discovered that the efficiency of the device ranges from 2.37% to 5.99% (given in Table 2).

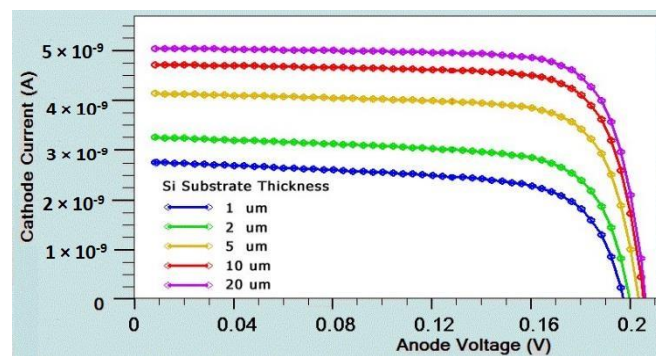


Figure 12. I-V curve of Si substrate with different thicknesses.

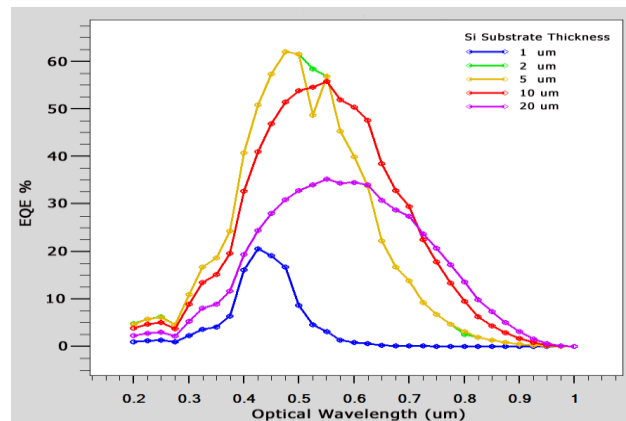


Figure 13. EQE of solar cell vs. different Si thicknesses.

Table 2. Performance of cell with substrate thickness (under n doping  $3 \times 10^{16} \text{ cm}^{-3}$  and work function 4.8).

Thickness ( $\mu\text{m}$ )	$J_{SC}$ ( $\text{mA}/\text{cm}^2$ )		$V_{OC}$ (V)		FF (%)		Efficiency (%)	
	GaAs	Si	GaAs	Si	GaAs	Si	GaAs	Si
1	6.10	2.76	1.00	0.29	51	28.69	3.29	2.37
2	6.80	3.26	0.97	0.29	51	31.88	5.03	3.11
5	7.90	4.14	0.94	0.18	49	58.08	4.74	4.51
10	8.40	4.72	0.93	0.19	45	60.21	4.58	5.47
20	9.00	5.05	0.91	0.19	45	60.95	4.58	5.99

#### 4.2. Graphene Work Function Effect

The difference between silicon  $\chi$  and graphene  $\phi_G$  is related to the barrier height  $\phi_B$ , as discussed in Section 3. Therefore, a higher work function will enhance the  $\phi_B$ , which will make the built-in potential  $V_{bi}$  increase according to the equation,  $V_{bi} = \phi_B - V_n$ , where  $V_n$  is the distance between  $E_c$  and  $E_f$  in silicon. Consequently, an enhanced graphene work function results in an increase in  $V_{bi}$  that corresponds to the upper limit of  $V_{oc}$ . As shown in Table 3, the built-in potential  $V_{bi}$  increases monotonically along with the  $FF$  and power conversion efficiency. This result is inconsistent with Y.F. Li's group's experimental findings [25].

**Table 3.** Performance of cell with graphene work function (under optimal 10  $\mu\text{m}$  si-thickness).

Graphene Work Function	$J_{SC}$ (mA/cm <sup>2</sup> )		$V_{OC}$ (V)		$FF$ (%)		Efficiency (%)	
	GaAs	Si	GaAs	Si	GaAs	Si	GaAs	Si
4.4	6.10	4.72	1.00	0.18	51	50.34	3.29	4.9
4.6	6.10	4.72	0.97	0.16	51	48.21	5.03	5.3
4.8	6.10	4.72	0.94	0.19	49	60.21	4.74	5.4

#### 4.3. GaAs and Silicon n-Type Doping Effect

The ability of silicon's N-type doping to raise the photogeneration carrier intensity and energy level of Fermi is well recognised. Due to the larger barrier height compared to a substrate made of pure silicon, both  $V_{OC}$  and  $I_{SC}$  increase for doping concentrations below  $3 \times 10^{15} \text{ cm}^{-3}$ . When the doping concentration exceeds  $3 \times 10^{15} \text{ cm}^{-3}$ , the cell's performance is radically different. The mechanism for electron emission could be the origin of this phenomenon. The emissions of a carrier from silicon to graphene are dominated by the tunnelling emission process rather than the thermionic emission mechanism. As a result, there is a slight decrease in the open-circuit voltage. Second, a high doping level reduces the photogeneration carriers' lifetime, particularly for light that has a long wavelength. These losses in the carrier collection result in a reduction in  $I_{SC}$ . Thirdly, as indicated in Table 4, the  $3 \times 10^{16} \text{ cm}^{-3}$  doping level has the largest fill factor, despite having a lower power conversion efficiency than the other two doping concentrations. Therefore, the optimal efficiency is found at a moderate doping level of  $3 \times 10^{15} \text{ cm}^{-3}$ .

**Table 4.** Performance of cell with doping concentrations (under optimal 10  $\mu\text{m}$  si- thickness).

Doping of n-Type Effect (/cm <sup>-3</sup> )	$J_{SC}$ (mA/cm <sup>2</sup> )		$V_{OC}$ (V)		$FF$ (%)		Efficiency (%)	
	GaAs	Si	GaAs	Si	GaAs	Si	GaAs	Si
$3 \times 10^{14}$	6.10	4.7	1.38	0.20	68	57.04	9.54	5.65
$3 \times 10^{15}$	6.10	4.7	1.37	0.19	66	59.73	9.52	6.50
$3 \times 10^{16}$	6.10	4.3	1.36	0.18	67	60.21	9.50	5.47

In order to improve the design, it is also necessary to identify different performance parameters. A solar cell I-V curve with varying substrate thicknesses is depicted in Figure 12. We determine the current–voltage curves and external quantum efficiency (EQE) for GaAs, as shown in Figures 14 and 15, respectively. It is found that Si EQE has well above 60% and GaAs EQE has 50%, which is optimized at the (2–5)  $\mu\text{m}$  substrate thickness due to the high photogeneration rate found at this substrate thickness.

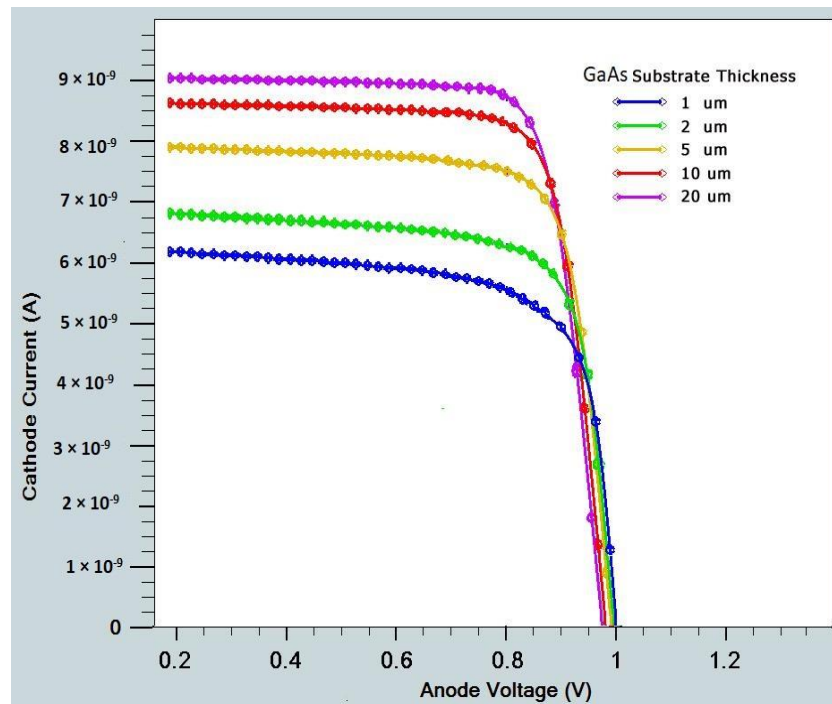


Figure 14. I-V curve of GaAs substrate with different thicknesses.

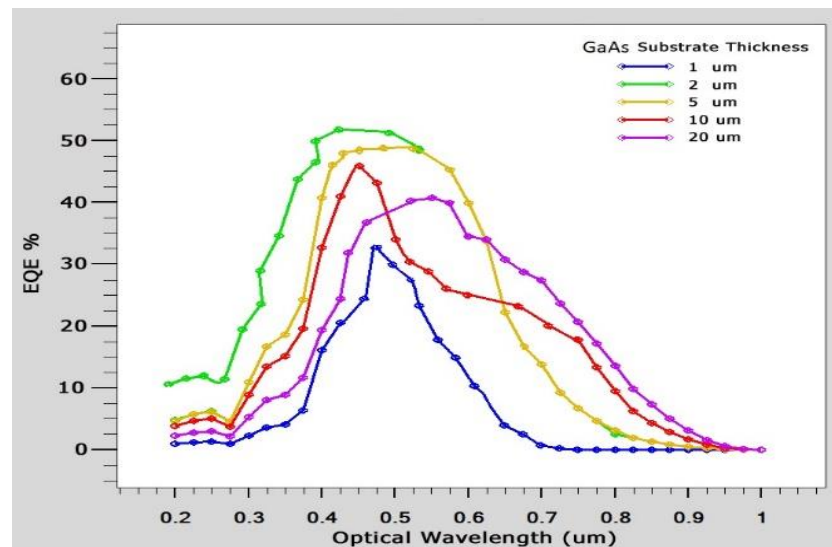


Figure 15. EQE of solar cell vs. different GaAs thicknesses.

The absorption and transmission co-efficient of the cell is depicted in Figure 16. The proposed cell works effectively in a wavelength range of 300 to 700 nm. After 700 nm, the efficiency starts decreasing due to an increase in transmittance and less absorptivity of photons, as shown in Figure 16. Most of the spectrum is found to be utilized in the generation of the carrier in the optimal 10 μm thickness Silicon substrate. Equation (7) can be used to determine  $J_{SC}$  using the measured  $EQE$ .

$$J_{SC} = q \int F(\lambda)EQE(\lambda)d\lambda \tag{7}$$

where  $F(\lambda)$  = intensity spectrum of AM1.5G sunlight, and  $q$  is electron charge. It is found that  $EQE$  is well above 60%, which is an indication of an effective cell structure. Table 5 provides a tabular comparison that demonstrates that the Si substrate is significant when

compared with existing results. Through comparison with the existing results, it is found that graphene-based Schottky solar cells with Si and GaAs as substrates have increased efficiency of GaAs (4.74%) and Si (5.99%) over conventional Schottky junction solar cells.

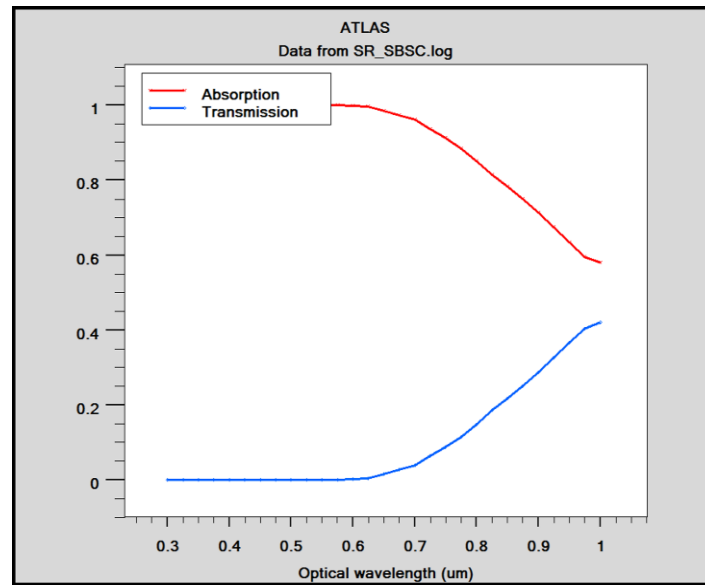


Figure 16. Absorption and transmission co-efficient of solar cells.

Table 5. Comparison of various factors, such as substrate thickness, work function, and doping concentration, with existing device.

	GaAs Thickness (μm)	Work Function (ev)	N-Type Doping (/cm <sup>3</sup> )	<i>J</i> <sub>sc</sub> (mA/cm <sup>2</sup> )	<i>V</i> <sub>oc</sub> (V)	<i>FF</i> (%)	Efficiency (%)
GaAs junction solar cell [26]	5	4.8	1 × 10 <sup>14</sup>	7.966	0.301	49	1.518
Our proposed work	5	4.8	3 × 10 <sup>16</sup>	6.10	0.94	49	4.74
	Si Thickness (μm)	Work Function (ev)	N-Type Doping (/cm <sup>3</sup> )	<i>J</i> <sub>sc</sub> (mA/cm <sup>2</sup> )	<i>V</i> <sub>oc</sub> (V)	<i>FF</i> (%)	Efficiency (%)
Si junction solar cell [27]	20	4.8	1 × 10 <sup>17</sup>	5.72	0.158	58	0.874
Our proposed work	20	4.8	3 × 10 <sup>16</sup>	5.05	0.19	60.95	5.99

### 5. Conclusions

Silvaco ATLAS software was used to model graphene-based GaAs solar cells and graphene-on-Si Schottky junction solar cells in a unique way for photovoltaic applications. Numerical simulation in two dimensions was used to analyze the output performance. Additionally, we thoroughly examined the performance vs. various graphene work functions, substrate thicknesses, and N-type doping concentrations. The findings demonstrate that greater graphene work function, adequate absorption thickness, and mild silicon doping are superior for increasing the power conversion efficiency. Further analysis revealed that the anode’s vicinity experienced the development of the highest potential, which leads to improved charge collection and an improvement in the solar cell’s overall performance. It is possible to research, design, and construct various structures of graphene-based solar cells using this remarkable optimization technique and data. The conversion of the emission electron mechanism from the thermionic mechanism to the tunnelling emission mechanism is due to the implementation of high-level doping, resulting in maximum *FF* but lower efficiency. For GaAs, under low illumination, the majority of the carriers created in the region reside relatively near to the interface. When compared to graphene’s lower transmittance and greater work function regarding cell performance, the work function is effective for increasing the cell performance. GaAs with moderate n-type doping has a significant increase in power con-

version efficiency; however, this form of device is significantly more sensitive to open-circuit voltage than short-circuit current. Therefore, Si has maximum conversion efficiency in terms of thicker absorption, larger graphene work function, and average doping in semiconductor substrates. As a result, it can be concluded from this work that graphene can function as a semi-transparent charge collector electrode and Schottky junction with a thermionic emission phenomenon for improved efficiency in SBSC solar cells.

**Author Contributions:** L.K.P., R.S.D. and K.J.S. conducted the experiment, design, material preparation, data analysis, and prepared most of the figures. R.S.D. Supervisor and K.J.S. Co-Supervisor of L.K.P. initiated the research and study and also contributed to the modeling and developing the novel idea and improvements in the manuscript. A.B. supported the work for the manuscript. All the authors discussed the results and contributed to the manuscript at various stages. R.S.D. and A.B. are the corresponding authors. The paper has two corresponding authors. All authors have read and agreed to the published version of the manuscript.

**Funding:** This work is partially supported by DST/TDT/DDP-38/2021, Device Development Programme (DDP), by the Department of Science & Technology (DST), Ministry of Science and Technology, Government of India.

**Data Availability Statement:** Not applicable.

**Acknowledgments:** The completion of this work would not have been possible without the support from Electronics and Communication Engineering Department, National Institute of Technology Mizoram, India.

**Conflicts of Interest:** The authors declare no conflict of interest.

## References

1. Avouris, P.; Freitag, M. Graphene photonics, plasmonics, and optoelectronics. *IEEE J. Sel. Top. Quantum Electron.* **2014**, *20*, 6000112. [[CrossRef](#)]
2. Chen, D.; Zhang, H.; Liu, Y.; Li, J. Graphene and its derivatives for the development of solar cells, photoelectrochemical, and photocatalytic applications. *Energy Environ. Sci.* **2013**, *6*, 1362–1387. [[CrossRef](#)]
3. Gao, P.; Ding, K.; Wang, Y.; Ruan, K.; Diao, S.; Zhang, Q.; Sun, B.; Jie, J. Crystalline Si/graphene quantum dots heterojunction solar cells. *J. Phys. Chem. C* **2014**, *118*, 5164–5171. [[CrossRef](#)]
4. Zhang, Z.; Cui, T.; Lv, R.; Zhu, H.; Wang, K.; Wu, D.; Kang, F. Improved efficiency of Graphene/Si heterojunction solar cells by optimizing hydrocarbon feed rate. *J. Nanomater.* **2014**, *2014*, 359305. [[CrossRef](#)]
5. Miao, X.; Tongay, S.; Petterson, M.K.; Berke, K.; Rinzler, A.G.; Appleton, B.R.; Hebard, A.F. High Efficiency Graphene Solar Cells by Chemical Doping. *Nano Lett.* **2012**, *12*, 2745–2750. [[CrossRef](#)]
6. Lei, Y.; Li, R.; Chen, F.; Xu, J. Hydrothermal synthesis of graphene-CdS composites with improved photoelectric characteristics. *J. Mater. Sci. Mater. Electron.* **2014**, *25*, 3057–3061. [[CrossRef](#)]
7. Zhang, L.; Fan, L.; Wang, K. Graphene CdSe nanobelt solar cells with tunable configurations. *Nano Res.* **2011**, *9*, 891–900. [[CrossRef](#)]
8. Luo, L.B.; Chen, J.J.; Wang, M.Z.; Hu, H.; Wu, C.Y.; Li, Q.; Wang, L.; Huang, J.-A.; Liang, F.-X. Near-infrared light photovoltaic detector based on GaAs nanowire array/monolayer graphene Schottky junction. *Adv. Junctional Mater.* **2014**, *24*, 2794–2800. [[CrossRef](#)]
9. Jie, W.; Zheng, F.; Hao, J. Graphene/gallium arsenide-based Schottky junction solar cells. *Appl. Phys. Lett.* **2013**, *103*, 233111. [[CrossRef](#)]
10. Aukerman, L.W.; Dvis, P.W.; Graft, R.D.; Shilliday, T.S. Radiation effects in GaAs. *J. Appl. Phys.* **1963**, *34*, 3590–3599. [[CrossRef](#)]
11. Dohler, G.H.; Kunzel, H.; Olego, D.; Ploog, K.; Ruden, P.; Stolz, H.J.; Abstreiter, G. Observation of tunable band gap and two-dimensional subbands in a novel GaAs superlattice. *Phys. Rev. Lett.* **1981**, *47*, 864. [[CrossRef](#)]
12. Tingting, F. Graphene based schottky junction solar cells on patterned silicon pillar array substrate. *Appl. Phys. Lett.* **2011**, *99*, 23505.
13. Behura, S.K.; Nayak, S.; Mukhopadhyay, I.; Jani, O. Junction characteristics of chemically-derived graphene/p-Si heterojunction solar cell. *Carbon* **2014**, *67*, 766–774. [[CrossRef](#)]
14. Li, X. Graphene on silicon schottky junction solar cells. *Adv. Mater.* **2010**, *22*, 2743–2748. [[CrossRef](#)] [[PubMed](#)]
15. Xie, C.; Jie, J.; Nie, B.; Yan, T.; Li, Q.; Lv, P.; Li, F.; Wang, M.; Wu, C.; Wang, L.; et al. Schottky solar cells based on graphene nanoribbon/multiple silicon nanowires junctions. *Appl. Phys. Lett.* **2012**, *100*, 193103. [[CrossRef](#)]
16. Zhang, X. High efficiency graphene/Si nanoarray schottky junction solar cells via surface modification and graphene doping. *J. Mater. Chem. A* **2013**, *1*, 6593–6601. [[CrossRef](#)]
17. Nair, R.R.; Blake, P.; Grigorenko, A.N.; Novoselov, K.S.; Booth, T.J.; Stauber, T.; Peres, N.M.R.; Geim, A.K. Fine Structure Constant Defines Visual Transparency of Graphene. *Science* **2008**, *320*, 1308. [[CrossRef](#)]

18. Weber, J.W.; Calado, V.E.; Van De Sanden, M.C.M. Optical constants of graphene measured by spectroscopic ellipsometry. *Appl. Phys. Lett.* **2010**, *97*, 091904. [[CrossRef](#)]
19. Arefinia, Z.; Asgari, A. A new modeling approach for graphene based silicon nanowire Schottky junction solar cells. *J. Renew. Sustain. Energy* **2014**, *6*, 043132. [[CrossRef](#)]
20. Silvaco. *Atlas User's Manual*; Silvaco: Santa Clara, CA, USA, 2014; pp. 163–165.
21. Lancellotti, L.; Polichetti, T.; Ricciardella, F.; Tari, O.; Gnanapragasam, S.; Daliento, S.; Di Francia, G. Graphene applications in Schottky barrier solar cells. *Thin Solid Film.* **2012**, *522*, 390–394. [[CrossRef](#)]
22. Cui, T. Enhanced efficiency of graphene/silicon heterojunction solar cells by molecular doping. *J. Mater. Chem. A* **2013**, *1*, 5736–5740. [[CrossRef](#)]
23. Sze, S.M.; Li, Y.; Ng, K.K. *Physics of Semiconductor Devices*; John Wiley & Sons: Hoboken, NJ, USA, 1981.
24. Singh, K.J.; Chettri, D.; Singh, T.J.; Thingujam, T.; Sarkar, S.K. A performance optimization and analysis of graphene based Schottky barrier GaAs solar cell. In Proceedings of the International Conference on Aerospace, Mechanical and Mechatronic Engineering, Bangkok, Thailand, 21–23 April 2017; IOP Publishing: Bristol, UK, 2017; Volume 211, p. 012024.
25. Li, Y.F.; Yang, W.; Tu, Z.Q.; Liu, Z.C.; Yang, F.; Zhang, L.Q.; Hatakeyama, R. Schottky junction solar cells based on graphene with different numbers of layers. *Appl. Phys. Lett.* **2014**, *104*, 043903. [[CrossRef](#)]
26. Kaung, Y. Modeling and design of graphene GaAs junction solar cell. *Hindawi. Adv. Condens. Matter Phys.* **2015**, *2015*, 326384. [[CrossRef](#)]
27. Kaung, Y.; Lui, Y.; Ma, Y.; Xu, J.; Yang, X.; Feng, J. TCAD analysis of graphene silicon Schottky junction solar cell. In Proceedings of the International Symposium on Photonics and Optoelectronics, Shanghai, China, 22–24 August 2015; Volume s9656.

**Disclaimer/Publisher's Note:** The statements, opinions and data contained in all publications are solely those of the individual author(s) and contributor(s) and not of MDPI and/or the editor(s). MDPI and/or the editor(s) disclaim responsibility for any injury to people or property resulting from any ideas, methods, instructions or products referred to in the content.





# Carbon Quantum Dots for Sustainable Energy and Optoelectronics

Woodhead Publishing Series in Electronic and Optical Materials

2023, Pages 455–472

## 19 - Nanodiamonds for advanced photonic and biomedical applications

[Daksh Agarwal](#)<sup>1,2</sup>, [Nikhil Dole](#)<sup>3</sup>, [Aditya Banerjee](#)<sup>4</sup>, [Amit Banerjee](#)<sup>5</sup>

[Show more](#) ▾

[Outline](#) | [Share](#) [Cite](#)

<https://doi.org/10.1016/B978-0-323-90895-5.00009-6> ↗

[Get rights and content](#) ↗

### Abstract

Nanocrystalline diamonds or nanodiamonds (NDs) have many interesting properties leading to various extreme applications, including in emerging areas of high-power high-temperature electronics, field emission, photonics and biomedical e.g., drug delivery and medical imaging. Fascinatingly, NDs' properties could be tailored to applications dependent on particle size: nanocrystalline (particle size  $\sim 1$  to  $\geq 150$ nm), ultrananocrystalline ( $\sim 2$  to  $10$ nm), and diamondoids ( $\sim 1$  to  $2$ nm). NDs, being the hardest materials, find mechanical applications as wear-resistant coatings, lubrication; with its high thermal-conductivity used in heat-sinks and heat-propagators, and with high negative electron affinity, NDs can be also used as electron emitters. NDs are optically transparent in the ultraviolet to far-infrared (IR), and are employed in IR and high-power laser lenses, and in window-coatings in hazardous environment like reactors, satellites, or space shuttles. The exciting emerging applications of NDs in advanced photonics and biomedical have been elaborated in the current chapter with comprehensive literature study.

[Recommended articles](#)

### References (0)

### Cited by (0)

[View full text](#)

Copyright © 2023 Elsevier Ltd. All rights reserved.



## In Silico Strategy to Control or Treat Nipah Virus Infection in Humans Through Saikosaponin Biomolecules

Dr. Sriparna Ray<sup>1</sup> and Dr. Jayanta Sinha<sup>2\*</sup>

<sup>1</sup>Department of Zoology, Bidan Chandra College, Asmeri, West Bengal, India  
<sup>2</sup>P.G. Department of Zoology, Vivekananda College, Kolkata, West Bengal, India

**Abstract:** The penetrance of deadly Nipah virus causing high mortality in humans is mediated by bats and pigs; and there is lack of licensed drugs against it till date. In India the transmittance is caused among humans through direct contamination of secretion and excretion. In order to combat the fatal Nipah virus, so far one strategy has been concerned in this paper; exploiting extract and resources that are of botanical origin. Usually in India, Favipiravir (T-705) is used as anti-viral medicine against Nipah virus. Chemically it is a pyrazinocarboxamide derivative and is an experimental antiviral drug being developed by Toyama Chemical of Japan with activity against many RNA viruses. As Favipiravir is a synthetic analogue, it may cause some side effects in renal function. This paper aims towards identifying various Saikosaponins as an anti-Nipah viral agent and establish its efficacy in binding of these molecules with a viral phosphoprotein. Thus with such an aim and considering the limitation of synthetic drugs, this paper focuses on the interaction between Nipah virus and natural bioactive compounds Saikosaponins (A, B, C, D, etc.), which are triterpene glycosides (naturally occurring) being isolated from medicinal plants such as *Bupleurum* spp, *Heteromorpha* spp, and *Scrophularia scorodonia*. Molecular docking of these herbal compounds with Nipah virus phosphoprotein was carried out through Molecular docking server. Lower energy scores represent better binding between Nipah virus phosphoprotein target and Saikosaponins as ligands. It is observed that best binding occurred between Nipah virus and saikosaponins K among the Saikosaponins clearly indicates its importance to be served as a potent drug. Ligolot+ server revealed polar and hydrophobic residues mainly involved in docking.

**Keywords:** Nipah Virus, In Silico, Bioactive Compounds, Docking, Saikosaponins.

### Article History

Date of Receiving: 18 April 2022

Date of Revision: 01 July 2022

Date of Acceptance: 15 July 2022

Date of Publishing: 29 July 2022

### \*Corresponding Author

Dr. Jayanta Sinha, P.G. Department of Zoology, Vivekananda College, Kolkata, West Bengal, India

**Funding:** This research did not receive any specific grant from any funding agencies in the public, commercial or not for profit sectors.

This article is under the CC BY-NC-ND Licence (<https://creativecommons.org/licenses/by-nc-nd/4.0>)

Copyright © International Journal of Pharma and Bio Sciences, available at [www.ijpbs.net](http://www.ijpbs.net)

Int J Pharma Bio Sci, Volume 13, No 3 (July) 2022, pp. 664-75



**Citation:** Dr. Sriparna Ray and Dr. Jayanta Sinha. In Silico Strategy to Control or Treat Nipah Virus Infection in Humans Through Saikosaponin Biomolecules (2022). Int J Pharm Sci. 13(3), 664-75 <http://dx.doi.org/10.22376/ijpbs.2022.13.3.664-75>

## Certificate of Collaboration

I am pleased to write this certificate of ongoing collaboration, details of which are as follows:

**Collaboration Between:**

**Faculty of Science and Engineering,**

**Jharkhand Rai University, Ranchi**

**Principal Investigator:** Dr Shraddha Prasad,

Associate Professor, Jharkhand Rai University, Ranchi

Jharkhand- 834010

and

**Department of Physics,**

**Bidhan Chandra College, Asansol**

**Principal Investigator:** Dr Ajay Kumar Sharma,

Department of Physics, B.C. College, Asansol

West Bengal- 713304

**Duration of Collaboration:** 2017-2023 and continuing.

**Details of Collaboration:** Research collaboration related to Electronic, Opto-electronic, Mechanical, Electrical Properties of Ternary Chalcopyrites.

**Output of Collaboration:**

● **Research Publications:**

**Journal Publication:-**

- “Optical properties of  $CuInS_2$ ,  $AgAlTe_2$ ,  $CdSiP_2$ ,  $ZnSiP_2$ ,  $CdSnAs_2$ - ternary chalcopyrites”, Ajay Kumar Sharma, Shraddha Prasad, Sanjay Kumar Gorai, Akshar Wangmay, October 2022, Special Issue-V, 147-151.

**Book Chapter Publication:**

- “Di-electric Constant of Ternary Chalcopyrites”, Ajay Kumar Sharma, Shraddha Prasad, Paradigmatic Research (2023), Shree Siddhivinayak Global Publication, 1<sup>st</sup> Edition, pp-29-33, ISBN-978-93-91773-43-4.



**Dr. Shraddha Prasad**

Associate Professor

Faculty of Science and Engineering

Jharkhand Rai University, Ranchi



**Dr. Ajay Kumar Sharma**

Assistant Professor

Department of Physics

Bidhan Chandra College, Asansol





# Bidhan Chandra College

[Govt. Sponsored], ESTD: - 1961, NAAC Accredited

Recognized by U.G.C. (Govt. of India) and affiliated to Kazi Nazrul University

## ONE DAY ONLINE SEMINAR ON

# Cyber Security and Ethical Hacking

## ARDENT COMPUTECH PVT. LTD.

in collaboration with

## BIDHAN CHANDRA COLLEGE



Date: 29/4/2023

Time: 12PM Onwards

Platform : Google Meet (Link will be shared)

Webinar registration Link-

<https://forms.gle/RJcc6bb3rbVjra7KA>

**REGISTER NOW**



**N·E·A·T**  
प्रौद्योगिकी के लिए राष्ट्रीय शैक्षणिक सहयोग  
National Educational Alliance for Technology



 *Forwarded*

**Speaker-** Mr. Dipan Mondal

**Subject Matter Expert-** Cyber Security & Ethical Hacking

Having 7 years of experience in Corporate Training , Product Delivery & High End Research Based Project.

Dipan Mondal is associated with **ardent** since last 7 years & delivered several session in PAN India basis.

He is also an HPE & Microsoft Certified Technology Associate & having publications in reputed journals & conferences.

11:16 am 



# Bidhan Chandra College

[Govt. Sponsored], ESTD: 1961

Recognized by U.G.C (Govt. of India) and affiliated to KAZI NAZRUL UNIVERSITY

Department of Professional studies

Asansol – 4, Dist – Paschim Bardhaman, West Bengal, Ph 0341 2283020 / 3058 / 3200; www.bccollegeasansol.org

Date: 24<sup>th</sup> April, 2023

## NOTICE

It is hereby informed to all the students of Bidhan Chandra College that an online seminar will be held in collaboration with ARDENT COMPUTECH PVT LTD ON 29<sup>TH</sup> April (Saturday) at 12 noon. The interested candidates are informed to register themselves in the Google form link given below.

SEMINAR TOPIC: - Cyber Security and Ethical Hacking

Date: 29<sup>th</sup> April, 2023(Saturday)

Time: 12 noon.

Registration link: <https://forms.gle/RJCc6bb3rbVjra7KA>

Platform for the seminar: Google MEET

Principal  
Bidhan Chandra College  
Asansol-4

Principal  
Bidhan Chandra College  
Asansol



*2 Rkaly...*







# Proposal for Webinar on Cyber Security and Ethical Hacking (Bidhan Chandra College, Asansol)

1 message

Mon, Apr 24, 2023 at 2:15 PM

Sukhendu Ghosh <sukhendu@ardentcollaborations.com>  
To: office@bccollegeasansol.ac.in, office.bccollege@gmail.com  
Cc: rajdipchat@gmail.com, Indranil De Sarkar <indranil@ardentcollaborations.com>, Rajmohan De Sarkar <rajmohan@ardentcollaborations.com>, jit dutta <jit.dutta@ardentcollaborations.com>, rajesh mitra <rajesh@ardentcollaborations.com>

*To Rajdip for 11:55 AM*

To  
The Principal  
Bidhan Chandra College, Asansol  
West Bengal

Respected Sir,

**In response to our meeting at your esteemed institution we are very much pleased to submit the proposal for a webinar on " Cyber Security and Ethical Hacking " for 1st year 2nd year & 3rd year students of all departments.**

ARDENT'S mission is to transform lives through technical up-gradation. To carry on the learning process which has been impacted by the corona-virus (COVID-19) outbreak ARDENT is providing online free technical workshops to assist universities, colleges & students online. These workshops will help students to gather knowledge on the latest technologies. We look forward to organizing a webinar for the students of your esteemed university.

*Jit Dutta*

**Participation E – Certificates shall be issued to all participants.**

Topic for Webinar: " Cyber Security and Ethical Hacking "

The duration of the webinar will be ( 2 hrs ).

Target Audience - 2nd yr & 3rd Year students mainly. 1st year students can also join.

Date: To be finalized on mutual discussion

Time: 12 PM Onwards

We are sharing the registration link: <https://forms.gle/RJCc6bb3rbVjra7KA>

**Participants are instructed to fill up the registration form within 28th April 2023 at 11pm (Friday).**

In case of any requirement feel free to Contact Mr Goutam Ghosh: 9933188883

Kindly send a confirmation from your end.

Thanks & Regards

Sukhendu Ghosh  
Manager - Marketing

Ardent Computech Pvt. Ltd. (An ISO 9001:2015 Company)  
SDF Building, Ground Floor,  
Module Number - 132, Sector 5, Salt Lake,  
Kolkata, Pin - 700091.

O: +91 33 4007 3507  
Call : + 91 9933188883



[Need some help?](#) [Click here to book a call with me or schedule a meeting](#)

S.N	Email Id	name	Ph Number	College	Dept.	Year	Dept.	Webinar Topic
1	chirdeepdev@gmail.com	Chirdeep Dev	9123220076	Bidhan Chandra College	BCA	2nd	BCA	Cyber Security and Ethical Hacking
2	nehakaur20002@gmail.com	Harpreet kaur	7061394104	Bidhan Chandra College	BCA	6th	BCA	Cyber Security and Ethical Hacking
3	denabandhupanidikelahi@gmail.com	Dinabandhu Pandit	8877817120	Bidhan Chandra college Asansol	BCA	4th	BCA	Cyber Security and Ethical Hacking
4	snigdharoy651@gmail.com	Snigdha Roy	7478757945	Bidhan Chandra College	BCA	4th	BCA	Cyber Security and Ethical Hacking
5	ziqrazain316@gmail.com	Ziqra Zain	8918684331	Bidhan Chandra College	B.Sc	4th	Mathematics	Cyber Security and Ethical Hacking
6	bose0737@gmail.com	Debjani Bose	7047742329	Bidhan Chandra College	BCA	4th	BCA	Cyber Security and Ethical Hacking
7	rajib.asn1617@gmail.com	Rajib Mahato	8910564224	Kazi Nazrul University	Msc	4th	Physics	Cyber Security and Ethical Hacking
8	alamp4094@gmail.com	Panwez Alam	7701966361	Bidhan Chandra College	B.Sc	2nd	B.Sc	Cyber Security and Ethical Hacking
9	mdashrafalimurtaza@gmail.com	MD ASHRAF ALI MURTAZA	7001233592	BIDHAN CHANDRA COLLEGE	BSC	2nd	Mathematics	Cyber Security and Ethical Hacking
10	singhamanindian82@gmail.com	Aman Kumar Singh	8617508472	B.C COLLEGE	Bsc Maths	2nd	Mathematics	Cyber Security and Ethical Hacking
11	ashishdennis123@gmail.com	ASHISH LALL	7001100663	Bidhan Chandra College	BCA	6th	BCA	Cyber Security and Ethical Hacking
12	khanzenat08@gmail.com	Rishi kesh Routh	9609213337	KNU	BCA	4th	BCA	Cyber Security and Ethical Hacking
13	usamapanwaiz91344@gmail.com	Osama panwaiz	9134475091	Bidhan Chandra college	B.A	4th	B.A	Cyber Security and Ethical Hacking
14	suvrax@gmail.com	Subhraman Sarkar	7557083935	The University of Burdwan	M.Sc. (Com)	4th	Physics	Cyber Security and Ethical Hacking
15	ghausiazulfequar27@gmail.com	Ghausia zulfequar	8509722154	Bidhan Chandra college	BA History	2nd	BA History	Cyber Security and Ethical Hacking
16	nawejakhatar10063@gmail.com	Nawej Akhatar	9.18797E+11	Bidhan Chandra College	BCA	4th	BCA	Cyber Security and Ethical Hacking
17	dasguptasourav15112003@gmail.com	SOURAV DASGUPTA	8918295343	College	Bsc ( Maths	4th	Department of Math	Cyber Security and Ethical Hacking
18	shivams52@gmail.com	Shivam choudhary	9474925772	Bidhan chandra college	BCA	2nd	BCA	Cyber Security and Ethical Hacking
19	nawazakram547@gmail.com	Nawaz Akram	6296536453	BC college	BSC	2nd	MP	Cyber Security and Ethical Hacking
20	zakiyahmed058@gmail.com	Mid Zaki Ahmad Ansari	7001494543	Bidhan Chandra College	BA	1st	History	Cyber Security and Ethical Hacking
21	mdsaquibkhan29910@gmail.com	Mid Saquib Khan	8537008706	Bidhan Chandra College Asansol	BA	6th	URDU	Cyber Security and Ethical Hacking
22	farhanpanwez6543@gmail.com	Mid farhan panwez	6297735300	BC college	BA	6th	BA PROGRAM	Cyber Security and Ethical Hacking
23	sk.nadeem2704@gmail.com	Nadeem Ahmed SK	9121755191	Bidhan Chandra college Asansol	BCA	6th	BCA	Cyber Security and Ethical Hacking
24	devdiwan10@gmail.com	Yash diwan	7001097073	Bidhan Chandra college	BCA	4th	BCA	Cyber Security and Ethical Hacking
25	ghazalaperween48@gmail.com	Ghazala perween	9609561084	Bidhan chandra college	BBA	4th	BBA	Cyber Security and Ethical Hacking
26	qsaba2279@gmail.com	Shaheena khatoon	8509747638	College	B.A	1st	B.A	Cyber Security and Ethical Hacking
27	asnmuskan8906@gmail.com	Muskan parween	7477702249	college	B.A	4th	Urdu	Cyber Security and Ethical Hacking
28	ajaymahato7671@gmail.com	Ajay Mahato	7679280919	Bidhan Chandra College	B.Sc (Hons)	2nd	Mathematics	Cyber Security and Ethical Hacking
29	souravhere03@gmail.com	Sourav Das	9382941429	Bidhan Chandra college	B.Sc Math h	2nd	Mathematics	Cyber Security and Ethical Hacking
30	shuvamkumar777@gmail.com	Shuvam Kumar	9.19047E+11	Kazi nazrul University	M sc Physics	2nd	Physcis	Cyber Security and Ethical Hacking
31	razikhan9333@gmail.com	MD RAZI KHAN	9733710595	BIDHAN CHANDRA COLLEGE	BA	1st	ME	Cyber Security and Ethical Hacking
32	suphailiansari8940@gmail.com	SUHAIL ANSARI	7679982271	BC COLLEGE / KNU	B.A (Hindi)	4th	B.A (Hindi Honours)	Cyber Security and Ethical Hacking
33	awbabashaw173@gmail.com	Avinaba shaw	9382670219	Bidhan chandra collage	Bsc	4th	Physics	Cyber Security and Ethical Hacking
34	kateerh1234@gmail.com	KAHKASHAN ABEDIN	7797896027	Bijoy Pal Memorial B.ed College	B.Ed	1st	Education	Cyber Security and Ethical Hacking
35	playngreenking@gmail.com	Nayan maji	9382716856	b.c college	B.sc in math	4th	Department of math	Cyber Security and Ethical Hacking
36	playngreenking@gmail.com	Reyaz Ahmed	7001359605	Bidhan Chandra College	BA	4th	BA Urdu hons	Cyber Security and Ethical Hacking
37	playngreenking@gmail.com	Mid Amir Ali	9508148286	Bidhan Chandra college	BCA	2nd	BCA	Cyber Security and Ethical Hacking
38	parijit667@gmail.com	Arijit Paul	9832296381	Bidhan Chandra College, Asansol	BCA	2nd	BCA	Cyber Security and Ethical Hacking





39	singhanuragkumar56@gmail.com	Anurag Kumar Singh	9264271011	College	BCA	2nd	BCA	Cyber Security and Ethical Hacking
40	nelufar26082003@gmail.com	Nelufar	7001088954	Bidhan chandra college	BBA	2nd	BBA	Cyber Security and Ethical Hacking
41	m.sonukhan0786@gmail.com	Md Sonu Khan	7866073499	Bidhan Chandra college	B.A	4th	Urdu	Cyber Security and Ethical Hacking
42	rahulyadav953202@gmail.com	Rahul yadav	7393021108	B C College	BCA	4th	BCA	Cyber Security and Ethical Hacking
43	swetakumar99019@gmail.com	SWETA KUMARI	7318900672	BIDHAN CHANDRA COLLEGE	BA	2nd	HISTORY HONS	Cyber Security and Ethical Hacking
44	mr.sarfarazofficial001@gmail.com	Md Sarfaraz Ansari	9832341778	Bc college	BCA	2nd	BCA	Cyber Security and Ethical Hacking
45	subhroghosh1024@gmail.com	Subhra Ghosh	9679490112	Bidhan Chandra college	BCA	6th	BCA	Cyber Security and Ethical Hacking
46	gorainilkantha83@gmail.com	Neelkantha Gorai	6295373405	Bidhan Chandra College	B SC (Hons)	4th	Mathematics	Cyber Security and Ethical Hacking
47	mukherjeechiranjit035@gmail.com	CHIRANJIT MUKHERJEE	9832897146	Bidhan chandra college	Bsc.in Math	4th	Mathematics	Cyber Security and Ethical Hacking
48	hrithikgsurana14@gmail.com	Hrithik G Surana	8250800543	BC COLLEGE ASANSOL	BCA	2nd	BCA	Cyber Security and Ethical Hacking
49	debashishmukherjee486@gmail.com	DEBASHISH MUKHERJEE	9563072237	BIDHAN CHANDRA COLLEGE	BSC HONO	4th	PHYSICS	Cyber Security and Ethical Hacking
50	srijitbhattacharjeegaddu@gmail.com	SRIJIT BHATTACHARJEE	7407186638	BC college	BCA	2nd	BCA	Cyber Security and Ethical Hacking
51	rishikeshch7890@gmail.com	Rishikesh Choudhury	9475758965	Bidhan Chandra College	Bsc	4th	Physics	Cyber Security and Ethical Hacking





# Bidhan Chandra College

NAAC Accredited, Govt. Sponsored, ESTD: - 1961

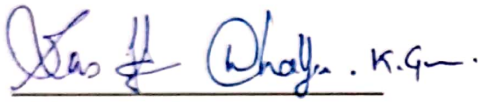
Recognized by U.G.C. (Govt. of India) and affiliated to Kazi Nazrul University

Asansol, Paschim Bardhaman, West Bengal, Pin-713304 Ph: 0341-2283020, [www.bccollegeasansol.ac.in](http://www.bccollegeasansol.ac.in)

22 September 2022

## NOTICE

This is to inform to all the students of BBA & BCA that an "Employability and Career Awareness Program" in collaboration with George Telegraph, Asansol (National Skill Development Corporation of India) will be held on 24th September 2022 (Saturday) from 11:30 am – 12:30 pm



Head of Professional Studies



Principal  
Bidhan Chandra College  
Asansol

Principal  
Bidhan Chandra College  
Asansol





"Employability and Career Awareness Programme  
 in Collaboration with George Telegraph, Asansol (National Skill  
 Development Corporation of India)  
 Attendance of Students Date: 24.09.22

- |                              |  |
|------------------------------|--|
| 1. Rahul Dubhaz (BBA)        | 38) Anli Prasad (BBA)                            |
| 2. Sunny Singh (BBA)         | 39) Uday Narayan Mohanajer (BBA)                 |
| 3. Md. Faizan Wasim (BBA)    | 40) Md. Saifullah Ansari (BBA)                   |
| 4. Kalayami Paul. (BBA)      | 41) Aioke Kr Pathak (BBA)                        |
| 5. ZAFAR HUSSAIN (BBA)       | 42) Kishav Kumar Verma (BBA)                     |
| 6. Babita Kumari (BBA)       | 43) Md. Shaqib Wari (BBA)                        |
| 7. Shilpi Datta (BBA)        | 44) Suman Borei (BBA) Rd-24                      |
| 8. Simhana Saha (BBA)        | 45) Md. Farhan Akhter (BBA-24)                   |
| 9. Lekha Dey (BBA)           | 46) Shams Raza (BBA-19)                          |
| 10. Biyanshu Kumari (BBA)    | 47) Md. Umarul Sulayman (BBA-1)                  |
| 11. Parambeer Singh (BBA)    | 48) Imran Nazir (BBA) (1 <sup>st</sup> sem) (35) |
| 12. Priyotosh Bawri (BBA)    | 49) Shahim Reza BBA 1 <sup>st</sup> semester     |
| 13. Satyajit Singh (BBA)     | 50) Md. Faraz BBA 1 <sup>st</sup> semester       |
| 14. Anurag Dey (BBA)         | 51) Ketan Kumar BBA                              |
| 15. Anjan Roy (BBA)          | 52) Spider Man America Marvel                    |
| 16. Kharisha Sikdar (BBA)    | 53) Bipin Bismwal (BBA)                          |
| 17. Junaid Akhtar (BBA)      | 54) Somnath Lama (BBA)                           |
| 18. Abdul Aziz Mustafa (BBA) | 55) Lazia Nayeem (BBA)                           |
| 19. Aditya Kumar Singh (BBA) | 56) Priyanka Sarkar (BCA)                        |
| 20) Syed Saahil Rashid (BBA) | 57) Amira Khatoon (BCA)                          |
| 21) Abhilaasha Sakshi Roy    | 58) Koushiki Roy (BCA)                           |
| 22) Vishal Kumar Mahto (BBA) | 59) Debjeet Halder (BCA)                         |
| 23) Md. Asif Ali (BBA)       | 60) Pratima Patwa (BCA)                          |
| 24) Sukanya Pal (BBA)        | 61) Masum Gupta (BCA)                            |
| 25) Anita Maji (BBA)         | 62) Hrithik . G. Surana (BCA)                    |
| 26) Sahil Raza (BBA)         | 63) Rohit Kurrao (BCA)                           |
| 27) Md. Shahar Khan (BBA)    | 64) Md. Amir Ali (BCA)                           |
| 28) Animesh Chand (BBA)      | 65) Santosh Kr. Bismwal (BCA)                    |
| 29) Susmita Dutta (BBA)      | 66) Munna Tripathi (BCA)                         |
| 30) Nisha Singh (BBA)        | 67) HABIBI SHAHIDI (BBA)                         |
| 31) Sandeep Mohato (BBA)     | 68) Afifa Ashrafi (BBA)                          |
| 32) Shahbaz Khan (BBA)       | 69) Athinto Gope (BBA)                           |
| 33) Anisha Kumari (BBA)      | 70) Shreya Roy (BBA)                             |
| 34) Beauty Kumari Ray (BBA)  | 71) Pooja Dae (BBA)                              |
| 35) Raju Mondal (BBA)        | 72) Pooja Sinha (BCA)                            |
| 36) Manash Kumar Shaw (BBA)  |  |
| 37) Hridyesh Bismwal (BBA)   |  |



24/09/22  
 K. G. M



# NIIT

## Student Connect Session:

Unsure of what skills you should have to be successful in this Digital Age?

Enrol for a Student Connect Session on **New Age Career in Digital Era**

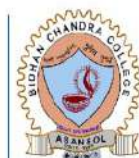


Organised by NIIT Ltd. in collaboration with Bidhan Chandra College

Patron:

Dr Falguni Mukhopadhyay

Principal, Bidhan Chandra College, Asansol



**Bidhan Chandra College**

[Govt. Sponsored], ESTD: - 1961, NAAC Accredited

Recognized by U.G.C. (Govt. of India) and affiliated to Kazi Nazrul University

Date: 12<sup>th</sup> April, 2023

Time: 12:00 pm

Seminar at college campus

For more detail, contact

Contact person: Sourav Chakraborty

Contact number: +91 8100075669

## BE SURE WITH NIIT



# Bidhan Chandra College

[Govt. Sponsored], ESTD: 1961

Recognized by U.G.C (Govt. of India) and affiliated to KAZI NAZRUL UNIVERSITY

Department of Professional studies.

Asansol – 4, Dist – Paschim Bardhaman, West Bengal, Ph 0341 2283020 / 3058 / 3200; www.bccollegeasansol.org

Date: - April 10, 2023

## NOTICE

It is hereby informed to all the Final year students of Bidhan Chandra College that a Seminar has been organized with the collaboration with **NIIT** on 12th April 2023 from 12 noon to 1PM.

**Venue:- Seminar Hall, Bidhan Chandra College.**

**Seminar Topic:- Data Science, Digital Marketing and Banking.**

**Time : 12 noon**

**Date : 12th April 10, 2023.**

All the interested students are informed to be present and participate in the seminar.

Wha...  
10/4/22



Principal  
Bidhan Chandra College  
Asansol-4  
Principal  
Bidhan Chandra College  
Asansol





To, Rajdeep (BCA)  
for action. *[Signature]*  
8/4/23

Office BC College <office@bccollegeasansol.ac.in>

## Requesting permission to host a seminar for your prestigious College

1 message

**Sourav Chakraborty** <Sourav.Chakraborty@niit.com>

To: "office@bccollegeasansol.ac.in" <office@bccollegeasansol.ac.in>

Fri, Apr 7, 2023 at 12:22 PM

Cc: Debjit Chowdhury <Debjit.Chowdhury@niit.com>, Snahajit Nair <Snahajit.Nair@niit.com>

To,  
The Principal  
Bidhan Chandra College

Requesting permission to host a seminar for your prestigious College.

Respected Sir,

Greetings for the day.

It was a please interacting with you yesterday at your college premises. As discussed, seeking for your support to connect with your final year and alumni students.

We understand that college education is the backbone of every student's professional career. The pride of every college is its successful alumni. However, in a country like India, graduation is not the end. It is in fact the start of a long and more arduous road to learning. Today, professional knowledge is as important as academic qualification, and this is where we come in.

Over the last 40+ years, NIIT has upskilled more than 4 Crore learners through its cutting-edge professional programs, not only in India but in 30 other countries. We have been the **most trusted training brand** for corporates consistently.

A look at today's fast-evolving technological scenario and the immense number of opportunities it is unfolding in front of us, NIIT plans to conduct a **knowledge session for all alumni and final year final semester students** of your esteemed institution on **New Age Careers like Full Stack Software Engineering, Data Science and Digital Marketing.**

This will help the graduates to understand the relevant skills needed in the industry and how they can prepare for the same with NIIT's specially designed curriculum. Our programs are highly hands-on and builds role-specific competencies. They are mapped to Global Certifications and are designed by practitioners. Learners will work in an environment that mirrors the real work environment, hence they become a preferred choice for employers. We also support the learners who are seeking for career support.

Your college is one of the prestigious institutions in this region and is engaged in creating the future Indian Workforce. Both our institution shares the same synergy of honing the skill sets of graduates and making them equipped with the specialized skills that are needed for the industry.

We pray for your support in helping us connect with your final year and alumni students by next week in April '23. In case if it is permissible from the college management end, you can also share your alumni contact details so that we can connect with them and keep the institution posted on the progress.

Looking forward for your support.

Best Regards,

**Debjit Chowdhury**

Manager-SNC, NIIT Digital

NIIT Limited | 85, Sector 32, Institutional Area, Gurgaon  
122001,

India | [www.niit.com](http://www.niit.com)

M: +91-8240311413



Visit us at: <https://www.niit.com>  
Follow us on: <https://www.twitter.com/niittd>

---

**DISCLAIMER**

This email and any files transmitted with it are confidential and are solely for the use of the individual or entity to which it is addressed. Any use, distribution, copying or disclosure by any other person is strictly prohibited. If you receive this transmission in error, please notify the sender by reply email and then destroy the message. Opinions, conclusions and other information in this message that do not relate to official business of the company shall be understood to be neither given nor endorsed by NIIT Ltd. Any information contained in this email, when addressed to Clients is subject to the terms and conditions in governing client contract.



# NIIT SEMINAR- 12/04/2023

Sr No	Name	Signature	Department	Contact No
1	Rohul Kumar Yadav	Rohul Yadav	B.C.A.	8604651108
2	Yash Diccyan	Yash Diccyan	BCA	7001097023
3	Pabitra Baral	Pabitra Baral	B.Com (P)	8927277536
4	Santosh Bhowmal	Santosh Bhowmal	B.C.A	8599797335
5	Hrithik. G. Surana	H.G. Surana	B.C.A	8230800543
6	Anurag Mandal	Anurag	B.Sc	8340558299
7	Snehajish Chakraborty	Shakraborty	B.B.A	8372804431
8	Aloke K. Palhak	Aloke K Palhak	B.B.A	7866044022
9	Sarosi Mandal	Sarosi Mandal	BSc	6297839619
10	Ananti kumar Das	Ananti kumar Das	B.Sc	8327495112
11	Subham Shaw	Subham Shaw	BSC	8327510244
12	Mriganka Nad	Mrid	B.Sc	9609674695
13	Shruti Mandal	Shruti Mandal	B.com(H)	9339053474
14	Riya Kumari Shawa	Riya Kumari Shawa	B.com(H)	7047329758
15	UPratima Patwa	Pratima Patwa	BCA	7029042700
16	Suramjam Samjhal	Suramjam Samjhal	BCA	9064509680
17	Babita - kumari	Babita kumari	B.B.A	9091180713
18	Kalayani paul.	Kalayani paul	B.B.A	9064592428
19	Saikat Bhikumar Shaw	Saikat Bh. Shaw	B.B.A	7679722842
20	Shilpi Dutta	Shilpi Dutta	B.B.A	7541055525
21	Khusboo Agarwal	Khusboo Agarwal	B.B.A	6296663157
22	Nyasha Bhardi	Bhardi	B.B.A	6372939008
23	Kishan Shaw	Kishan Shaw	B.B.A	8218823006
24	Rajshree shaw	Rajshree shaw	B.B.A	7811092404
25	Animesh Chand	Animesh Chand	B.B.A	7047987999
26	Rohul Dasgupta	Rohul Dasgupta	B.B.A	9609152270
27	Ritik Tewari	Ritik Tewari	B.O.A	974992054
28	SAMANTHA SNEHA PAUL	Samantha Sneha Paul	Dsc.	9635315634
29	MAMTA SHRESTHA	Mamta Shrestha	B.Sc (Hons)	8906237717
30	Priyotosh Bauri	Priyotosh Bauri	B.B.A	8101737509
31	Sunny Singh	Sunny Singh	BBA	9507038471
32	Ankit Kumar Thg	Ankit Kumar Thg	BBA	9608566612
33	Sujal Prasad Nongia	Sujal Prasad Nongia	BBA	7407275159
34	Rishikesh Choudhury	Rishikesh Choudhury	B.Sc (Hons)	9475758965
35	Debashish Mukherjee	Debashish Mukherjee	B.Sc (Hons)	9563072237
36	Mantu yadav	Mantu yadav	B.Sc (Hons)	7029362437
37	Ravi Thakur	Ravi Thakur	B.Sc (Hons)	980197986
38	souvik chakraborty	Souvik chakraborty	B.Sc (Hons)	9735240602



